Dynamics of polyamide in the solid state in presence of solvents and in the molten state

Florentina Maria Preda

Université Claude Bernard Lyon 1

UNIVERSITÉ DE LYON

Numéro d'ordre: 01 - 2016 Année: 2016

THÈSE DE L'UNIVERSITÉ DE LYON

Délivrée par

l'Université Claude Bernard Lyon 1
École Doctorale Matériaux

DIPLÔME DE DOCTORAT

(arrêté du 7 août 2006)

Soutenue publiquement le 5 Janvier 2016 par

Florentina Maria PREDA

Dynamics of polyamide in the solid state in presence of solvents and in the molten state

Devant la commission d'examen formée de :

Christian CARROT	*Examinateur*
Eliane ESPUCHE	*Examinateur*
Henk HUININK	*Rapporteur*
Peter VAN PUYVELDE	*Rapporteur*
Paul SOTTA	*Directeur de thèse*
Louise-Anne FILLOT	*Correspondant industriel*

Daca nu exista ferestre, ele trebuie inventate.
(If there are no windows, invent them)

Iona - Marin Sorescu

Remerciements

Je voudrais remercier tout d'abord Ludovic Odoni, Florence Clément, Jean-Yves Delannoy et Didier Long de m'avoir permis de réaliser ce travail au sein du Laboratoire Polymères et Matériaux Avancés, UMR 5268 CNRS/Solvay.

Mes plus profonds remerciements vont à mon directeur de thèse, Paul Sotta et mon encadrante Solvay, Louise-Anne Fillot. Paul, je te remercie pour ta disponibilité, tu as toujours trouvé du temps pour nos discussions. Merci de m'avoir guidé dans la découverte du monde de la recherche en physique des polymères, toujours à l'écoute et avec pédagogie. Ton calme perpétuel a apaisé ma nature sanguine. Louise-Anne, je te remercie de m'avoir instigué à chercher les conclusions de mon travail et à les traduire en messages claires pour le monde industriel. Merci d'avoir été proche professionnellement et humainement jusqu'à la fin de ma thèse, malgré ton changement de poste. Tes conseils restent gravés dans ma mémoire.

I would also like to express my deepest gratitude to Frank Snijkers, who supervised closely the research on polyamide viscoelasticity. You were relentless in teaching me rheometry and the scientific approach in investigating the rheology of polymer melts. My friend, I am forever in your debt.

I gratefully acknowledge Professors Henk Huinink and Peter van Puyvelde for accepting to examine this thesis and Eliane Espuche and Christian Carrot for accepting to be part of the jury. Thank you for your interest in this PhD work.

Moreover, I would like to express my gratitude to all our external collaborators: Ruben Vera (Centre de Diffractométrie Henri Longchambon), who spent late afternoons to finish XRD measurements, Jean-Charles Majesté (IMP Saint-Etienne), who received us with open arms each time we needed their equipment, Angel Alegria and Silvia Arrese Igor (Centro de Fisica de Materiales, Spain, through an ESMI grant), best tutors in dielectric spectroscopy and Evelyne van Ruymbeke and Alexei Likhtman, who helped us with data and discussions on rheology.

J'adresse des remerciements particuliers à Anthony Bocahut, Nadia Delon-Anik, Danielle Lamberet, Didier Long et Marie-Laure Michon pour l'expertise et l'aide précieuse que vous avez apportés par des discussions, des mesures expérimentales ou par la synthèse des matériaux. Sans vous ce travail n'aurait pas été abouti.

Je suis extrêmement reconnaissante à toutes les personnes du R & I Centre Lyon de Solvay pour leur aide pendant ces trois ans. Je remercie chaleureusement le laboratoire d'Analyse, Nadia Delon-Anik, Pauline Grau, Clémence Abadie, Baptiste Gros et Frederic le Guyader pour avoir traité mes demandes avec le maximum d'attention. Merci à l'équipe transformation, Vincent Curtil, Michel Sorin et Olivier Chaubet ainsi que l'équipe Synthèse, Marie-Laure Michon, Vincent Mollet, René Rossin et Franck Touraud dirigées par Véronique Bossennec. Les matériaux que vous avez transformé ou synthétisé ont été au cœur de cette thèse. Un grand merci à Sylvie Ghiringhelli et Alexandre Comment pour avoir rempli la documentation sécurité et avoir fait tout le possible pour que mes manips contraignantes se fassent, toujours avec le sourire et la bonne volonté.

De manière générale, merci à tout le personnel Solvay qui s'est rendu disponible pour des discussions formelles et informelles: merci à Olivier Andres, Alexandra Argoud, Alexandre Corbin, Martine Collomb, Daniel Duchène, Léo Georges, Olivier Gilbain, Jean-Claude le Thiesse, Stéphane Lousteau, Sonia Perosino, Christiane Prebet, Olivier Sanseau, Elodie Seignobos, Lise Trouillet-Fonti, Didier Tupinier, Caroll Vergelati, ...

Pour finir, je souhaite en particulier remercier tous mes amis thésards, post-docs, alternants et stagiaires sans lesquels l'ambiance au bureau n'aurait pas été la même. Je garderai toujours dans le cœur nos pauses thé/café, la tablette de Crunch - craquage en fin d'après-midi, les déjeuners internationaux, les restaurants, l'accrobranche, la galette des rois, les gâteaux du

jeudi matin, le tiramisu, les discussions philosophiques, la piscine et la course à pied... Vous allez me manquer.

Et il ne faut pas oublier les amis de Chimie Paris, en thèse ou pas, avec qui j'espère on partagera toujours des fous rires et on retrouvera le sentiment paisible d'être chez soi. Malgré la distance, on arrive toujours à se retrouver.

Dar cel mai important, as vrea sa multumesc familiei mele, care mi-au dat aripi sa zbor departe de casa, oricat de greu a fost pentru ei. Tataie, iti dedic teza aceasta, as vrea sa ma poti vedea azi...

Summary in English

Dynamics in the solid state in presence of solvents: Polyamides are a family of semi-crystalline thermoplastic polymers widely employed in the automotive industry due to its excellent thermal stability and mechanical properties. However, polyamide can be significantly affected by the absorption of low molecular weight penetrants like water. The rate of sorption and amount of absorbed solvent depend on the mechanisms of interaction between solvent and polyamide, along with sorption and diffusion mechanisms. Diffusion and sorption of solvents in polymers can be very complex because of the existence of specific interactions (non-polar or polar), dynamic heterogeneities in the amorphous phase, modification of the polymer dynamics induced by the solvents and different crystalline phases. In polyamide/solvent systems, all of these factors have to be taken into account.

A first part of this study focused on the accessibility of the amorphous phase in semi-crystalline polyamides. A comparison between a 100% amorphous polyamide and its semi-crystalline counterpart of equivalent chemical structure suggests that the amorphous phase in semi-crystalline polyamide is not entirely accessible to the solvents. A second part of this study focused on the diffusion mechanisms of water and ethanol in polyamide. Fickian or non-Fickian diffusion mechanisms could be explained by the variation of the diffusion coefficients as a function of solvent concentration. Moreover, the relationship between water diffusion and the dynamics of the amorphous phase in polyamide was investigated. A simple comparison of dielectric characteristic relaxation times with the timescale of diffusion suggests that diffusion and polyamide α relaxation (associated to the glass transition) should not be directly correlated. However, diffusion is correlated to the secondary β relaxation, which encompasses the local chain dynamics of hydrogen bonded amide groups in the presence of water. A mechanism of diffusion based on the trapping of water molecules between neighboring sorption sites (amide groups) is proposed in these strongly interacting polymers.

Dynamics in the molten state: Although polyamide is an industrially important polymer, systematic studies of its rheological behavior are scarce. The main reasons are the difficulties related to chemical stability and to the presence of a crystalline phase that limits the measurement range to temperatures above the melting point. The aim of our investigation is to gain understanding of the effects of the strength and density of hydrogen bonds on the dynamics in the molten state in polyamides. In order to achieve this goal, a class of amorphous, blocked polyamides was designed to remove the above-mentioned limitations inherent to polyamide. The strength of the interactions is varied by the introduction of lateral groups on a constant PA6I backbone.

The complete master curves of the dynamic moduli for polyamide were obtained for the first time. As the molecular weight increases, a clear rubbery plateau appears and the longest relaxation time is shifted to lower frequencies. The introduction of functional groups results in an increase of the glass transition temperature by 10 to 40° C, probably due to their ability to form strong interactions with the amide groups. Surprisingly, when polymers of similar molecular weight and molecular weight distribution are compared at the same $T - T_g$, their master curves overlap, indicating that the strength of interaction does not affect their dynamics above T_g. To confirm this point, we described the master curves of the unentangled polyamides with a regular Rouse model. An investigation by Broadband Dielectric Spectroscopy gives some elements for understanding the lack of influence of interactions on polyamide viscoelasticity.

Keywords: polyamide, crystallinity, strong interactions, hydrogen bonds, dynamics, solvents, rheology

Résumé en français

Dynamique du polyamide dans l'état solide en présence de solvants: Les polyamides sont une famille de polymères thermoplastiques semi-cristallins largement utilisés dans l'industrie automobile grâce à leur excellente stabilité thermique et propriétés mécaniques. Cependant, ces propriétés peuvent être affectées par la sorption de l'eau présente dans l'atmosphère ou de l'éthanol présent dans les biocombustibles. Les cinétiques de sorption et la sorption à l'équilibre dépendent des mécanismes d'interaction entre le solvant et le polyamide et des mécanismes de sorption et de diffusion. La diffusion et la sorption de solvants dans les polyamides sont des phénomènes complexes à cause de l'existence d'interactions spécifiques (liaisons hydrogène), d'hétérogénéités dynamiques dans la phase amorphe, de changements dans la dynamique du polymère en présence de solvants et de l'existence d'une phase cristalline.

Puisque l'accessibilité de la phase amorphe peut avoir une influence sur les mécanismes de diffusion et de sorption, la diffusion et la sorption de différents solvants (eau, alcools de tailles différentes) ont été comparés dans un polyamide 100% amorphe et son homologue semi-cristallin. Nous avons confirmé que la phase amorphe d'un polymère semi-cristallin n'est pas entièrement accessible à l'eau, ce qui est en accord avec la littérature. Une deuxième partie de cette étude a été consacrée à la relation entre la diffusion de solvants et la dynamique de la phase amorphe. Premièrement, nous avons mis en évidence que les mécanismes de diffusion Fickien et non-Fickien peuvent être expliqués par la variation des coefficients de diffusion avec la concentration de solvant. Deuxièmement, l'influence de la relaxation du polymère a été évaluée par Spectroscopie Diélectrique. Une simple comparaison des échelles de temps de la diffusion et de la relaxation α, associée à la transition vitreuse, indique que les deux phénomènes ne sont pas directement corrélés. Cependant, la diffusion semble corrélée à la relaxation secondaire β, qui décrit la dynamique locale des groupements amide en présence d'eau.

Dynamique du polyamide à l'état fondu: Bien que le polyamide soit un polymère industriel de grande importance, les études systématiques de son comportement rhéologique sont rares dans la littérature. Les raisons principales sont les difficultés liées à la stabilité chimique de ce polymère et à l'existence d'une phase cristalline. Le but de notre étude est de comprendre les effets de la force et de la densité de liaisons intermoléculaires (liaisons hydrogène, interactions ioniques) sur la dynamique du polyamide à l'état fondu. Pour atteindre ce but, des polyamides amorphes ayant des bloqueurs de chaînes ont été synthétisés. La force d'interaction a été variée en introduisant des groupements latéraux sur des chaines polymères par ailleurs identiques.

Les courbes maîtresses complètes pour les modules dynamiques ont été obtenues pour la première fois pour le polyamide. Quand la masse moléculaire augmente, un plateau caoutchoutique distinct apparaît et le temps de relaxation le plus long est déplacé vers les fréquences plus basses. L'introduction de groupements fonctionnels provoque une augmentation de la température de transition vitreuse de 10 à 40°C respectivement, ce qui est probablement dû à leur capacité à former des interactions plus fortes avec les groupements amide. De manière surprenante, les courbes maîtresses des polymères de masse moléculaire comparable se superposent à même distance à la T_g, ce qui indique que la force d'interaction n'influence pas leur dynamique en fondu. Pour confirmer cette hypothèse, nous avons décrit la variation des modules dynamiques des polymères non-enchevêtrés avec un modèle classique de Rouse. Une étude de ces matériaux par Spectroscopie Diélectrique nous donne des éléments pour comprendre l'absence d'influence des liaisons intermoléculaires.

Mots clés: polyamide, cristallinité, interactions fortes, liaison hydrogène, dynamique, solvants, rhéologie

Table of Contents

List of symbols and abbreviations

Symbols

a	activity
a_T	horizontal shift factor for time-Temperature Superposition
A	parameter in GAB model
A_{VFT}	constant in VFT law
b	Kuhn length
b_T	vertical shift factor for tTS
c	concentration
C	parameter in GAB model
C_1, C_2	empirical constants WLF law
C_p	heat capacity
D	diffusion coefficient
d	distance
G	shear modulus
G'	storage shear modulus
G''	loss shear modulus
k	equilibrium constant (also $k_{condensation}$ and $k_{hydrolysis}$)
E_a	activation energy
I	isophthalic
J	diffusive flux of penetrant molecule
$J(t)$	compliance
k_B	Boltzmann constant
M	molecular weight
M^*	complex dielectric modulus
M'_{dielec}	real part of the complex dielectric modulus
M''_{dielec}	imaginary part of the complex dielectric modulus (loss modulus)
$M(t)$	mass of solvent at time t
M_c	critical molecular weight
M_e	molecular weight between entanglements
M_K	molecular weight of a Kuhn segment
M_{eq}	mass of solvent at sorption equilibrium
M_m	solvent content correponding to saturation of all primary sites by one solvent molecule (monolayer)
M_n	number average molecular weight
M_w	weight average molecular weight
M_{PA}	molecular weight/amide group
N_A	Avogadro's number
p	monomer conversion or probability to react in polycondensation (Flory distribution)
P	(partial) vapor pressure
P_{sat}	saturated vapor pressure, *i.e.* vapor in equilibrium with the liquid

q	scattering vector
R	ideal gas constant
S	solubility
t	time
T	terephthalic acid monomer *or* temperature
T_0	Vogel temperature
T_2	transversal decay time in NMR; with superscript *s, i, l* = short, intermediate, long
T_g	glass transition temperature
T_{ref}	reference temperature
w_x	weight fraction of polymer chains of x repeating units
$X\,(Y)$	molar fraction in liquid (gas) phase of a mixture

Greek symbols

α	polymer main relaxation process, associated to the glass transition *or* crystalline lattice in polyamide
α_I, α_I	forms of α phase in PA6,6
β	polymer secondary relaxation process *or* metastable crystalline phase in PA6
β_{dry}	β relaxation of dry polyamide
β_w	β relaxation of water/polyamide system
β_{imm}	chain immobilization factor
γ	polymer secondary relaxation process, at lower temperatures than β *or* crystalline lattice in polyamide *or* shear strain
γ_0	shear strain amplitude
$\dot{\gamma}$	shear rate
δ	phase angle
δ_i	Hildebrand solubility parameter
ΔH	enthalpy
$\Delta H_{100\%}$	enthalpy of melting for a 100% crystalline polymer
ΔH_{cryst}	enthalpy of cold crystallization
ΔH_m	enthalpy of melting
ΔS	entropy
$\varepsilon*$	complex permittivity
ε'_{dielec}	real part of complex permittivity
ε''_{dielec}	imaginary part of complex permittivity or loss permittivity
ε_∞	permittivity in the limit of infinite temperature
ζ	monomeric friction coefficient
η	viscosity
η_0	zero shear viscosity
θ	scattering angle
λ	wavelength
μ	chemical potential

ν	molar volume
ξ	tortuosity factor
ρ	density
σ	stress
$\sigma*$	complex conductivity
τ	relaxation time
τ_0	relaxation time in the high temperature limit
τ_e	entanglement relaxation time
τ_p	characteristic relaxation time of polymer segment p
τ_R	longest (Rouse) time of a polymer chain
τ_{rep}	reptation time of a polymer chain
φ	coverage of sorption sites
ϕ	solvent volume fraction
χ	Flory interaction parameter
χ_C	crystalline ratio
ω	frequency

Abbreviations

AA	Acrylic Acid
AP	Acrylaminopyridine
BDS	Broadband Dielectric Spectroscopy
BHT	Bis(hexa-methylene) triamine
CEA	Carboxyethylacrylate
CR	Chill Roll
CuK_α	X-ray generated by copper anode
DMA	Dynamic Mechanical Analysis
DSC	Differential Scanning Calorimetry
DVS	Dynamic Vapor Sorption
EPR	Electron Paramagnetic Resonance
FID	Free Induction Decay
FTIR	Fourier Transform Infrared
GAB	Guggenheim, Anderson and de Boer
GPC	Gel Permeation Chromatography
GT	Terminal Group
HFIP	Hexafluoroisopropanol
KF	Karl Fischer
linPG-OH	linear polyglycerol
linPG-OMe	linear permethylated polyglycerol
LNCS	Liquid Nitrogen Cooling System
MAF	Mobile Amorphous Fraction
MCS	Mean Cluster Size
MDSC	Modulated Differential Scanning Calorimetry
MSE	Magic Sandwich Echo
MWD	Molecular Weight Distribution
NIR	Near Infrared
NMR	Nuclear Magnetic Resonance

NTFA-PA	N-trifluoroacetylated polyamide
PA	Polyamide
PA6,6	Polyamide 6,6
PA6,10	Polyamide 6,10
PA6HIA	Polyamide 6 Hydroxy-Isophthalic acid
PA6LiSIPA	Polyamide 6 Lithium Sulfonate IsoPhthalic Acid
PA6I	Polyamide 6 Isophthalic acid
PA6T	Polyamide 6 Terephthalic acid
PBd	Poly(butadiene)
PnBA	Poly(n-butyl) acrylate
PC	Polycarbonate
PDMS	Poly(dimethylsiloxane)
PEO	Poly(ethylene oxide)
PIB	Poly(isobutylene)
PMMA	Poly(methyl methacrylate)
PMTO	Poly(tetramethylene oxide)
PS	Poly(styrene)
PVC	Poly(vinyl chloride)
PDI	Polydispersity Index
RAF	Rigid Amorphous Fraction
RCS	Rapid Cooling System
SANS	Small Angle Neutron Scattering
SAXS	Small Angle X-Ray Scattering
SEM	Scanning Electron Microscope
SPS	Sulfonated Poly(styrene)
tTS	time-Temperature Superposition
UPy	Ureido-pyrimidinone acrylate
VFT	Vogel-Fulcher-Tammann
WAXS	Wide Angle X-Ray Scattering
WLF	Williams-Landel-Ferry
XRD	X-Ray Diffraction

Introduction

This PhD thesis was carried out in the Laboratoire Polymères et Matériaux Avancés (LPMA, UMR 5268), a joint research unit between the CNRS and the company Solvay. This work was done within the framework of a fundamental understanding of the dynamics of polyamide in the solid and in the molten state.

Polyamides are a family of thermoplastic polymers widely employed in the various applications (textile, automobile, food packaging) due to their excellent thermal stability and mechanical and barrier properties. The chemical structure of polyamide consists of aliphatic or aromatic sequences separated by amide groups, which can form hydrogen bonds between them. At a larger scale, a hydrogen bonds network exists, which is thought to be intimately related to the unique properties of polyamide in terms of resistance to heat, oil or wear combined with toughness and stiffness [1].

The presence of strong interactions makes the study of polyamide interesting both from the fundamental and the industrial point of view. On one hand, it is important to understand how hydrogen bonds influence the dynamics of a polymer or how they relate to its properties. From the industrial point of view, this understanding opens a path for manipulating strong interactions (strength, density) in order to obtain specific combinations of polymer properties (*e.g.* improved barrier properties without compromising on impact strength). Due to its industrial importance, polyamide has been intensively studied in the literature. However, several aspects related to the polymer dynamics have not yet been elucidated.

To begin with, polyamide can be significantly affected by the absorption of low molecular weight penetrants [1] like water from the air humidity or ethanol in biofuels. Solvent sorption is accompanied by an large decrease in the glass transition temperature [2, 3], which strongly affects mechanical properties [1]. The rate of sorption and amount of absorbed solvent depend on the mechanisms of interaction between the solvent and polyamide, along with sorption and diffusion mechanisms. It would be therefore interesting to relate the polymer dynamics due to solvent/polyamide interaction and the sorption and diffusion mechanisms.

Moreover, there has been a growing interest on the influence of strong interactions (hydrogen bonds, ionic etc.) on polymer dynamics in the molten state. First studies have been limited to monodisperse polymers with a low density of interactions. In this context, the study of polyamide would ensure the transition towards the investigation of more complex systems, with an extremely high density of interactions.

The first chapter of this manuscript presents the state of the art on polyamide chemistry, its semi-crystalline structure and its interaction with solvents. Then, a background review on the influence of strong interactions on viscoelasticity is presented. The scientific approach of the thesis emerges from this first chapter. The materials and methods used to adress this scientific approach are further presented in Chapter 2.

Before analyzing the interaction with solvents, it is crucial to assess the influence of the semi-crystalline nature of polyamide on diffusion and sorption. The third chapter focuses therefore on the comparison of these two processes in a 100% amorphous polyamide and its analogous semi-crystalline polyamide. The semi-crystalline structure of polyamide will always be taken into account in the next chapters, which focus on the diffusion mechansims in relation to solvent type and polyamide dynamics and on the sorption modes in these strongly interacting polymers. A model for solvent diffusion at molecular level is proposed.

Lastly, the dynamics of polyamide in the molten state have been studied on specifically designed polyamides. The viscoelastic response of these materials is described as a function of increasing molecular weight and strength and density of interacting groups. The potential effect of the dynamics of interacting groups in the molten state is discussed.

Chapter 1

State of the art

Polyamides (PAs, also known as Nylons) are defined as the family of polymers that contain an amide group, $-NHCO-$, as a recurring part of the chain. Since their commercial introduction by DuPont in 1938, these thermoplastic polymers have been widely employed as engineering plastics due to their excellent thermal stability and mechanical properties [1]. Historically, polyamides are aliphatic and semi-crystalline (*e.g.* PA6, PA6,6 or PA6,10). Other chemical structures (cyclic, aromatic), as well as amorphous polyamides have been developped over the years for specific applications.

This first chapter is a review of the structural characteristics and properties of polyamides, in order to better grasp the interest in studying this specific class of polymers.

1.1 Polyamide synthesis

The nomenclature of polyamide is generally PAx, given by the number of carbon atoms between amide groups (x) or PAx,y, given by the number of carbon atoms in the diamine (x) and diacid (y) starting blocks. For example, PA6 is obtained from ε-caprolactam, a monomer with 6 carbon atoms between amide groups and PA6,10 is obtained from the reaction of monomers with 6 carbon (hexamethylenediamine) and 10 carbon (sebacic acid) atoms.

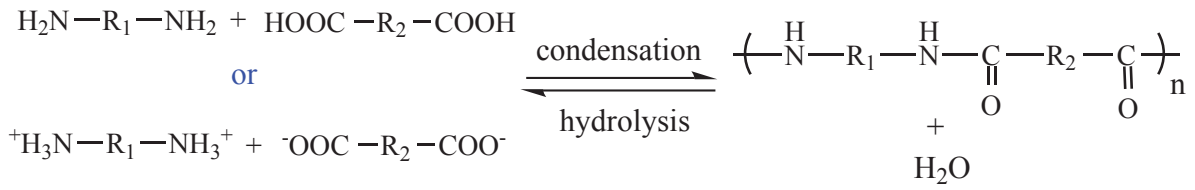

Scheme 1.1: Polycondensation equilibrium for polyamide synthesis

The most common synthetic route for PAx,y polyamides is via the polycondensation reaction of a diamine (AA) and a diacid (BB) or their corresponding salts (Scheme 1.1) [1] in the melt. An acid catalyst can also be added to the reaction medium in order to increase the monomer conversion. The reaction is a chemical equilibrium that can be shifted towards condensation or hydrolysis depending on the concentrations of the species. The equilibrium constant of polycondensation is given by equation (1.1). For PA6, Tai and Tagawa [4] determined a value of approximately 4 J $mol^{-1}K^{-1}$ for the entropy of reaction and -24 kJ/mol for the enthalpy of reaction.

$$k = \frac{k_{condensation}}{k_{hydrolysis}} = \frac{[CONH][H_2O]}{[NH_2][COOH]} = \exp\left(-\frac{H - ST}{RT}\right) \tag{1.1}$$

In parallel with this equilibrium, a trans-amidation reaction occurs, redistributing the molecular weights through chain rupture and re-combination (Scheme 1.2) [5]. Polyamide is industrially synthesized in pressure reactors. The molecular weight depends on the reaction stoichiometry and the condensation reaction can be favored by the extraction of water vapor under vacuum, which lowers the water concentration and shifts the chemical equilibrium to the right. Inversely, if the concentration of water is too high, the hydrolysis reaction is favored

and the molecular weight decreases. Therefore, a certain molecular weight of polyamide is accompanied by a certain concentration of water at equilibrium $[H_2O]_{eq}$.

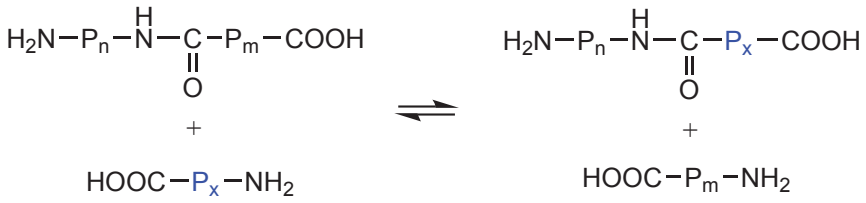

Scheme 1.2: Trans-amidation equilibrium during polyamide synthesis

The most probable molecular weight distribution can be determined based on statistical considerations. This theory was developped by Flory [6] and is based on the assumption that only linear polycondensation occurs and that functional groups have equal reactivity, independently of the size of the molecule. In a Flory distribution for linear polycondensation, the weight fraction of chains of x repeating units (w_x) is expressed as a function of the monomer conversion or probability to react p:

$$w_x = x(1-p)^2 p^{x-1} \tag{1.2}$$

The expected (theoretical) polydispersity index (PDI, ratio of the polymer weight average molecular weight M_w over the number average molecular weight M_n) is given by equation (1.3) when the reaction goes to completion:

$$PDI = \frac{M_w}{M_n} = 1 + p \simeq 2 \tag{1.3}$$

If polycondensation is not linear, Flory's distribution does not apply in its simple form (equation (1.2)). In PA, "non-linear" side reactions can occur, which include the formation of cyclic or branched chains. In particular, branching can have an important influence on rheological properties [7] and will therefore be presented in more detail below.

Branching occurs when a parallel reaction between amine chain ends takes place, which leads to the formation of bis(n-alkyl)triamine. In its turn, the amine becomes a site for branching (Scheme 1.3) [8]. The amount of branching can be estimated by analytical methods, which will be presented in Chapter 2.

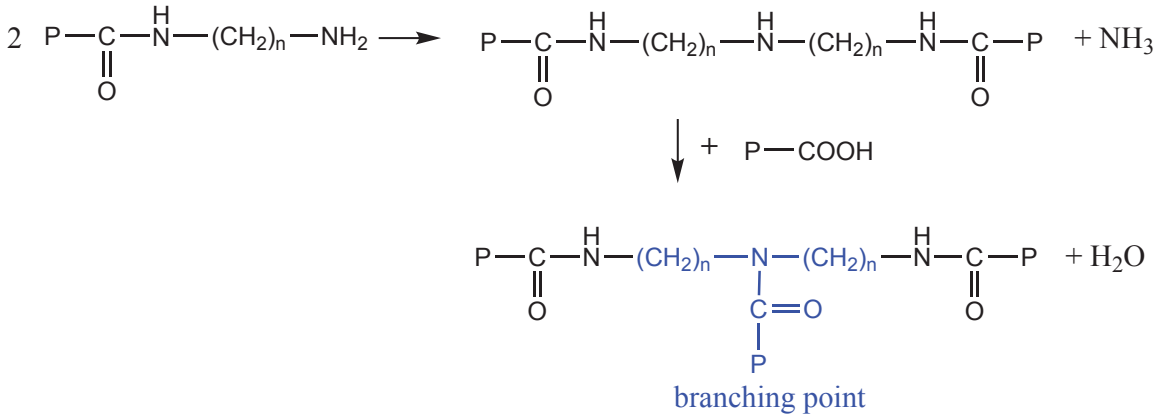

Scheme 1.3: Side reaction in polyamide synthesis leading to branching [8]

It should be stressed that, at high temperature in the melt, polyamide will continue to react as long as its molecular weight is not matched by the corresponding water concentration at equilibrium. Also, molecular weights are continuously redistributed by trans-amidation until a Flory distribution is reached (in absence of branching). Lastly, if the water concentration is too high, the hydrolysis reaction is favored and the molecular weight will decrease. Controlling the water content and ambient humidity is therefore crucial in processing, applications etc.

1.2 Structure, morphology and dynamics of polyamide

1.2.1 Crystalline phase

The chemical structure of polyamides consists of amide groups separated periodically by methylene or aromatic sequences. The amide groups can form strong hydrogen bonds (25 KJ/mol [9]) between the lone pairs of the carbonyl oxygen and the hydrogen of the NH (Figure 1.1). FTIR studies showed that nearly 100% NH groups in polyamide (crystalline and amorphous) participate in hydrogen bonds at room temperature and around 10-20% in the molten state (at T=260°C) [10, 11].

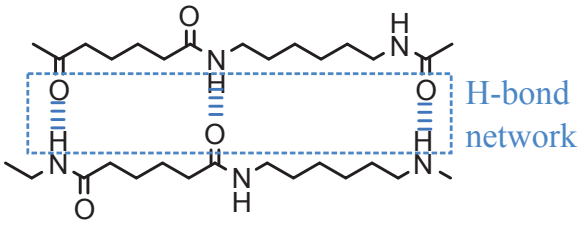

Figure 1.1: Hydrogen bond (H-bond) network in polyamides (Case of PA6)

If the chain order persists on a long range, crystalline domains appear. Two stable crystal structures (α and γ) have been identified in polyamides. In the α structure, the polymer chains unfold in a zig-zag conformation with amide and methylene groups being coplanar. Hydrogen bonds form between polymer chains, in the same plane as the methylene backbone (Figure 1.2). In even (x even) or even-even (x,y even) polyamides, two successive amide groups along a chain are rotated 180°. α crystals are triclinic (PA6,6 or PA6,10) or monoclinic (PA6). Most polyamides (even PA with more than seven carbons, even-odd, odd-even and odd-odd PA) crystallize primarily in the γ form, in which the polymer chains are slightly distorted (Figure 1.3). The amide group rotates by 30° with respect to the methylene backbone and the hydrogen bonds are formed between parallel chains. Therefore, the amide and the methylene groups are no longer in the same plane. This structure is described as pseudo-hexagonal, *i.e.* it forms a hexagonal lattice in the plane perpendicular to the chain axis [1]. For polyamides that can crystallize in both types of lattices, the different crystalline structures may be obtained by applying different cooling conditions from the melt. In some cases, cooling conditions can also lead to variations from the thermodynamically stable lattices.

For the polyamides mentioned in this thesis, the following stable crystalline structures have been recorded in the literature: α for PA6, PA6,6 and PA6,10 and γ for PA6. For all these polymers, metastable structures have also been identified, corresponding to different types of lattices.

Besides the stable α (T_{melt}=222°C) and γ (T_{melt}=214°C) phases, a metastable phase called β has been described in the literature for PA6 [13]. The β phase exhibits a hexagonal symmetry, with hydrogen bonds forming between parallel and anti-parallel chains. The density of this phase (1.14 g/cm^3) is lower than α (1.23 g/cm^3) or γ (1.18 g/cm^3), and is much closer to the

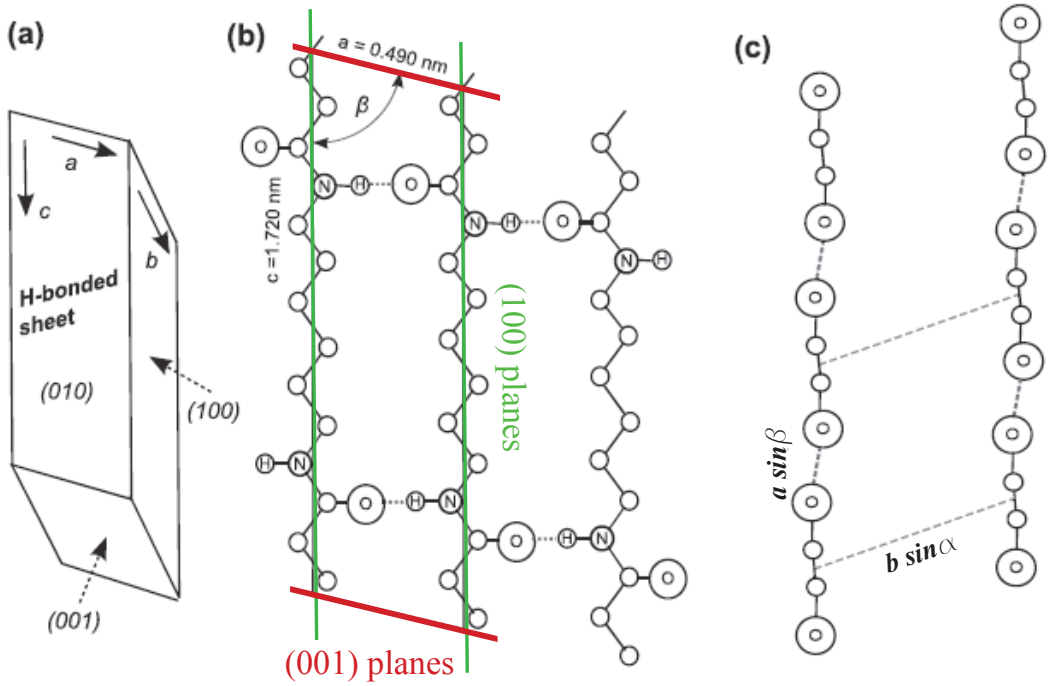

Figure 1.2: Schematic representation of an α crystalline lattice in PA6,6 (a) triclinic unit cell with base vectors (chain axis is along $\vec{c}$), (b) chain arrangement in the *a*-*c* plane where H-bonds are formed (H-bonds are depicted by dashed line segments) and (c) chain arrangement in plane perpendicular to chain axis. Adapted from [1, 12]

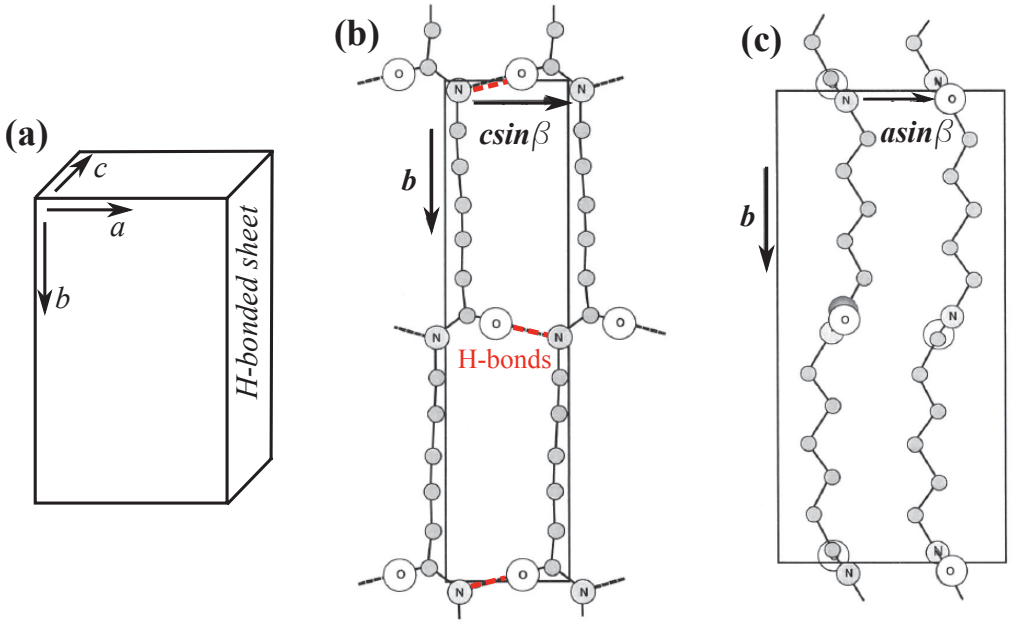

Figure 1.3: Schematic representation of a γ crystalline lattice in PA6 (a) monoclinic unit cell with base vectors (chain axis is along $\vec{b}$), (b) projection along the *a* direction showing the *b*-*c* faces and (c) projection along the *c* direction showing the *a*-*b* faces. Adapted from [1]

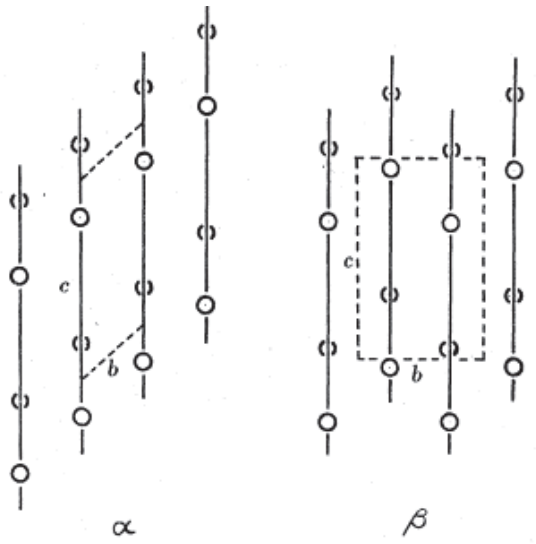

Figure 1.4: Arrangement of sheets of molecules in α and β crystals in PA6,10. Lines represent chain molecules, circles oxygen atoms. H-bonds are perpendicular to the plane of the figure. From [19]

density of the amorphous phase (1.08 g/cm^3) [13, 14]. Upon heating above 130°C, this phase transforms into α and the process can be followed in Differential Scanning Calorimetry (DSC) or X-Ray Diffraction (XRD).

In the case of PA6,6, two forms of the α phase exist. α_I is the stable phase obtained by solution crystallization. This phase is triclinic, has a high density (1.24 g/cm^3) and a high melting point (T_{melt}=265°C) [14]. α_{II} is the metastable phase obtained at low temperatures or quenching. Therefore, the crystalline lattice is less perfect and it is thought that a fraction of the H-bonds shift from the methylene zig-zag plane, leading to a pseudo-hexagonal lattice [15]. The crystalline density is lower (1.16 g/cm^3) and the melting temperature is higher (T_{melt}=262°C) [16]. The two forms of the α structure can easily be identified in XRD by their specific 2θ spacing (3.55° for α_I and 0.72° for α_{II}) [17]. In normal processing conditions, an intermediate structure α_{I-II} is obtained. During storage at ambient temperature or in a humid environment, α_{I-II} slowly evolves towards the thermodynamically stable phase α_I [18].

In PA6,10, Bunn and Garner [19] found an α triclinic phase (1.18 g/cm^3, $T_{melt} \simeq$ 220°C [14]) with a general organization similar to that of PA6,6 (Figure 1.2) and traces of a similar packing to α, which they called β. They suggest that the only difference between α and β crystals is the placement of the successive hydrogen bond lattice planes. In the α form, successive planes are always displaced in the same direction by a fixed distance 3.55Å, whereas in the β form the planes are staggered up and down. A right angle is formed in the *b*-*c* plane (Figure 1.4). There has been no study in the literature on the existence of a metastable phase α_{II} in PA6,10. However, since the α triclinic phase in PA6,10 is almost identical to the α triclinic phase in PA6,6, the analogy could apply also to the α_{II} phase obtained by quenching.

The different lattices can be identified through their DSC, Fourier Transform Infrared (FTIR) or XRD signature. Since XRD allows a straightforward identification of the crystalline phases, this technique is generally preferred. In the case of PA6 with the largest number of different crystalline lattices, XRD provides a specific signature for each of them in 2D patterns and in 2θ scans (Figure 1.5). The α phase of PA66 and PA610 give similar diffractograms as the α of PA6, the variable being the distance $\Delta 2\theta$ between the main two peaks. The signature of the main peaks in different crystalline lattices evidenced by X-ray diffraction is summarized in Table 1.1.

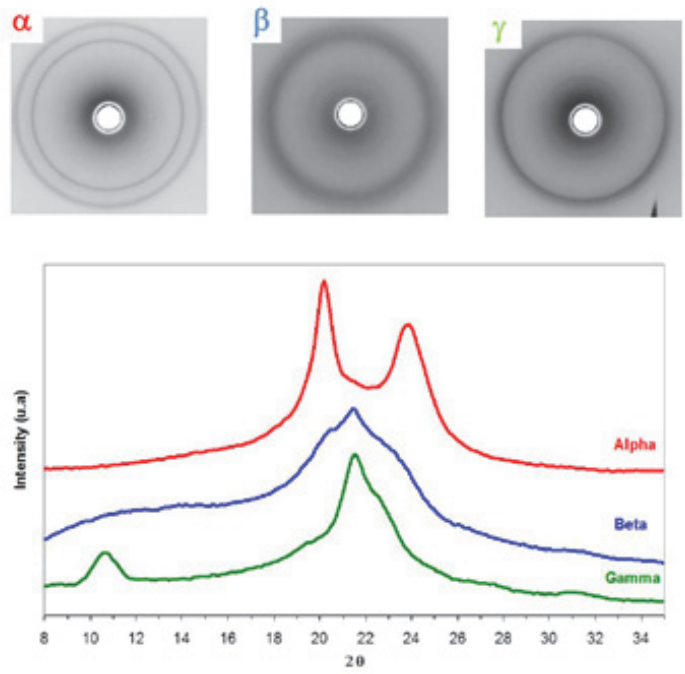

Figure 1.5: Wide Angle X-ray Scattering (WAXS) scans of PA6 films containing mainly α, β or γ phase. Adapted from [20]

Polymer	Phase	Peak	(hkl) plane	2θ (°)
PA6	α	α1	200	20
		α2	002/202	24
	β	β1	200	21.5
	γ	γ1	020	10.5
		γ2	200	21.5
PA66	α_I	α1	001	6
		α2	002	13
		α3	100	20
		α4	010/110	23
PA610	α	α1	001	5
		α2	002	10
		α3	100	20
		α4	010/110	23

Table 1.1: Parameters associated to the main crystalline phases of PA6, PA6,6 and PA6,10 as measured by X-ray diffraction (CuK_α)

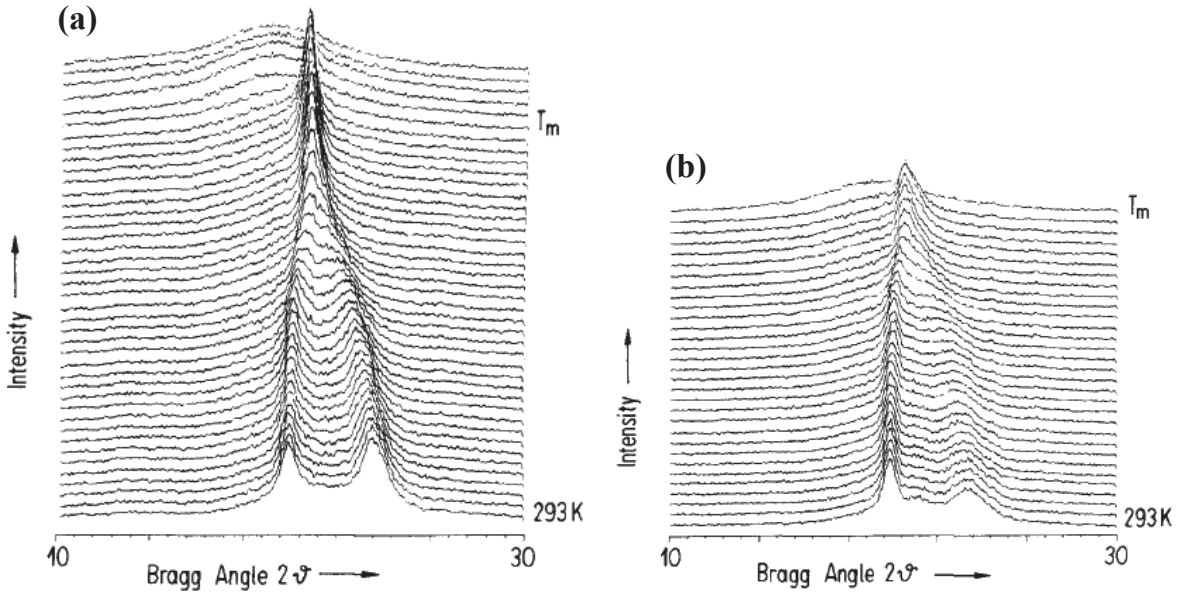

Figure 1.6: WAXS scans of (a) PA6,6 and (b) PA6,10 measured during continuous heating. $\Delta T = 7K$ between successive scans. From [23]

Last, it has been observed that as the temperature increases, the main peaks of the α phase progressively merge into one at 175-200°C. This transition was first observed by Brill [21, 22] and corresponds to a transformation into a pseudo-hexagonal phase. Figure 1.6 illustrates the Brill transition in PA6,6 and PA6,10.

In conclusion, several crystalline lattices (*i.e.* polymorphism) have been identified in polyamides. Among them, the metastable phases have the tendency to transform into the stable phases upon temperature treatment or storage in a humid environment.

In presence of solvents: The crystalline lattices are considered impermeable to solvents but they could affect sorption and diffusion properties. First, crystalline domains constitute obstacles on the diffusion paths and create an additional "tortuosity" factor that can delay diffusion. Second, the structure of the amorphous phase could depend on the type of crystalline lattice and its evolution in presence of solvents. The structure of the amorphous phase will be presented in the next section. The influence of the crystalline phase on diffusion and sorption will be presented in sections 1.3 and 1.4.

1.2.2 Amorphous phase

1.2.2.1 Heterogeneity of the amorphous phase

At scales larger than the dimensions of the crystalline lattice, single crystals of polyamides are lamellae formed by folding of the chains during crystallization. At a higher scale, lamellae organize into stacks that then form spherically shaped aggregates called spherulites (Figure 1.7). These three hierarchical structures can give a large range of lamellae sizes, long periods of lamellar stacks and spherulite sizes, with the amorphous part occupying the spaces between the lamellae, the stacks and the spherulites [1]. Based on this approach, polyamide can be commonly described by a two-phase model assuming the existence of two homogeneous phases: amorphous and crystalline. However, the mobility of a chain that participates in both amorphous and crystalline phases should not be similar to the mobility of a chain in the amorphous bulk. Moreover, as polymers crystallize in the form of folded-chain lamellae, amorphous chain

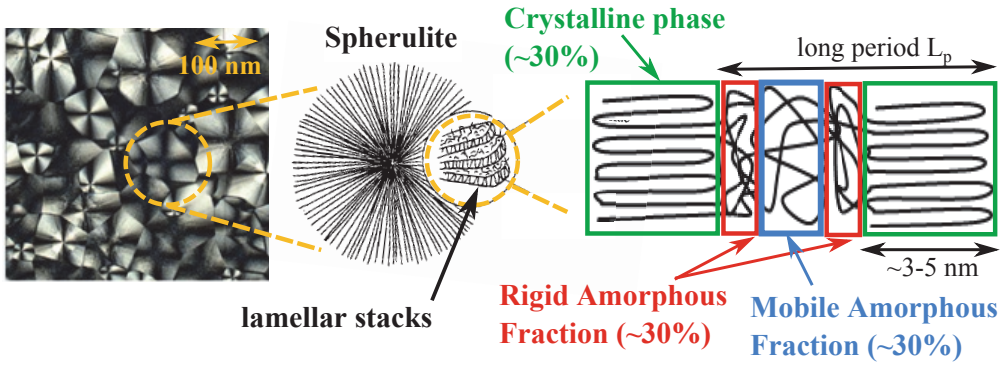

Figure 1.7: Schematic representation of crystalline lamellae, Rigid Amorphous Fraction (RAF) and Mobile Amorphous Fraction (MAF)

segments remain in the inter-lamellar spaces. Some chain segments are also in between the lamellar stacks or between spherulites and should have a mobility close to the bulk amorphous. The two-phase model does not distinguish among the amorphous segments situated close to or far away from the crystals.

These considerations led to the description of an "interphase" region, which was named Rigid Amorphous Fraction (RAF), as opposed to the Mobile Amorphous Fraction (MAF) (Figure 1.7). Since its introduction by Flory in the early sixties [24], the hypothesis of the existence of an "interphase" has received increasing support from experimental results. In most techniques (Dynamic Mechanic Analysis, Broadband Dielectric Spectroscopy, Differential Scanning Calorimetry, Modulated DSC, low-resolution Nuclear Magnetic Resonance), RAF assessment consists in quantifying the extent to which polyamide deviates from a two phase model. In standard polyamides exhibiting typical crystalline fractions of 30%, the order of magnitude of RAF is estimated to be 35% (+35% MAF)[1]. Therefore, the RAF percentage is quite important and its existence should not be neglected.

In presence of solvents: For diffusion in semi-crystalline polymers, it is generally accepted that small molecules cannot penetrate the crystalline phase and therefore that diffusion and sorption only occur in the amorphous phase. However, it is difficult to assess if solvent molecules can access the whole amorphous phase, including the less mobile RAF chains close to the crystal. This notion of accessibility of the amorphous sites is essential for sorption equilibrium, since the solvent mass intakes are reported to the number of supposedly accessible sorption sites.

Solvents have two effects on the amorphous phase: (1) they decrease the glass transition temperature or equivalently increase the large scale chain mobility (for details see next section) and (2) they can induce a swelling of the amorphous phase. Swelling can be estimated from density or SAXS measurements. The latter provides an estimation of the long period of the lamellar stacking L_p (Figure 1.7). If the crystalline structure does not change, an increase in the long period of the lamellar stacks could be related to the swelling of the amorphous phase.

To sum up, the diffusion and sorption of solvents occurs in a heterogeneous amorphous phase (RAF and MAF), whose accessibility is difficult to assess between constrained and bulk amorphous. Moreover, the mobility of the polymer chains increases significantly as solvents are absorbed, which could lead to a reorganization of the different phases and/or to swelling. In case of swelling for example, additional volume would become available for solvents and the solvent mass intake would increase. More details on the heterogeneity of the amorphous phase in relation to diffusion and sorption will be presented in the corresponding sections 1.3 and 1.4.

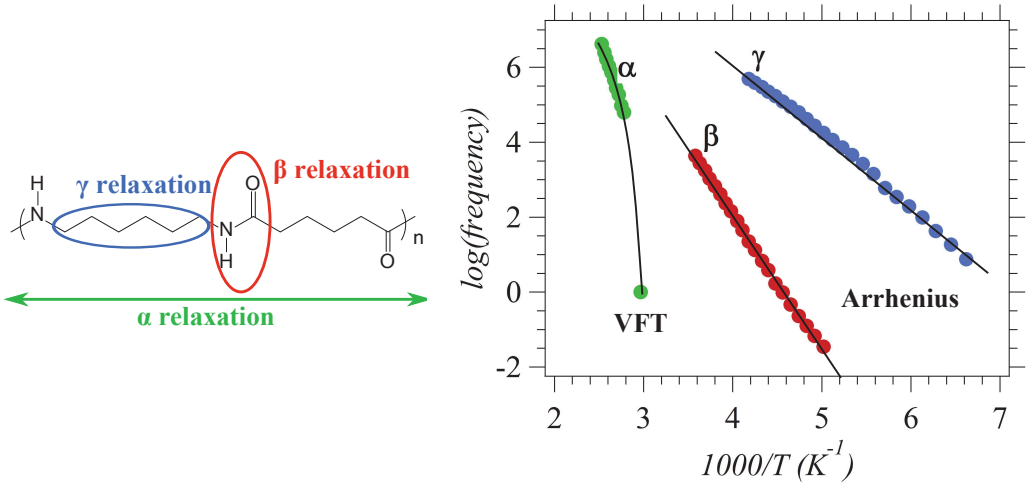

Figure 1.8: Schematic representation of PA6,6 molecular relaxations and the corresponding relaxation chart. Adapted from [27]

1.2.2.2 Dynamics of the amorphous phase

Molecular dynamics of polymers take place on a hierarchy of different lengths and timescales. Several relaxation processes have been identified in polymers: local motions due to molecular groups, segmental relaxations on a larger spatial scale and the global chain dynamics. Motional processes depend on the morphology and micromorphology of polymer systems so the investigation of molecular mobility can also be an excellent probe for microstructure [25].

Three main relaxation processes due to the onset of successive molecular motions have been identified in polyamides (Figure 1.8) [26]. At highest frequency, the γ relaxation is generally attributed to very fast rotation of the aliphatic sequences. These very local motions are internal to the monomer. The β relaxation is generally attributed to the motions of the amide group dipoles (changes in configuration and hydrogen bond association/dissociation), while the α relaxation is related to larger scale motions of the chain associated to the glass transition.

The presence of a crystalline phase has as effect on the α relaxation, but not on the more local, secondary relaxations [25]. The position and the shape of secondary relaxations show no significant difference in homologous amorphous and semi-crystalline polymers. However, the heterogeneity of the amorphous phase in semi-crystalline polymers induces a broadening in the α relaxation and a shift of relaxation times to longer timescales [25].

Polymer relaxation times or glass transition temperature can be measured either by Dynamic Mechanical Analysis (DMA) or, more precisely, by Broadband Dielectric Spectroscopy (BDS). The glass transition temperature can also be measured by Differential Scanning Calorimetry (DSC). The characteristic relaxation times are obtained from the analysis of DMA or BDS spectra. Their variation with temperature is represented in relaxation charts (log(*frequency*)=f(1/T), *e.g.* in Figure 1.8). The variation of the α relaxation times in polymers generally follows a Vogel-Fulcher-Tammann (VFT) [28, 29, 30] temperature dependence:

$$\tau(T) = \tau_0 \exp\left(\frac{A_{VFT}}{T - T_0}\right) \tag{1.4}$$

where τ is the relaxation time, τ_0 the relaxation time in the high temperature limit, A_{VFT} is a constant and T_0 denotes the Vogel temperature, generally found to be 30 – 70 K below the glass transition temperature T_g [25]. For secondary relaxations, an Arrhenius-like dependence is observed (equation (1.5)); τ_0 is the relaxation time at infinite temperature, E_a is the activation

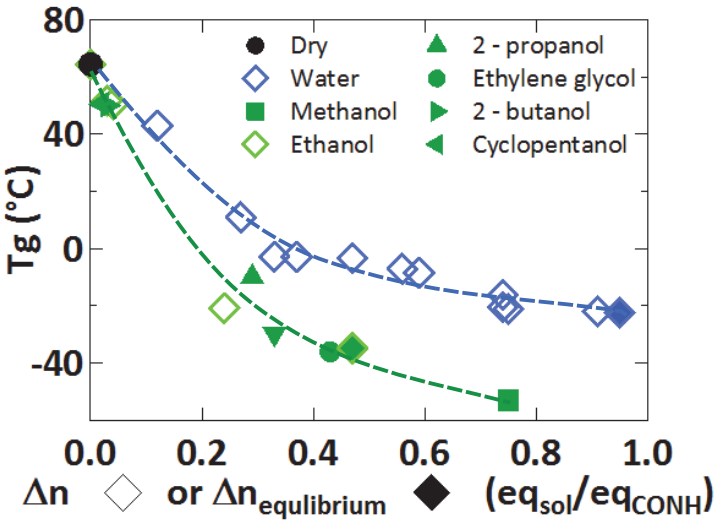

Figure 1.9: Decrease in the glass transition temperature of PA6,6 in the presence of solvents vs. the equivalent number of solvent molecules/amide groups. From [27]

energy, R is the ideal gas constant (8.314 J/g mol) and T is the temperature.

$$\tau(T) = \tau_0 \exp\left(-\frac{E_a}{RT}\right) \tag{1.5}$$

In presence of solvents, molecular relaxations are affected. In polyamides, it is generally accepted that polar solvents interact with amide groups to replace the initial hydrogen bonds between them [9, 10, 31, 32]. A large number of studies on the mobility of the amorphous phase have highlighted that the glass transition temperature of polyamide decreases significantly in presence of solvents [2, 3, 27, 33]. For instance, the sorption of ethanol in PA66 results in a decrease of 110 degrees of the glass transition temperature (Figure 1.9). Secondary relaxations are also affected [27, 34]; their characteristic relaxation times are shifted to lower temperatures.

Figure 1.9 also shows that the decrease of the glass transition temperature depends on the type of molecule. For example, water has a more limited effect than ethanol. We can question to what extent the increase of the mobility of the polymer chains upon solvent sorption could lead to a local reorganization and a change in the distribution of constrained (RAF) and bulk amorphous (MAF). Also, it would be interesting to investigate if polymer dynamics are correlated to solvent diffusion and sorption mechanisms.

1.3 Diffusion

Diffusion is the process of transfer of a fluid into a system due to random molecular motions or under the influence of a concentration gradient. It is a kinetic process that illustrates the mobility of a molecule into a phase.

The diffusion of small molecules into polymers depends on several parameters:

- the molecular size of the diffusant
- polymer morphology and physical state (glassy, rubbery)
- the compatibility between the solute and the polymer matrix
- the surface or interfacial energies of the monolayer films

1.3.1 Fick's law of diffusion

The first law of diffusion was established by Adolf Eugen Fick in 1855, by analogy to Fourier's Law of heat transport. Fick stated that "the rate of transfer of diffusing substances through a unit area of section is proportional to the concentration gradient measured normal to the section" [35].

The diffusive flux of a penetrant molecule (J) is equal to the quantity of penetrant (Q) which crosses the polymer membrane (surface A, thickness l) during one unit of time and by unit of area:

$$J = \frac{Q}{Al} \tag{1.6}$$

Fick's first law is valid in the steady state and its mathematical expression is the following:

$$\vec{J} = -D\vec{\nabla}C \tag{1.7}$$

where C is the concentration of diffusing substances and D is the diffusion coefficient (length^2/time). Fick's second law is a conservation law:

$$\frac{\partial C}{\partial t} = -\nabla\vec{J} = \frac{\partial}{\partial x}\left(D\frac{\partial C}{\partial x}\right) + \frac{\partial}{\partial y}\left(D\frac{\partial C}{\partial y}\right) + \frac{\partial}{\partial z}\left(D\frac{\partial C}{\partial z}\right) \tag{1.8}$$

Depending on the boundary conditions, different solutions are available for equation (1.8). It is important to keep in mind that the diffusion coefficient is not necessarily constant. For instance, D can depend on penetrant concentration. If the diffusion is unidirectional and the diffusion coefficient is constant, the solution to equation (1.8) gives the concentration profile at a time t, where C_0 is the solvent concentration on the polymer surface:

$$C(x) = C_0 \exp\left(-\frac{x^2}{2Dt}\right) \tag{1.9}$$

When D is a function of the concentration C only, equation (1.8) can be rewritten for unidirectional diffusion as:

$$\lambda\frac{\partial C}{\partial \lambda} = \frac{\partial}{\partial \lambda}\left(D\frac{\partial C}{\partial \lambda}\right) \tag{1.10}$$

where λ is the reduced variable $\lambda = x/t^{1/2}$. This shows that the concentration profile is a function of the reduced variable λ only, and thus the sorbed amount evolves as a function of $t^{1/2}$ even if D is not a constant. This is no longer true if the diffusion coefficient D depends on time, *e.g.* due to slow relaxation of the polymer matrix (see below).

1.3.2 Diffusion mechanisms

Based on the impact of the penetrant on the polymer matrix, different types of diffusion may occur [36]:

- *Case I or normal diffusion*: diffusion occurs in a polymer matrix which is unperturbed by the presence of solvent and the diffusion coefficient of the solvent is independent of the solvent concentration, within the duration of the sorption experiment (in this case diffusion is called Fickian). The concentration profile is described by equation (1.9) and depicted in Figure 1.10(b). A typical sorption kinetics curve is shown in Figure 1.10(a).

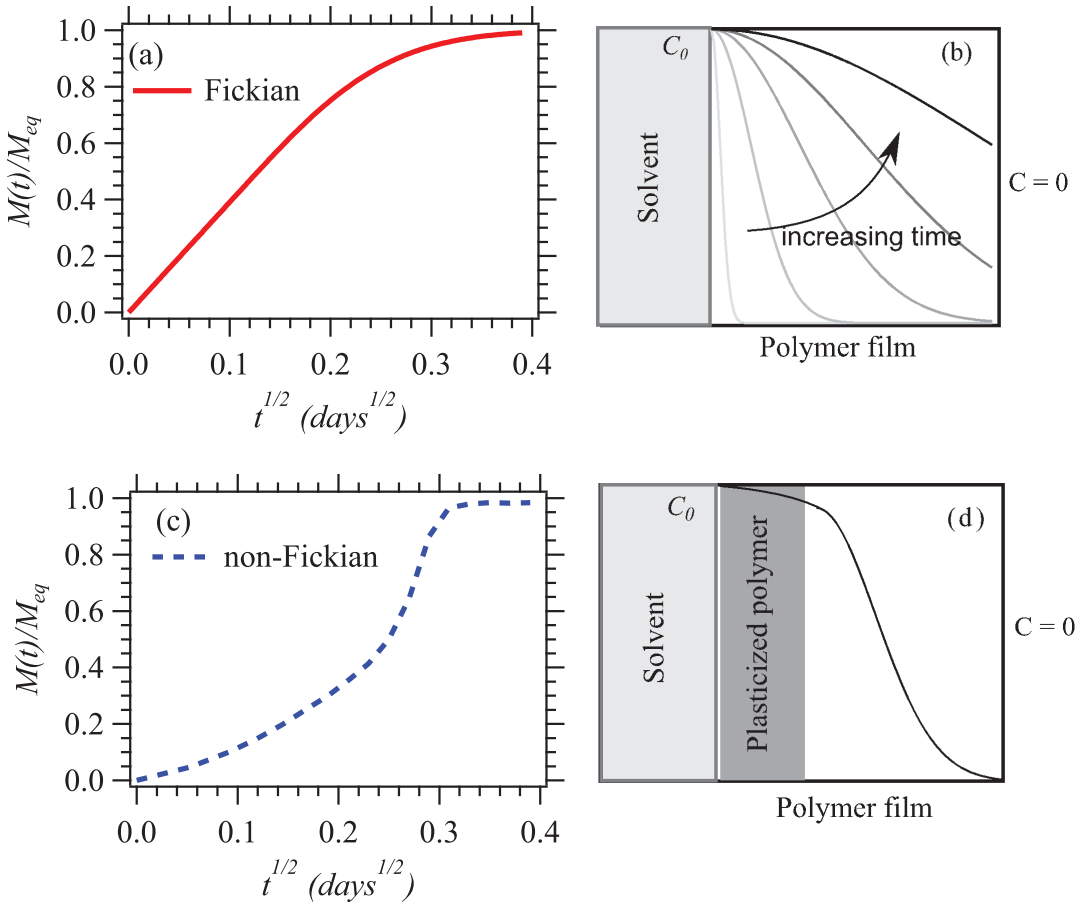

Figure 1.10: Schematic representation of sorption kinetics curves following (a) Fickian and (c) non-Fickian diffusion mechanisms and (b), (d) their corresponding solvent concentration profiles

- *Case II*: the diffusion coefficient of the solvent depends on the solvent concentration because the polymer matrix is affected (plasticized) by the solvent. The polymer relaxation rate becomes faster than the diffusion rate. Consequently, the penetrant moves into a polymer with a steep concentration front separating regions of swollen, penetrant saturated, plasticized polymer behind the front and unswollen, "dry" polymer ahead of the front.

- *"Anomalous" or non-Fickian diffusion* [37]: polymer relaxation rates and diffusion rates are similar. As in Case II diffusion, the penetrant induces swelling in the polymer matrix but the phenomenon is delayed. Therefore, a slowly advancing front of swelling is preceeded by a Fickian diffusion tail. A typical non-Fickian sorption kinetics curve is illustrated in Figure 1.10(c) with its corresponding concentration profile in Figure 1.10(d).

In order to properly interpret sorption kinetics curves, it is therefore esssential to (1) check the variation of the diffusion coefficient along the sorption process and (2) relate diffusion time scale to the characteristic relaxation time related to the various relaxation processes displayed by the polymer chains.

The sorption data acquired for the polymer-solvent system is generally represented as the normalized mass intake $M(t)/M_{eq}$, which is the ratio between the mass uptakes at time t and at

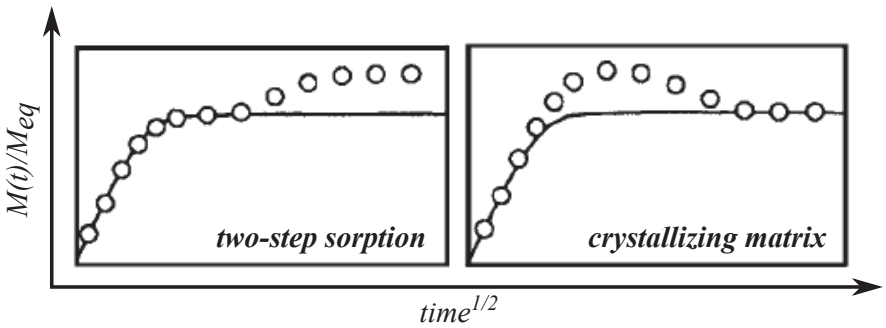

Figure 1.11: Schematic representation of diffusion curves following non-Fickian diffusion mechanisms: (a) two step sorption and (b) diffusion in a matrix that crystallizes. Adapted from [38]

equilibrium. We consider the case of one-dimensional diffusion in a polymer film so thin that all the penetrant enters through the plane faces and a negligible amount through the edges. The film of thickness l is suspended in a sorption cell where the solvent activity ($a = \frac{P}{P_{sat}}$) remains constant. In this geometry, diffusion with a constant diffusion coefficient D is described by an exact mathematical model [35]:

$$\frac{M(t)}{M_\infty} = 1 - \sum_{n=0}^{\infty} \frac{8}{(2n+1)^2\pi^2} exp\left(\frac{-D(2n+1)^2\pi^2 t}{l^2}\right) \tag{1.11}$$

At short times, equation (1.11) gives a linear increase of the normalized mass intake $M(t)/M_{eq}$ as a function of $t^{1/2}$ and the diffusion coefficient D is simply extracted from the slope of this curve (for $M(t)/M_{eq} < 0.5$, $M(t)/M_{eq} = \left(\frac{16D}{\pi l^2}\right)^{1/2} t^{1/2}$). Thus, the shape of the $M(t)/M_{eq}$ curve as a function of $t^{1/2}$ gives a first information on the diffusion mechanism (Figure 1.10). In the case of Fickian diffusion, a linear increase with the square root of time is observed for the normalized mass intake, whereas in a non-Fickian mechanism the curve is generally a sigmoid exhibiting an inflexion point. Other types of non-Fickian behaviour are for example two-step sorption (explained by delayed swelling after first equilibrium) or diffusion in a polymer matrix that crystallizes (sorption overshoot explained by expulsion of the solvent as the matrix crystallizes) [38]. Typical shapes of the curves are presented in Figure 1.11.

Several mathematical models have been suggested to analyze non-Fickian diffusion. Berens and Hopfenberg [39] proposed a heuristic model based on the linear superposition of Fickian diffusion and relaxation processes (detailed in Chapter 5). A more complete model was proposed by Hedenqvist and Gedde [40], who took into consideration the solute-concentration dependence of diffusivity, swelling, time-dependent surface boundary concentration and swelling-induced mechanical stresses. However, all these models have a large number of adjustable parameters so their physical relevance can be argued. To check the relevance of either model, it is crucial to be able to relate time scales associated to diffusion to the relaxation time of the polymer matrix.

1.3.3 Influence of crystalline phase

Diffusion in semi-crystalline polymers is altered because of the crystalline phase. The polymer processing method and conditions give a certain distribution and aspect ratio of the crystallites in the amorphous phase. In order to diffuse, molecules have to go around impermeable crystallites. In addition, the existence of a gradient of mobility in the amorphous phase (rigid and mobile) might lead to different accessibility on the diffusion path.

To illustrate both effects, Michaels *et al.* [41, 42] introduced the "tortuosity factor" ξ and the "chain immobilization factor" β_{imm}. The measured diffusion coefficient D is expressed by:

$$D = \frac{D^*}{\xi \beta_{imm}} \tag{1.12}$$

where D^* is the diffusion coefficient in the bulk amorphous polymer, β_{imm} is the chain immobilization factor that relates to the reduced mobility of the polymer chains in the proximity of the crystals and ξ is the tortuosity factor that accounts for the increased diffusion path in order to bypass crystallites [43]. One expression for the tortuosity factor proposed in the context of polymers nanocomposites with layered clay fillers of aspect ratio f is of the form $\xi \simeq 1 + \frac{f}{6} X_c$, where X_c is the volume fraction of layered objects (taken to be here crystalline lamellae or lamellar stacks) and integration has been done over all possible lamella orientations [43, 44].

The accessilibity of the amorphous phase can be evaluated by different techniques but is specific to each polymer. This aspect will be presented in the next section for the case of polyamide.

All existing models have failed in providing satisfactory descriptions of semi-crystalline systems. This is mainly due to the fact that it is difficult to obtain a strictly amorphous polymer as a reference and that many factors influence the results (degree of crystallinity, the characteristics of crystallites, morphology, processing conditions etc.) [45].

1.3.4 Case of polyamide

1.3.4.1 Diffusion mechanisms

Diffusion in polyamides might be more complex than in non-polar polymers because of the existence of specific interactions. Several literature studies have been focused on sorption or diffusion experiments of solvents in dry polyamide at a certain activity. The diffusion mechanisms are either Fickian [2, 3, 46, 47] or non-Fickian [27, 48], depending on the solvent type, polymer characteristics and processing conditions.

Starting simple, Kwan *et al.* [46] studied the diffusion of n-alkanes. N-alkanes are non polar and have no affinity with the polyamide matrix; the observed diffusion mechanism is Fickian. The authors showed that the diffusion coefficients decrease when the size of the molecule increases (linear variation on a log-log scale, Figure 1.12). In a next step, the authors investigated the diffusion of an equivalent series of esters. The esters are more polar and have a higher compatibility with the polyamide matrix but no strong interaction with amide groups. The diffusion mechanisms were still Fickian. However, the variation of diffusion coefficients with size was different (non-linear on a log-log scale, Figure 1.12). Therefore, these strongly interacting systems do not have a simple behavior.

To the next level, it is interesting to understand how diffusion occurs if penetrating molecules have the ability to form hydrogen bonds with the matrix. This is the case for water and alcohols for example.

In one of the most complete studies on water diffusion in polyamide, Lim *et al.* [2] observed a Fickian behavior and determined that diffusion coefficients increase as a function of water activity and temperature in PA6,6. Recently, Broudin *et al.* [49] made the same observations by investigating diffusion coefficients as a function of water activity in PA6,6 between 25 and 80°C. In other studies, Camacho *et al.* [48] or Rios de Anda *et al.* [27] observed non-Fickian diffusion for water in PA6,6. Polymer processing was not the same in the different studies, which might have an effect on the type of diffusion mechanism.

More interesting, strongly non-Fickian behavior was observed for the diffusion of ethanol in PA6 [50] and methanol and ethanol in PA6,6 [27] (Figure 1.13). This behavior was explained

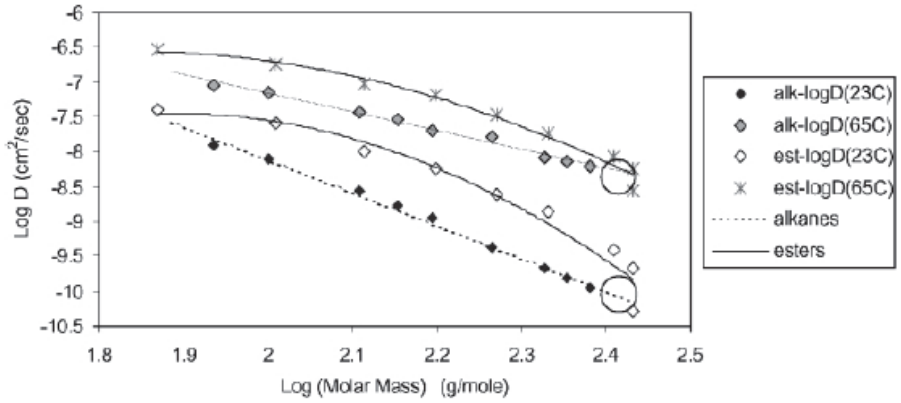

Figure 1.12: Variation of diffusion coefficients as a function of molar mass for n-alkanes and the homologous series of esters at 23 and 65°C. From [47]

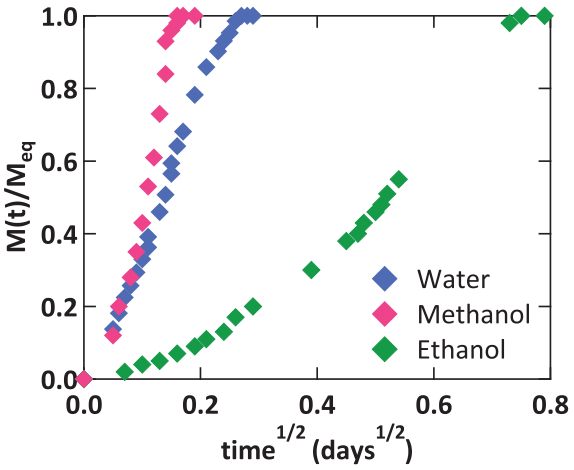

Figure 1.13: Diffusion profiles for methanol, water and ethanol in PA6,6. From [27]

by a higher affinity of alcohols with polyamide, which might lead to a higher swelling of the matrix. It should be noted that all H-bonding solvents plasticize the polyamide matrix, leading to a shift in the glass transition temperature down by -120°C [27]. Therefore, molecules diffuse through a matrix with varying chain mobility in time.

In conclusion, it would be interesting to understand how diffusion occurs when penetrating molecules can form hydrogen bonds with polyamide. Diffusion mechanisms can be non-Fickian in presence of water and strongly non-Fickian in presence of alcohols. All of these species plasticize polyamide. To the best of our knowledge, there has been no investigation on the direct influence of polymer relaxations (glass transition, secondary relaxations) on diffusion processes in polyamide.

1.3.4.2 Influence of crystalline phase

The accessibility of the amorphous phase was intially evaluated by Murthy *et al.* [51, 52, 53] by Small Angle Neutron Scattering (SANS) and solid state Nuclear Magnetic Resonance (NMR). The authors studied water sorption in PA6 and showed that water diffused exclusively in the amorphous region. Two distinct water populations exist: one in the interlamellar regions (1/3) and one in the amorphous phase outside the lamellar stacks (2/3). Water molecules in the

constricted amorphous of the interlamellar regions are thought to be strongly immobilized because of hydrogen bonds.

In the past years, low-resolution ^{1}H NMR studies have been widely employed for probing the phase distribution in semi-crystalline polyamides [33, 54, 55, 56, 57, 58, 59]. Low-resolution ^{1}H NMR distinguishes between the relaxation times of a rigid (crystalline?), a semi-rigid (RAF?) and a soft phase (MAF?). It was suggested that water fully plasticizes only a small amount of the amorphous phase ($\sim$ 10%), typically located between the crystalline domains. It is unclear however if water can penetrate the semi-rigid phase, since this fraction has its relaxation only slightly affected by the presence of water. The authors conclude that either water does not penetrate the semi-rigid phase, or it is highly immobilized by hydrogen bonds. The last explanation seems more plausible, since it has already been observed by Hutchison and Murthy [52]. It should be noted that this series of studies showed an important effect of the processing method, processing conditions and crystalline ratio on the RAF and MAF distribution. The diffusion coefficient might depend on the morphology of the amorphous phase. For instance, it was highlighted that the diffusion coefficient of water in the skin of a fast-crystallizing PA4,6 plate was higher than in the core of the plate, which had more time to crystallize in a stable form [54].

A recent NMR study done by Reuvers *et al.* [59] focused on the coupling between diffusion and plasticization. It was evidenced that a plasticization lag exists in polyamide, *i.e.* a few percentages of water are already absorbed by the material before the mobility of the amorphous phase increases.

To the best of our knowledge, there has been no systematic study on how the diffusion coefficient varies between a 100% amorphous polyamide and the amorphous phase in a semi-crystalline polyamide. Also, although the plasticization of polyamide has been investigated by NMR, there has been no attempt to investigate how polymer relaxation could influence diffusion. Since polymer relaxation during diffusion can give a non-Fickian mechanism, this is an important aspect to analyse.

1.4 Sorption

Sorption is defined as the process in which one substance takes up or holds another one. It includes absorption, adsorption as well as trapping in the microvoids or the clustering of aggregates. In polymer/solvent systems, the amount of absorbed solvent depends mainly on the affinity between the penetrant and the polymer matrix. Generally, the amount of sorbed molecules is represented in sorption isotherms as a function of activity. Several mathematical models have been developed in order to characterize sorption isotherms. In this section, we will present the thermodynamics of sorption, the sorption models and how sorption is influenced by the existence of a crystalline phase in semi-crystalline polymers.

1.4.1 Sorption mechanisms

When a polymer is put into contact with a solvent under partial vapor pressure P, the solvent molecules penetrate into the polymer matrix up to a certain equilibrium concentration. The sorption equilibrium in presence of a vapor pressure P is defined by the equation:

$$\mu_{ads}(c, T) = \mu_{gas}(P, T) \tag{1.13}$$

where $\mu_{ads}(c, T)$ is the chemical potential of adsorbed molecules, which depends on the concentration c in the material and on T and $\mu_{gas}(P, T)$ is the chemical potential of the gas. If the

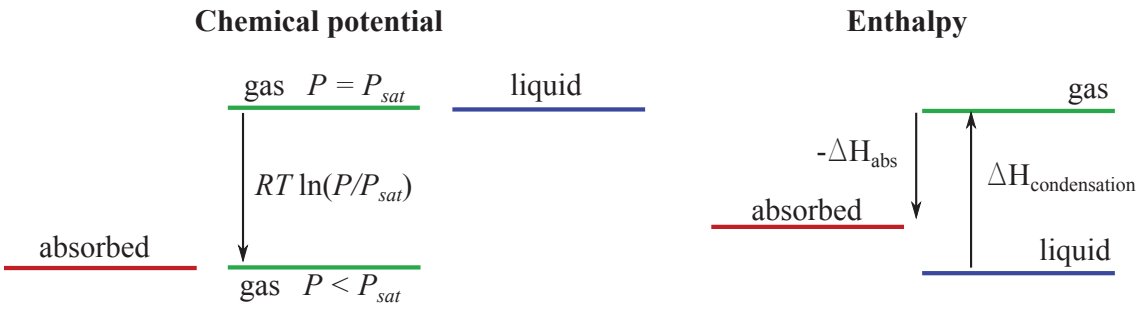

Figure 1.14: Schematic representation of sorption thermodynamics

zero level of chemical potential is taken as the chemical potential of the saturating vapor (gas at $P = P_{sat}$), $\mu_{gas}(P,T)$ is given by:

$$\mu_{gas}(P,T) = RT \ln\left(\frac{P}{P_{sat}}\right) = RT \ln a \tag{1.14}$$

which is negative if $P < P_{sat}$. $a = \frac{P}{P_{sat}}$ is the activity in the vapor phase. The sorption thermodynamics is schematically illustrated in Figure 1.14. Equation (1.13) gives the equation of sorption isotherms, which relates the concentration c in the material to the pressure or activity of the vapor, at temperature T. The chemical potential $\mu_{ads}(c,T)$ contains an enthalpic contribution (enthalpy of adsorption ΔH) and an entropic term ΔS which depends on concentration c: $\mu_{ads}(c,T) = \Delta H - T\Delta S$. Note that ΔH may depend on temperature.

By measuring sorption isotherms at various temperatures T and taking points at constant concentration c, the following curve is obtained [60]:

$$\ln a_c(T) = \frac{\Delta H_{st}}{RT} + constant \tag{1.15}$$

Then ΔH_{st} (at a given concentration c) can be obtained from the slope of the curve $\ln a_c$ as a function of $1/T$. This quantity is called the net isosteric heat of sorption and is equal to $\Delta H_{st} = \Delta H_{abs} - \Delta H_{condensation}$. The sorption enthalpy $\Delta H_{abs} = H_{gas} - H_{ads}$ contains the contribution of molecular interactions of water molecules in an adsorbed state compared to water molecules in a gaseous state. In order to compare the interactions of water molecules sorbed in the polymer to those in liquid water, the heat of liquefaction $\Delta H_{condensation}$ must be substracted [60] (Figure 1.14).

Note that equation (1.15) is analogous to the Clayperon equation for liquefaction [61], obtained by substituting $a = P/P_{sat}$, derivating with respect to T and using the ideal gas constitutive equation $PV = RT$:

$$\frac{\partial P}{\partial T} = \frac{P\Delta H}{T^2} \tag{1.16}$$

Several models have been developed in order to relate the equilibrium penetrant concentration to the penetrant activity, *i.e.* to describe the shape of sorption isotherms. The most simple one is *Henry*'s law. This model applies to the sorption of ideal gases at low activities and states that at a constant temperature, the amount of gas that dissolves in a polymer (C_D) is directly proportional to the activity of that gas in equilibrium with the polymer:

$$C_D = aK_D \tag{1.17}$$

K_D is called Henry's constant and depends on the solute, the polymer and the temperature. This model applies to solutes that are sorbed at very low activity or that have a low solubility

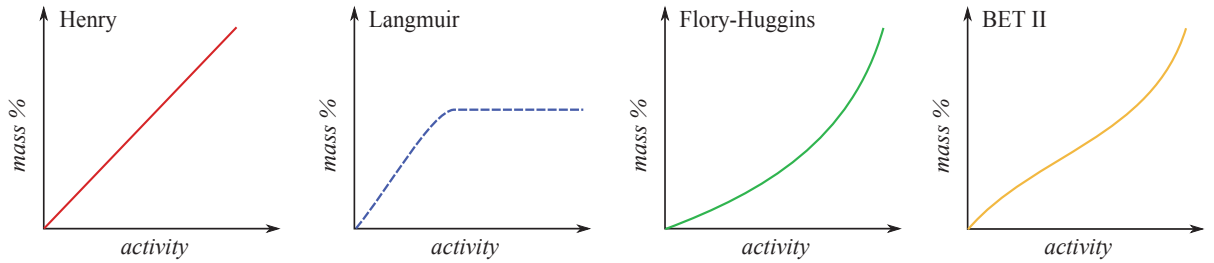

Figure 1.15: Schematic representation of typical sorption isotherms following Henry, Langmuir, Flory-Huggins and BET II modes

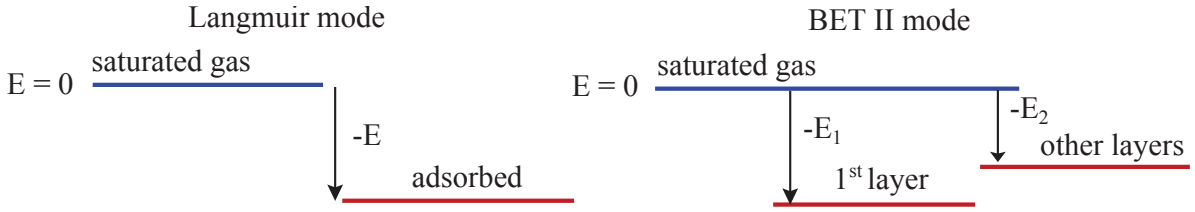

Figure 1.16: Adsorption enthalpies in the Langmuir (monolayer) and BET (multilayer) sorption modes. The reference level for energies is the saturated gas. E_2 is analogous to the heat of liquefaction and is positive and $\Delta E>0$ is both models.

in the polymer matrix. In this case, K_D is equivalent to the solubility coefficient (S). A typical isotherm is illustrated in Figure 1.15. Henry's law is valid for any sorption mode at low solute activity.

The *Langmuir* [62] sorption mode assumes the existence of a fixed number of preferential sorption sites. It applies for instance to polymers containing specific functional groups, micro-voids or high-area inorganic fillers. In this type of sorption isotherm the solvent concentration increases rapidly at the beginning but slows down at higher activities, when the sorption sites become saturated (Figure 1.15).

For N sorption sites, $n<N$ molecules are absorbed as a monolayer. The free energy per absorption site is given by equation (1.18), where the quantity $\varphi = n/N$ is defined as the coverage.

$$f = \varphi \ln(\varphi) + (1-\varphi)\ln(1-\varphi) - E\varphi \tag{1.18}$$

For a solvent chemical potential μ (or activity a), the sorption at equilibrium is given by the condition:

$$\frac{\partial f}{\partial \varphi} = \mu(T,P) - \mu(T,P_{sat}) \tag{1.19}$$

that is

$$\ln a = \ln \varphi - \ln(1-\varphi) - E \tag{1.20}$$

or

$$\varphi = \frac{a e^{E/RT}}{1 + a e^{E/RT}} \tag{1.21}$$

For small activities, equation (1.21) is reduced to Henry's law with $K_D = e^{E/RT}$.

The sorption is enthalpy driven, *i.e.* the system gains the energy E (see Figure 1.16). The energy E may be positive or negative. For $E > 0$, sorption is exothermic. In this case, adsorption of a molecule results in a *gain* in energy because of attractive non polar - van der Waals or

polar interactions developed with the surface, which are stronger than interactions within the liquid. The driving force for adsorption is enthalpic, entropy acts against adsorption. It is thus expected that sorption will *decrease* as temperature increases.

For $E < 0$ (endothermic sorption), molecules have to overcome an energy barrier to adsorb. The driving force for adsorption is entropy. Sorption will thus *increase* as temperature increases.

The *Flory-Huggins* [6] sorption mode is used to describe non polar polymer-solvent mixtures. This model takes into account the swelling of the polymer matrix. A typical isotherm is presented in Figure 1.15. Flory introduced an interaction parameter χ, which accounts for the affinity between the penetrant and the polymer matrix. χ is a dimensionless measurement of the differences in interaction energies between species i and j in a mixture. The value of the interaction parameter χ can be estimated with the following equation [63]:

$$\chi = \frac{(\delta_i - \delta_j)^2}{RT} \sqrt{v_i v_j} \tag{1.22}$$

where δ is the Hildebrand solubility parameter, R is the gas constant, T is the temperature and v is the molar volume of each specie.

By deriving the expression of the free energy of mixing between a long polymer chain and a solvent, the following expression is obtained for the variation of the solvent volume fraction ϕ as a function of solvent activity a [6] :

$$\ln a = \ln \phi + (1 - \phi) + \chi(1 - \phi)^2 \tag{1.23}$$

In order to describe systems with strong interactions between the penetrant and the polymer, other models were developed, which combine the previous ones or have a different approach for calculations. Among them, the *Brunauer, Emmett and Teller* (BET II, Figure 1.15) [64] model assumes the existence of preferential sorption sites like in the Langmuir mode. However, the BET model allows sorption in several layers and differentiates between the water molecules from the first sorbed layer (energy E_1) and the ones from the additional layers (energy E_2, see Figure 1.16). The sorption isotherms are described by the *Guggenheim, Anderson and De Boer* (GAB) [65, 66, 67] equation:

$$M(a) = \frac{M_m A C a}{(1 - Aa)(1 - Aa + ACa)} \tag{1.24}$$

where $M(a)$ is the solvent uptake at activity a, M_m is the solvent content corresponding to saturation of all primary absorption sites by one solvent molecule (monolayer), C is the Guggenheim constant and represents the difference in the adsorption energy for the first layer and the other successive layers and A is a factor correcting the properties of the multilayer molecules with respect to the bulk liquid.

Solvent molecules in multilayers on a sorption site can be seen as a cluster. The GAB parameters can also be used to estimate the size of the solvent clusters (Mean Cluster Size, *MCS*) with the following equation (1.25) [68]:

$$MCS = -(1 - \phi)\left[\frac{\phi}{M_m C}(-2 + 2Aa - 2ACa + C) - 1\right] \tag{1.25}$$

where ϕ is the solvent volume fraction in the polymer.

1.4.2 Influence of crystalline phase

Solvents are supposed to be exclusively absorbed in the amorphous phase [41, 42]. However, as discussed before, the presence of a crystalline phase induces a gradient of mobility in the

amophous phase. The polymer chains connected to the crystals (RAF) are more supposedly closely packed that the polymer chains in the amorphous bulk (MAF). Therefore, one can question if all the amorphous phase is accessible to the solvent.

Several studies on poly(ethylene terephthalate), PA6,10 or polyethylene [42, 69] showed that the solubility S of water or gas molecules in a semi-crystalline polymer could be represented by a simple linear variation with respect to the solubility in the amorphous phase $S_{amorphous}$ and the volume fraction of the amorphous phase $\Phi_{amorphhous}$:

$$S = \Phi_{amorphous} S_{amorphous} \tag{1.26}$$

Therefore, the whole amorphous fraction seems to behave as a homogeneous phase for sorption. Note that all polymers crystallized in the same crystalline lattice so the influence of polymorphism is not taken into account. It should also be highlighted that these results are based on small gas or water molecules; it might not be the case for larger molecules. This aspect will be discussed in the next section dedicated to polyamide.

Deviations from equation (1.26) have been observed in samples that crystallize during sorption or that have a less stable crystalline phase with lower density [70]. As a consequence, the evolution of the amorphous and crystalline phase during sorption should be taken into account in all sorption analysis.

Last, there is a lack of litterature data on a pure amorphous polymer and its semi-crystalline equivalent. This can be explained by the fact that it is difficult to have the same chemical structure without it crystallizing. Semi-crystalline polymers can be quenched at low temperature or copolymerized in order to obtain the amorphous equivalents. However, these polymers do crystallize in time or in presence of solvents. *A study between a semi-crystalline and its equivalent 100% amorphous would allow to shed some light on the accessibility of the amorphous phase.*

1.4.3 Case of polyamide

1.4.3.1 Sorption isotherms

Sorption isotherms of water in polyamides are well illustrated in the literature [1, 2, 31, 50, 60, 71], with data for different temperatures and solvents (water, alcohols) activities. For instance, Figure 1.17 presents the isotherms of water in nylon 6,6, as studied by Lim *et al.* [2].

Figure 1.17 shows that water is less absorbed by PA6,6 at higher temperatures. The GAB model fits well the experimental data and allows to calculate the mean cluster size. Water is absorbed in preferential sites (amide groups) and the cluster size varies depending on the type of polyamide and the function used to estimate it. Table 1.2 shows examples of Mean Cluster Sizes (MCS), as calculated by different authors.

Author	Polyamide	T(°C)	MCS
Starkweather *et al.* [31]	PA6,6	25	3
Lim *et al.* [2]	PA6,6	25	2
Sabard *et al.* [50]	PA6	40	2.3

Table 1.2: Mean Cluster Size for PA/water systems, as calculated by different authors

At room temperature, water seems to form clusters of 2-3 molecules in PA6,6 and approximately 2 molecules in PA6. Skirrow and Young [60] highlighted clustering in PA6/water and PA6/methanol systems but did not find conclusive data on the clustering of ethanol and 1- and 2-propanol. Sabard *et al.* [50] calculated the mean cluster size at different ethanol activities in

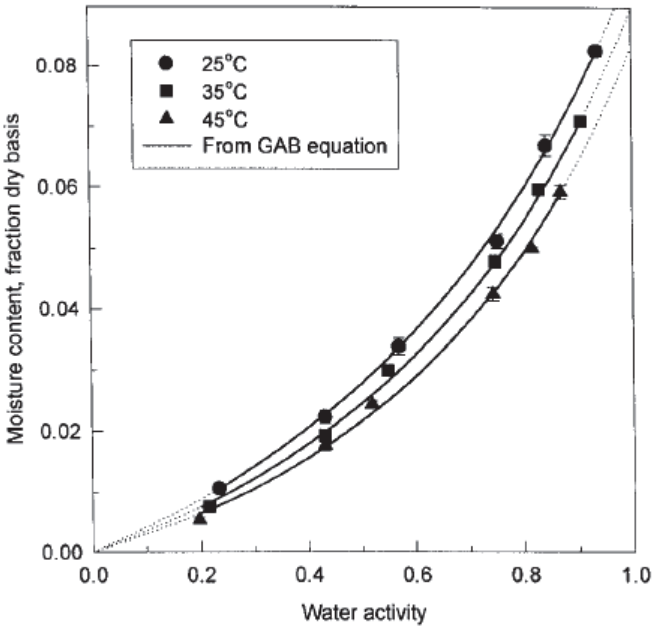

Figure 1.17: Sorption isotherms of water in PA6,6 at different temperatures. The solid lines are derived from the GAB equation. From [2]

pristine and filled PA6 samples. The GAB model provided a MCS value of 1.5 for an ethanol activity of 0.9.

The net isosteric heat of sorption $\Delta H_{st} = \Delta H_{abs} - \Delta H_{condensation}$ was calculated by Skirrow and Young [60] for PA6 with several solvents and Lim *et al.* [2] for PA6,6 with water. The authors found enthalpies of sorption slightly positive for water and methanol. For alcohols, the heat of sorption is of the order of 4 kJ/mol for ethanol and 10 kJ/mol for propan-1-ol and propan-2-ol. This difference is given by the heat of absorption which is more negative for water than alcohols, whereas the heat of condensation has small variations for the different solvents [60]. Lastly, the net isosteric heat of sorption increases with water concentration, which was associated to clustering by the authors [60].

In conclusion, the sorption of water, methanol and ethanol seems to follow a GAB model and allow small clustering at high solvent activity. The amide groups act as preferential sites, due to their polarity and their ability to form hydrogen bonds with these solvents.

1.4.3.2 Accessibility of amorphous phase

As presented before in section 1.3, the accessibility of the amorphous phase was studied with Small Angle Neutron Scattering (SANS) and solid Nuclear Magnetic Resonance (NMR), always in presence of water as a solvent. It was found that water might penetrate in all the amorphous phase but plasticizes only a small amount of it ($\sim$ 10%), typically located between the crystalline domains. It should be noted that this series of studies showed an important effect of the processing method, processing conditions and crystalline ratio on the RAF and MAF distribution.

If studies of water sorption in polyamide are abundent, much less literature data can be found on the sorption of other solvents. Water molecules are small and might therefore easily access both rigid and mobile amorphous phases. However, larger molecules might have a limited accessibility. Rios de Anda *et al.* [27] studied the sorption of a series of alcohols with increasing size. It was shown that solvent intake at equilibrium decreased when the size of the

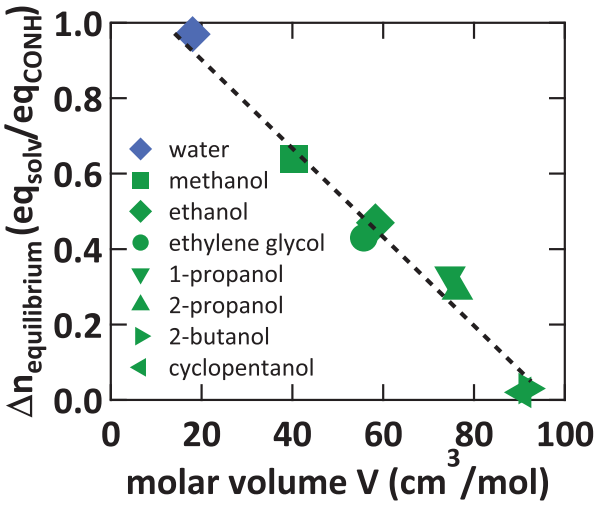

Figure 1.18: Solvent molar intake at equilibrium as a function of solvent molar volume. From [27]. Lines are guides for the eye.

solvent increased (Figure 1.18). However, since the polarity of the molecule varied at the same time, it is difficult to draw conclusions. The lower solvent intake results from the combination of the higher molar volume and lower compatibility with the matrix (lower polarity).

Therefore, it would be interesting to analyse the influence of the solvent type and size without having to take into consideration the accessibility of the amorphous phase. This study could be done in a 100% amorphous polyamide.

1.4.3.3 Structural changes in presence of solvents

Solvents cannot penetrate the crystalline phase in polyamides. However, XRD scans show changes after solvent sorption. This phenomenon has been observed in PA6 [51], PA6,6 or PA6,6/6T [12] (Figure 1.19).

Two observations can be made based on Figure 1.19:

1. An unannealed/as-processed sample evolves in presence of solvents: it is the case of all three PA. Characteristic crystalline peaks appear or are better resolved after sorption.

2. An annealed, stable crystalline phase does not evolve in presence of solvents. The XRD scans in Figure 1.19(a) are identical in the dry and water saturated PA6.

An atomistic simulation study proposed an explanation for the changes in the crystalline phase [18]. Small amounts of water are absorbed on the crystal surface and interact with amide groups. This facilitates the rotation of the polymer chains from the crystal surfaces, leading to a more stable crystalline lattice.

The underlying question is whether or not sorption equilibrium is affected by the structural changes. It is unclear at what point structural chages occur (during diffusion, after equilibrium?). Moreover, none of the above studies did sorption/desorption cycles to evaluate sorption at equilibrium before and after the structural changes.

Another study was performed on the specific case of fast-crystallizing PA4,6 [54]. It was observed that PA4,6 absorbed a higher molar amount of water than PA6 or PA6,6 because the fast crystallization rate imposed an out-of-equilibrium crystalline phase. After annealing, PA4,6 had a similar water molar sorption as the other two polyamides. Sabard *et al.* [50] studied a PA6

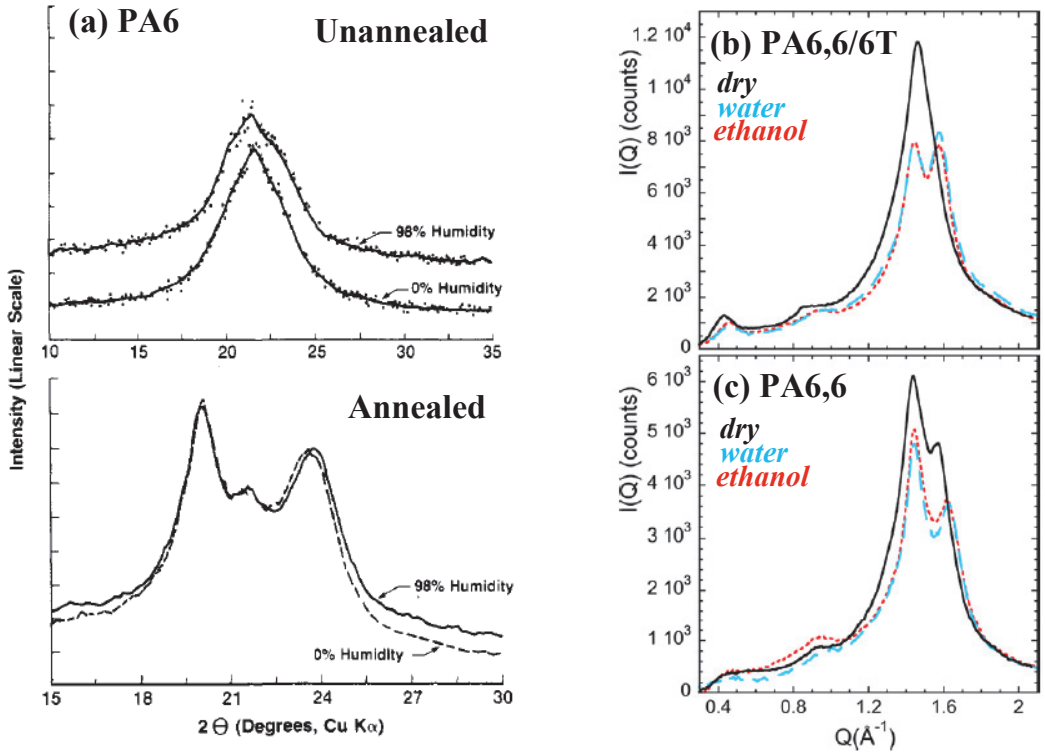

Figure 1.19: XRD scans for (a) PA6 unannealed and annealed in presence of water. From [51] (b) PA6,6/6T and (c) PA6,6 in presence of water and ethanol. From [12]

crystallized under different Chill Roll (CR) temperatures (50 and 125°C): PA6-CR50 and PACR-125. PA6-CR50 absorbed a similar amount of water but much more ethanol than PA6-CR125 (Figure 1.20(a)). It was evidenced in a Solvay internal study that the PA6-CR50 crystalline phase transformed upon solvent sorption, whereas the PA6-CR125 crystalline phase did not change (Figure 1.20(b) and (c)). These two studies show that the presence of a metastable phase can have an important effect on sorption at equilibrium.

Last, it has also been observed that amorphous polyamide crystallized in presence of solvent: PA6I [72], PA6,6/6I [12] or poly(metaxylene adipamide) (MXD6) [73]. Depending on crystallization kinetics, this can happen either during solvent sorption (MXD6) or after the sorption equilibrium has been reached (PA6,6/6I). For pure PA6I, the authors did not specify when crystallization occurred [72].

In conclusion, special care must be taken in analyzing solvent sorption in polyamide. Sorption is affected by the presence of highly metastable phases, which systematically evolve towards a stable crystalline phase. It is unclear when this evolution occurs and if the "transformed" material has the same sorption properties as the initial material.

1.5 Viscoelasticity of polymer melts

Rheology can be defined as the science of deformation and flow of materials (E.C. Bingham and M. Reiner, April 29, 1929 [74]). One of its goals is the development of quantitative relationships between deformation and force and the development of the understanding of how the flow behavior depends on the structure and composition of the material. This section begins with a small introduction to viscoelasticity and the rheology of polymer melts in the linear viscoelastic region. Then, the effect of strong interactions of the viscoelasticity of polymer melts is discussed.

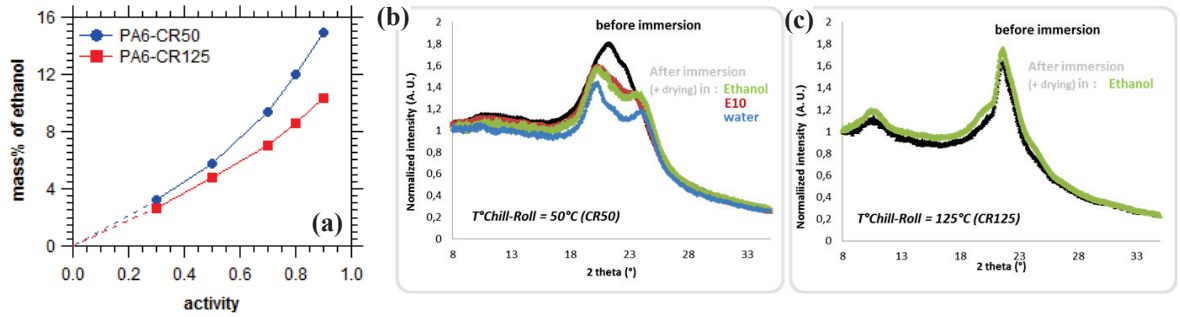

Figure 1.20: (a) Sorption isotherms of ethanol in two PA6 with different crystalline lattices (Adapted from [50]) and XRD scans (Solvay internal study) of (b) PA6-CR50 and (c) PA6-CR125 before and after sorption of solvents

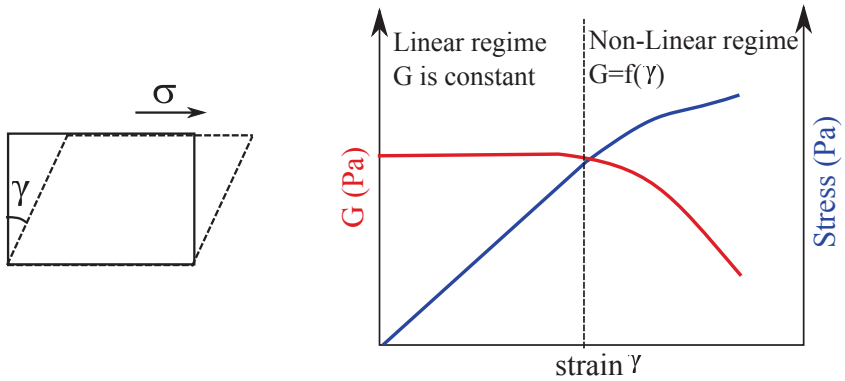

Figure 1.21: Schematic representation of the response of a Hookean solid upon the application of a shear strain

Lastly, a review of literature studies on polyamide rheology is presented.

1.5.1 Solids, liquids and viscoelastic materials

The most common rheological experiment is to subject a thin sample to small amplitude sinusoidal shear oscillations $\gamma = \gamma_0 sin(\omega t)$ (where γ_0 is strain amplitude, ω is the angular frequency and t the time) and measure its stress response.

Under the application of an oscillatory strain γ, an ideal elastic solid will respond following Hooke's law in the linear regime (*i.e.* the limit of small deformations, where the response is always proportional to the stimulus, see Figure 1.21) [75]:

$$\sigma = G\gamma = G\gamma_0 \sin(\omega t) \tag{1.27}$$

where γ is the shear strain and G is the shear modulus, which quantifies the resistance of a material to the deformation. For an oscillatory shear, the response of a Hookean solid is in phase with the sollicitation. Under the application of an oscillatory shear γ, an ideal viscous liquid on the other hand will respond following Newton's law [75]:

$$\sigma = \eta\dot{\gamma} = G\gamma_0\omega \cos(\omega t) \tag{1.28}$$

where $\dot{\gamma}$ is the shear rate and η is the viscosity. The response of a viscous material is therefore out of phase with the stimulus.

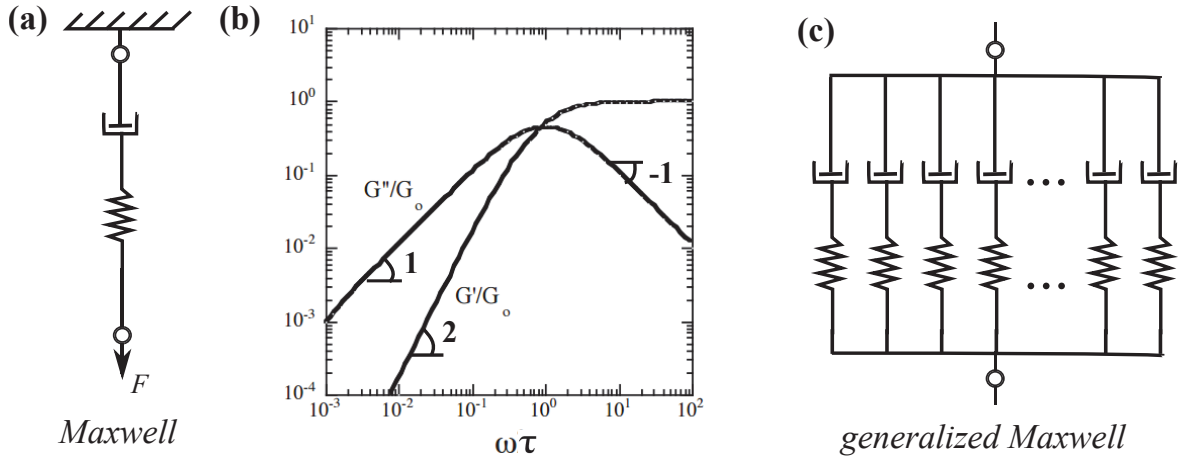

Figure 1.22: Mechanical analog models of a (a) viscoelastic liquid (Maxwell), (b) Dynamic moduli for the Maxwell model and (c) polymer melt (generalized Maxwell model)

A material that exhibits both viscous and elastic behavior is called viscoelastic. Several models have been developed to describe the responses of viscoelastic materials to stress or strain. The simplest examples are combinations of elastic (a spring) and viscous (a dashpot) elements, being able to store and dissipate energy respectively (*e.g.* Figure 1.22(a)). The models endow the material with a characteristic time and make its behavior time-dependent. In a Maxwell model (Figure 1.22(a)), the stress response to the application of an oscillatory shear is still sinusoidal but shifted by a phase angle δ [75]

$$\sigma = \sigma_0 \sin(\omega t + \delta) \tag{1.29}$$

The stress can then be separated into two components, one in phase with the strain (elastic contribution) and one in phase with the shear rate (viscous contribution)[75]:

$$\sigma = G^* \gamma_0 \sin(\omega t + \delta) \tag{1.30}$$

$$\sigma = G^{'} \gamma_0 \sin(\omega t) + G^{''} \gamma_0 \cos(\omega t) \tag{1.31}$$

with G' being the elastic "storage" modulus and G'' the viscous "loss" modulus. The ratio of the moduli is the tangent of the phase angle, $\tan\delta$, or the "damping factor":

$$\tan\delta = \frac{G''}{G'} \tag{1.32}$$

For a Maxwell model, the exact expressions of the elastic and loss modulus can be calculated [75]. Their formulas are given in equations (1.33) and (1.34) respectively and the resulting curves are shown in Figure 1.22(b).

$$G'(\omega) = G_0 \frac{\omega^2\tau^2}{1+\omega^2\tau^2} \tag{1.33}$$

$$G''(\omega) = G_0 \frac{\omega\tau}{1+\omega^2\tau^2} \tag{1.34}$$

In equations (1.33) and (1.34), $\tau = \eta_0/G_0$ and gives the link between liquid and solid behavior. Note that when $\omega \to \infty$, $G' \sim G_0$ (solid) and when $\omega \to 0$, $G'' \sim \eta\omega$ (liquid).

Polymer melts are viscoelastic materials. However, they cannot be described by a simple Maxwell model with a single characteristic time. In reality, polymer melts have a spectrum of relaxation times, that can be obtained by adding individual elements with different relaxation times, *i.e.* as in the generalized Maxwell model, Figure 1.22(c).

The behaviour of real polymer systems can be described by using the mechanical analog models. Nevertheless, they do not relate the viscoelastic behavior to the chemical or molecular structure (*e.g.* the molecular weight...). The linear viscoelastic behaviour of polymeric liquids is generally determined with creep/creep recovery, stress relaxation and/or small amplitude oscillatory shear experiments using a rheometer. In principle, in the linear viscoelasticity regime all these measurements provide the same information and the different material functions can be converted into one another.

Small amplitude oscillatory shear experiments for a viscoelastic material were decribed at the beginning of this section. In a stress relaxation experiment, a small shear strain is suddenly applied to a material for a long time and the relaxation of the stress is measured. The stress relaxation modulus defined as $G(t) = \sigma(t)/\gamma$ is independent of γ. In a creep experiment, a constant shear stress is suddenly applied to a material at time $t=0$ and the shear strain $\gamma(t)$ is monitored as function of time. The creep compliance is defined as $J(t) = \gamma(t)/\sigma$. In the linear viscoelasticity region, the creep compliance is independent of σ.

Shear creep measurements are particularly interesting because they allow the study of the linear viscoelastic behavior at very long times. An experiment of several hours can give access to frequencies down to 10^{-4} rad/s, which would be too low to reach in dynamic oscillatory measurements. In principle, a simple relationship exists between the relaxation modulus and the experimentally accessible compliance:

$$\int_0^\tau G(t)J(t-\tau)dt = \tau \tag{1.35}$$

The relaxation modulus can be extracted by deconvolving equation (1.35) using for example Fourier transform. In reality, this conversion is not trivial and has been intensively discussed in the literature [76, 77, 78].

1.5.2 Polymer melts

1.5.2.1 Influence of molecular weight

A polymer chain is an array of atoms linked by covalent bonds with characteristic angles and orientations. The most simple picture of a polymer chain is the freely-jointed chain, in which each polymer segment can orient freely with respect to its neighbours. Assuming that each configuration is equally probable, a Gaussian distribution is obtained for the mean squared average end-to-end distances. Therefore, the freely-jointed chain is also called a Gaussian chain. At a next level, the bond angle and rotational energy potentials have to be taken into account, thus limiting the motions of the chain [7].

Polymer molecules constantly exhibit Brownian motion. They can diffuse past each other and adopt multiple conformations due to their length and flexibility. In polymer melts of sufficiently high molecular weight, the motion of an individual chain can be inhibited by the motion of its neighbours. This is referred to as chain entanglement [7].

The dynamics and viscoelasticity of polymer melts is highly dependent on molecular weight, molecular weight distribution, chemical structure, architecture and temperature. Focusing on linear monodisperse polymers, the earliest observation of this dependency was made by analyses of the variation of the zero shear viscosity (*i.e.* viscosity at the limit of low shear rate) as a function of molecular weight (Figure 1.23(a)) [80]. The melt viscosity varies linearly with

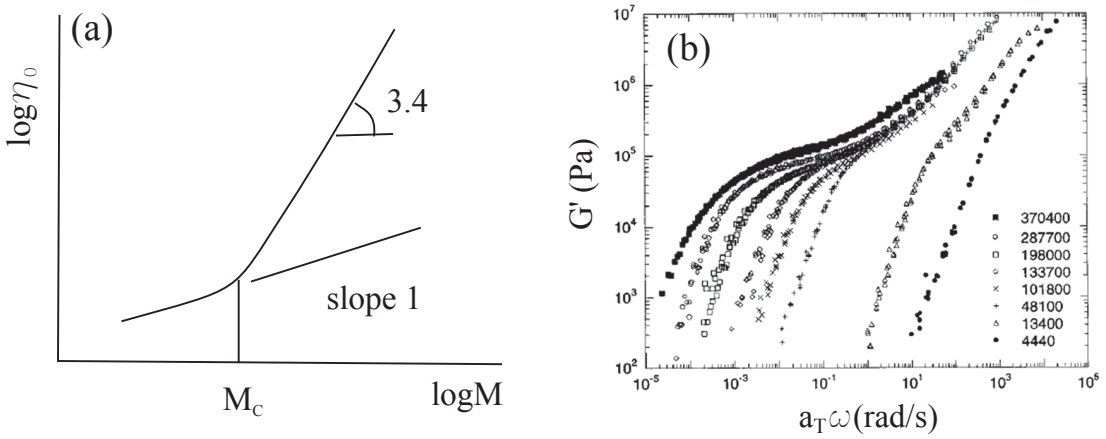

Figure 1.23: (a) Variation of zero shear viscosity of a polymer melt as a function of molecular weight (b) Variation of the elastic modulus of a hydrogenated polystyrene melt as a function of molecular weight (T_{ref} = 187°C, numbers in legend correspond to M_n in g/mol). From [79]

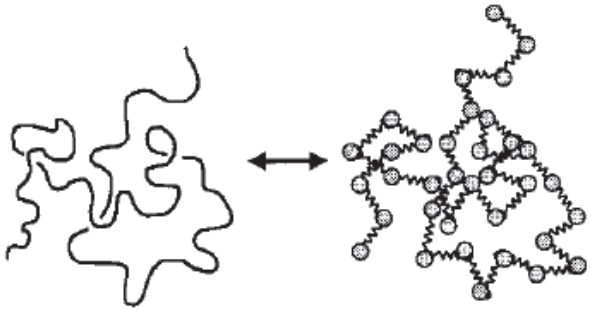

Figure 1.24: Mapping of a polymer chain onto a bead-spring chain. From [7]

molecular weight below a critical value M_C. Above M_C, the viscosity varies with $M^{3.4}$. The critical molecular weight M_C is linked to the molecular weight between entanglements M_e. M_C is generally thought to be approximately 2-3 times M_e, but this value can vary depending on the polymer chemical structure [81].

The master curves of the dynamic relaxation moduli (obtained by time-temperature superposition, detailed in Section 2.2.5) also show different types of behavior depending on the molecular weight. Figure 1.23(b) illustrates the variation of the dynamic elastic moduli with frequency for a linear polymer of varying molecular weight. It can be seen that, as molecular weight increases, a plateau appears in G'. In order to explain this behavior, several molecular models were proposed. For this work, the most important molecular model is the Rouse model, which can describe the dynamics of unentangled, short chains [76]. The polymer chain is represented as *N* beads connected by *N-1* springs (Figure 1.24). Each bead has a friction coefficient ζ and interacts with other beads via the springs. Because of the many degrees of freedom in the chain, the relaxation is governed by a series of relaxation times as in the generalized Maxwell model. In the Rouse Model, each relaxation mode p has a characteristic relaxation time τ_p and the dynamic moduli are given by the sum of all relaxation modes [76]:

$$G'(\omega) = \frac{\rho RT}{M} \sum_{p=1}^{N} \frac{\omega^2 \tau_p^2}{1 + \omega^2 \tau_p^2} \tag{1.36}$$

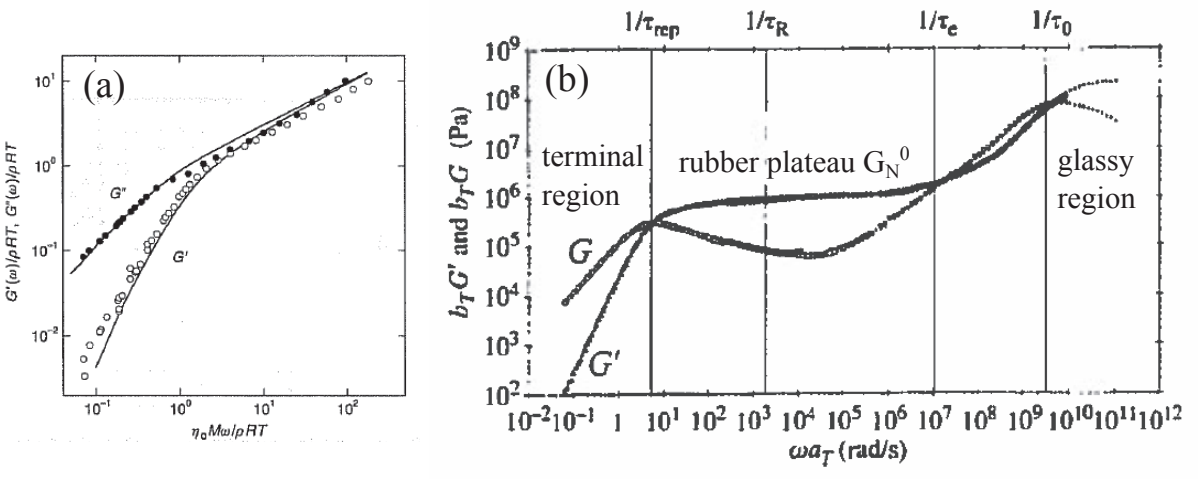

Figure 1.25: (a) Relaxation moduli for an unentangled hydrogenated polystyrene melt (M_w = 5000 g/mol, T_{ref} = 187°C), as predicted by the Rouse model. From [76] based on data from [79]; (b) Relaxation moduli for an entangled monodisperse polymer melt; master curve at 25°C for 1,4-polybutadiene (M_w = 130000 g/mol). Adapted from [7]

$$G''(\omega) = \frac{\rho RT}{M} \sum_{p=1}^{N} \frac{\omega \tau_p}{1 + \omega^2 \tau_p^2} \tag{1.37}$$

where ρ is the polymer density, R is the gas constant, T is the temperature in K and M is the molecular weight of the polymer. The characteristic relaxation times τ_p are:

$$\tau_p = \frac{1}{p^2} \times \frac{M^2 N_A}{6\pi RTM_0} \times \frac{\zeta b^2}{M_K} = \frac{\tau_R}{p^2} \tag{1.38}$$

where N_A is Avogadro's number, M_0 is the molecular weight of the monomer unit, b and M_K are the length and the molecular weight of a Kuhn segment respectively. The longest relaxation time τ_R is obtained when p=1 and is typically called the (longest) Rouse time of the chain.

At low frequencies (*i.e.* the terminal regime), equations (1.36) and (1.37) predict a slope of two and one for G′ and G″ respectively on a log-log plot. At higher frequencies, G′ is equal to G″ and the model predicts a slope of 1/2. As it can be seen in Figure 1.25(a), the Rouse model fits well the experimental data for unentangled polymer melts.

For higher molecular weights, entanglements come into play and the dynamic moduli display a distinct plateau on G' over a certain range of frequencies (Figures 1.23(b) and 1.25(b)). Focusing on Figure 1.25(b), at extremely short times, the large scale motions of the chain are frozen and the only mechanism for relaxation is the stretching and bending of bonds ($\tau_0 = \frac{\zeta b^2}{kT}$). The polymer is in its glassy state and its characteristic modulus is of the order of the GPa. At longer times ($\tau_0 < 1/\omega < \tau_e$), short-range molecular motions come into play and there is a transition zone during which there is a significant relaxation of stress. Up to this point, entanglements do not influence the relaxation. Afterwards, the chains "find out" that their motion is topologically hindered by surrounding chains (entanglements), which prevent further relaxation and lead to a plateau. The typical value of the rubbery plateau modulus ($G_N^0 = \frac{4}{5}\frac{\rho RT}{M_e}$, analogous to the rubber theory [76]), is of the order of the MPa. For long linear chains, the rubbery plateau can span many decades in time. At sufficiently long times, the polymer chain can escape its entanglement constraints by diffusion. This leads to the terminal zone ($1/\omega > \tau_{rep}$), in which the chains are relaxed and the slopes of 1 and 2 are reached.

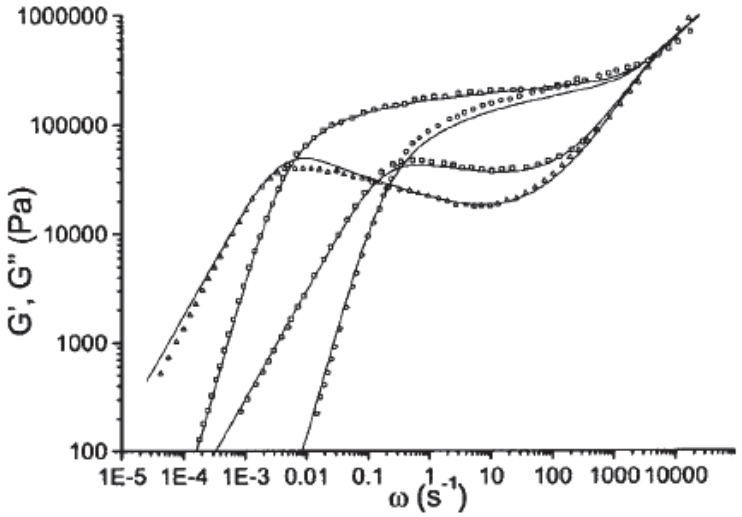

Figure 1.26: Dynamic moduli for linear polystyrene and the best fit by the tube theory. T_{ref} = 169.5°C and M_w = 275 and 860 kg/mol, respectively. From [85]

A breakthrough in the understanding of this behavior came with the tube idea originating from Edwards, de Gennes and Doi [82, 83, 84]. They assumed that the effects of entanglements on a certain test chain could be replaced by a tube, thereby simplifying the dynamics of the melt to the diffusion of a single chain in a tube. The "tube" ansatz led to the prediction of $\eta_0 \sim M_w^3$, remarkably close to the experimental observations. Later theories include several different relaxation mechanisms (e.g. dynamic dilution, contour length fluctuations, constraint release [7]), a discussion of which lies beyond the scope of the present work. Figure 1.26 shows the predictions of an up-to-date theory and one can observe that the dynamic moduli are well described.

1.5.2.2 Influence of polydispersity and branching

The above sketched situation is typical for linear, monodisperse polymer melts. However, real industrial polymers are seldom monodisperse nor linear. Depending on the chemistry and synthesis route, polydispersity can be far from 1 and secondary reactions can occur as well (leading to branching, cyclic oligomers etc.). For instance, details on polyamide side reactions have been provided in Section 1.1. Since rheology is very sensitive to the molecular structure, these features can give distinct signatures in the variation of the relaxation moduli.

If the sample is polydisperse, each molecular weight relaxes with its own characteristic time spectrum. This results in the loss of the flat rubbery plateau in favor of a smooth transition towards the terminal regime. For un-entangled polymer melts, the effects of polydispersity are additive as the chains have no mutual influence. The Rouse model can hence be applied by summing over the entire molecular weights distribution:

$$G'(\omega) = \sum_i \frac{\rho RT w_i}{M_i} \sum_{p=1}^{N} \frac{\omega^2 \tau_{i,p}^2}{1 + \omega^2 \tau_{i,p}^2} \tag{1.39}$$

$$G''(\omega) = \sum_i \frac{\rho RT w_i}{M_i} \sum_{p=1}^{N} \frac{\omega \tau_{i,p}}{1 + \omega^2 \tau_{i,p}^2} \tag{1.40}$$

where w_i is the weight fraction of chains of average molecular weight M_i (obtained experimentally from GPC) and $\tau_{i,p} = \tau_p(M_i)$ in equation (1.38). In entangled melts however, polydispersity has to be taken into account differently and led to the development of other models (*e.g.* double reptation [86]).

The effect of branching on rheological properties cannot be easily generalized. There is a very large variety of branching structures: short and long side-chains, comb structures, star polymers, hyperbranched structures etc. [87], which are very difficult to characterize. Generally, the terminal regime is delayed to lower frequencies and several inflection points can appear in the plateau region, indicating the existence of distinct relaxation mechanisms (*e.g.* backbone and arms) [87]. In order to draw any conclusions from the rheological data or apply any model, detailed information on the branching structure is usually needed [88].

Last, if the branching is not regular and controlled, a broad distribution of structures can exist. In this case, it is difficult to distinguish between the effect of branching and polydispersity.

1.5.3 Effects of interchain interactions on polymer viscoelasticity

It is well-accepted that the rheological properties of polymers depend on their macromolecular architecture. It is however unclear how enthalpic interactions (*e.g.* ionic association or hydrogen bonds) influence the rheological properties.

The study of the influence of strong interactions has been done on model monodisperse, linear polymers with a low density of interactions. Typically, first literature studies were concentrated on systems consisting of polymers with low polydispersity, containing a small amount of lateral groups forming so-called "stickers" capable to interact with each other. The strong interactions form a thermoreversible network, which subsequently gave the “transient network” name for these systems. The most extensive experimental study of transient networks was initially done by the group of Stadler [89, 90, 91, 92]. The authors investigated entangled polybutadienes of narrow molecular weight distribution, modified by the addition of small amounts of 4-phenyl-1,2,4-triazolidine-3,5-dione (urazole) groups. The transient network and interaction groups are illustrated in Figure 1.27. Typical master curves of the relaxation moduli for increasing amount of stickers are illustrated in Figure 1.28.

The key conclusions can be summarized as:

1. The longest relaxation time shifts to lower frequencies with increasing concentration of stickers.

2. The slopes of G' and G'' in the terminal zone decrease with increasing concentration of stickers.

3. The value of the plateau modulus increases with increasing concentration of stickers.

4. An additional relaxation can be observed in the plateau region for the loss modulus (arrow in Figure 1.28). It could be related to the association/dissociation dynamics of the stickers.

5. Time-Temperature Superposition works relatively well with some minor deviations in the rubber plateau region.

Interestingly, the stickers association/dissociation times could be investigated by Dielectric Spectroscopy measurements [93]. Figure 1.29 presents the relaxation chart of the polybutadiene/stickers systems. Polybutadiene has a glass transition temperature that is sufficiently low (inferior to -90°C [14]) to occur before the stickers can relax. The characteristic relaxation times of the stickers (given by the α^* relaxation) were found at temperatures above the glass transition. As the concentration of stickers increased, both the α and α^* relaxation times are

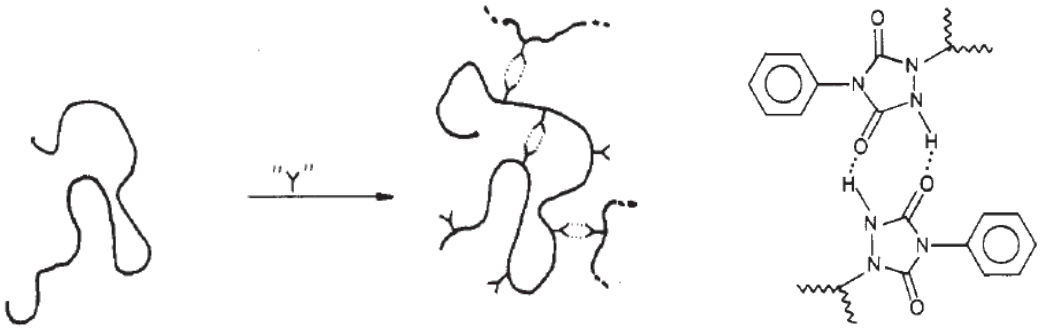

Figure 1.27: Schematic representation of the introduction of specifically interacting groups ("Y") on a linear polymer chain and the structural details of the Y stickers (urazole). From [90]

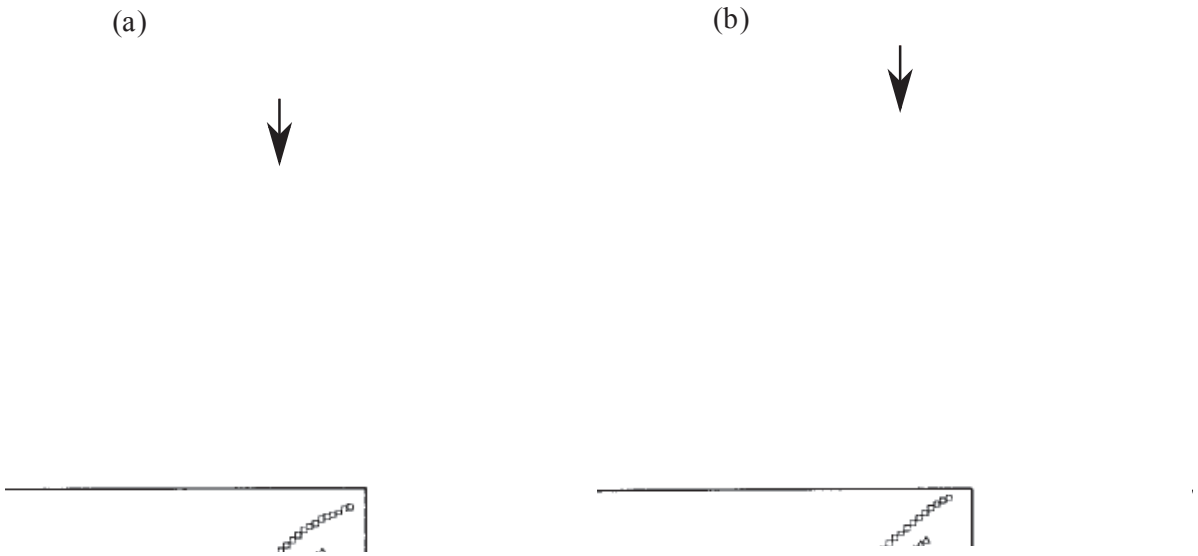

Figure 1.28: (a) Master curves of the loss (G″) and (b) storage (G′) moduli at T_{ref}=233K for polybutadiene with ∘ 0 mol%, ▽ 2 mol%, △ 3 mol% and □ 4 mol% urazole groups. The solid lines indicate behavior in the terminal zone. The master curves are vertically shifted by half a decade for clarity. From [92]

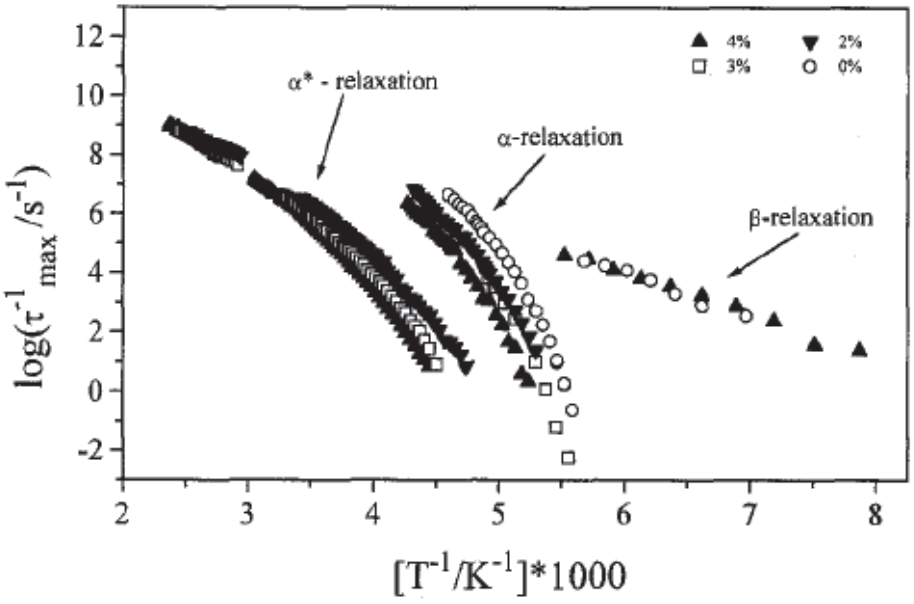

Figure 1.29: Relaxation charts of polybutadiene/phenyl urazole systems evidencing the characteristic relaxation times for increasing concentrations of stickers. From [93]

shifted to higher temperatures. As highlighted in Dielectric Spectroscopy, *the relaxation of the stickers occurs on a different time and temperature scale than the polymer glass transition* .

Based on this experimental data, Leibler, Rubinstein and Colby developed a theoretical model called sticky reptation [94]. In this model, hydrogen bonds between stickers are considered as reversible crosslinks that relax with a single relaxation time $\tau_{sticker}$. On time scales shorter than the average lifetime of a sticker in the associated state $\tau_{sticker}$, the reversible network is indistinguishable from a permanent network. On longer time scales however, the bonds break and re-attach rapidly, rendering the diffusion of the chain possible. It is assumed that the chain conformation and topological state are not significantly changed by the presence of the stickers. Based on these hypotheses, the variation of the shear modulus was predicted as shown in Figure 1.30.

At times shorter than the entanglements relaxation times τ_e, there is no difference between a polymer with and without stickers (assuming the glass transition temperature T_g is not affected at low sticker %). On intermediate time scales (inferior to $\tau_{sticker}$), a new plateau appears due to the contribution of interactional cross-links. Once the bonds break, the plateau modulus reaches the same level as the corresponding linear polymer without stickers. This model predicts two maxima in the loss modulus, as was also suggested by the experimental data in Figure 1.28. However, time-Temperature superposition failed in the rubbery plateau region for the experimental data, indicating that *the relaxation of the stickers had a different dependency on temperature than the chain dynamics*. The sticky reptation model was further developed in the following years by Rubinstein and Semenov [95, 96] for entangled polymer solutions, to include the case of a high degree of stickers association and a distribution in the stickers relaxation times.

These benchmark studies opened the path for the investigation of associating polymers in the molten state. Several points remained unadressed in the polybutadiene systems: 1. the addition of stickers modified the PB backbone (and hence also the local stifness of the chain), 2. the polymers were entangled, which did not allow to discriminate between the role of interactional and topological entanglements and 3. the density of interactions was always very low. In the following years, several studies were dedicated to un-entangled and entangled

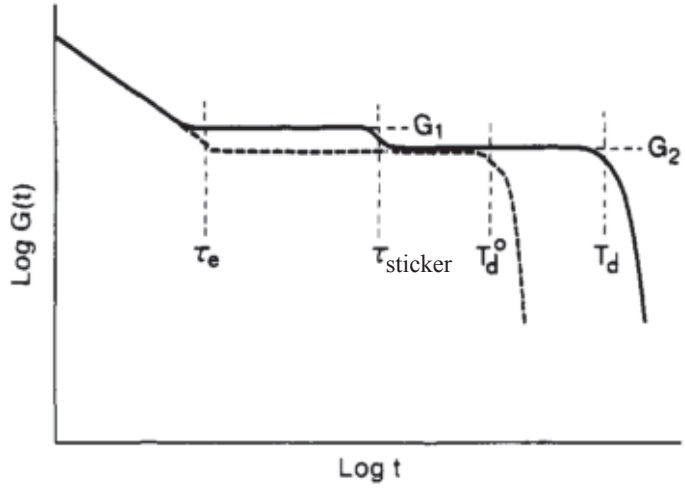

Figure 1.30: Comparison of the time-dependent relaxation moduli for an entangled linear polymer chain with (solid line) and without stickers (dashed line). Adapted from [94]

polymers with various stickers, with no modification of the backbone and increased strength and density of interactions. An overview of the literature studies most relevant for this work is presented in Table 1.3. The chemical structure of referenced stickers is illustrated in Figure 1.31. Different studies are compared based on : the chemical structure of the backbone and of the stickers, how much T_g changes in presence of stickers (T_g shift), if the chains are entangled or not, the bond density (% of stickers), the bond strength (bond type and its energy) and the key rheological observations (time-Temperature Superposition works or not, increase of plateau modulus, longer relaxation time, decrease of slopes in terminal regime, *i.e.* gel-like behavior).

As can be seen in Table 1.3, the key observations made by Stadler *et al.* were confirmed by most studies: T_g shift, increase of the plateau modulus, increase of the longest relaxation time and slopes inferior to 1 and 2 in the terminal regime. Time-temperature superposition (tTS) failed in some frequency ranges and the master curves of unentangled polymers could not always be described by a sticky Rouse model. One of the most complete studies was done by Lewis *et al.* [97]. The authors added stickers of different chemical structures on an unentangled PnBA backbone. A plateau was observed only in the case of the UPy stickers, which form high energy complexes of 4 hydrogen bonds (70 kJ/mol). Therefore, the interaction strength between the stickers needs to be high enough at the temperatures where the polymer is molten in order to have an impact on rheology.

Recently, an interesting observation was made by Shabbir *et al.* [98]. The studied polymer was PnBA, hydrolyzed in different proportions. The authors suggested that the increase in modulus with the percentage of associating groups could be explained by the decrease in packing length induced by hydrolysis. Therefore, one of the observed effects is due to the change in packing length and not to the stickers association.

Ref.	Chemistry	T_g shift	Entangled?	Bond density	Bond strength	Key rheological observations
Stadler *et al.* [89]	PBd + urazole (Fig 1.31(a))	162 to 170K	Yes	0-2 mol%	2 H-bonds	tTS works, plateau modulus increases, longer terminal relaxation time, gel-like behavior in terminal regime
de Lucca *et al.* [90]	PBd + urazole (Fig 1.31(a))	162 to 170K	Yes	0-7.5 mol%	2 H-bonds	tTS works, plateau modulus increases, longer terminal relaxation time, gel-like behavior in terminal regime
Muller *et al.* [92]	PBd + urazole (Fig 1.31(a))	175 to 182.5K	Yes	0-4 mol%	2 H-bonds	tTS fails in the rubbery plateau, plateau modulus increases, longer terminal relaxation time, gel-like behavior in terminal regime
Feldman *et al.* [99]	PnBA + UPy (Fig 1.31(e))	-50 to -10°C	No	0-13 mol%	4 H-bonds (70 kJ/mol [97])	tTS works, plateau modulus increases, longer terminal relaxation time, gel-like behavior in terminal regime, plateau due bonds (backbone unentangled)
Oster-winter *et al.* [100]	linPG-OH, linPG-OMe	248 to 263K, 198 to 212K	from un- to entan-gled	each monomer	1 H-bond	tTS works, plateau modulus increases, longer terminal relaxation time for linPG-OH compared to linPG-OMe
Lewis *et al.* [97]	PnBA + AP, AA, CEA and UPy (Fig 1.31(b-e))	-50 to -40 or -12°C	No	0-23 mol%	1 to 4 H-bonds, from 25 to 70 kJ/mol	tTS works, higher modulus, longer terminal relaxation time, plateau only for UPy, gel-like behavior in terminal regime

Table 1.3: Literature overview of chemistry and main rheological observations for polymer melts with interacting groups

Ref.	Chemistry	T_g shift	Entangled?	Bond density	Bond strength	Key rheological observations
Shabbir *et al.* [98]	PnBA hydrolyzed	?	Yes	3-38 mol% hydrolyzed	2 H-bonds	tTS works over certain range, higher modulus, longer terminal relaxation time, gel-like behavior in terminal regime for 38% only
Callies *et al.* [101]	PnBA center-functionalized with bis-urea (Fig 1.31(f))	No	from unto entangled	max. 2.2 mol%	4 H-bonds	tTS fails, for entangled : higher modulus, longer terminal relaxation time, gel-like behavior in terminal regime
Weiss *et al.* [102]	sulfonated PS	No	Yes	0-1.71 mol%	ionic, 65 kJ/mol [103]	tTS works, higher plateau modulus, longer terminal relaxation time
Weiss *et al.* [104]	sulfonated PS	80 to 90°C	No	0-4.8 mol%	ionic	tTS fails for ionomers; comparison between PS and H-sulfonated PS shows that H-bonds have no influence on rheological behavior
Chen *et al.* [105]	polysiloxanes + phosphonium ions	189 to 204K	No	0-26 mol%	ionic	tTS works, no plateau; master curves fitted with sticky Rouse and KWW
Chen *et al.* [103]	PEO-f%Na	228 to 271K	No	0-100 mol%	ionic, 8-13 kJ/mol	tTS ok, no plateau; master curves fitted with sticky Rouse and KWW
Chen *et al.* [103]	PMTO-f%Na	No	No	0-100 mol%	ionic, 58 kJ/mol	very long plateau, tTS fails on plateau; sticky Rouse + KWW do not describe the master curves accurately

Table 1.3 (continued): Literature overview of chemistry and main rheological observations for polymer melts with interacting groups

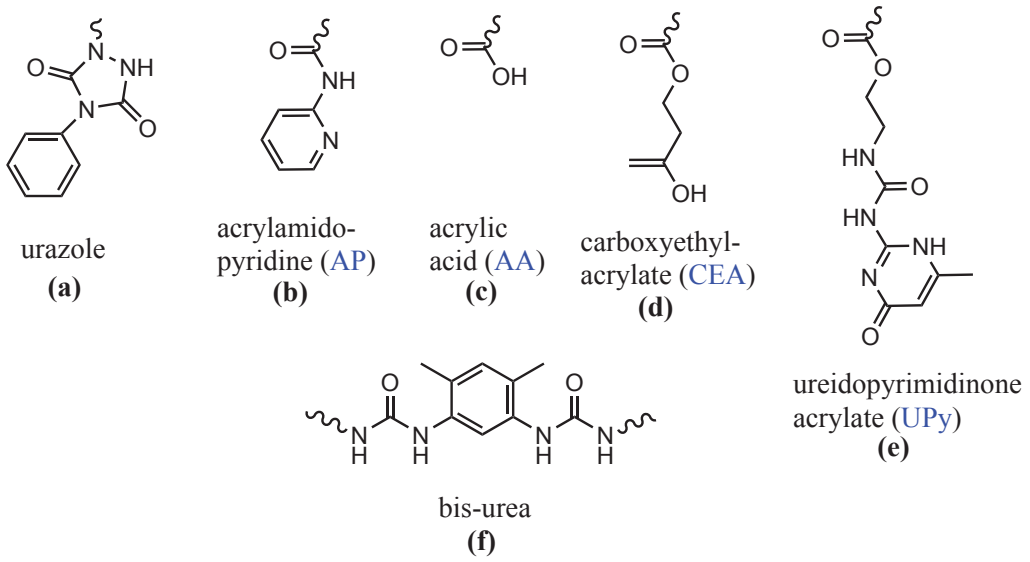

Figure 1.31: Chemical structure of stickers referenced in Table 1.3

It should also be highlighted that in most of the listed studies, the master curves were compared at a fixed temperature. However, the glass transition of the polymers varied systematically with the introduction of the stickers. This "T_g effect" is not always taken into account and might also influence the interpretations.

Lastly, another class of transient networks is represented by ionomers. In contrast with the low T_g systems with hydrogen bonds, the ionomers can have high glass transition temperatures up to 100°C and more. The same effects were observed in ionomers, *i.e.* increase of modulus plateau and shift of the longest relaxation time. In a study on sulfonated polystyrene PS-SO_3X, Weiss *et al.* [104] also compared a possibly hydrogen bonding PS (X=Hydrogen) to a reference PS. At high temperature (130°C), no effect of the hydrogen bonds was observed on the rheological properties, while the corresponding ionomers (X=cation) displayed a plateau modulus at the same temperature (Figure 1.32).

Recently, a unique study of ionomers with high concentrations of interacting groups was done by Chen *et al.* [105, 103]. The authors studied the linear viscoelasticity (LVE) and the dielectric response of polysiloxane-based phosphonium ionomers (chemical structure in Figure 1.33(a)) up to high percentages of ionic contents [105]. It was observed that a sticky Rouse model [94] described the data well up to 11% ionic content but that at higher concentrations one broad relaxation was observed from glassy to flow 1.33(b). This broad process can be described phenomenologically by a single Kohlrausch-Williams-Watts (KWW) equation. An important observation was that dielectric spectroscopy and rheology provided independent measures of the same ionic dissociation process, similar to the observations of the Stadler group [93] mentioned previously. The ionic association/dissociation times obtained from dielectric spectroscopy measurements could be successfully used to predict the dynamic moduli of these ionomers (up to 11% ionic content).

In conclusion, there is great interest in understanding the rheological behavior of polymers with interactions. Most literature studies have been done on low T_g polymers with a limited amount of H-bonding stickers or on ionomers with high interaction energy and high percentage of stickers. Dielectric Spectroscopy has proved to be a valuable complementary technique to analyse the relaxation of these interactions. Several common observations have been made for these interacting systems but some points are yet to be elucidated: taking into account the

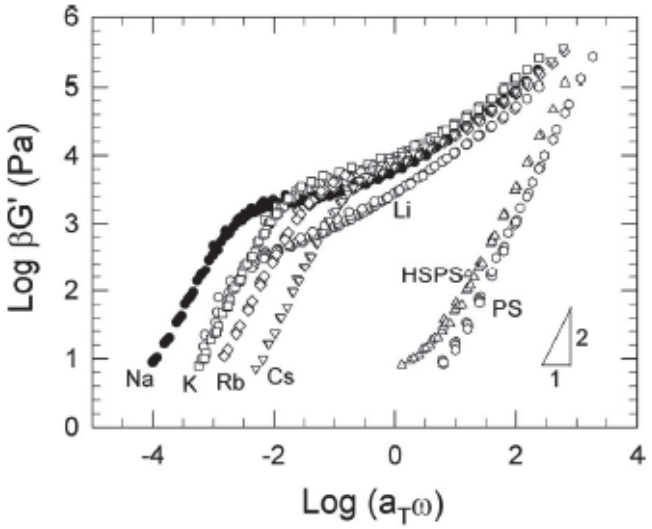

Figure 1.32: G′ master curves for polystyrene and PS-SO_3X, where X=H or metal. T_{ref} = T_g + 45°C. From [104]

(b)

(a)

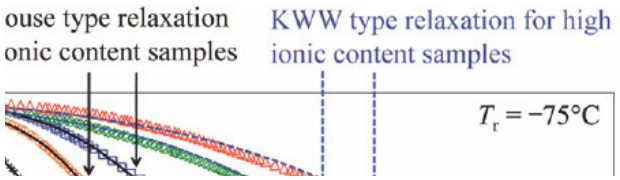

Figure 1.33: (a) Chemical structure of polysiloxane-based phosphonium ionomers and (b) Master curves of dynamic modulus *G(t)* as function of time for phosphonium ionomers (chemical structure to the left) with different ionic contents. From [105]

T_g effect, why tTS fails in some cases, why the sticky Rouse model does not describe systems with a high density of interactions or why the presence of the interactions is expressed on the rubbery plateau and/or in the terminal region.

1.5.4 Viscoelasticy of polyamide

1.5.4.1 Literature review

In the context of polymers with interactions, polyamide is interesting to study because of its extremely high bond density (each monomer) compared to previous studies. The literature on polyamide rheology is scarce. It has long been known experimentally that PA pellets have to be dried thoroughly (<0.2%) before processing in order to avoid bubble formation and hydrolysis [1]. However, to the best of our knowledge, it was only in 1964 that a first study was made on starting materials with variable moisture contents [106]. The authors showed that the melt viscosity increased with time for samples with low water content (<0.24%) and decreased with time for samples containing a higher amount of water. The first studies were aimed at calculating the flow activation energy and the variation of viscosity with molecular weight. By using samples dried at less than 0.2% water, different authors [106, 107, 108] found flow activation energies between 40 and 100 kJ/mol (temperature ranges of approximately 200-300°C).

The first systematic study of the influence of moisture content was done by Khanna *et al.* [109]. The authors analysed PA6 samples of molecular weight M_v between 30 and 70 kg/mol. Firstly, they showed that extreme drying conditions (T>150°C) led to an important increase of the viscosity, suggesting that solid state polymerization had occurred. Secondly, the shear rate viscosity of the samples decreased with the moisture content in the 0.02 to 0.2% range. The activation energies for flow were between 40 and 70 kJ/mol.

All the above studies were mainly done with a capillary rheometer, without checking the possible evolution of the molecular weight (except for [108]). In a recent study [110], it was shown that water concentration is an essential parameter for polyamide stability. Figure 1.34 illustrates the evolution of the apparent viscosity for PA6 samples with varying initial water contents.

In capillary rheometry, the high temperature and hydrostatic pressure ensure the dissolution of the water molecules in the polymer matrix. Therefore, the molecular weight will remain constant if the polymer sample contains the equilibrium water concentration. In Figure 1.34, it can be observed that the viscosity of PA6 with 1150 ppm water does not change with time, meaning that this is the equilibrium water concentration for this particular PA6. If the sample contains less water, post-condensation occurs and the molecular weight increase leads to a viscosity increase. If the sample contains more water, hydrolysis occurs and the molecular weight decreases, leading to a decrease of the viscosity. In addition, water may act as a plasticizer and lower the viscosity of the melt. In all the previous capillary rheometry studies, the polymers were dried well below their equilibrium water concentration and their viscosity probably varied during the measurements.

In oscillatory rheometry, the polymer melt is at atmospheric pressure so excess water is no longer dissolved in the matrix. Moreover, the polymer lateral surface is in contact with a hot flux of nitrogen or air. These experimental conditions favor the drying of the sample and therefore post-condensation, which should lead to an increase in viscosity. A first study done with a parallel plate rheometer in oscillatory mode [111] highlighted the evolution of polyamide viscosity as a function of time. The authors followed the viscosity of PA11 as a function of moisture content and temperature. It was shown that polymers evolved faster when they were very dry at a high temperature (Figure 1.35).

post-condensation

equilibrium

hydrolysis

Figure 1.34: Apparent viscosity vs. residence time at 260°C in capillary flow of a medium molecular weight commercial PA6 at different initial moisture contents (Karl Fischer measurements at 160°C). From [110]

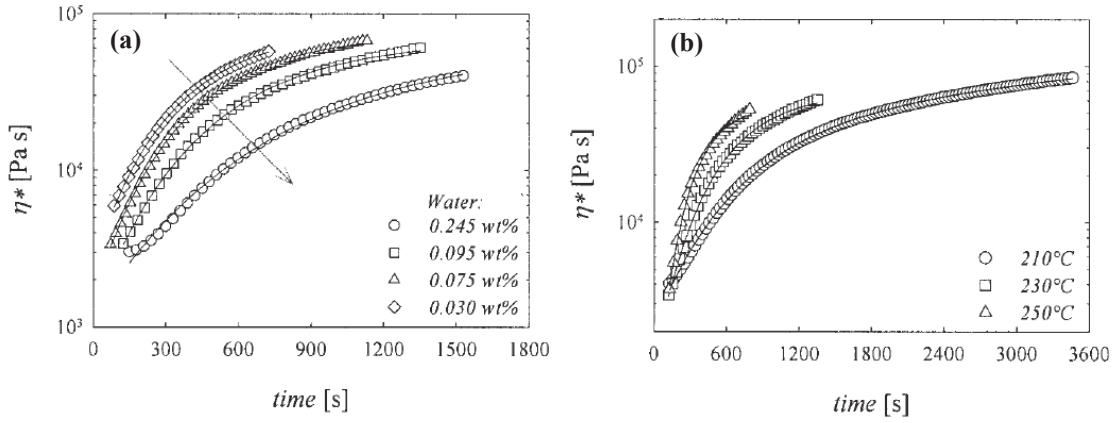

Figure 1.35: Evolution of the complex viscosity of PA11 at (a) different initial moisture levels at 230°C and (b) as a function of temperature for 0.095% initial moisture. The arrow in (a) points in the direction of increasing moisture. From [111]

In order to limit variability in oscillatory measurements, a IUPAC technical report was written so as to give guidelines for the rheological characterization of polyamide melts [110]. The authors highlighted once again the increase of viscosity with measurement time in oscillatory rheometry. Moreover, they observed a shouldering in the elastic modulus G' at low frequencies, which they associated to the formation of water bubbles, as in emulsions, blends or foams [112, 113, 114].

Recently, van Ruymbeke *et al.* [88] studied the viscoelasticity of end-capped linear and branched PA6. The capping of the chain ends ensured the stability of the polymer during measurements. Size Exclusion Chromatography data was fitted to provide an analysis of the sample composition in terms of architecture and molecular weight. This distribution was then used in the tube model, which provided predictions in good agreement with the experimental data. Although this study allowed the authors to discuss the role of polymer architecture in the viscoelastic response, the experimental data was limited to the terminal regime because the studied samples were semi-crystalline.

In conclusion, the polyamides investigated in the literature are water-sensitive and all semi-crystalline, rendering tTS impossible. There is no information available on the modulus in the rubber plateau or in the glass transition zone. To the best of our knowledge, there has been no attempt in the literature to perform time-Temperature superposition on polyamide in order to obtain the full spectrum of the dynamic shear moduli.

1.5.4.2 Challenges for PA

The aim of this investigation is to study the relationship between viscoelasticity and the molecular structure of polyamide. In order to do so, two criteria must be valid. First, the polymer must not evolve during the measurement time, *i.e.* there must be no change in molecular weight. Second, the polymers need to be amorphous to be able to access the full frequency spectrum of the moduli. In the case of polyamide, neither condition is generally fulfilled.

To begin with, polyamide molecular weight can vary to a large extent, depending on the experimental conditions. As presented in Section 1.1, polyamide is formed by a condensation reaction between (di-)amine and (di-)acid monomers or their corresponding salts. Since the reaction is a chemical equilibrium, the molecular weight of the polymer is given by the concentration of reacting groups and water. A certain molecular weight has a corresponding water quantity, called the equilibrium concentration $[H_2O]_{eq}$. If the water concentration is lower than $[H_2O]_{eq}$, the equilibrium will try to compensate this loss by creating additional water molecules through condensation. In the process, new amide $-NHCO-$ bonds will be created and the molecular weight will increase. If the water concentration is higher than $[H_2O]_{eq}$, the chemical equilibrium will favor the hydrolysis reaction in order to consume water. In this case, the molecular weight will decrease. Moreover, the reaction rate will also depend on the product of the concentration of end/terminal groups (GT). A polyamide with a high product of GT has a higher potential of evolution towards condensation because of the reaction equilibrium (equation (1.1)). If condensation occurs in previously synthesized polyamide, the process is called post-condensation.

It should also be highlighted that the reaction rates increase with temperature. At ambient temperature the rate is low and the molecular weight does not change, ensuring for instance its stability during storage or in end-use applications. At an intermediate temperature inferior to the melting point (typically 110-200°C), the reaction rate is also intermediate and has been exploited for example in solid-state post-condensation [115] for obtaining higher molecular weight polymers that were too viscous for classic synthesis or processing. At high temperatures, above the melting point, the reaction rate is fast and special precautions have to be taken in order to preserve the desired molecular weight of polyamide melts. For instance, polyamide

pellets are always dried in industrial processing (e.g. extrusion, injection) and the processing time is kept short to avoid post-condensation [1]. In rheological studies, post-condensation in the melt is hard to avoid, which is one of the reasons why literature data are scarce.

Another reason for the lack of data on polyamide rheology is that most polyamides are semi-crystalline. The shear modulus of the polymer increases significantly upon crystallization and cannot be measured with typical rheometers. In addition, the measured properties would be mainly given by the existence of the crystalline phase, whose mechanical effect is dominant over the polymer structure, topological or interactional crosslinks. All literature studies have therefore been limited to polyamide above melting temperature. This is justified in capillary rheometry, since the study of the melt is relevant for processing conditions. However, for a more fundamental study of the influence of molecular structure on polyamide rheology we would need to eliminate the crystalline phase and have access to the full frequency spectrum of the dynamic moduli G' and G''. To the best of our knowledge, a complete spectrum has never been measured experimentally for PA. Special care has to be taken as well to account for polydispersity and possible branching.

1.6 Approach of the current study

1.6.1 Solid state diffusion and sorption

Diffusion and sorption of solvents in polymers can be very complex because of the existence of specific interactions (non-polar or polar), dynamic heterogeneities in the amorphous phase, modification of the polymer dynamics induced by the solvents and different crystalline phases. In polyamide/solvent systems, all of these factors have to be taken into account. To begin with, solvents can interact strongly with amide groups and lead to the decrease of the glass transition temperature, or plasticization of the amorphous phase, *i.e.* an increase in the mobility of the polymer chains. Secondly, although the crystalline phase is considered impermeable to the solvent, its existence induces a gradient of mobility in the amorphous phase, which has often been depicted as a Rigid and Mobile Amorphous Fraction. An important number of literature studies have been dedicated to elucidating the accessibility of the amorphous phase. Murthy *et al.* [53] concluded from Small Angle Neutron Scattering measurements that one third of the amorphous phase is in the interlamellar space and two thirds outside the lamellar stacks. Water was found to diffuse in all regions. The water molecules in the interlamellar regions are thought to be highly immobilized [52]. These findings were confirmed later on by NMR studies [33, 55, 56, 58, 59]: water diffuses preferentially in the soft amorphous phase, which is then plasticized by the water molecules. Recent studies have also shown that a plasticization lag exists, meaning that a few percentages of water were absorbed in the material before the plasticization was visible [59].

Thus, it would be interesting to study if there is a correlation between penetrant diffusion and the mobility of the polymer chains due to amorphous phase heterogeneity or plasticization. To the best of our knowledge, no previous study has investigated the correlation between the diffusion coefficient and polymer dynamics (main α relaxation and more local, secondary relaxations) in polyamides.

Since the amorphous phase accessibility might be of importance for diffusion and sorption mechanisms, the first part of this study was dedicated to model polyamides. A 100% amorphous polyamide and its homologous semi-crystalline were compared for the diffusion and sorption of different solvents (water, alcohols of increasing size). The conclusions of this part would give us premises to compare other commercial polyamides of different crystallinity.

A second part of this study investigated the relationship between solvent diffusion and

the dynamics of the amorphous phase in two polyamides with slightly different ratios of amide/methylene groups (PA6,6 and PA6,10). The first purpose is to study each polymer matrix individually (water sorption, diffusion coefficients, relaxation times) and understand diffusion mechanisms, in particular whether or not diffusion is coupled to polymer relaxation. The second is to assess the influence of the ratio of amide/methylene groups, *i.e.* the density of hydrogen bonds.

1.6.2 Linear viscoelasticity

Polyamide is an important industrial polymer but systematic studies of its rheological properties are scarce. The main reasons are the difficulties related to chemical stability and to the presence of a crystalline phase that limits the measurement range to temperatures above the melting point. However, polyamide contains a very high density of hydrogen bonds, which is poorly understood and seemingly highly interesting as discussed in Section 1.5.3 [99, 105]. Previous literature studies have explored model polymers and increased gradually the concentration of interactions up to 1 group/nm^{-3}. In this context, the present study increases the level of complexity by focusing on a commercial polydisperse polymer (polyamide) with a higher density of interactions (5 groups/nm^{-3}).

The aim of our investigation is to understand the role of strength and density of bonds in polyamides. A class of polyamides was designed for this study in order to remove the limitations inherent to polyamide. First of all, polyamide stability could be ensured by incorporating inert terminal groups (see Chapter 2).

Second, limitations related to the presence of a crystalline phase can be removed by using an amorphous polyamide. There has been important progress in synthesizing amorphous polyamides over the past decades, and the choice is wide between monomer structures that can ensure the amorphous character [116].

Third, since rheological properties are dependent on the chemical structure, special precautions have to be taken in order to keep the polymer backbone intact and add lateral groups of limited length. The hydrogen bond strength and density must be modified while keeping stiffness and free volume as constant as possible.

In conclusion, the limitations inherent to polyamide can be circumvented by using amorphous, blocked polyamides. Several materials have been selected to allow us to investigate the influence of the density and strength of hydrogen bonds and to distinguish between the contribution of entanglements and physical crosslinks. The study of the relationship between viscoelasticity and the molecular structure of stable, amorphous polyamide is also important in knowing physical parameters (friction, free volume, molecular weight between entanglements) that might be linked in the future to semi-crystalline polyamides.

This manuscript is divided in three main parts. The first part presents the studied polyamides, as well as the methods and setups that were used in order to characterize the structure, dynamics in the solid and molten state and the diffusion and sorption of solvents. The second part presents different investigations in the solid state in presence of solvents: influence of crystallinity, diffusion mechanisms with a focus on the influence of polyamide dynamics, sorption models, influence of solvent type and size on sorption and phenomena occuring at long immersion times. The third part is dedicated to polyamide dynamics in the molten state: the investigation of the role of interactions on the viscoelasticity of polyamide.

Chapter 2

Materials and methods

2.1 Materials

2.1.1 Polyamides for sorption and diffusion studies

2.1.1.1 Model amorphous and semi-crystalline aromatic polyamides

In order to evaluate the influence of the existence of a semi-crystalline phase on sorption and diffusion properties, an amorphous and semi-crystalline polyamide of equivalent chemical structure were needed. Random copolymers of PA6I and PA6T satisfy this criterium. Isophthalic (I) and terephthalic (T) acid monomers differ only by the position of their substituents on the aromatic ring (*meta* for I and *para* for T, for the chemical structure please refer to Table 2.1). The stereochemical configuration of the carboxyl functions in the isophthalic acid monomer "bends" the polyamide chains, thus preventing them from aligning and crystallizing [116]. On the other hand, the linear configuration of the carboxyl functions of the terephthalic acid monomer do not prevent crystallization. By adjusting the molar percentage of I or T monomer, amorphous or semi-crystalline polyamides can be obtained [116]. It is the case of amorphous Selar commercialized by DuPont and semi-crystalline Amodel A1007 commercialized by Solvay. The characteristics of these polymers can be found in Table 2.1.

Despite its unfavorable configuration, PA6I was found to crystallize to some extent in presence of solvents [72]. The crystallization was indisputable in the case of alcohols but uncertain in the case of water. Also, there was no specification if the process occurs before or after the sorption equilibrium is reached. At this point, it was questionable if the current study would reach its aim. However, the polymer choice was preserved for several reasons:

1. these polymers were the only amorphous and semi-crystalline polyamides of equivalent chemical structure available to us

2. PA6I did not crystallize in presence of water so at least the case of water could be studied

3. the crystallization kinetics of the amorphous PA6I was unknown, the process might occur after sorption equilibrium is reached, as it was suggested for the copolymer PA6,6/6I [12]

Pure PA6I of molecular weight equivalent to Selar was also added to the study. The polymer was synthesized by the Polymers Process & Synthesis Laboratory in Solvay (M.-L. Michon, V. Mollet); its characteristics can also be found in Table 2.1.

Last, it was observed in Differential Scanning Calorimetry scans that A1007 cold-crystallized upon heating (Figure 2.5). By annealing for 2h at 173°C, the cold crystallization peak was removed and the crystalline fraction of the polymer increased from 16 to 26%. This sample will be referred to as *A1007 annealed*.

2.1.1.2 Commercial aliphatic polyamides

The conclusions of the first study on model amorphous and semi-crystalline polyamide were applied on two industrial polyamides, PA6,6 and PA6,10 provided by Solvay. The characteristics of these polymers can be found in Table 2.2.

Polymer	PA6I	Selar Dupont	A1007
Chemical formula	PA6I	PA6I/6T 70/30 molar, random copolymer	PA6I/6T 30/70 molar, random copolymer
Chemical structure	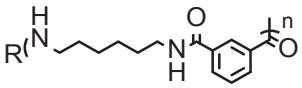	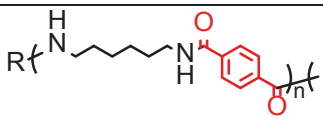 6 Terephthalic (T)	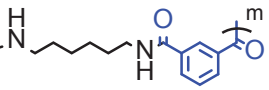 6 Isophthalic (I)
Glass transition temperature T_g (°C)	126	130	133
Melting point T_m (°C)	-	-	323
Crystalline fraction DSC (%)	amorphous	amorphous	16±2*
Average number molecular weight M_n (g/mol) - GPC	12 000	12 000	12 000

*the enthalpy of fusion of pure PA6T is not available in the literature so an average value of 200±20 J/g was used to determine the crystalline fraction of A1007

Table 2.1: Polymer characteristics for amorphous and semi-crystalline aromatic polyamides for diffusion and sorption studies

Polymer	PA6,6	PA6,10
Chemical structure	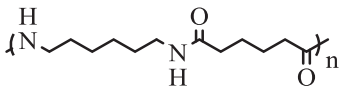	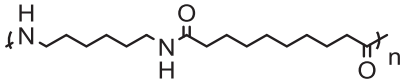
Glass transition temperature T_g (°C)	64	53
Melting point T_m (°C)	260	222
Crystalline fraction DSC (%)	38	23
Average number molecular weight M_n (g/mol)	25000	37000

Table 2.2: Polymer characteristics for aliphatic polyamides for diffusion and sorption studies

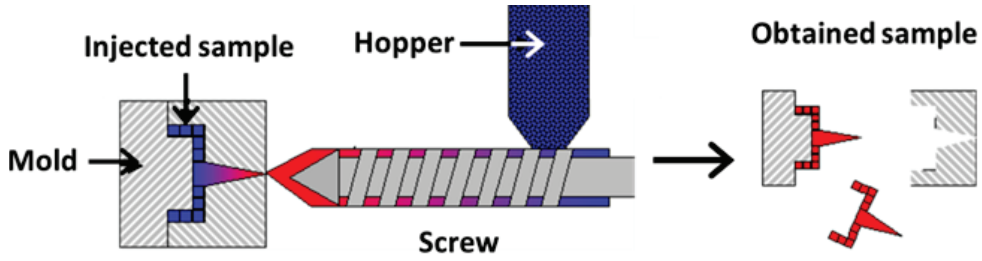

Figure 2.1: Injection-molding setup. From [27]

Polymer	Temperature (°C)		Molding cycle time (s)
	Screw	Mold	
PA6I	310	80	62
Selar	310	80	64
A1007	335	90	40
PA6,10	245	80	20

Table 2.3: Injection conditions for PA6I, Selar, A1007 and PA6,10

2.1.1.3 Polymer processing

All polymers were in the form of pellets. PA6I, Selar and A1007 pellets were injected in a Fanuc S-2000i 150A(180T) press (D. Delcourt, Solvay Brussels) in order to obtain injection molded plates of 125 x 125 x 1 mm. PA6,10 pellets were injected in a DEMAG H200-80T press (E. Seignobos, Solvay Belle-Etoile) in order to obtain injection molded plates of 100 x 100 x 0.8 mm.

The principle of injection molding is illustrated in Figure 2.1. The polymer pellets are introduced in a hopper and carried by the screw into areas with increasing temperature. A motor coupled to the screw pushes the molten polymer into the mold, where it will take the desired shape and cool down. The polymer is maintained in the mold by applying a counter-pressure. Depending on polymer rheology, a few parameters have to be adjusted in order to fill the mold: the screw temperature, the injected quantity, the mold temperature, the counter-pressure and the piece retention time. The processing conditions are presented in Table 2.3. After injection, all plates were thinned on one side at a thickness of 300 μm using a planer.

PA6,6 films were used from the PhD of Agustin Rios de Anda [27] for Solvay. The films were prepared by film-cast extrusion. The pellets were introduced in a Leistritz extruder with a L/D ratio of 33 and an output of 10 kg/h. Figure 2.2 illustrates the principle of film-casting: the polymer is introduced via a hopper in the extruder, in which the polymer melts. At the exit of the extruder, a die gives the polymer a planar form. Then the polymer is carried through a series of chill-rolls that will cool it down and draw it to a given thickness.

The processing was done at the Polymer Processing Facility of the CRTL (Vincent Curtil, Olivier Andrès, Thomas Jacquin, and Sandrine Rossi). The processing conditions are shown in Table 2.4. The Chill-roll temperature corresponds to the temperature of the rolls that cool down the polymer after it exits through the die. The film casting speed corresponds to the speed at which the films are stretched, giving the draw ratio between the polymer at the exit from the die and the obtained film. The desired thickness is obtained by modulating the film cast speed and the draw ratio.

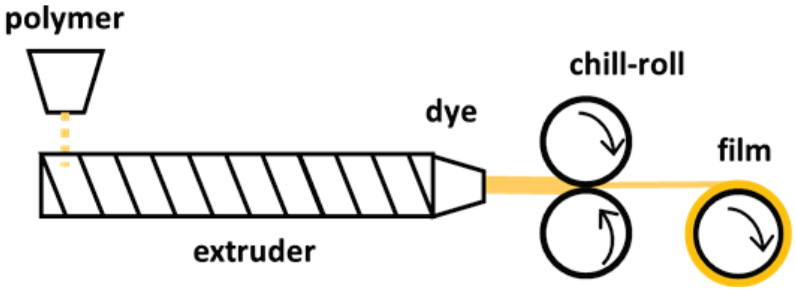

Figure 2.2: Film-cast extrusion setup. From [27]

Polymer	Temperature (°C)		Film casting speed (m/min)	Draw ratio	Film thickness (µm)
	Extruder	Chill Roll			
PA6,6	282	125	4.5	6	100

Table 2.4: Film-casting processing conditions for PA6,6

2.1.2 Semi-aromatic polyamide for rheology studies

A new class of polyamides had to be designed for rheological studies in order to remove the experimental limitations inherent to polyamide (post-condensation and crystallinity).

To begin with, polyamide post-condensation can be avoided by blocking the terminal groups, as illustrated in Scheme 2.1. The amine terminal groups can react with a blocker terminated with a non-reactive -*R* group (*e.g.* mono-acid). The chain ends no longer bear functional groups and therefore cannot react with other terminal groups. Post-condensation issues are thus solved.

Scheme 2.1: Blocking of polyamide amine terminal groups with a mono-acid

Second, limitations related to the presence of a crystalline phase can be removed by using an amorphous polyamide. There has been important progress in synthesizing amorphous polyamides over the past decades, and the choice is wide between monomer structures that can ensure the amorphous character [116]. Since rheological properties are dependent on the chemical structure, special precautions have to be taken in order to keep the polymer backbone intact and add lateral groups of limited length. For these reasons, we have chosen to test PA6I, PA6HIA and PA6LiSIPA, whose amorphous character is given by the isophthalic acid (substituted or not) (Figure 2.3).

Compared to PA6I, PA6HIA has an additional OH group capable of forming hydrogen bonds with amide groups. These hydrogen bonds have a higher energy than amide-amide hydrogen bonds (approx. 40 kJ/mol compared to 25 kJ/mol [117]). PA6LiSIPA was used as a copolymer with PA6I in a proportion of 95/5 molar. The ion-amide interactions were thoroughly investigated in the literature by Electron Paramagnetic Resonance (EPR), FTIR, Near Infrared (NIR) and solid-state ^{15}N Nuclear Magnetic Resonance (NMR) spectroscopies [118, 119, 120, 121]. It was highlighed that an ionomer-amide groups complex exists, which involves coordination of the carbonyl group by the metal cation. The different stages of the interaction between lithium sulfonate and the amide groups are illustrated in Figure 2.4. Initially, the positive charge of the cation is balanced by at least one sulfonate in its environment (Stage A). When introduced in

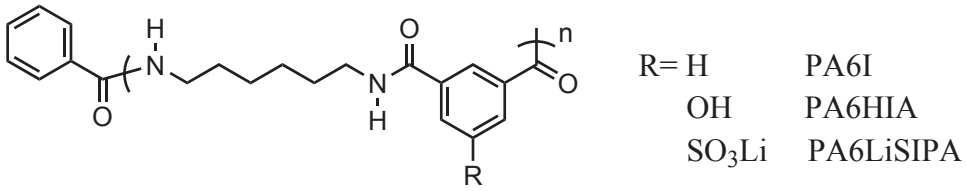

Figure 2.3: Chemical structure of polyamide based on hexamethylene diamine and isophthalic (I), 5-hydroxyisophthalic (HIA) and lithium 5-sulfoisophthalic (LiSIPA) acids

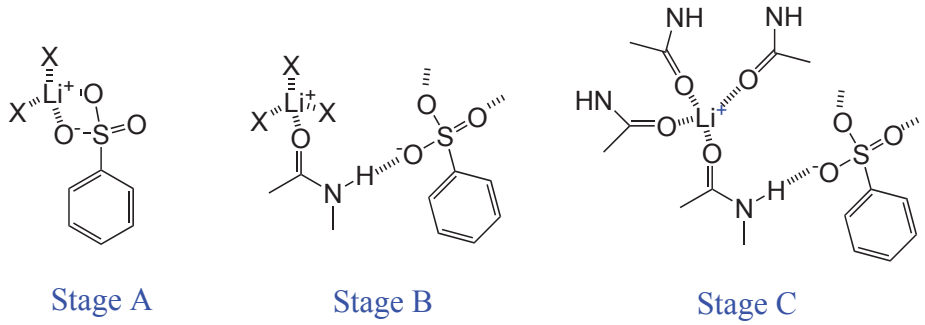

Figure 2.4: Schematic representation of the different stages of interaction between lithium sulfonate and polyamide. [118]

polyamide, the sulfonate could be displaced by a carbonyl group and the resulting SO_3^- could form a hydrogen bond with the *NH* from the amide group (Stage B). When enough amide groups are available, Li^+ can be surrounded by maximum four carbonyls (Stage C). The energy gained by coordinating one carbonyl group is around 10-15 kJ/mol and the energy of a tetra-coordinated complex is approximately 50 kJ/mol [122], which is much higher than the energy of an amide-amide H-bond (25 kJ/mol [117]).

These three polyamides will allow the investigation of the influence of hydrogen bonds on the rheological properties. Moreover, the contribution of entanglements can be assessed by synthesizing polymers with a molecular weight below and above the molecular weight between entanglements (approx. 2000-2500 g/mol for PA6 [123]).

None of the selected polyamides are commercially available and were synthesized by the Polymers Process & Synthesis Laboratory in Solvay (M.-L. Michon, V. Mollet). The complete list of materials and their molecular weight can be found in Table 2.5. A deep knowledge of the structure of the polymer backbone (linear, branched...) and of the molecular weight distribution is needed for rheological studies. The full characterization of these polymers will be presented in Chapter 6.

Polymer reference	M_n (g/mol) - GPC
PA6I	2000
PA6I	10000
PA6I	12000
PA6HIA	2000
PA6I/6LiSIPA 95/5	2000
PA6I/6LiSIPA 95/5	10000

Table 2.5: List of synthesized aromatic polyamides and their number average molecular weight

2.2 Methods

2.2.1 Determination of chemical structure

2.2.1.1 Molecular weight and molecular weight distribution

The (number and/or mass) average molecular weight was measured by End-group titration, by Nuclear Magnetic Resonance (NMR) in solution and by Gel Permeation Chromatography (GPC). The latter also gives access to the molecular weight distribution, which is particularly important for interpreting rheological data.

End-group titration gives access to the concentration of terminal groups in the polymer sample. Polyamide is dissolved in a trifluoroethanol/chloroform mixture and the $-NH_2$ and $-COOH$ groups are titrated by potentiometric back titration (Solvay Analytical Lab, K. Longé). Amine end group concentration $[-NH_2]$ and acid end group concentration $[-COOH]$ are obtained in mmol/kg. The molecular weight is then calculated with equation (2.1) [1]. The concentration of blockers is known from the reaction recipe.

$$M_n = \frac{2 \times 10^6}{[-NH_2] + [-COOH] + [blockers]} \tag{2.1}$$

Solution NMR can be used to determine the average number molecular weight of short polymer chains. PA6I 2k and PA6HIA 3k were dissolved in hexafluoroisopropanol (HFIP) and their NMR spectra were recorded on a Bruker spectrometer operating at 250 MHz for ^1H (Solvay Analytical Lab, F. le Guyader). The degree of polymerization and the average molecular weight are calculated from the integration of monomer peaks over the end group peaks.

In GPC, polymer chains are separated based on their hydrodynamic volume (radius of gyration). As a polymer solution passes over a column containing porous beads, the small chains are trapped in the pores while the long chains flow with the solvent. The weight concentration of the polymer in the eluting solvent is monitored continuously with a detector. The output in GPC is the polymer concentration as a function of elution time. This curve is compared to the one of a standard polystyrene (PS) and the molecular weight in PS equivalents is obtained. If the GPC is equiped with a triple detector (concentration, viscosity, refractive index), absolute molecular weight are obtained. The advantage of GPC over the other techniques is that it also provides the molecular weight distribution and polydispersity index. Since polyamides are polydisperse because of the polycondensation reaction, this aspect is very important.

GPC curves can be used to check if the polycondensation reaction lead to statistical, linear chains. For this purpose, the experimental GPC distribution is fitted with a Flory model for linear polycondensation (equation (1.2), Chapter 1) [6]. If the GPC experimental data cannot be fitted with the Flory equation, side-reactions probably occurred during synthesis. These side reactions can either be formation of cyclic chains or branching.

GPC measurements were done on a GPC PL Lab 120 device with double detection (viscometer and concentration detector) in the Solvay Analytical Department (N. Delon-Anik). Since polyamide is not soluble is usual solvents at room temperature, dissolution by N-trifluoroacetylation was used [124]. As the hydrogen of amide groups reacts with trifluoroacetic anhydride (Scheme 2.2), the hydrogen bonds between chains are broken. N-trifluoroacetylated polyamides (NTFA-PA) are therefore soluble in most common organic solvents at room temperature. Once prepared, NTFA-PA solutions are unstable in presence of atmospheric humidity and should be used immediately. This derivatization technique gives similar results as GPC at high temperature or with fluoroalcohols as solvents. However, GPC characterization of the derivatized product might be highly dependent on the presence of unsubstituted amide groups and results should be carefully evaluated.

Scheme 2.2: Chemical reaction between amide groups and trifluoroacetic anhydride for GPC derivatization

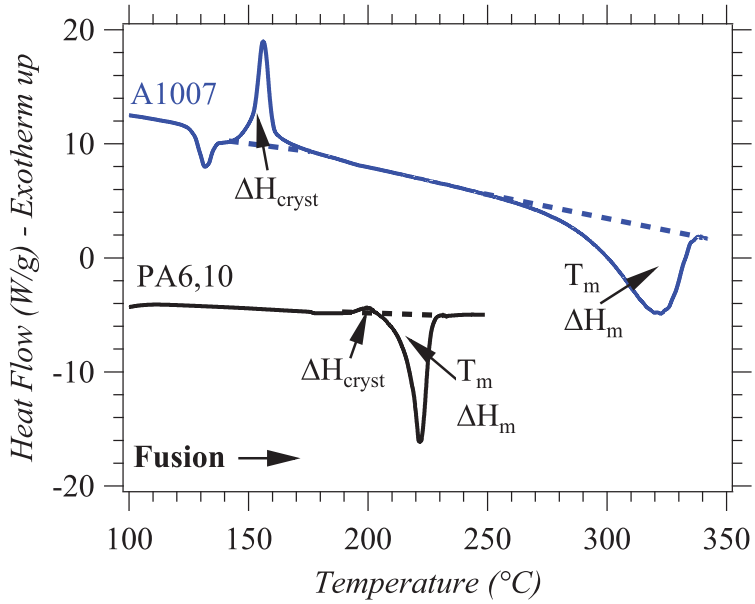

Figure 2.5: Typical DSC thermograms for (a) PA6,6 and (b) Amodel A1007. The curves have an offset for better observation.

2.2.1.2 Branching

As explained Chapter 1, branching can occur by forming bis(hexa-methylene) triamine (BHT) (see Scheme 1.3). The concentration of BHT can be determined by dosage after hydrolyzation of polyamide. The dosage was performed following an internal protocol from the Solvay Analytical Lab (Nadia Delon-Anik). The determined BHT concentration is in ppm (parts per million) with report to the initial polyamide weight.

2.2.2 Structural characterization

2.2.2.1 Crystalline fraction

The melting point, crystallisation temperature and crystalline fraction of polyamide were determined by Differential Scanning Calorimetry (DSC). As a sample undergoes a physical transformation (glass transition, melting, crystallization, reticulation etc.) in a DSC device, more or less heat has to flow to it in order to maintain it at the same temperature as the reference. This heat flow is recorded by the device as a function of time and temperature. Typical DSC thermograms for PA6,6 and Amodel A1007 are shown in Figure 2.5.

In both polyamides, the polymer chains crystallize or reorganize upon heating before the polymer melts (ΔH_{cryst}), also called cold-crystallization. The enthalpy of melting ΔH_m contains therefore both the contribution of the initial crystals and the ones formed upon heating. The contribution of cold-crystallization ΔH_{cryst} must be removed in order to calculate the initial crystalline fraction χ_C:

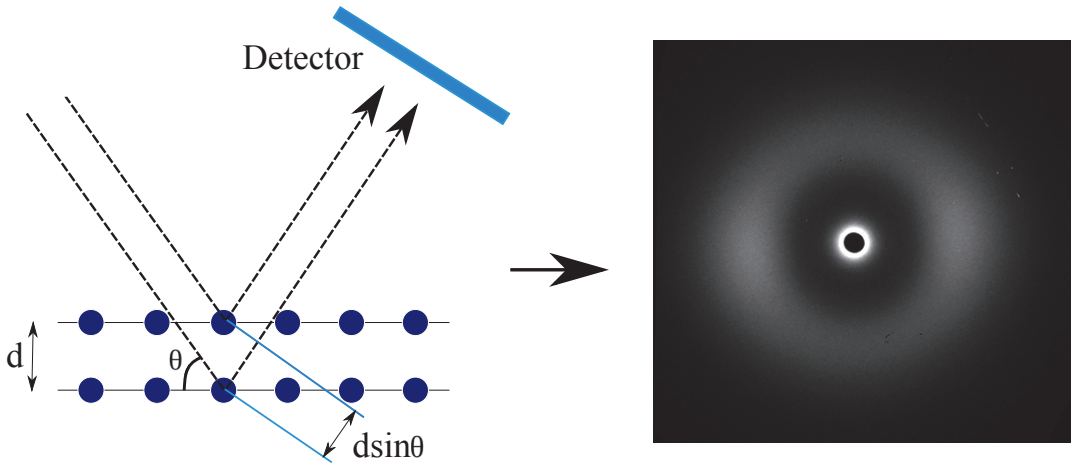

Figure 2.6: Illustration of X-Ray scattering by crystalline planes and an example of the resulting 2D interference pattern for PA6,6

$$\chi_C = \frac{\Delta H_m - \Delta H_{cryst}}{\Delta H_{100\%}} \times 100 \tag{2.2}$$

where $\Delta H_{100\%}$ is the enthalpy of melting for the 100% crystalline polyamide. This value can be found in the litterature for PA6,6 (188 J/g [14]) and PA6,10 (207 J/g [14]), but not for the crystalline PA6T part of A1007. As a consequence, an average value of 200 ± 20 J/g was chosen for A1007 to provide an estimation of the crystalline fraction.

A TA Instruments DSC Q2000 was used in the standard mode to determine the melting point and the ethalpy of melting. A Rapid Cooling System (RCS) with a nitrogen flow of 50 ml/min was used down to -85°C. Samples (between 7 and 15 mg) were placed in non-hermetic aluminium pans and heated from -85 to 250 or 350°C at a heating rate of 10°C/min.

2.2.2.2 Crystalline structure

X-Ray Scattering techniques have been used to provide information on the crystalline structure of polymers. When X-Rays are scattered by atoms, every atom emits spherical wavelets from its position. The scattered X-rays come from interferences between these wavelets at the detector position. These interferences depend on the observation angle 2θ, the orientation and the distance d between atoms. A 2-dimensions (2D) scattering pattern specific to the material is thus obtained, where the intensity varies from position to position in the detection plane (Figure 2.6).

After integration of the 2D pattern over all azimuth angles, the variation of the intensity is obtained as a function of the scattering angle 2θ. The scattering vector q is defined as:

$$q = \frac{4\pi \sin(\theta)}{\lambda} \tag{2.3}$$

where λ is the X-ray wavelength. The distance d between atomic planes can be retrieved from Bragg's law for constructive interferences (equation (2.4)), where n is a positive integer:

$$q = n\frac{2\pi}{d} \tag{2.4}$$

Following Bragg's law, the scattering angle θ determines the size of the structures that can be measured. If the measurement is done at wide angles, small distances of ~ 0.5 nm (e.g.

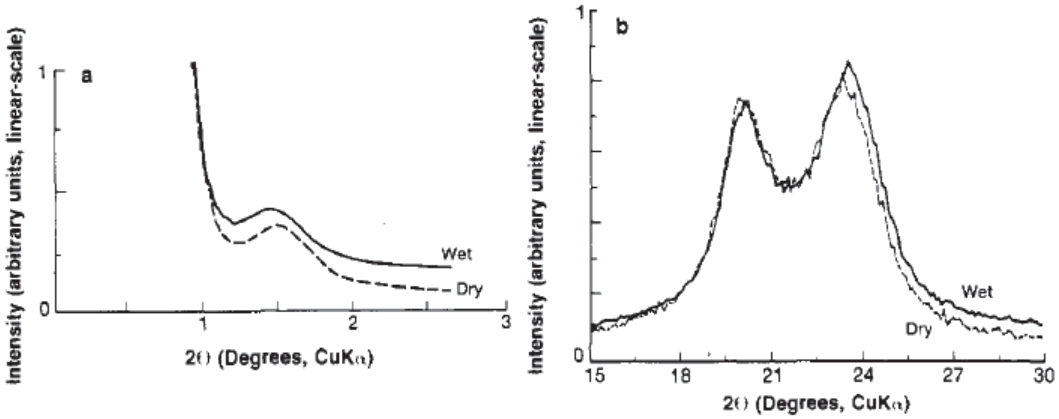

Figure 2.7: Illustration of a (a) SAXS and (b) WAXS scan for PA6 dry and wet fibers [51]

distance between crystalline planes) are available. If the measurement is done at small angles, larger distances up to 100 nm can be accessed (e.g. lamellar spacing). Examples of Wide and Small Angle X-Ray Scattering scans (WAXS and SAXS) are shown in Figure 2.7.

The XRD scan of a semi-crystalline polyamide consists of an amorphous halo on which crystalline peaks are superimposed. All polyamides in this study crystallize in the α form, which has a triclinic unit cell (see Figure 1.2). The peak position is associated to different crystallographic planes: around 6° the (001) perpendicular to chain axis, around 20° the (100) plane along molecular chains and cutting through H-bonded sheets and around 23° a superposition of the (010) plane parallel to H-bonded sheets and the (110) diagonal plane.

WAXS measurements were performed on a Bruker D8 Advance (reflection geometry) and an Oxford Xcalibur Mova diffractometer at the Henri Longchambon Diffraction Center (R. Vera). The pristine polymer was dried under vacuum at 80 (PA6,10) or 110°C (PA6,6, aromatic PA). The films saturated with solvent were measured before and after drying (desorbing at room temperature or at 50°C under vacuum). Measurements were performed on 2 x 2 cm cuts in a film, at room temperature, with the angle 2θ varying from 4 to 50° (CuK_α). A copper anode was used to generate X-rays of wavelength 1.54Å (CuK_α) in reflection geometry and a molybdenum anode was used to generate X-rays of wavelength 0.707Å in transmission geometry. For clarity, all diffractograms presented in this manuscript were converted to 2θ (CuK_α).

In reflection, the measurements are done on 2 x 2 cm cuts in a film of 5 x 5 cm so the influence of the cutting position was analyzed. In PA6,6, analyses on two samples gave similar results (Figure 2.8(a)). However, in PA6,10 some differences were noticed either on dry samples (Figure 2.8(b)) or on samples immersed in water (Figure 2.8(c)). These slight differences suggests that there could be a higher crystalline heterogeneity in our PA6,10 samples. Depending on where the cuts were made in the PA6,10 films, the WAXS peaks are more or less well resolved. The two main peaks position is not much affected but an additional peak appears around 21° in some samples (perhaps due to the coexistence of the α_I and α_{II} phases?).

In addition, the influence of drying of the samples with solvents was assessed. Gravimetric measurements showed that a minimum of 6 days at 50°C under vacuum was necessary to remove all the solvent (water or ethanol). Figure 2.9 illustrates the diffractograms of a PA6,10 sample equilibrated with solvent and a sample dried under vacuum. The peak position is similar but the dried sample seems better resolved. Since samples cut from different areas of the film already give this difference, it is difficult to say whether the improved resolution comes from the drying or from the sample itself. For this reason, all WAXS data in this report will be presented for samples containing the solvent.

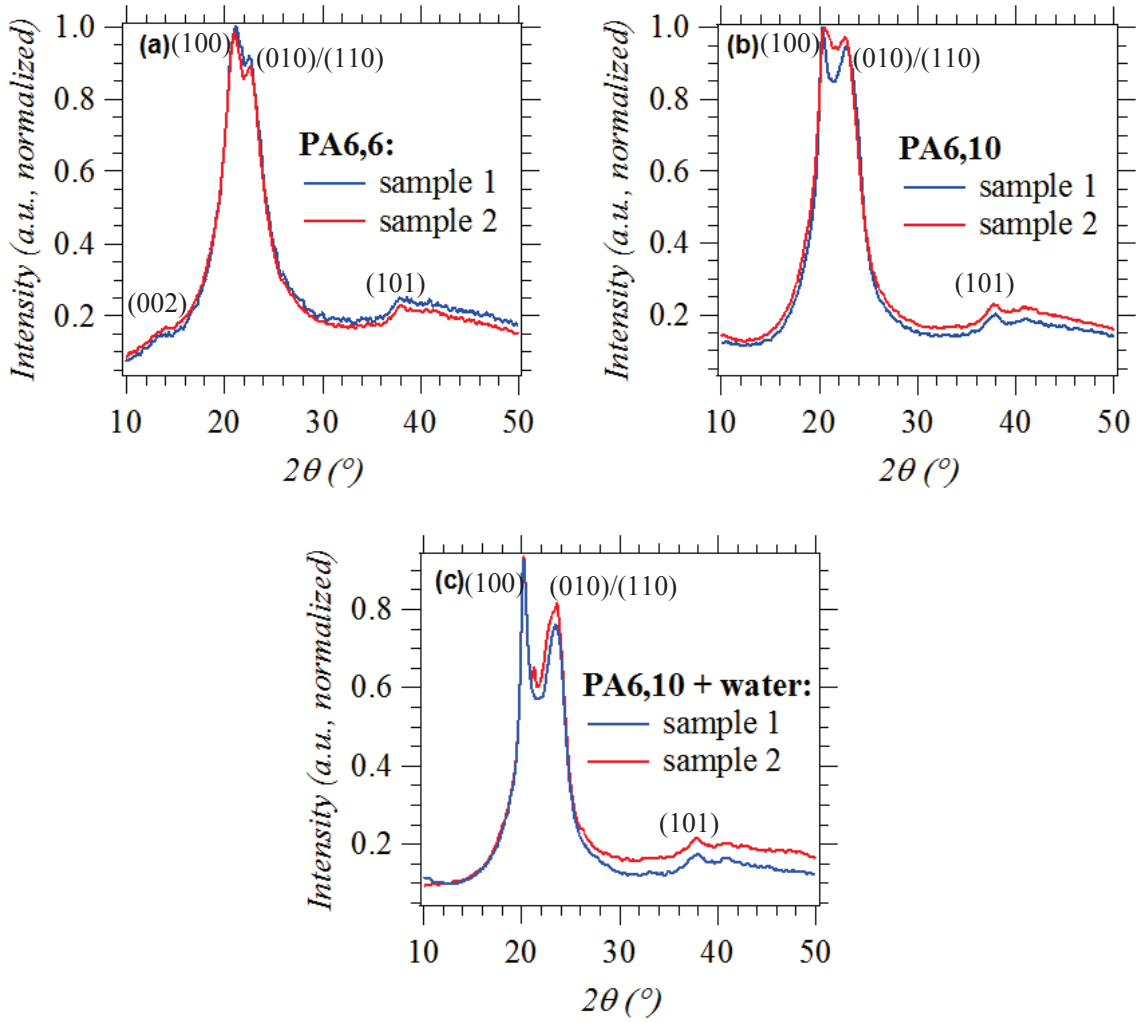

Figure 2.8: WAXS diffractogram of (a) PA6,6 (b) PA6,10 and (c) PA6,10+water for cuts in different areas of the films

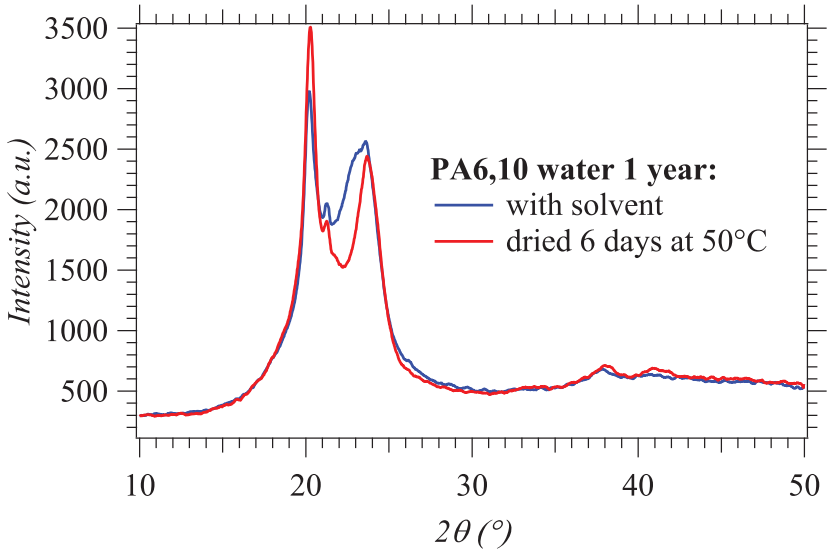

Figure 2.9: WAXS diffractogram of PA6,10 samples containing solvent and dried for 6 days at 50°C

SAXS measurements for PA6,6 and PA6,10 with solvents were done at the European Synchrotron Radiation Facility (ESRF Grenoble). SAXS scattering patterns will be presented as a function of the length of the scattering vector q.

2.2.3 Quantification of the dynamics of the amorphous phase

2.2.3.1 Differential Scanning Calorimetry

The glass transition of amorphous polymers is easily identified as a step in the heat flow from DSC measurements in standard mode. On the other hand, the glass transition of the heterogeneous amorphous phase in semi-crystalline polymers is a broad phenomenon that often cannot be identified easily in standard mode. A better precision can be obtained by using Modulated Differential Scanning Calorimetry (MDSC).

The total heat flow is expressed by equation (2.5) in DSC measurements, where H is the heat flow, C_p is the heat capacity of the sample, T is the temperature and $f(T,t)$ is the kinetic contribution to the heat flow:

$$\frac{dH}{dt} = C_p \frac{dT}{dt} + f(T,t) \tag{2.5}$$

Compared to the standard mode in which a temperature ramp is applied linearly, in MDSC the temperature is modulated by a few degrees around an average value (Figure 2.10(a)). Two independent heating rates exist (average and modulated). For a modulated heating rate equal to zero, the heat flux due to the heat capacity is zero and only the kinetic term $f(T,t)$ is measured. By substraction of the kinetic term from the total heat flow, the heat flow due to C_p can be obtained. MDSC provides therefore a separation of the total heat flow signal into its thermodynamic (heat capacity, reversing) and kinetic components (non-reversing).

Thermodynamic processes like the glass transition temperature are time independent and appear in the Reversing component of the heat flow. Time-dependent processes like ageing or solvent evaporation appear in the Non-reversing component. An example of the decomposition

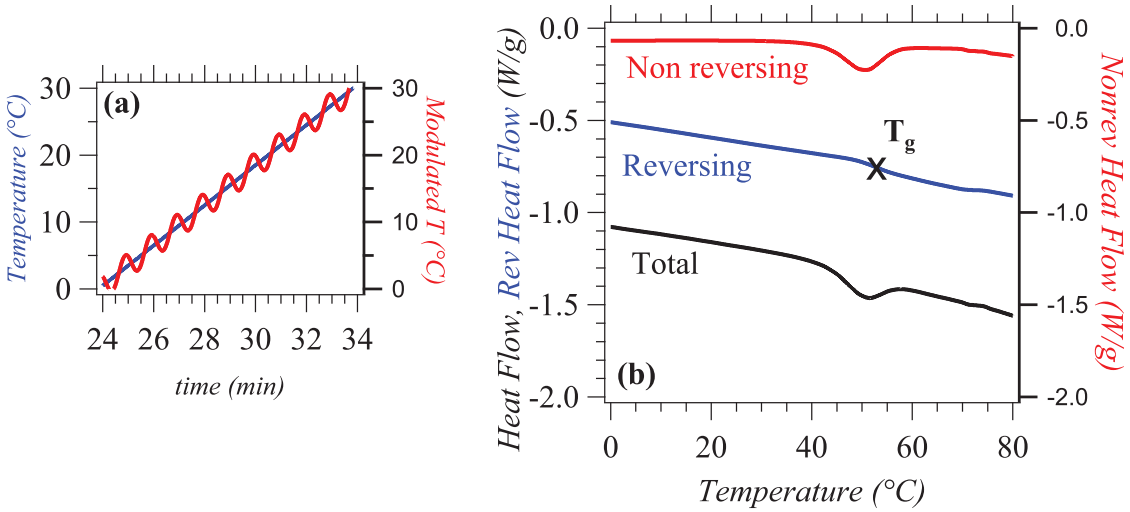

Figure 2.10: Illustration of (a) temperature modulation in MDSC and (b) the resulting separation of the heat flow into reversing and non-reversing contributions. The curves were offset for a better observation.

of the total heat flow is shown in Figure 2.10(b): the enthalpic peak due to polymer ageing at T_g can be deconvoluted from the C_p jump at T_g.

By making the hypothesis that only the mobile amorphous phase contributes to the step in the heat capacity, the amount of Mobile Amorphous Fraction can be estimated from MDSC measurements. The area below the glass transition peak in the reversing C_p ($RevC_p$) signal can be integrated and provides $\Delta C_p^{experimental}$. The MAF% is then given by equation (2.6):

$$MAF\% = \frac{\Delta C_p^{experimental}}{\Delta C_p^{theoretical}} \times 100 \tag{2.6}$$

where the theoretical heat capacity for a 100% amorphous polymer is 0.51 J/gK for PA6,6 and 0.418 J/gK for PA6,10 [125]. The RAF% is obtained by substracting the MAF% and the crystalline ratio.

A TA Instruments DSC Q2000 was used in the modulated mode to determine the glass transition temperature T_g of pristine and solvent equilibrated polymer. A Rapid Cooling System (RCS) with a nitrogen flow of 50 ml/min was used down to -85°C. For lower temperatures down to -150°C, a Liquid Nitrogen Cooling System (LNCS) was used with a Helium flow (25 ml/min). Samples (between 7 and 15 mg) were placed in non-hermetic aluminium pans and heated from -150 or -85 to 200°C at a heating rate of 3°C/min with a temperature modulation of ± 2°C every 60 s. The solvent-swollen samples were transferred rapidly between the sorption cell and the DSC pans in order to limit solvent evaporation. The glass transition temperature was determined at the mid-height or inflexion point in the reversible heat flow or equivalently the maximum in the peak of the time derivative of Reversible C_p.

2.2.3.2 Dielectric Spectroscopy

In dielectric spectroscopy, the response of a dielectric polymer sample to an electric field is measured. Under the action of a frequency dependent electric field $E(\omega)$, the dipoles present in the material can reorient to better align with the field (Figure 2.11). Other effects like charge

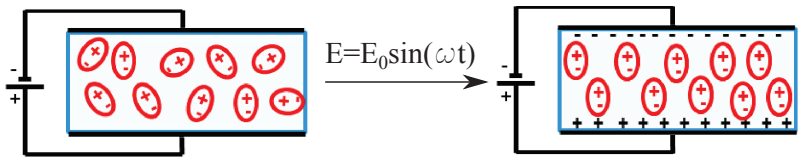

Figure 2.11: Schematic representation of dipole orientation (polarization) in a polymer film between two electrodes when an electrical field is applied

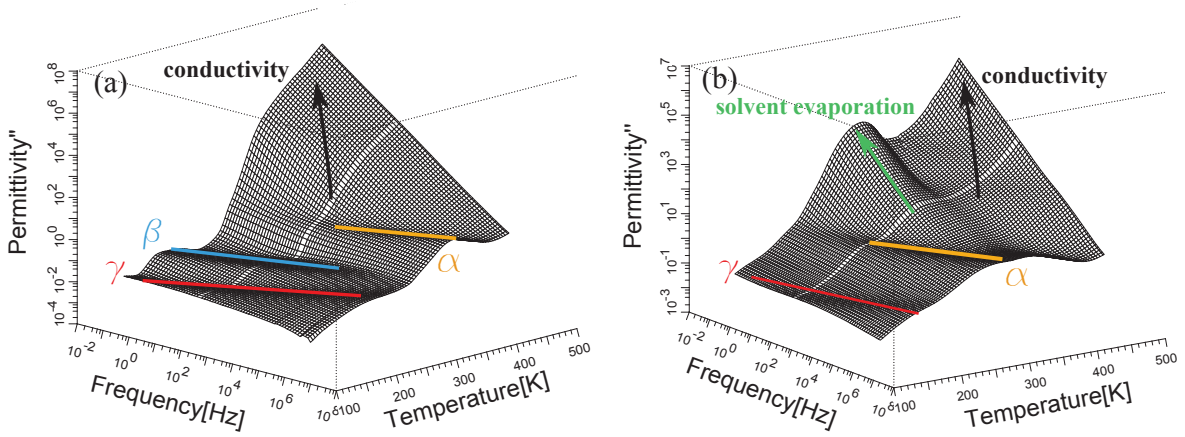

Figure 2.12: 3D map of loss permittivity ε'' as a function of frequency and temperature for (a) dry PA6,10 and (b) ethanol saturated PA6,10

transport and interfacial polarization can also take place. The relaxation processes can be identified in the variations of the frequency dependent complex permittivity $\varepsilon^*_{dielec}(\omega) = \varepsilon' + i\varepsilon''$, or equivalently complex modulus $M^*_{dielec}(\omega) = \frac{1}{\varepsilon^*_{dielec}(\omega)}$ or complex conductivity $\sigma^*(\omega)$.

As presented in Chapter 1, three main relaxation processes (α, β, γ) due to rotational fluctuations of the molecular dipoles have been identified in polyamide [26]. Motions involved in the α and β relaxations may potentially be coupled to or influenced by the motions of solvent molecules [126, 127, 128, 34]. *Therefore, the present study will focus on these processes. Their corresponding relaxation times have been measured by dielectric spectroscopy as a function of temperature and at various solvent concentrations.*

The output signal in dielectric spectroscopy is a 3-dimension (3D) map of the permittivity as a function of frequency and temperature (Figure 2.12). Loss permittivity ε'' is preferred for the analysis of the data, since each relaxation can be easily indentified by a peak. Other processes (e.g. conductivity, solvent evaporation) are also visible in this representation. These processes can be more intense than the polymer relaxations and thus limit the analysis range.

For the data analysis, isochronal (constant frequency, varying temperature, similar to a Dynamic Mechanical Analysis) or isothermal (constant temperature, varying frequency) representation can be used. The isothermal representation is generally preferred because it gives access to the distribution of relaxation times at each temperature. However, the fitting of the data is not trivial.

The most simple model for the distribution of the relaxation times is the Debye model [26], which assumes that a relaxation has a single characteristic time at a certain temperature (Figure 2.13). The complex dielectric permittivity is given by:

$$\varepsilon^*(\omega) = \varepsilon_\infty - \int_0^\infty \frac{d\varepsilon}{dt} \exp(-i\omega t) dt \tag{2.7}$$

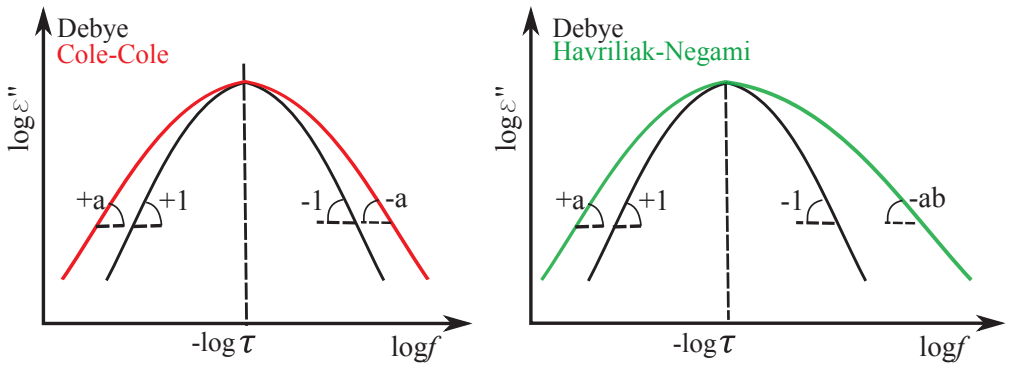

Figure 2.13: Models for describing the isothermal relaxation spectrum obtained in Dielectric Spectroscopy [26]

which gives equation (2.8), in which ε_∞ is the permittivity at infinite temperature, $\Delta\varepsilon$ is the intensity of the relaxation, τ_D is the Debye relaxation time:

$$\varepsilon^*(\omega) = \varepsilon_\infty + \frac{\Delta\varepsilon}{1 + i\omega\tau_D} \tag{2.8}$$

A Debye-like relaxation behavior is rarely observed. Usually the measured dielectric functions are much broader than predicted by the Debye function. Broadened relaxation processes can be formally described by a superposition of Debye functions with different relaxation times:

$$\varepsilon^*(\omega) = \varepsilon_\infty - \Delta\varepsilon \int_{-\infty}^{\infty} L(\tau)\frac{1}{1 + i\omega\tau}d\tau \tag{2.9}$$

where $L(\tau)$ is the relaxation time distribution function.

For practical use, empirical models have been developped to describe the complex permittivity. For example, the Cole-Cole model [26] ((Figure 2.13)) accounts for a symmetrical broadening of the relaxation times by introducing an exponent a (0<a<1) at the denominator:

$$\varepsilon^*(\omega) = \varepsilon_\infty + \frac{\Delta\varepsilon}{1 + (i\omega\tau)^a} \tag{2.10}$$

The most complete is the Havriliak-Negami model[129, 26], which allows an assymetrical broadening of the relaxation times ((Figure 2.13)). Havriliak-Negami model is expressed by equation (2.11), in which a and b are the Havriliak-Negami exponents following conditions $0<a<1$ and $ab<1$. Debye and Cole-Cole are specific cases of the Havriliak-Negami equation with ($a=1$ and $b=1$) and $a=1$ respectively.

$$\varepsilon^*(\omega) = \varepsilon_\infty + \frac{\Delta\varepsilon}{(1 + (i\omega\tau)^a)^b} \tag{2.11}$$

In practice, a relaxation spectrum will be fit by a sum of Havriliak-Negami functions and other contributions if present (conductivity, electrode polarization etc.). It is well-established that secondary relaxations are generally symmetric so the exponent b is fixed at one in this case. An exemple of a data fit is shown in Figure 2.14. This example clearly shows that two distinctive peaks, corresponding to distinct relaxation processes, must be used in order to fit the β relaxation in a PA6,10 film.

The α relaxation time τ_α is often difficult to measure because it is accompanied by a strong increase of the sample conductivity. For amorphous polyamides, τ_α was determined from the Havriliak-Negami fit of isothermal relaxation spectra. For semi-crystalline polyamides, τ_α

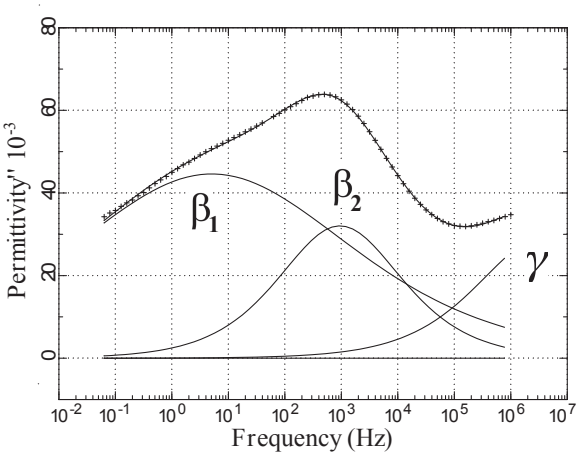

Figure 2.14: Example of an isothermal relaxation spectrum (markers) and its fit by summing three Havriliak-Negami functions (solid line curves) in the region of the β relaxation (PA6,10 at T=255K)

was determined by using the maximum of the loss permittivity and/or the loss modulus in isochronal curves (Figure 2.15). Although this method may seem less precise than fitting the relaxation curves in isothermal representation, it was preferred because it provides relaxation times over a larger temperature range. When both isochronal and isothermal representations could be used, it was checked that the data coincide. The loss modulus representation is less sensitive to contributions from sample conductivity and gives a well-defined peak. The values obtained from the loss modulus are shifted with respect to the values obtained from the loss permittivity but allow a verification of the latter. A typical curve of obtained τ_α is shown in Figure 2.16. As it can be seen, the two curves are roughly parallel but shifted in frequency.

A Novocontrol Alpha Analyzer and a Quatro temperature control system were used to conduct experiments under a voltage of 3V in the temperature range of −130 to 200°C with 4°C steps. For each temperature, the frequency range was 10^{-2} Hz to 10^6 Hz (Broadband Dielectric Spectroscopy - BDS). For dry samples, additional experimental points in the frequency range 10^6 Hz to 10^9 Hz were obtained by High Frequency Dielectric Spectroscopy (HFDS) under a voltage of 0.5 V in the temperature range −130 to 200°C with 1°C steps. The HFDS measurements were done at the Centro de Fisica de Materiales in San Sebastian (A. Alegría, S. Arrese-Igor) under an European Soft Matter Infrastructure grant (no. 262348). Polymer films were cut into disks of 30 mm (BDS) and 10 mm (HFDS) diameter and placed between gold plated electrodes. For solvent-equilibrated samples, the electrode/polymer film/electrode sandwich was immediately quenched at −130°C to avoid solvent evaporation. Measurements were performed on heating. Polymer films kept a constant weight up to 25 – 35°C, depending on the initial solvent concentration. Above this temperature, solvent evaporation started to occur as was illustrated by the decrease in the real part of permittivity ε'.

2.2.3.3 Low-resolution ^{1}H Nuclear Magnetic Resonance (NMR)

Proton NMR transverse magnetization relaxation experiments (T_2 relaxation) are commonly used for the investigation of morphology and molecular mobility in polymers [55, 130]. This technique consists in measuring the NMR response (Free Induction Decay - FID) upon excitation of a polymer sample with a radio frequency magnetic pulse. The measured signal is an average of all the contributions from the sample protons. When the sample is semi-crystalline, the hard (crystalline) and soft (amorphous) regions have different decay times. Rigid, dense protons in

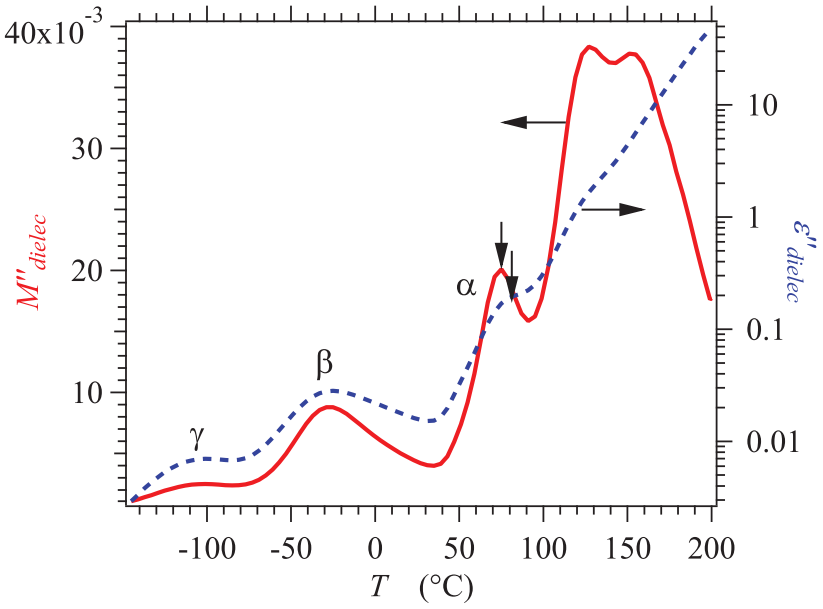

Figure 2.15: Isochronal representation of loss permittivity (dotted curve) and loss modulus (full curve) as a function of temperature for dry PA6,6 at the frequency of 133 Hz. The maximum of the α relaxation peak is pointed by arrows.

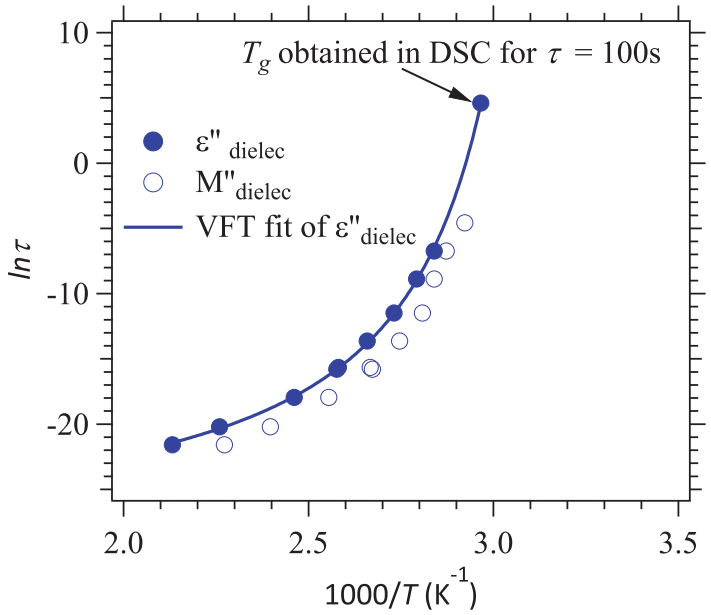

Figure 2.16: Relaxation times as a function of temperature obtained from ε''_{dielec} and M''_{dielec} isochronal representation for dry PA6,6. Solid line represents a Vogel-Fulcher-Tammann (equation (1.4)) fit of the data.

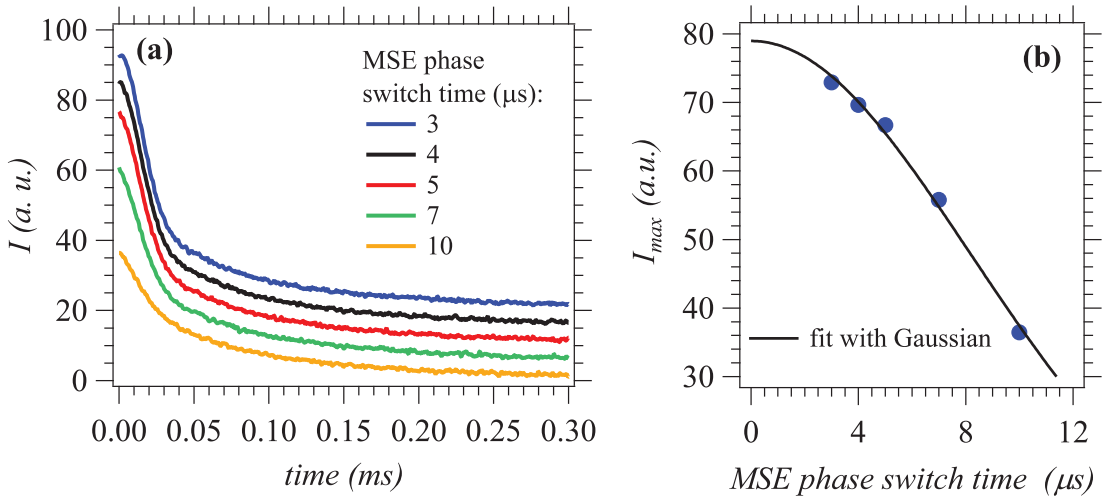

Figure 2.17: PA6,6 100 μm film at 125°C (a) MSE signals at different phase switch times. The curves were offset vertically by 5 units for clarity. (b) Maximum intensity of the MSE signal as a function of the phase switch time. The solid line corresponds to the fit with a Gaussian function.

the crystalline phase have limited orientation freedom so their signal decays fast, within 20 μs [130]. The signal from more mobile protons in the amorphous phase takes longer time to decay, of the order of hundred μs.

Proton low-resolution NMR T_2 relaxation experiments were performed on a Bruker Minispec MQ-20 spectrometer, operating at a proton resonance frequency of 20 MHz. The temperature gradient within sample volume was less than 1°C. Temperature control was ensured by a BVT3000 unit within an accuracy of ±0.1°C. The polymer films were cut into 8 mm diameter disks. The disks were stacked in the NMR tube up to a height of maximum 5 mm. For samples swollen with deuterated water (D_2O), the solvent was added at this step in sufficient amount to cover the polymer films. The NMR tube was flashed with dry argon to remove air that contains water vapor. The tube was then rapidly sealed with a cover and parafilm. The measurement temperature range was -50 to 160°C for dry samples and -50 to 90°C for D_2O-saturated samples.

The NMR spectra were first recorded with a Free Induction Decay (FID) method, in which a 90° pulse excitation is applied and the amplitude of the transverse magnetization is recorded after a dead time. The initial part of the FID is therefore not detected after the 90° pulse excitation because of the dead time of the receiver (typically 0.015 ms). The initial part of the transverse magnetization decay is essential for a quantitative deconvolution of the spectrum in the structural components (crystalline, rigid and mobile phase) [55]. Therefore, a Magic Sandwich Echo (MSE) sequence was used with variable phase switch times τ_{MSE} (3, 4, 5, 7 and 10 μs). The principle of MSE can be found in Maus *et al.* [130]. MSE has the advantage of avoiding the dead time of the spectrometer. The measured signal depends on the phase switch time, as it is illustrated in Figure 2.17(a). The MSE intensity decreases as τ_{MSE} increases; the rigid component (starting at t=0) is not quantitative because the efficiency of the sequence is not 100% for the rigid signal. The maximum of the MSE signal is plotted as a function of the phase switch time in Figure 2.17(b) and fitted with a Gaussian function. The intensity of the MSE at $\tau_{MSE} = 3\ \mu s$ is very close to the extrapolated value at $\tau = 0$, supposed to represent the "exact" value. Thus, MSE signals at $\tau_{MSE} = 3\ \mu s$ were used to obtain the phase composition.

A comparison of FID and MSE signals can be found in Figure 2.18(a). Indeed, the FID and MSE signals are almost identical for $\tau_{MSE} = 3\ \mu s$ (for time > 15 μs). A three phase model (rigid,

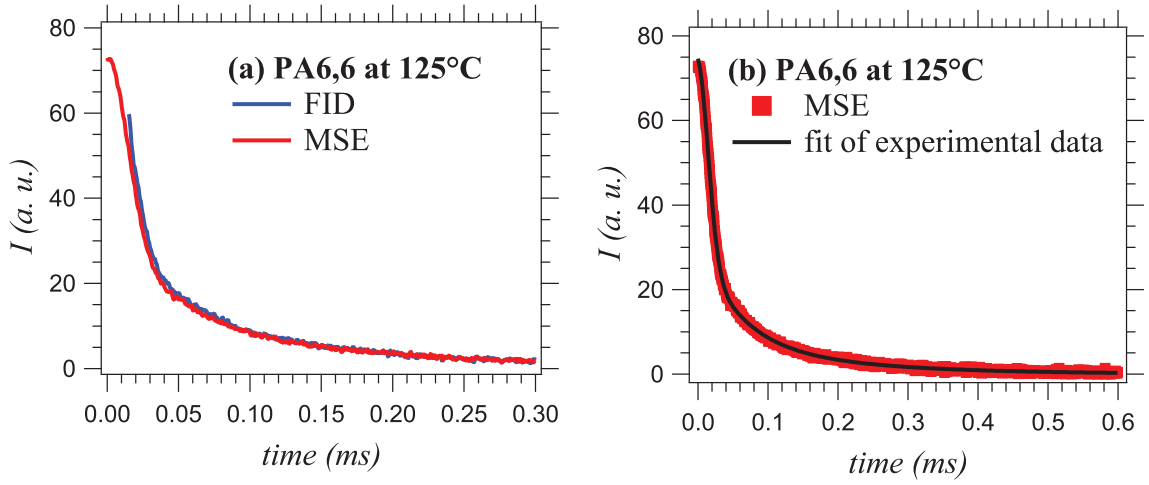

Figure 2.18: PA6,6 100 μm film at 125°C (a) FID and MSE spectra and (b) fit of MSE experimental data with a three component equation (2.12)

semi-rigid and soft) is used to fit the data, following the procedure by Litvinov *et al.* [55]. First the MSE, then the FID spectra are fitted with the 3-component equation (2.12), which is a linear combination of a Gaussian and two exponential functions.

$$I(t) = I(0)^s exp\left(-\left(\frac{t}{T_2^s}\right)^2\right) + I(0)^i exp\left(-\frac{t}{T_2^i}\right) + I(0)^l exp\left(-\frac{t}{T_2^l}\right) \tag{2.12}$$

The superscripts s, i and l stand for short, intermediate and long decay time, which are associated to the rigid, semi-rigid and soft phase, respectively. The relative intensity of each component gives its proportion in the material in terms of number of protons. An example of the fit of the MSE experimental data with equation (2.12) is shown in Figure 2.18(b).

In order to validate that low-resolution NMR provides a good estimation of the phase composition, mixtures of poly(methyl methacrylate) (PMMA) and poly(dimethylsiloxane) (PDMS) were measured. PMMA has a glass transition temperature of 105°C and acts as a rigid phase at room temperature, whereas PDMS has a glass transition temperature of -125°C and acts as a mobile phase at room temperature. PDMS/PMMA mixtures of determined composition in weight percentage were prepared: 0/100, 40/60, 50/50, 80/20, 100/0. The spectra for all compositions at 30°C are shown in Figure 2.19. It can be observed that PDMS and PMMA present the typical relaxations of a mobile and rigid matrix, respectively. The mixtures are intermediate cases, containing the signal of both components. A decomposition of the signal in a rigid and mobile component gave the same phase percentages as the prepared mixtures, within a ±5% error. Indeed, low-resolution NMR is a powerful technique for determining phase composition.

2.2.4 Sorption experiments

2.2.4.1 Sorption of liquid solvents

Several solvents of different size and polarity were chosen for this study. The complete list and their physical properties can be found in Table 2.6.

Polymer films were immersed in liquid solvents (Figure 2.20(a)) and removed regularly for weighing following a standard procedure: removal from sorption cell, pressing between absorbent paper, surface drying with compressed air, record of weight exactly at 1 minute after removal from sorption cell, re-immersion. The mass intake is recorded as a function of

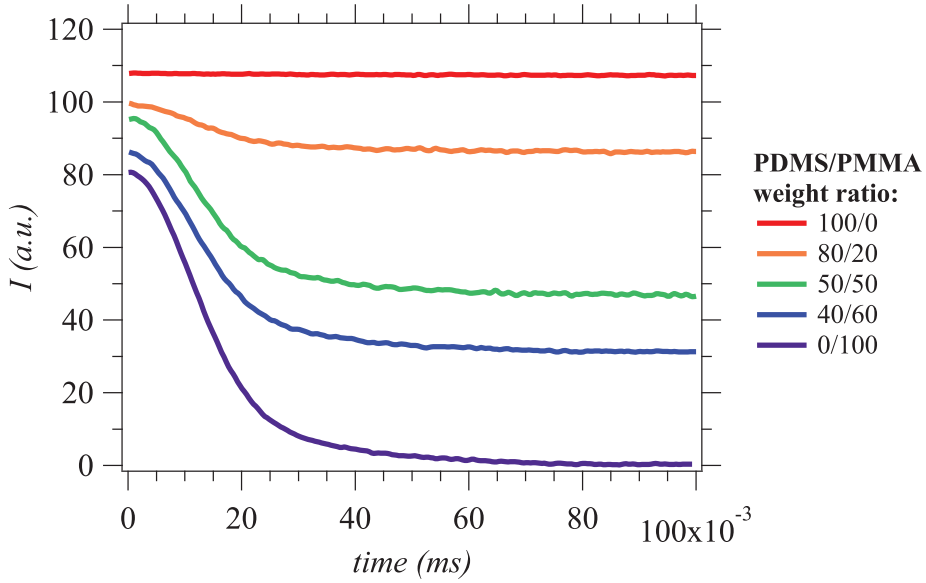

Figure 2.19: MSE spectra of PDMS/PMMA mixtures at 30°C. The curves were offset vertically for clarity.

Solvent	Water	Methanol	Ethanol	Ethylene glycol	2-propanol
Chemical structure	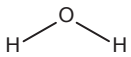		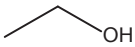	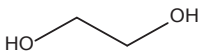	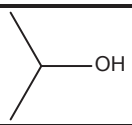
Density at 23°C (g/cm^3)	1	0.792	0.789	1.113	0.803
Boiling point (°C)	100	64.7	78.4	197.3	97.1
Molar volume at 25°C (cm^3/mol)	18	40.7	58.5	55.8	76.8
Dipole moment (x10^{30} C m)	6.7	5.5	5.7	6.7	5.5

Table 2.6: Chemical structure and physical properties of selected solvents [131, 132]

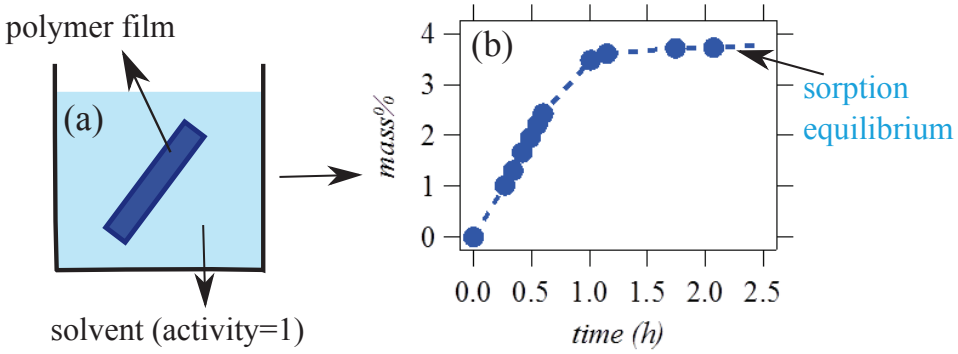

Figure 2.20: (a) Illustration of the sorption experiment in liquid solvent and (b) Example of a curve for mass increase as a function of time

immersion time (Figure 2.20(b)). Measurements were done at temperatures between 25 and 180°C, depending on the solvent and the polymer sample.

The mass percentage of solvent at time t was determined with equation (2.13) as a function of the mass of the polymer film at time t and the mass of the dry film m_0. Another representation is the normalized mass intake, with respect to the mass intake at equilibrium m_{eq} (equation (2.14)).

$$m\%(t) = \frac{m(t) - m_0}{m_0} \times 100 \tag{2.13}$$

$$\frac{M(t)}{M_{eq}} = \frac{m(t) - m_0}{m_{eq} - m_0} \tag{2.14}$$

Last, a useful quantity in these systems with specific sorption sites is the molar intake, *i.e.* the ratio of solvent molecules per amide groups in the amorphous phase:

$$\Delta n = \frac{n_{solvent}}{n_{amidegroups}} = \frac{m\% \times M_{PA}}{100 \times M_{solvent} \times (1 - \chi_C)} \tag{2.15}$$

where M_{PA} is the molecular weight/amide group (113 g/mol for PA6,6 and 141 g/mol for PA6,10), $M_{solvent}$ is the solvent molecular weight and χ_C is the crystalline ratio.

Demineralized water and absolute polar solvents were used for this study. However, it should be highlighted that the sorption cells are open systems in contact with ambient atmosphere. Under these conditions, the initially water-free polar solvents absorb water from air humidity until the thermodynamic equilibrium of solvent/water system is attained. Based on the phase diagram of water/ethanol mixtures at temperature T, one can calculate the amount of water that will be absorbed by ethanol if left at ambient atmosphere. For example, at 40 °C and 50% humidity in the air, a liquid ethanol/water mixture will contain 12% water. In order to avoid this phenomenon, a dessicant (molecular sieves) was added to the ethanol. In spite of this precaution, water was still absorbed by the polymer film. A Karl Fischer dosage allows to quantify the amount of water. For all our polyamide films, a maximum of 1-2% weight of water was absorbed in the same time as the polar solvents. For additional information on this experimental issue, a thorough description can be found in Appendix A.

2.2.4.2 Sorption of water at activity *a* using saturated salt solutions

For film conditioning with water at intermediate activities, two strategies were adopted. For water activity 0.5, the films were kept in a Solvay humidity-conditioned laboratory. For film

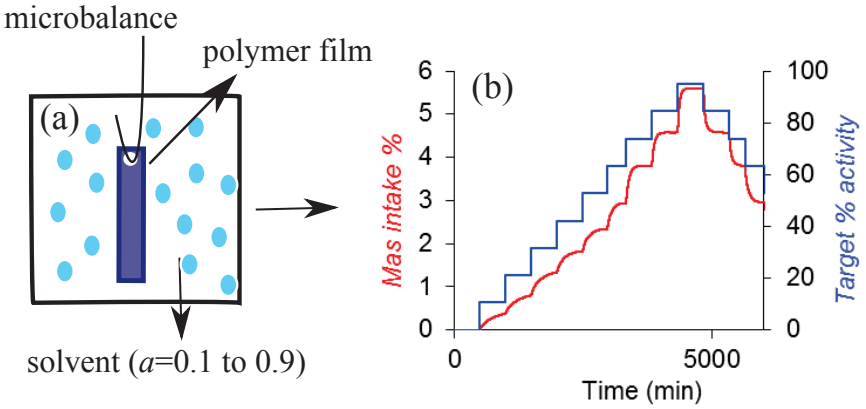

Figure 2.21: (a) Illustration of a Dynamic Vapor Sorption experiment in a solvent at activity a (b) Example of a sorption/desorption DVS curve for mass increase as a function of time, for successive values of activity

conditioning at activities 0.11, 0.33, 0.75 and 0.84, saturated salt solutions (LiCl, $MgCl_2$, NaCl, KCl) were used at room temperature (20°C). The humidity in the atmosphere above a saturated salt solution is tabulated in the literature [133] as a function of temperature. The saturated salt solution was placed at the bottom of a desiccator. The polymer film was left several days above the saturated salt solution in the closed desiccator until sorption equilibrium was reached. The conditioned films were used for Differential Scanning Calorimetry and Broadband Dielectric Spectroscopy measurements.

2.2.4.3 Sorption of intermediate concentrations of alcohols

For film conditioning at intermediate concentrations of alcohols (ethanol, ethylene glycol), the films were immersed in liquid solvent and the sorption was stopped when the desired concentration was reached. The films were then hot-sealed in an envelope and left to equilibrate for several months. During this period, there was few or no weight loss. DSC showed only one glass transition temperature, meaning that the solvent concentration was homogeneous throughout the film.

2.2.4.4 Dynamic Vapor Sorption (DVS)

A DVS Advantage device was used for the sorption of water and ethanol vapor at controlled activity ($a = P/P_{sat}$). In a DVS Advantage Analyzer, the polymer film is fixed on a ultra-microbalance hook inside a sample chamber (Figure 2.21(a)). Inside the chamber, a fixed value of solvent activity is obtained by mixing a flux of dry and solvent saturated nitrogen. Precise control of the ratio of saturated and dry gas flow is enabled with mass flow control combined with the use of real time vapor concentration monitoring. The internal ultra-microbalance (precision ± 0.0001 g) measures the change in weight of the polymer film. A typical DVS sorption/desorption curve is presented in Figure 2.21(b).

Before sorption, the films were dried under vacuum at 110 °C and then also dried inside the DVS chamber under nitrogen flow until their weight was stable. Activity steps of 0.1 were then applied in the range of 0.1 to 0.9. Each activity was maintained until the sorption equilibrium was reached. After equilibrium at activity a, the next activity $a+0.1$ is set almost instantaneously (equilibration time of new activity is shorter than 1 minute) and a new mass intake is recorded. Water sorption measurements were done at 29, 35, 40 and 51°C for PA6,6 and 29, 40 and 51°C

for PA6,10. For the two polymers, measurements at 51°C stopped at activity 0.4 for PA6,6 and activity 0.6 for PA6,10 because the experimental temperature was too close to the limit of the machine (60°C). Ethanol sorption was measured at 40 °C both for PA6,6 and PA6,10.

2.2.5 Rheometry

2.2.5.1 Small strain dynamic oscillatory measurements

Small strain dynamic oscillatory shear measurements were performed using an Advanced Rheometric Expansion System (ARES, from TA Instruments) strain-controlled rheometer equipped with an active Force Rebalanced Transducer 2kFRT-N1. Dry samples (less than 500 ppm water, as determined by Karl Fischer dosage) were placed between two 4 or 8 mm invar plates (Fe-Ni alloy with a low thermal expansion coefficient). Temperature was controlled with a forced convection oven and a nitrogen dewar. The temperature variation in the convection oven was better than ±0.2 °C. The polymer was molten at high temperatures (200-220°C for PA6I, 230°C for PA6HIA, 210°C for PA6I/6LiSIPA) and left to relax until the plate-plate geometry was correctly filled. The gap was always between 1.4 and 2 mm. Firstly, Time and Strain Sweeps were performed to check for polymer stability and determine the limits of the linear viscoelastic domain. Subsequently, frequency sweeps (100 to 0.1 rad/s, with a strain in the linear viscoelastic domain) were performed at different temperatures. For each temperature, the gap was adjusted so as to account for the thermal expansion of the plates. After each measurement series, the temperature was brought back to the initial value and a final frequency sweep was performed to check for polymer evolution by comparing with the initial frequency sweep. Temperature range was between 110 and 210°C for the PA6I samples, 155 and 200°C for PA6HIA, 127 and 210°C for PA6I/6LiSIPA.

A rheometer operating at a temperature T can usually provide dynamic information over only a few decades of time or frequency. Especially for polymer melts, this in generally insufficient to cover the variation of relaxation moduli from the glassy to the flow regime. However, it was observed in some cases that data obtained at several temperatures could be made to overlap by shifting them horizontally and vertically in order to obtain a mastercurve [77]. This process, illustrated in Figure 2.22, is called time-Temperature superposition (tTS). A material to which this technique can be applied is said to be thermorheologically simple.

Generally, loss and storage moduli are shifted vertically with a factor b_T calculated from:

$$b_T = \frac{\rho(T_{ref})T_{ref}}{\rho(T)T} \tag{2.16}$$

The vertical shift factors are hence not fitted and their value is close to 1. The horizontal shift factors a_T, on the other hand, are large and are determined by an error minimization method. Their dependency on temperature is more complex and can be generally described by a Williams-Landel-Ferry (WLF) [134] equation, for $T > T_g$:

$$\log a_T = -\frac{C_1(T - T_{ref})}{C_2 + T - T_{ref}} \tag{2.17}$$

where C_1 and C_2 are empirical constants. The WLF equation can be derived from the empirical Doolittle equation that relates viscosity to fractional free volume. C_1^g is related to the fractional free volume at glass transition temperature and C_2^g is related to the Vogel temperature (temperature where the free volume is zero). C_1^g and C_2^g were initially considered universal constants with the values 17.4 and 51.6 respectively [134]. Later, it was shown that they vary from one polymer to another. Typical values of the product $C_1^g C_2^g$ are in the range 449 to 2305, compared to the approximate "universal" value of 900 [77].

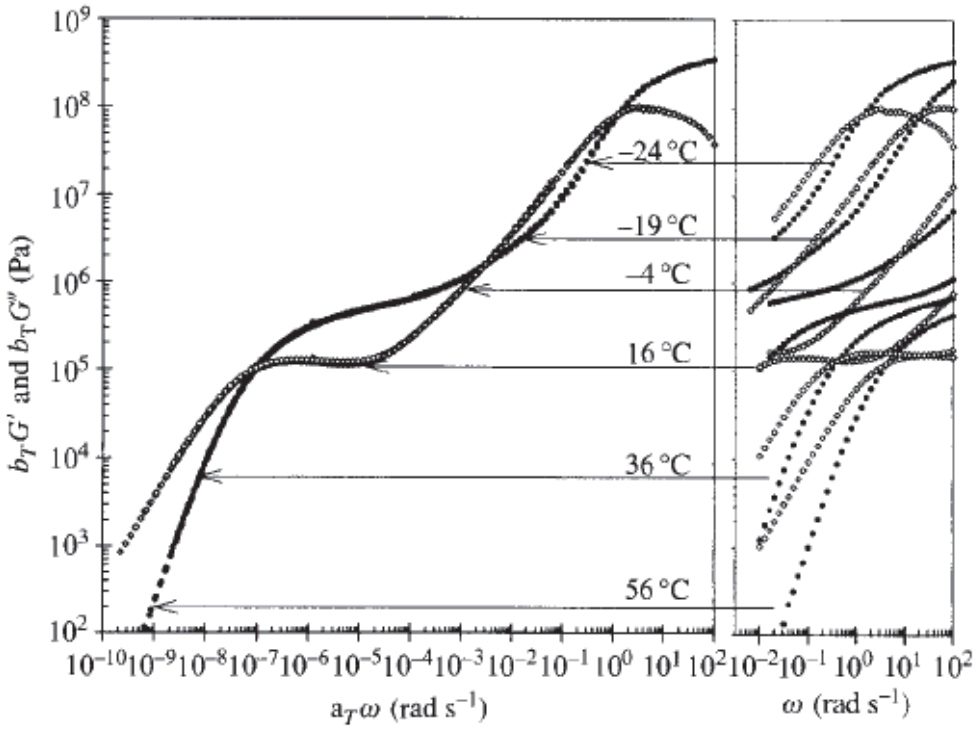

Figure 2.22: Illustration of the time-temperature superposition principle, using oscillatory shear data (G′, G″) for a poly(vinyl methyl ether) melt with M_w=124000 g/mol. The right-hand plot shows the data that were acquired at the six temperatures indicated, with T_g=-24°C chosen as reference temperature. From [7]

A material shows the so-called thermorheological simplicity when all relaxation mechanisms which are active on the experimental timescale have the same dependency on temperature. This condition is often valid for many polymers. For other systems, tTS fails and they are called thermorheologically complex (*e.g.* interacting polymers in Section 1.5.3). The quality of a tTS can be misleading if the assessment is done only based on graphical considerations. A summary of the methods to detect thermorheological complexity can be found in reference [135]. Nevertheless, a mastercurve representation can be useful even if the material is thermorheological complex. In this case, the master curve provides a general idea on the polymer behavior but no exact information can be extracted.

In our case, time-temperature superposition was applied by shifting experimental data horizontally and vertically to a reference temperature T_{ref}. When tTS did not work on the whole temperature range, T_{ref} was chosen as the lowest temperature for which tTS was still valid. Since the polymers density does not vary much in the tTS temperature range (results of molecular modelling for PA6I in [136]), the vertical shift factor was calculated based only on temperature variation assuming a constant temperature independent density. This is justified as the vertical shift factors are small in any case and measurements were only performed over small T ranges over which the density is not expected to vary much. The horizontal shift factors were fitted with a WLF equation (equation (2.17)). The obtained parameters C_1 and C_2 were used to calculate the horizontal shift factor at T_g. Then, mastercurves at T_{ref} were shifted to T_g by rescaling them with the horizontal and vertical shift factors at T_g.

2.2.5.2 Creep

To access longer times, creep measurements in the linear viscoelastic region were performed on a stress-controlled Anton Paar rheometer (Physica MCR301, Austria) in the Ingénierie des Matériaux Polymère laboratory in Saint-Etienne (J.-C. Majesté). Dry samples (less than 500 ppm water) were placed between 8 mm disposable parallel plates. Temperature was controlled with compressed air and the temperature variation in the convection oven was ±0.1 °C. The polymer was molten at 160°C for PA6I and 200°C for PA6HIA and left to relax until the plate-plate geometry was correctly filled. The gap was between 1.4 and 1.8 mm. For PA6I 2k, measurements were performed between 110 and 120 °C. For PA6HIA, measurements were performed between 155 and 165°C. At each temperature, a dynamic frequency sweep was done first. Then, creep measurements were done at three different stresses: 50, 100 and 300 Pa. An example of curves at different stresses is shown in Figure 2.23. Measurements took between 20 min and 3 hours, depending on the temperature. The three curves generally superimposed, except at short times in some cases. Only the data where the superposition worked were used.

The creep compliance data can be transformed into dynamic moduli, as presented in Chapter 1. Since the conversion itself was not the scope of this work, two external programs have been used to obtain dynamic moduli: NLReg (from Honerkamp *et al.* [137]) and Compliance to Complex Moduli V3 (from Evans *et al.* [78]). Both methods gave similar results (Figure 2.24) and a good superposition to the dynamic data. NLReg was chosen because the curves are smoother. This data was not used in the assessment of the influence of interchain interactions on viscoelasticity and is presented in Appendix D.

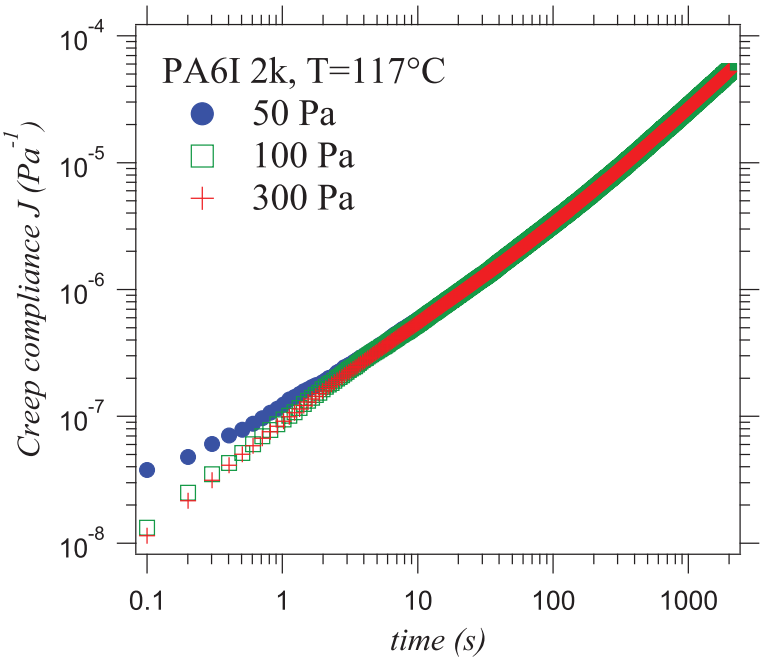

Figure 2.23: Example of creep measurement curves at three different stresses for PA6I 2k at 117°C

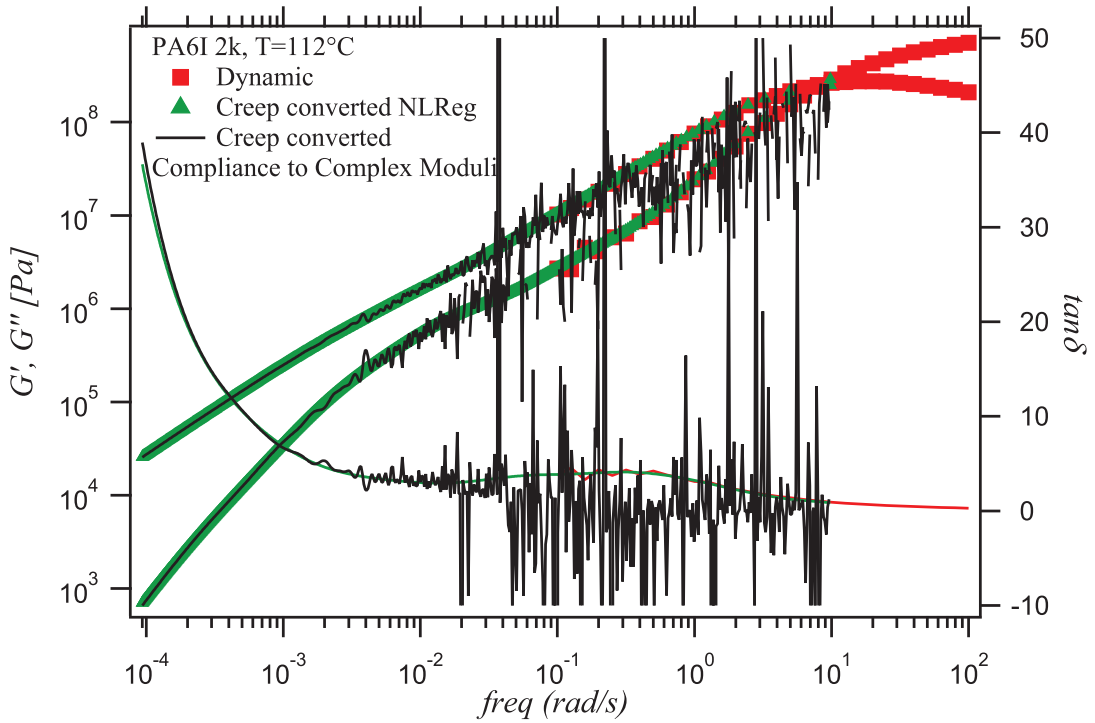

Figure 2.24: Example of creep compliance conversion to dynamic moduli by using NLReg and Compliance to Complex Moduli programs for PA6I 2k at 112°C

Chapter 3

Influence of crystalline phase on diffusion and sorption in polyamide

As presented in Chapter 1, both diffusion and sorption are influenced by the existence of a crystalline phase in polymers. For instance, diffusion coefficients in a semi-crystalline polymer might be inferior to those in an amorphous polymer because of increased tortuosity on the diffusion path and chain immobilization next to the crystals. In the case of sorption, a fraction of the amorphous phase might not be accessible to solvents. Sorption and diffusion are strongly influenced by the crystalline phase (lattice type, crystalline ratio), which is intimately related to processing method and conditions. If we want to compare two solvents of different size and polarity in the same polyamide matrix, more information is needed on their accessibility in the amorphous phase. Also, if we want to compare two polyamide matrices with different crystalline ratios and/or prepared by different processing conditions, a knowledge of their phase distribution is essential. To the best of our knowledge, no study has been reported for comparing a 100% amorphous polyamide and its semi-crystalline polyamide of analogous chemical structure. Chapter 3 will thus attempt to ellucidate if the amorphous phase of a semi-crystalline polyamide behaves as a 100% amorphous polyamide for sorption and diffusion of solvents.

3.1 Effect on diffusion coefficients

To begin with, the influence of crystallinity on diffusion was analyzed by comparing the 100% amorphous polyamides PA6I and Selar to the semi-crystalline A1007 (pristine or annealed) of equivalent chemical structure. Water and alcohols of different sizes (methanol, ethanol, ethylene glycol and propanol) were used as solvents. Mass intakes were measured at 25, 40 and 55°C.

3.1.1 Sorption kinetics of water

In order to analyse diffusion mechanisms, the normalized mass intake is represented as a function of the square root of time. Water sorption kinetics curves are illustrated for the four polymers in Figure 3.1.

As temperature increases, sorption kinetics become faster, which is in agreement with diffusion being a thermally activated process. Similar kinetics are observed for all samples, independently of the amorphous or semi-crystalline character. The normalized mass intake increases linearly with the square root of time for all polyamides, suggesting a Fickian diffusion mechanism. Indeed, equation (1.11) for Fickian diffusion gives an excellent fit of experimental data and provides the values of diffusion coefficients (Table 3.1). It should be noted that the obtained values of diffusion coefficients are very sensitive to the measured film thickness. A typical variation of $\pm 10 \mu m$ on the film thickness gives an uncertainty of ±10% on the values of the diffusion coefficients (main source of error). The variability on diffusion coefficients among different polymer films (repetability for one temperature) is indeed in the ±10% range.

The values of the diffusion coefficients are similar for all temperatures within the ±10% uncertainty range. Therefore, it would seem that the semi-crystalline structure has no influence on the diffusion of water. Assuming that the diffusion coefficient dependence on temperature

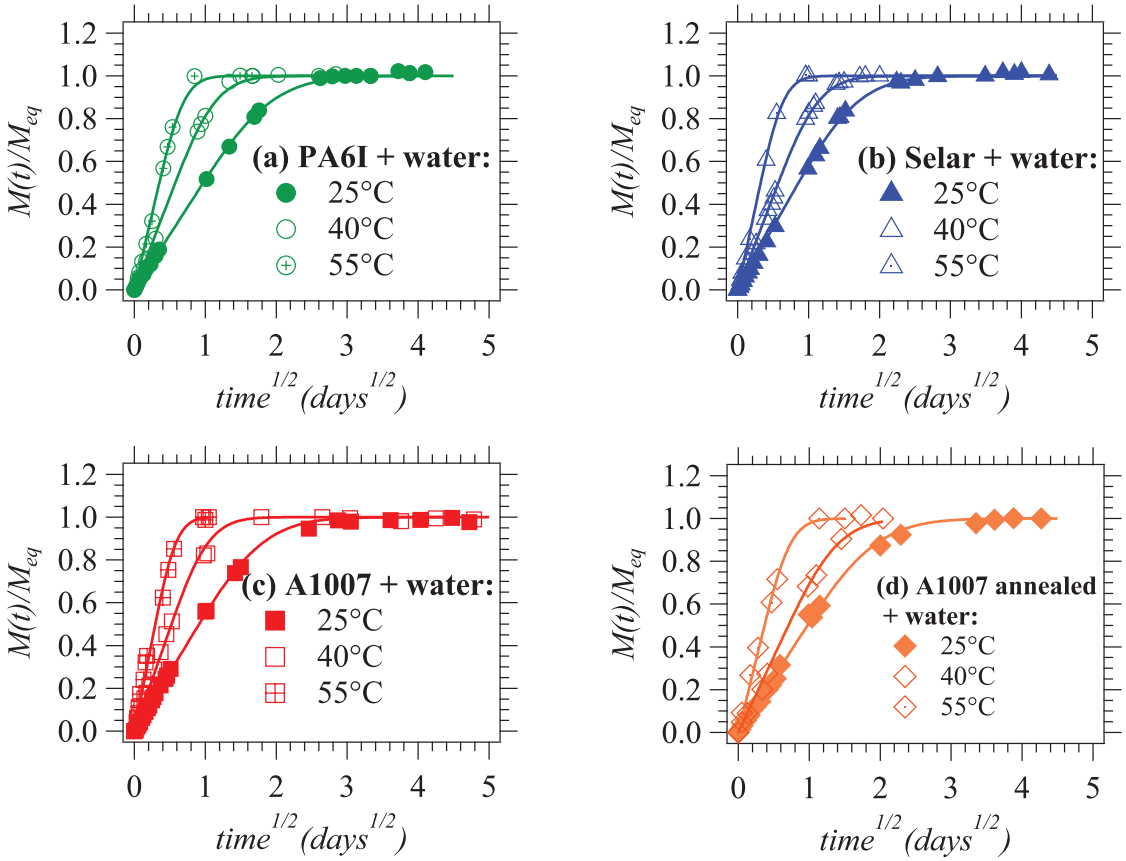

Figure 3.1: Sorption kinetics of liquid water at 25, 40 and 55°C in amorphous (a) PA6I (b) Selar and semi-crystalline (c) A1007 (χ_C = 16%) and (d) A1007 annealed (χ_C = 26%). Solid lines are obtained by fitting the data with equation (1.11) for Fickian diffusion.

	D (cm^2/s) at 25°C	D (cm^2/s) at 40°C	D (cm^2/s) at 55°C
PA6I	$5.4\ 10^{-10}$	$1.5\ 10^{-9}$	$4.1\ 10^{-9}$
Selar	$7.0\ 10^{-10}$	$1.6\ 10^{-9}$	$4.9\ 10^{-9}$
A1007	$6.2\ 10^{-10}$	$1.9\ 10^{-9}$	$5.8\ 10^{-9}$
A1007 annealed	$5.5\ 10^{-10}$	$1.0\ 10^{-9}$	$3.7\ 10^{-9}$

Table 3.1: Water diffusion coefficients in amorphous and semi-crystalline PA, obtained from the fit of experimental curves with equation (1.11) for Fickian diffusion

follows an Arrhenius law, an activation energy of 55 kJ/mol is obtained for the diffusion of water in these polyamides. This value is close to the range of 60 to 80 kJ/mol activation energies reported for diffusion of water in other polyamides [2, 14].

Before any interpretation, it is crucial to check the integrity of the samples. This resumes to verifying if there are structural changes and/or formation of cavities in presence of water.

To begin with, XRD scans were recorded before and after water sorption (Figure 3.2). As it can be seen in Figure 3.2, PA6I and Selar XRD scans have the typical shape of amorphous polymers. A1007 and A1007 annealed present crystalline peaks in positions close to the typical values for polyamide: 10° for (002) plane, 18.5° for (100) plane and 22° for (010)/(110) planes. The peak at 20° could correspond to the amorphous halo. Compared to known values for PA6,6 (see Chapter 1), the 2θ values are shifted towards smaller angles, *i.e.* larger distances d between crystalline planes. To the best of our knowledge, there is little information on the crystalline lattice of PA6T, which is the crystalline moiety of the A1007 copolymer of PA6I and PA6T.

The volume of the crystalline lattice can however be estimated from density considerations. One value was found in the litterature for the density of a pure PA6T polymer of medium crystalline fraction (1.2447 g/cm^3) [138]. The density of the PA6T amorphous phase can be estimated at 1.23 g/cm^3, based on the density values of a pure amorphous PA6I (1.16 g/cm^3 [136]) and an amorphous PA6I/6T 70/30 (Selar DuPont from this study, 1.19 g/cm^3 in the Material Safety Data Sheet). If we assume a medium crystalline ratio value of 30% for the pure PA6T in reference [138], a density of 1.28 g/cm^3 is obtained for the crystalline phase of PA6T. Considering a number of 4 monomers/crystalline lattice, the volume of a PA6T crystalline lattice is estimated at 1.22 nm^3. This value is higher than the volume of a PA6,6 crystalline lattice, estimated to 1.17 nm^3 based on the density of 1.23 g/cm^3 for the PA6,6 crystalline phase [14]. Therefore, it would seem that the volume of a crystalline lattice is slightly higher in PA6T than in PA6,6, which explains the shift towards higher values of d-spacing.

Back to Figure 3.2, the annealed films have better resolved crystalline peaks, indicating the existence of a more perfect crystalline lattice. Overall, there is no significant difference between the XRD scans of the dry and water saturated polymer films. These amorphous polyamides do not crystallize in presence of water, contrary to what was reported in the literature for PA6I [72].

Additionnally, the crystalline fraction of A1007 and A1007 annealed was measured after water sorption. DSC measurements (on water saturated films as such and after drying under vacuum) showed an increase in the crystalline ratio of A1007 from 16 to 25%. The DSC scan of the water saturated sample no longer presented the cold crystallization peak typical to A1007 (Figure 3.3). On the other hand, the scan showed a remarkable resemblance with that of A1007 annealed. The crystalline ratio of A1007 annealed did not change in presence of water.

In order to check if the increase in crystalline ratio has an influence on diffusion, water saturated A1007 films were dried under vacuum and re-immersed in water (second sorption cycle). The curves from the second sorption cycle superimpose almost perfectly with the first cycle, indicating that the change in crystalline ratio did not affect diffusion. However, as it will be discussed in Section 3.2, the water intake at equilibrium is lower for the second cycle for A1007.

In addition, cuts of the dry and water saturated films were analyzed with a Scanning Electron Microscope (SEM). The films were observed throughout their thickness in order to identify possible cavities. One amorphous (PA6I) and one semi-crystalline (A1007) polyamide were chosen for this study. The SEM images for PA6I and A1007 are shown in Figure 3.5. The surface of slices cut through the film thickness is smooth for both the dry and water equilibrated films, up to high magnification. Therefore, no cavities can be observed in the thickness of the polyamide films in presence of water on a scale down to 1 μm.

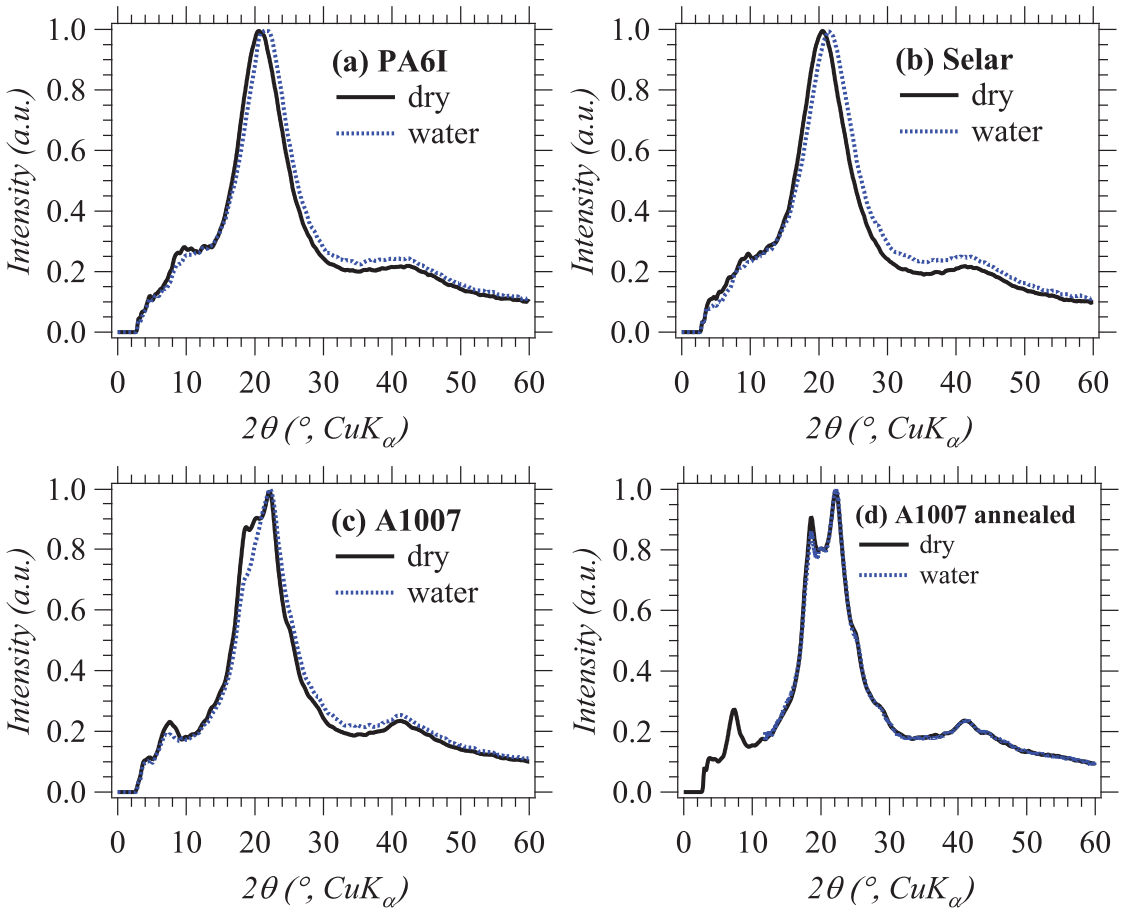

Figure 3.2: XRD scans of dry and water saturated polymer films: (a) PA6I (b) Selar (c) A1007 and (d) A1007 annealed. The same XRD scans were obtained on water saturated films after drying.

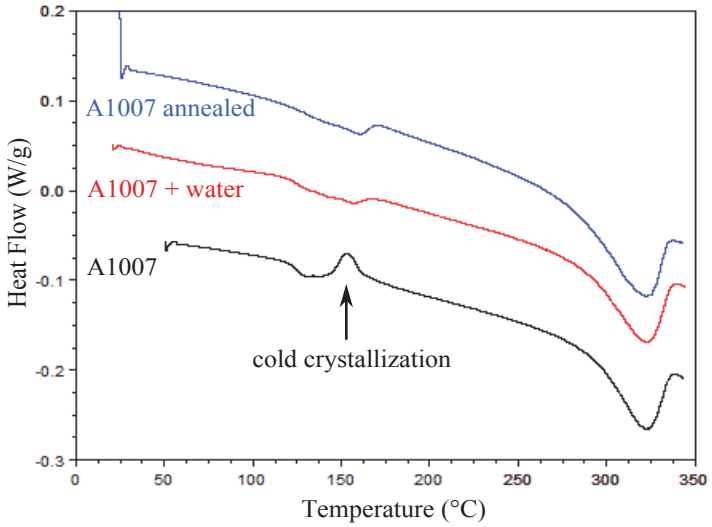

Figure 3.3: DSC scans of A1007 reference, A1007 after water sorption and A1007 annealed. Curves were shifted by 0.1 units for clarity.

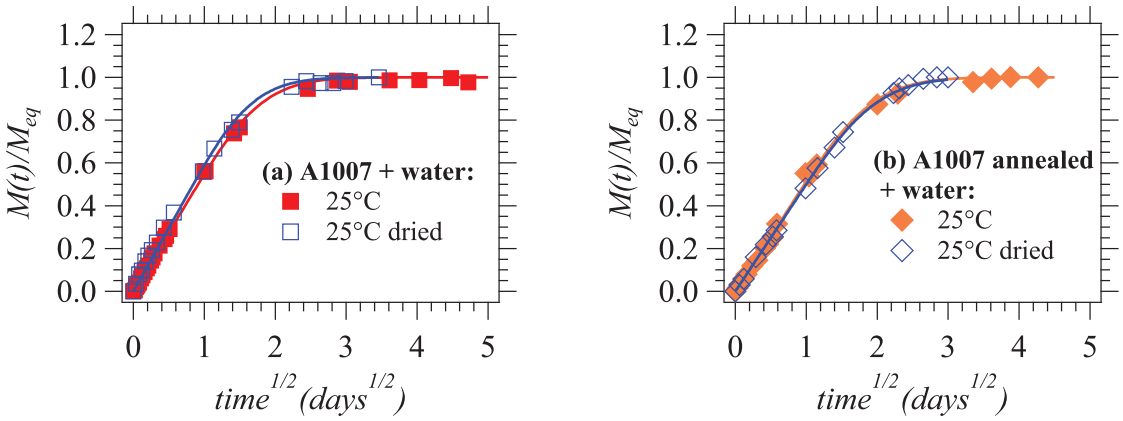

Figure 3.4: Sorption kinetics of liquid water at 25°C in (a) A1007 and (b) A1007 annealed, first and second cycle after drying. Solid lines are obtained by fitting the data with equation (1.11) for Fickian diffusion.

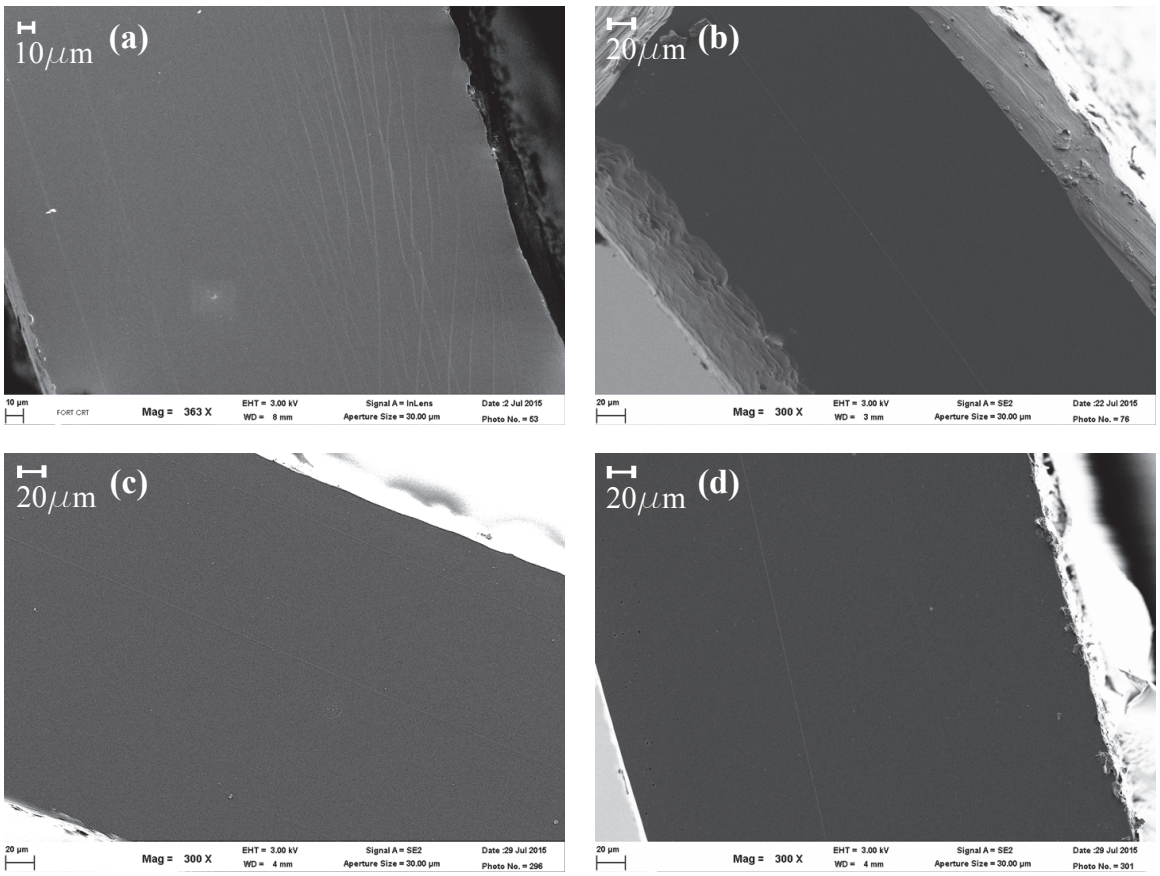

Figure 3.5: SEM images of dry and water saturated polyamide films: (a) PA6I dry, (b) PA6I+water, (c) A1007 dry and (d) A1007+water

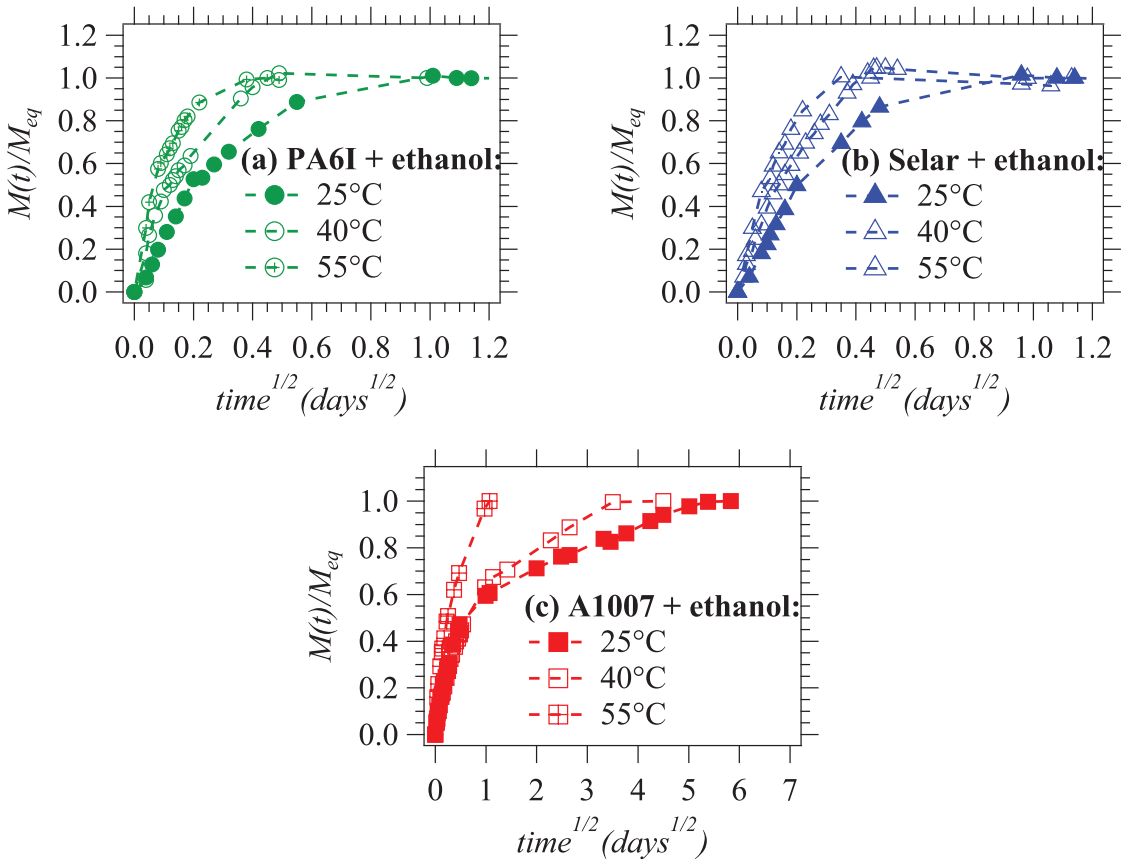

Figure 3.6: Sorption kinetics of liquid ethanol at 25, 40 and 55°C in (a) PA6I (b) Selar (c) A1007 and (d) A1007 annealed. Dashed lines are guides for the eyes.

3.1.2 Sorption kinetics of alcohols

Ethanol sorption kinetics curves are presented in Figure 3.6 for PA6I, Selar and A1007. In the case of ethanol, mass intake increases linearly with time in the first part of the curves. At $M(t)/M_{eq} \simeq 0.5$, the slope changes and equilibrium is reached slowly. The non-linear shape of the curve suggests that the diffusion mechanism is non-Fickian. As a consequence, diffusion coefficients cannot be calculated from these experimental curves.

Sorption kinetics were also measured for alcohols of different sizes: methanol, ethanol, propan-2-ol and ethylene glycol. The curves are presented in Figure 3.7 for PA6I and A1007. Methanol diffusion is the fastest, followed closely by ethanol and then by propan-2-ol and ethylene glycol, which are much slower. For comparison, in PA6I at 25°C, sorption equilibrium is reached in 4h for methanol, 24h for ethanol, 15 days for propan-2-ol and 2 months for ethylene glycol.

It was observed that in presence of alcohols the PA6I and Selar films become very soft before turning white. XRD scans of all films were therefore taken at $M(t)/M_{eq} \simeq 0.5$ (called 1st plateau) and at $M(t)/M_{eq} = 1$ (called 2nd plateau) in presence of ethanol. The XRD scans are shown in Figure 3.8. At the first plateau, both PA6I and Selar maintain their amorphous character, as indicated by the excellent superposition with the scan of the dry sample. On the other hand, crystalline peaks appear at the second plateau. The peaks are especially visible for PA6I and are in accordance with crystalline peak positions in A1007. To confirm crystallization, the PA6I and Selar films were dried under vacuum and measured in DSC. Distinct melting peaks appeared

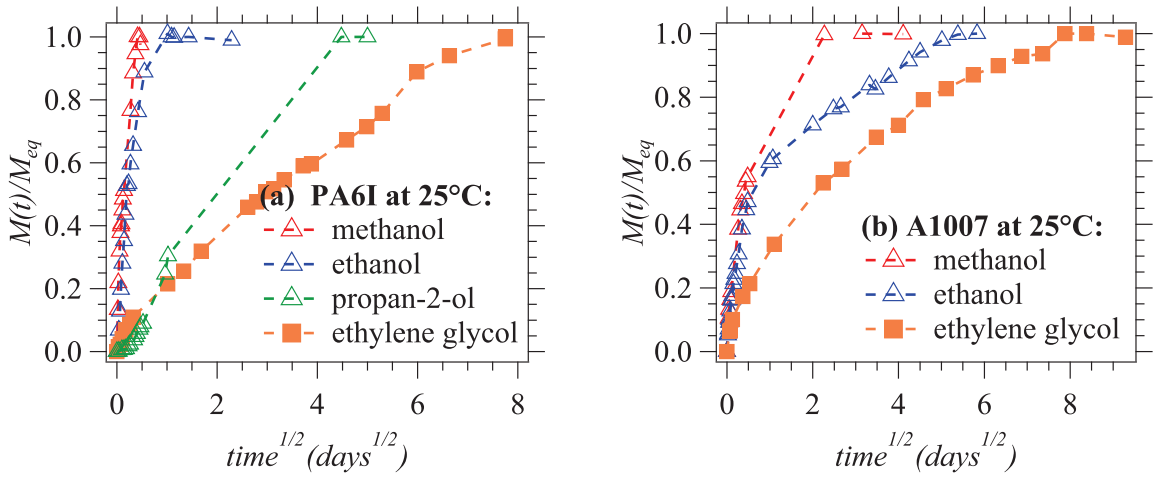

Figure 3.7: Sorption kinetics of liquid alcohols at 25°C in (a)PA6I and (b)A1007

in the temperature region 150-250°C (for DSC curves, please refer to Appendix B). Depending on the alcohol type, the crystalline ratio of PA6I varied between 20 and 28% and that of Selar between 15 and 22%.

For the semi-crystalline polyamides, no significant difference is observed in the XRD scans of the dry and ethanol swollen samples. Similarly to water, DSC measurements on the ethanol swollen A1007 films as such and on dried films showed an increase in the crystalline ratio from 16 to 25%. No difference was recorded for A1007 annealed after alcohols sorption. In this case, the second sorption cycle is different from the first one (*e.g.* methanol in Figure 3.9), although the same quantity of solvent is absorbed at equilibrium.

Film whitening can be explained by the onset of hetereogeneities at large scales (hundreds of nanometers). It might consist of crystallization but also of the formation of cavities. Therefore, PA6I films were observed in SEM. A1007 films were also observed to check for eventual cavities.

To begin with, the SEM images of dry and ethanol saturated A1007 films are shown in Figure 3.10. The films are smooth throughout their thickness, even at higher magnification. No cavities were observed in semi-crystalline A1007.

To continue with, Figure 3.11 shows the SEM images of dry and ethanol saturated PA6I (at three weeks of immersion). As it can be seen in Figure 3.11(b), the PA6I film presents cavities throughout its thickness, with a higher concentration in the central part. A closer look inside the cavities (Figure 3.11(c) and (d)) shows a globular structure at the interior. The globules are approximately 5 μm in diameter and have a rough surface. If the samples are irradiated with electrons for a short time period, the globular structure is evidenced throughout the thickness, not only inside the cavities (Figure 3.11(e)).

In order to investigate the formation of cavities and globular structure, a dry PA6I film was observed in SEM at intermediate immersion times in ethanol (0, 75, 225 min, 24h-equilibrium, 1 week, 2 weeks and 3 weeks). Figure 3.12 presents the cuts of the films at intermediate immersion times. The ethanol diffusion front can be observed on the side of the films, whose color changes from dark gray to white/transparent. The same type of solvent fronts have been observed by SEM in the literature in poly(ether ether ketone) films that crystallized and swelled in presence of solvents [139].

The 75 min of immersion correspond to the arrival at what will be defined as the first plateau, before the slope changes at $M(t)/M_{eq} \simeq 0.5$. By zooming on the film surface, three regions can be observed (Figure 3.13). The core of the film is dry and appears as a dark region. The white

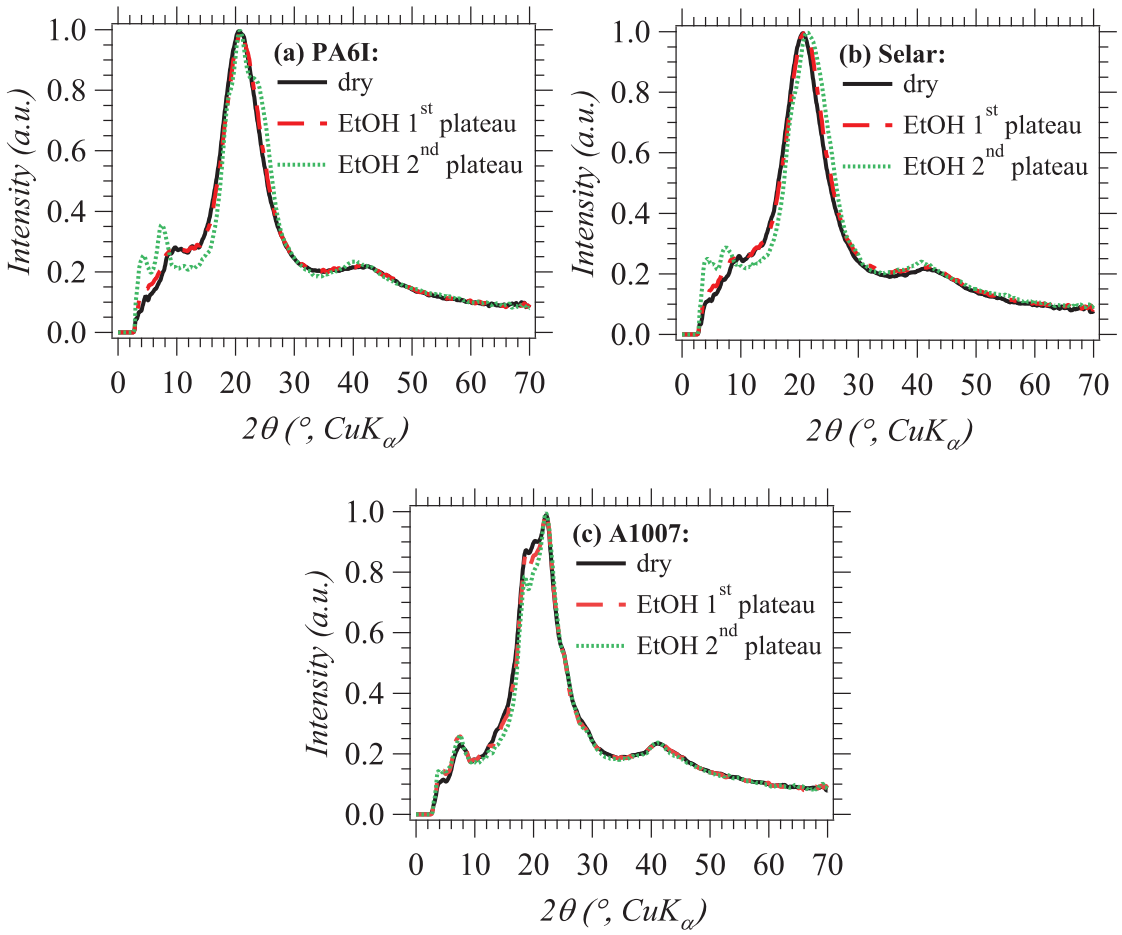

Figure 3.8: XRD scans of (a) PA6I (b) Selar (c) A1007 and (d) A1007 annealed, dry and in presence of ethanol (EtOH).

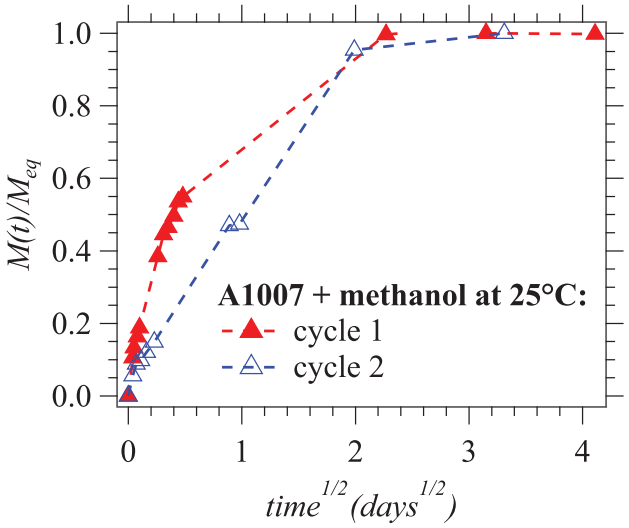

Figure 3.9: Sorption kinetics of methanol in A1007 at 25°C: cycle 1 (immersion of dry film) and cycle 2 (immersion of solvent-saturated film after drying)

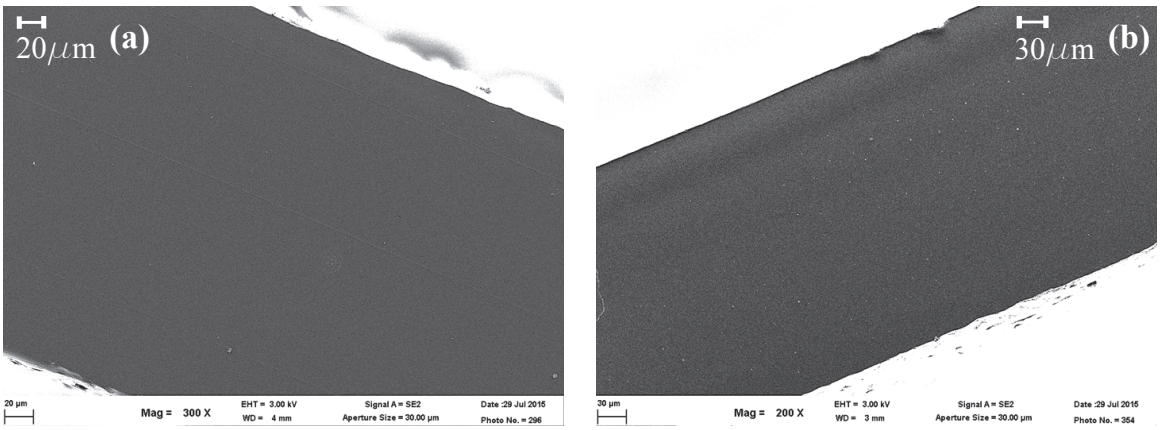

Figure 3.10: SEM images of (a) dry and (b) ethanol saturated A1007 films

region is assumed to correspond to the ethanol saturated region and a clear front of ethanol advancement can be seen between the two regions. On the extreme surface, a dark, thin layer exists. Small cavities are observed in this thin layer, meaning that there is a time lag between ethanol diffusion and cavitation. Therefore, the change of slope in the sorption kinetics curve at this point coincides also with the beginning of cavitation.

At an intermediate immersion time of 225 min (Figure 3.14), the three layers still exist but have different proportions. The dry core reduces as the ethanol diffusion continues. The damaged layer on the surface has increased in size and cavities can be observed in it. Interestingly, globular shapes are observed throughout the ethanol diffusion layer, their number being more important at the contact with the damaged layer. It would seem that the globular structure develops gradually, as ethanol advances in the polymer.

Immediately after equilibrium is attained at 24h, the PA6I film is uniformly covered in μm-sized cavities (Figure 3.15). One week later, the number and size of cavities increase in the middle of the polymer film. Up to three weeks, the cavities in the middle do not change shape or distribution. The average molecular weight and molecular weight distribution were measured by GPC. None evolved in presence of ethanol, even at long immersion times.

3.1.3 Discussion

This study was aimed at understanding the influence of crystallinity on diffusion coefficients in polyamide. It is generally accepted that crystallinity has a double effect on diffusion coefficients [41, 42]: the effective length of the diffusion path is increased as solvent molecules have to get around the crystals (tortuosity factor) and the accessibility of the amorphous phase might change due to the presence of a rigid amorphous fraction (chain immobilization factor).

Four polymers of equivalent chemical structure but different morphologies (amorphous or semi-crystalline) were compared for the diffusion of water and alcohols. In the case of water, diffusion follows a Fickian mechanism for both amorphous and semi-crystalline polyamide. The values of the diffusion coefficients were obtained by fitting the normalized mass intake curves. It was observed that diffusion coefficients are similar in the various polymer matrices (amorphous, 16 and 26% crystalline ratios). This would suggest that the presence of a crystalline phase has no significant incidence on water diffusion, at least in the 0-25% range of crystalline ratio. A hypothesis for this finding is that, due to its small size, water diffuses fast and can access most sorption sites in polyamide.

It was observed however that the crystalline ratio of A1007 increased after water sorption, approaching the one of A1007 annealed (26%). The cold crystallization peak identified in A1007

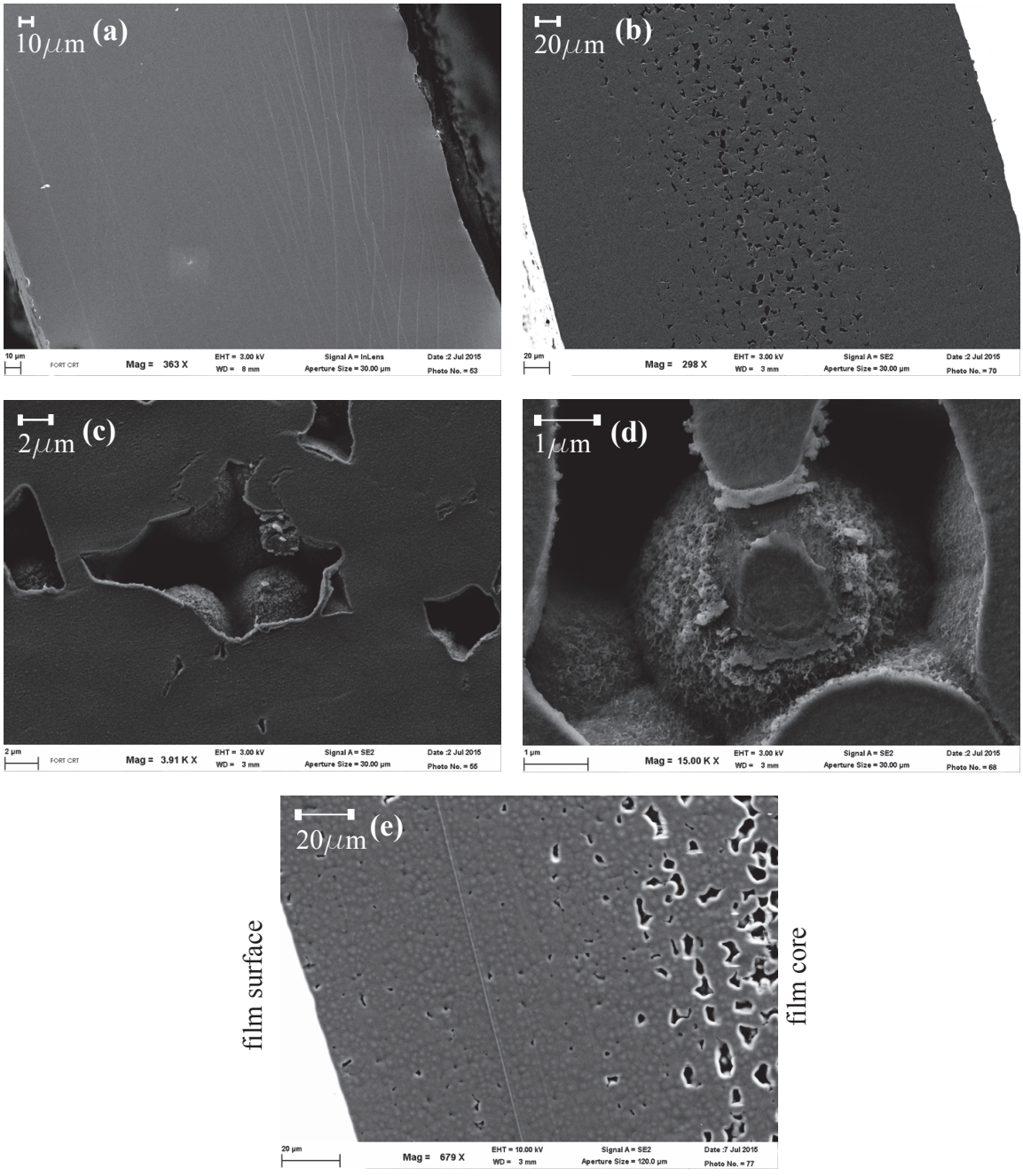

Figure 3.11: SEM images of dry and ethanol saturated PA6I films (3 weeks of immersion): (a) dry, (b)-(e) ethanol, (c) and (d) zoom of cavities, (e) surface after 5 min of electron irradiation

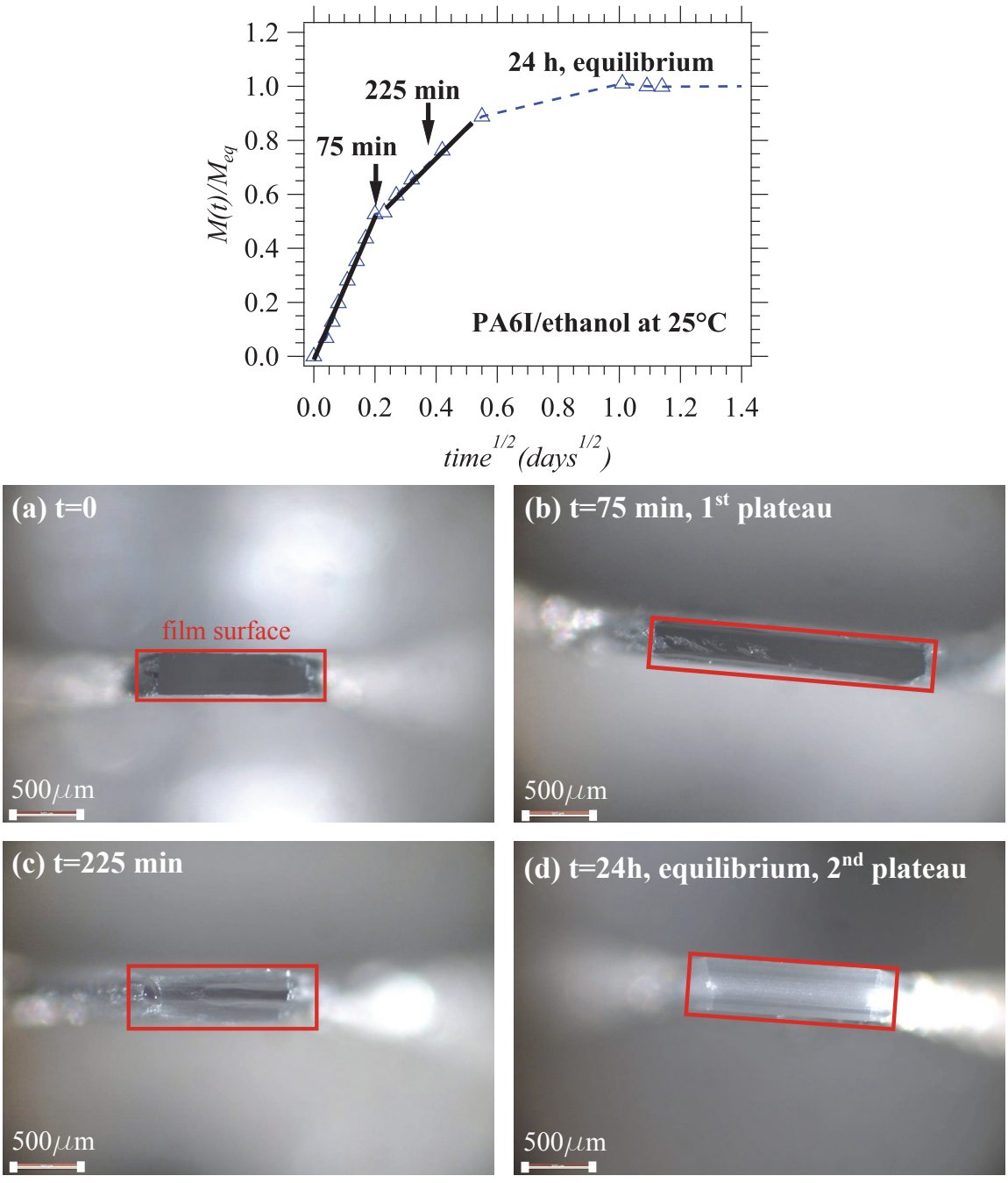

Figure 3.12: SEM images of PA6I immersed in ethanol for different periods of time. The SEM image at t = 75 min corresponds to the change in slope in the sorption kinetics curve (top graph).

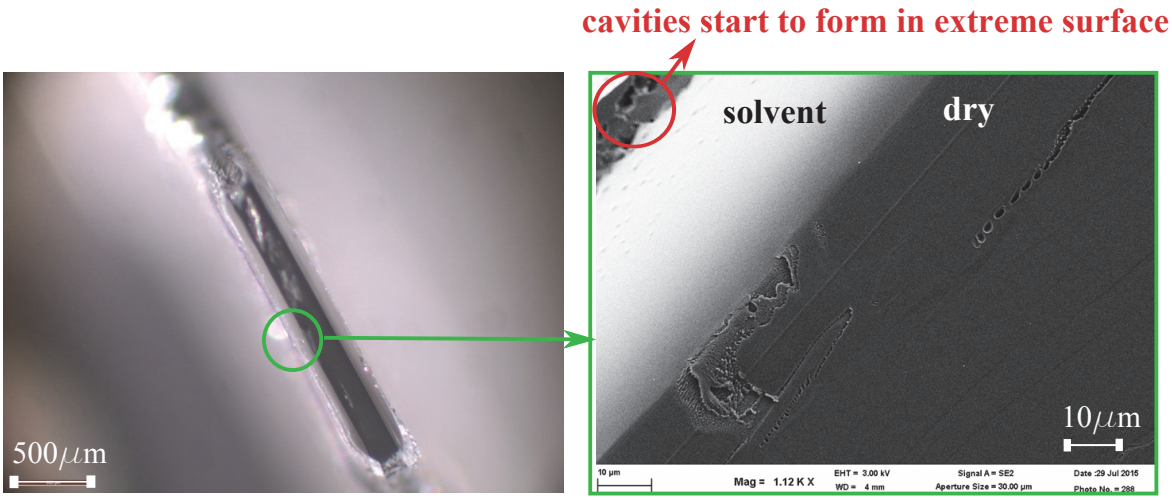

Figure 3.13: SEM images of PA6I film after 75 min immersion in ethanol

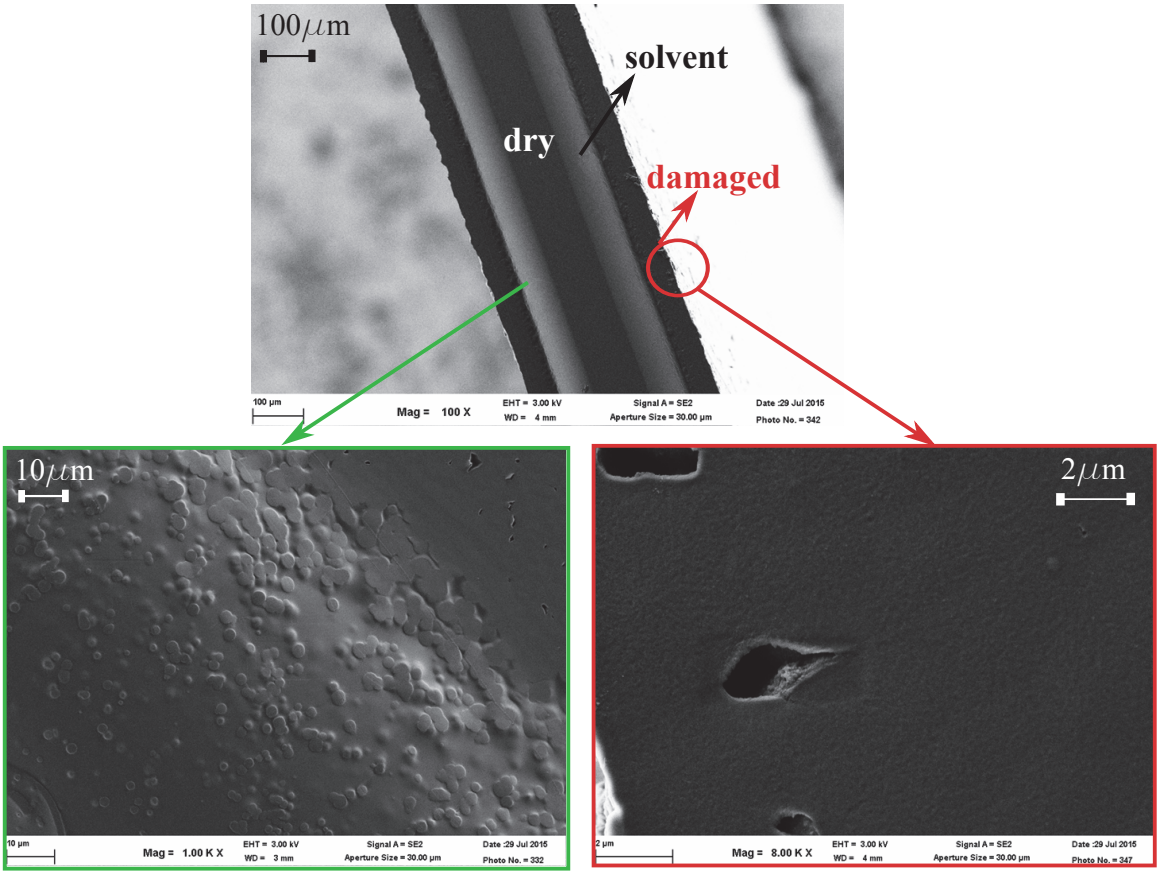

Figure 3.14: SEM images of PA6I film after 225 min immersion in ethanol. A globular structure is starting to form in the ethanol swollen area.

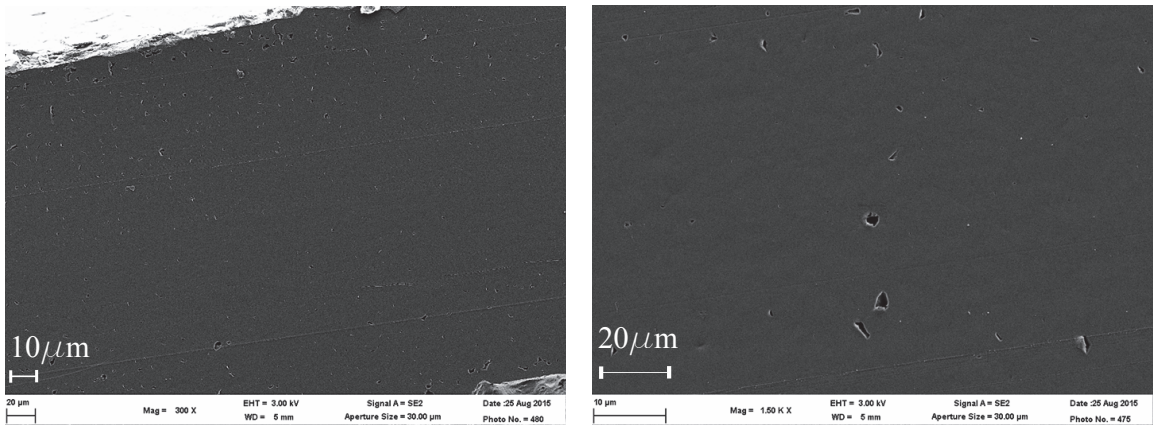

Figure 3.15: SEM images of a PA6I film at equilibrium (24h) showing a uniform distribution of small cavities

around 150°C dissappears in the water-swollen samples. Moreover, the DSC scans of the latter are similar to A1007 annealed. This would suggest that similar transformations occur under temperature treatment or in presence of water: A1007 transforms into A1007 annealed. The same observations were made for the sorption of alcohols in A1007.

A second sorption cycle on dried A1007 superimposed with the first cycle, suggesting that the change in crystalline ratio does not influence diffusion. The crystalline ratio of A1007 annealed did not change upon solvent sorption, which confirms that annealing gave a more stable crystalline structure. No cavitation or small scale structural changes were observed in presence of water.

In the case of alcohols, non-Fickian diffusion mechanisms are observed for all polymers. Amorphous polymers become white, indicating cavitation or crystallization of the samples. As it turns out, both phenomenons occur. XRD scans of PA6I and Selar showed crystalline peaks similar to those of A1007. However, DSC measurements evidenced a melting region between 150 and 250°C, which is much lower than the melting point of A1007 (325°C). The crystalline phase of PA6I and Selar melts at lower temperatures, suggesting that the crystalline structure is less organized. After solvent sorption, PA6I and Selar have crystalline ratios between 15 and 25%. PA6I crystallization in presence of solvents has already been observed in the polymer films at equilibrium [72]. As it turns out, crystallization occurs during the diffusion step, before equilibrium is attained.

SEM observations of PA6I films throughout their thickness showed large scale cavities. A study of the films at different immersion times showed a gradual advancement of the ethanol front towards the dry core. Up to $M(t)/M_{eq} \simeq 0.5$, the normalized mass uptake increases linearly with the square root of time (Figure 3.6). At this point, XRD scans show that PA6I does not crystallize and SEM images show no cavitation in the two main regions in PA6I films: the dry core and the ethanol saturated exterior of the film. However, a very thin third layer containing cavities is starting to form at the extreme surface. From this point, a change in the slope is observed in Figure 3.6. The softened polymer film hardens and becomes white. Immediately after sorption equilibrium is attained, an uniform distribution of cavities is observed in the film. On the next SEM images at longer immersion times, cavities appear in high number and a globular structure is starting to form in the PA6I bulk. Since PA6I crystallizes in presence of ethanol from $M(t)/M_{eq} > 0.5$ (XRD scans in Figure 3.8), these globules might be spherulites of very small sizes. The change in diffusion mechanism from Fickian to non-Fickian might therefore be due to the formation of cavities and crystallites. Indeed, these types of

diffusion profiles have been observed and simulated in polymers (poly(ethylene terephthalate), polycarbonate) that crystallize during diffusion [140, 141].

All alcohols give non-Fickian diffusion mechanisms, as it can be seen in Figure 3.7. Since several phenomena occur simulteneously (cavitation, crystallization), no models can be used to estimate the values of diffusion coefficients. However, it is obvious from Figure 3.7 that diffusion rate decreases for alcohols of bigger size. It is well known in the literature that the values of diffusion coefficients decrease when the size of the penetrant increases [46, 47]. The slowest diffusion was recorded for ethylene glycol, which takes 2 months before reaching sorption equilibrium at 25°C.

Up to this point, the influence of existence of strong interactions (hydrogen bonds) has not been discussed. The above observations could be valid for any non-polar polymer. However, in polyamide, both water and ethanol are capable of forming hydrogen bonds with the amide groups. Their energy (30-35 kJ/mol for water/amide [9, 142] and 25-30 kJ/mol for ethanol/amide [143]) is higher than an amide-amide hydrogen bond (25 kJ/mol [117]). In the next paragraph, the influence of the type of molecule on diffusion mechanisms will be discussed.

For this purpose, the diffusion of water and ethanol is compared in PA6I and A1007 (Figure 3.16). Ethanol diffuses faster than water in the two polymers. In A1007, diffusion is faster at the beginning and a marked change of slope is observed after one day. By assimilating this change to a first plateau and normalizing with respect to the corresponding intake value (Figure 3.16(c)), similar ethanol sorption kinetics curves would be obtained in A1007 and PA6I. The final equilibrium then takes one month to be established. Several changes of slope occur during ethanol diffusion in A1007 and it is unclear if the long time regime is not linked to other phenomena. It was highlighted before that A1007 crystallizes in presence of ethanol, which might explain the change in slope after one day of sorption.

In conclusion, if we want to compare water and ethanol, these systems are not the best suited to understand their respective Fickian and non-Fickian diffusion mechanisms. Although there is no cavitation in A1007, the polymer crystallized in presence of solvents. Also, the sorption equilibrium with ethanol is too long to attain. Therefore, other semi-crystalline polyamides are more adapted for this study (Chapters 4 and 5).

3.2 Effect on sorption at equilibrium

As for diffusion, the influence of crystallinity on sorption was analyzed by comparing amorphous PA6I and Selar to the semi-crystalline A1007. The sorption of water and alcohols of different sizes (methanol, ethanol, ethylene glycol and propanol) was measured at 25, 40 and 55°C.

3.2.1 Sorption of water

As discussed in Section 3.1, amorphous polyamides did not crystallize, nor cavitate in presence of water. On the other hand, the crystalline ratio of A1007 increased after water sorption. Moreover, less water was absorbed at the second sorption cycle (6.3% instead of 9%). It has been observed in the literature that the transformation of a metastable crystalline phase can have a huge impact on the sorption properties of polyamide (Figure 1.20 in Chapter 1). In A1007, the influence of crystallization during sorption cannot be properly assessed. For instance, crystallization results in the formation of a more dense phase, which might create extra free volume in the polymer. This free volume can be filled with water molecules, that would not be in direct interaction with the polymer. For the above reason, water mass intakes at equilibrium in A1007 were left out from the results.

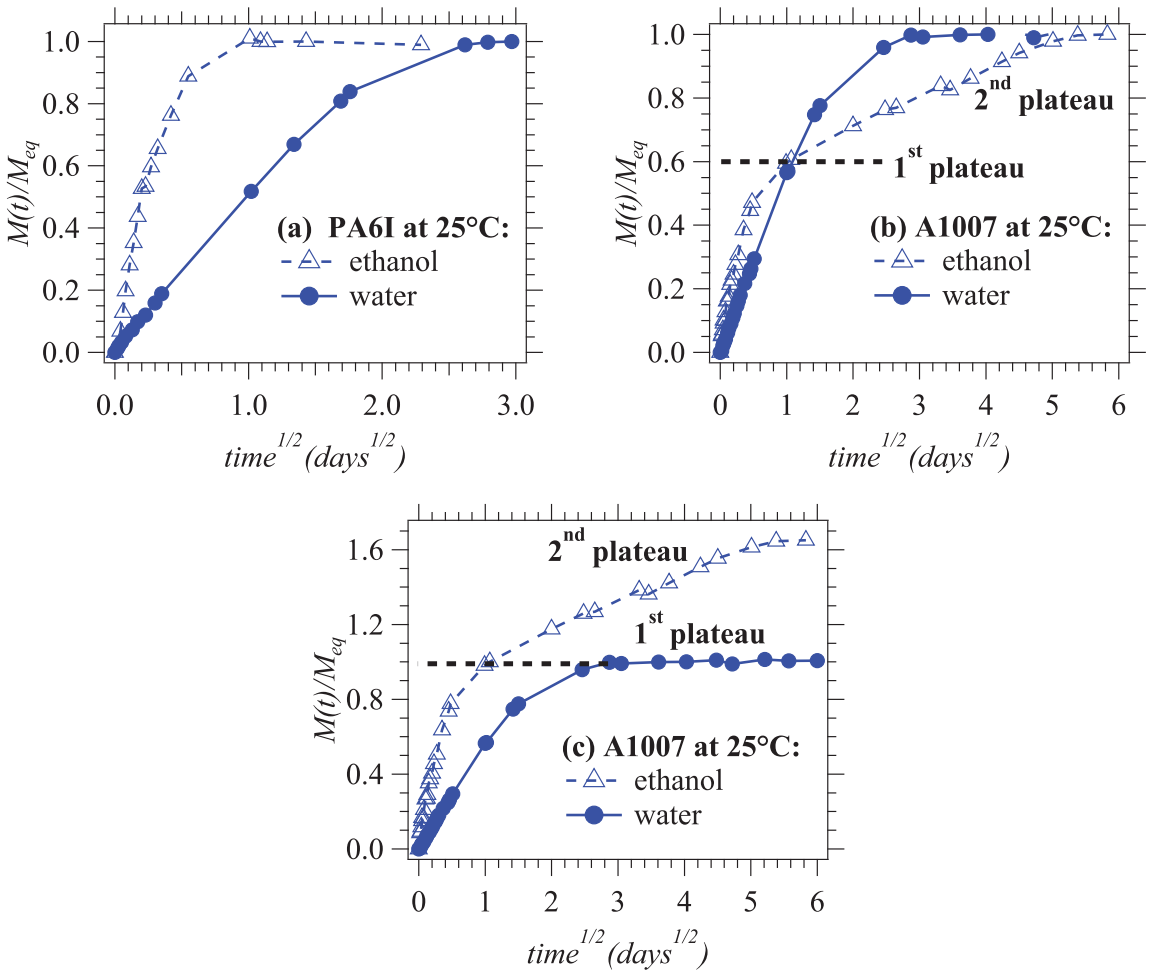

Figure 3.16: Comparison of sorption kinetics of water and ethanol at 25°C in (a) PA6I, (b) A1007 normalized at final equilibrium and (c) A1007 normalized at first plateau. Lines are guides for the eyes.

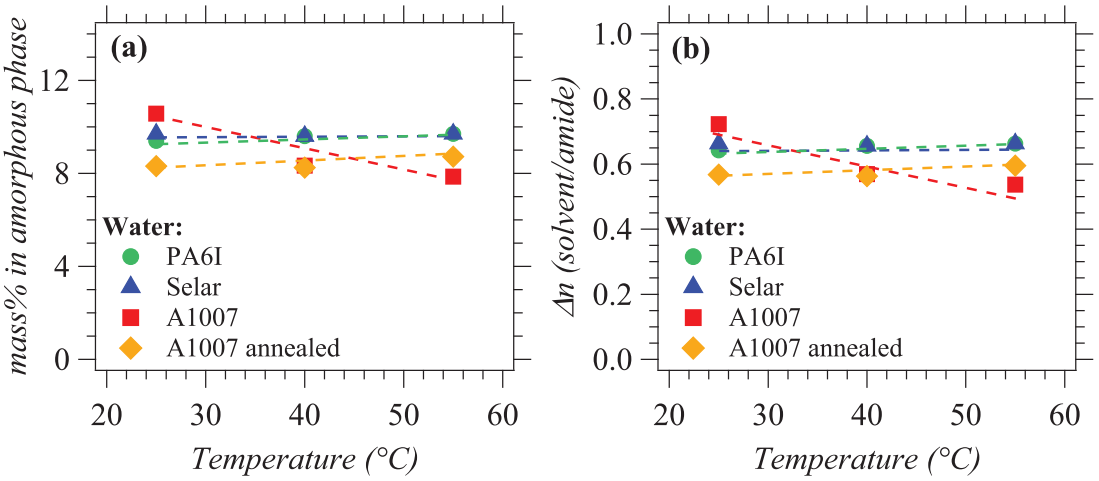

Figure 3.17: Water intake in the amorphous phase for model aromatic polyamides (a) mass percentage and (b) molar intake

Water intake at equilibrium in the amorphous phase is presented in Figure 3.17 for PA6I, Selar and A1007 annealed as a function of temperature, assuming that 100% of the amorphous phase is accessible in the semi-crystalline polyamide. It can be observed that water sorption in these polymers is independent of temperature.

The molar intake was calculated based on equation (2.15). This quantity is representative of the number of solvent molecules per amide sorption site in the amorphous phase. As illustrated in Figure 3.17(b), approximately half of the amide sorption sites are occupied by water. The ratio is slightly higher in amorphous polyamides compared to the semi-crystalline polyamide.

For better apprehending the influence of the crystalline phase, the water mass intake at equilibrium is presented as a function of the crystalline ratio in Figure 3.18. Since A1007 crystalline ratio changed during water sorption, only the data for A1007 annealed (26% crystalline ratio) was reported. In Section 3.1, it has been shown that the diffusion coefficients of water were similar in amorphous and semi-crystalline model polyamides. In the case of sorption however, the water intakes at equilibrium vary with the polymer matrix.

Previous studies on several polymers including semi-crystalline PA6,10 report a linear increase of solubility with the amount of amorphous phase $\Phi_{amorphous}$ (equation (1.26), $S = \Phi_{amorphous} S_{amorphous}$) [42, 69], which is in accordance with a two phase model. This linear variation is valid only for systems with a stable, non-evolving crystalline phase. The two-phase model is plotted in Figure 3.18 as a solid line. It should be highlighted that a literature study on PA6I calculated a Mean Cluster Size of 1.5 in PA6I [73]. It can be therefore considered that water is distributed at a molecular level in PA6I; the value of water mass intake is a characteristic of the PA6I/water system and a valid data point for the two phase model. Also, it should be noted that the glass transition temperature of water/aromatic polyamide systems is approximately 50°C (determined by DSC). Therefore, maybe except for 55°C, the systems are in their glassy state when the solvent equilibrium is reached.

From Figure 3.18, it is obvious that experimental mass intakes deviate from the two phase model, which suggests that not all the amorphous phase is accessible in polyamide. In the case of A1007 annealed at 26% crystalline ratio, 6.2% water is absorbed experimentally, compared to the 7.2% predicted by the two phase model. By a simple calculation, this would mean that 15% percent of the amorphous phase is unaccessible to the solvent. In the polymer film, the different phases would be distributed as such: 26% crystalline, 11% unaccessible amorphous

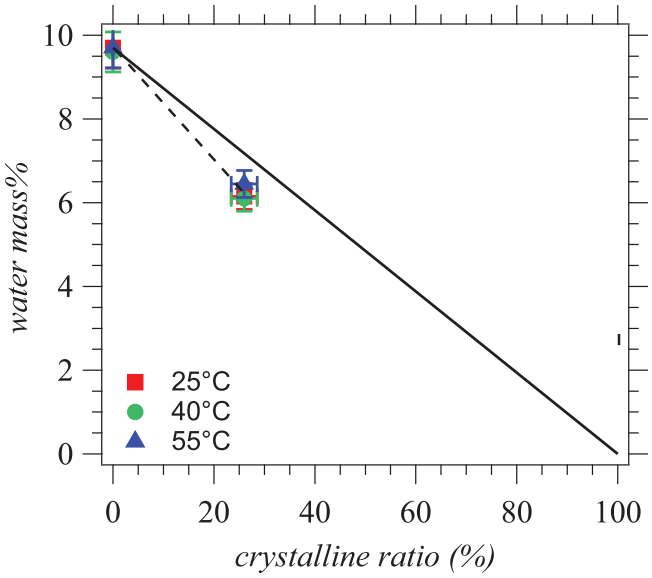

Figure 3.18: Water mass intake as a function of the crystalline ratio at different temperatures. The solid line is the prediction of linear variation for a two phase model (equation (1.26)).

and 63% accessible amorphous.

In A1007 annealed, the proportions of mobile and rigid amorphous fraction can be estimated by modulated DSC measurements, based on the value of experimental ΔC_p as shown in equation (2.6). The ΔC_p of the 100% amorphous is given by the measured ΔC_p of PA6I and Selar. The measured value of $\Delta C_p^{100\%amorphous}$ is 0.33 J/g °C (Figure 3.19). Based on this value, equation (2.6) provides a MAF% of 64% in A1007 annealed. By substraction (crystalline ratio 26%), the RAF accounts for approximately 10%. If we compare the RAF% to the estimated percentage of unaccessible amorphous, the two are in the same range of 10%. This would indicate that water penetrates little in the rigid amorphous phase.

Murthy *et al.* [51, 52, 53] showed by Small Angle Neutron Scattering that 1/3 of the amorphous phase was found in the interlamellar regions (constricted amorphous) and 2/3 in between the lamellar stacks (mobile amorphous). Water was identified in both constricted and mobile amorphous. However, it is unclear if some of the constricted amorphous remains inaccessible to water. Low-resolution NMR studies on hydrated PA [54, 55, 58] suggest that water plasticizes only a small portion of the polyamide matrix, depicted as the soft amorphous in between crystalline domains. Water molecules that are absorbed in the constricted amorphous are strongly immobilized by hydrogen bonds so water is thought to diffuse only through the soft amorphous.

This image is in accordance with our experimental results. If the amorphous phase is not entirely accessible to water, mass intake at equilibrium would be lower in semi-crystalline polymers. If water diffuses only through the soft amorphous, diffusion coefficients in semi-crystalline polyamide should be lower because of the tortuosity and chain immobilization factor. However, if the crystalline ratio is small, soft amorphous domains might be sufficiently percolated to give fast water diffusion like in a 100% amorphous. This would be the case of our polyamides, in which diffusion coefficients did not vary in the 0 to 25% crystalline ratio.

As-injected and annealed A1007 films give a weak response when observed by cross-polarization in microscopy (Figure 3.20). The films do not show a classical spherulitic growth but a more discrete distribution of the crystalline domains. The amorphous phase might there-

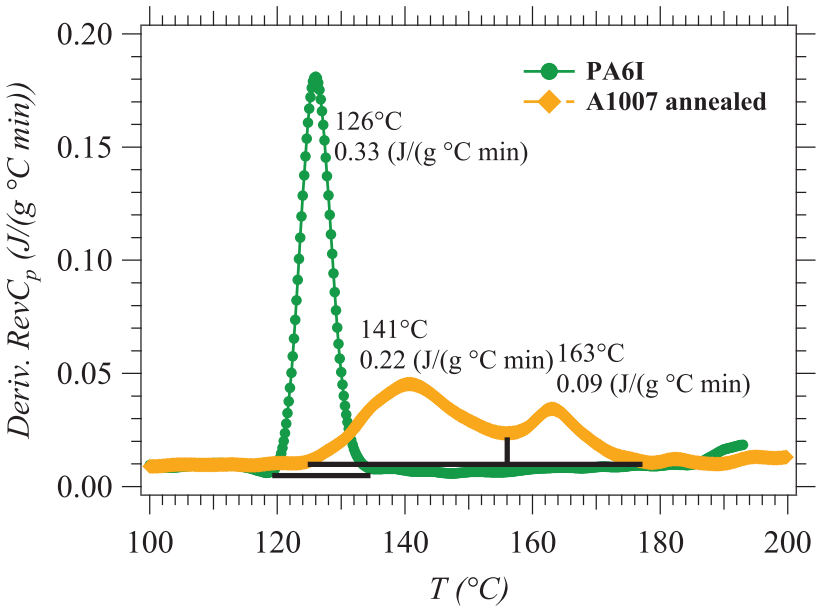

Figure 3.19: MDSC scans of PA6I and A1007 annealed (derivative of $RevC_p$ as a function of time). The value of the integrated area below the peak and the maximum of the peak are reported on the Figure. A1007 annealed presents two peaks: the first one is related to the glass transition temperature and the second one is an "artificial" peak given by the annealing temperature. If the annealing temperature changes, the second peak shifts accordingly. Note that the glass transition is much broader in semi-crystalline A1007 than in PA6I.

fore be sufficiently percolated. As measured by DSC, the MAF% in A1007 annealed is quite high (64%), which also supports this percolation hypothesis.

An additional confirmation of this hypothesis could be given by the quatification of Mobile and Rigid Amorphous Fraction by low-resolution NMR. However, these high T_g systems (130-140°C in DSC) cannot be analysed with this technique. In order to resolve the different components, the temperature for NMR experiments should substantially exceed T_g. However, Minispec spectrometers can reach a maximum temperature of 160-200°C, which is too close to the T_g of semi-aromatic PA (approx. 130°C) to differentiate crystalline and amorphous phases. Aliphatic PA of low T_g are more adapted to these studies.

3.2.2 Sorption of alcohols

As discussed in Section 3.1, secondary phenomena (cavitation, crystallization) occur in amorphous polyamides in presence of alcohols. For this reason, the alcohol intakes at equilibrium are not precise, since some of the solvent fills the cavities and the crystalline fraction cannot be accurately determined. The alcohol intakes presented in this section are therefore only estimates for the initially amorphous polyamides.

It was also observed that the crystalline ratio of A1007 increased after alcohols sorption. Interestingly, the mass intake at equilibrium did not evolve at the second cycle of sorption, although the crystalline ratio of the sample was 10% higher.

Ethanol intake at equilibrium is presented in Figure 3.21 for aromatic polyamides as a function of temperature, assuming that 100% of the amorphous phase is accessible in semi-crystalline A1007 and overlooking other phenomena in amorphous PA. Ethanol seems much more absorbed in amorphous PA but no conclusion can be drawn because the polymers structure

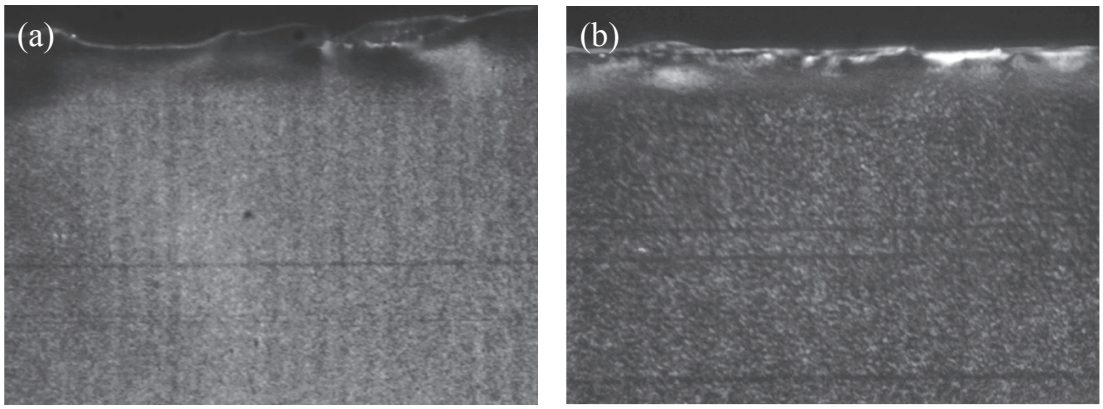

Figure 3.20: Observation of A1007 films (a) as-injected and (b) annealed by cross-polarization in microscopy. Magnification=100 × 1.6

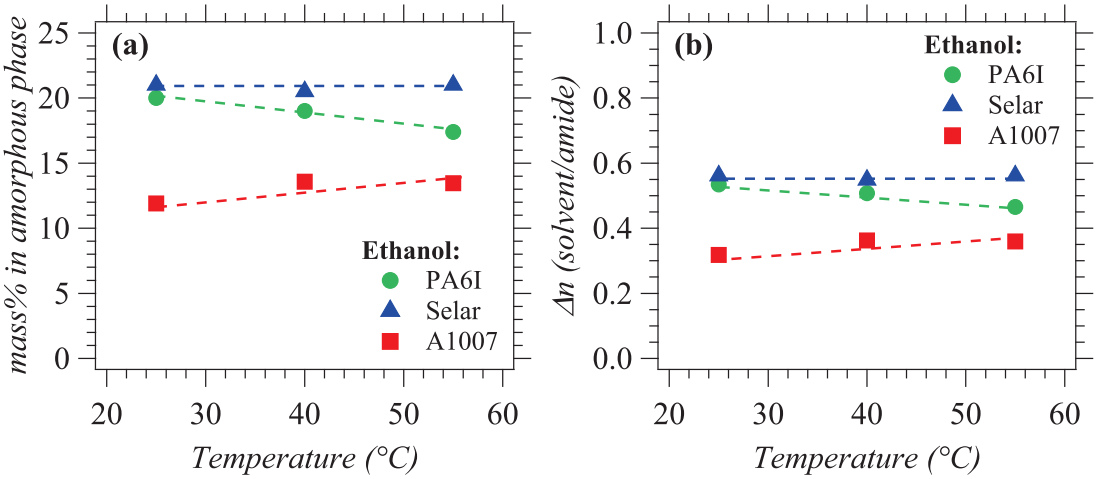

Figure 3.21: Ethanol intake in the amorphous phase for model aromatic polyamides (a) mass percentage and (b) molar intake

changed.

In addition to ethanol, the sorption of alcohols of different sizes was recorded at 25°C. The molar intakes are presented only for semi-crystalline A1007 in Figure 3.22 as a function of the solvent molar volume and as a function of the dipole moment/molar volume, which takes into account the changes in polarity that accompany changes in size. Both data from the first sorption cycle (crystalline ratio 16%) and second sorption cycle (crystalline ratio 25%) are shown. Water molar intake and data for PA6,6 (from reference [27]) and PA6,10 (measured during this PhD work) were added to the data for comparison.

3.2.3 Discussion

Because of side effects (cavitation, crystallization), the influence of crystallinity could only be assessed for water sorption. It was concluded that approximately 15% of the amorphous phase in semi-crystalline A1007 annealed is not accessible to water. This percentage corresponds roughly to the RAF% estimated by DSC. Therefore, it would seem that water penetrates little in the constricted amorphous phase.

In the next paragraphs, let us discuss solvent distribution in polyamide with respect to

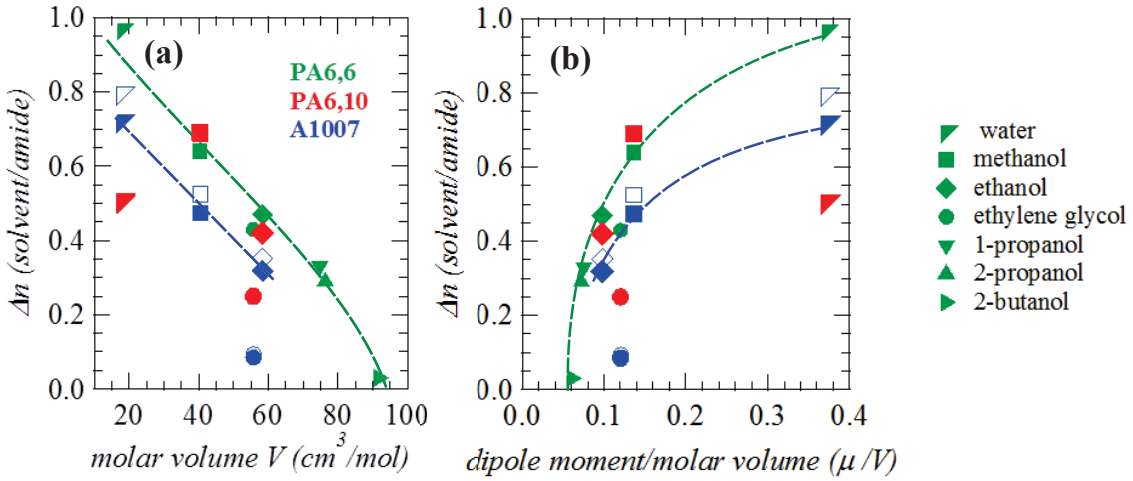

Figure 3.22: Solvent molar intake at 25°C in the amorphous phase of A1007 (blue, full symbols = cycle 1, empty symbols = cycle 2) as a function of solvent (a) molar volume or (b) dipole moment over molar volume. PA6,6 (green, from reference [27]) and PA6,10 (red) (measured in this PhD) are added for comparison. Lines are guides for the eye.

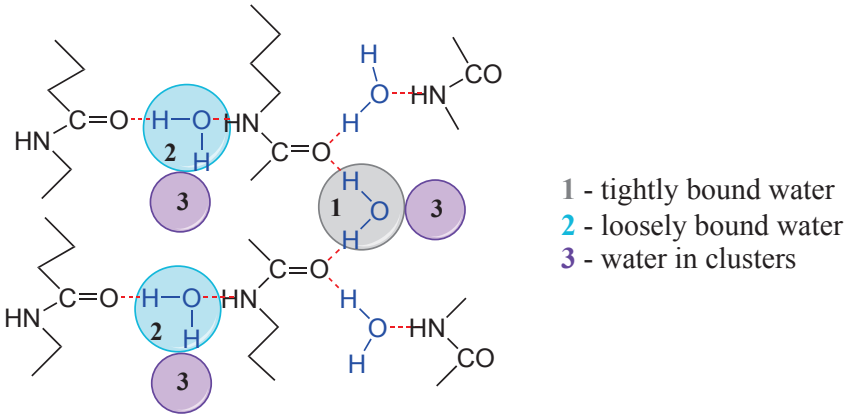

Figure 3.23: Schematic representation of water populations in polyamide as proposed by Puffr and Sebenda [71]

the amide groups. Water populations in polyamide are generally represented following the interpretation of Puffr and Sebenda (Figure 3.23). A water molecule can either be bound to two oxygen atoms from amide groups (tightly bound water), to an oxygen and hydrogen atom from amide groups (loosely bound water) or to another molecule of water (clusters). The stoichiometry is one tightly bound and two loosely bound water molecules for two amide groups, which gives a molar intake of 1.5.

In amorphous polyamide, the measured molar intake is 0.7 (≃2/3), which is significantly lower than the stoichiometric ratio of 1.5. Atomistic simulations on water sorption in PA6,6 [144] have shown that at a given time, roughly half of the amide groups are free, *i.e.* not bonded to water molecules, because they are burried in regions of high alkane moities density. If we accept this image, among the bonded sites in PA6I, 0.7/0.5=1.4 water molecules are found on average per amide group, which is in agreement with the 1.5 stoichiometry shown in Figure 3.23. Note however that molecular dynamics simulations have a very short time scale (order of ns); they provide a "snapshot" of the system, which is representative of the average equilibrium

state of the system (because of ergodicity).

Because of cavitation and crystallization, the same discussion cannot be done on alcohol sorption in amorphous polyamide. The different behavior of water and ethanol might be explained by the different compatibility of the PA6I or PA6I/6T matrix with water and ethanol. In this purpose, the Flory interaction parameter χ was calculated with equation (1.22) and the following values for the Hansen interaction parameters δ: 48 $MPa^{1/2}$ for water [145, 146], 25.4 $MPa^{1/2}$ for ethanol [147] and 24.5 $MPa^{1/2}$ for the 6I or 6T unit (calculated with the group contribution [148]). The obtained Flory interaction parameters are 7.45 for water/PA6I and 0.02 for ethanol/PA6I. Based only on the value of the Flory interaction parameter, water is a very bad solvent for PA6I and ethanol is a very good solvent, that should dissolve PA6I. A higher compatibility might explain the behavior of ethanol/PA6I systems. However, it should be highlighted that Flory-Huggins theory gives an idea of the compatibility of the solvent and the polymer but is adapted to non-polar systems with no strong interactions, which is not the case of solvent/polyamide systems. Water does penetrate into PA6I up to a high percentage of 10% in weight and ethanol does not entirely dissolve PA6I films, although the structural integrity of the films is strongly altered by the formation of cavities. Moreover, GPC shows no difference in the molecular weight distribution after ethanol sorption. This indicates that ethanol does not have a chemical effect (like hydrolysis in the case of water) and suggests that there is no dissolution of polyamide chains.

The alcohol molar intake at equilibrium in the amorphous phase can be calculated for semi-crystalline A1007. The results are presented in Figure 3.22, along with PA6,6 and PA6,10 for comparison. The same trends are observed in all polyamides for the alcohol series: small, polar alcohols are more absorbed. The difference can arise either from the compatibility with the matrix or from the molecule size (accessiblity of the amorphous phase), or both. The study of an amorphous polyamide would have allowed us to rule out between the two effects. A better knowledge of the accessibility of the amorphous phase is needed to compare polyamides between them.

Ethylene glycol seems to be a specific case, its molar intake being below the general trend for alcohols. Contrary to the other alcohols, ethylene glycol has two hydroxyl groups and is therefore a multifonctional molecule, like water. Although the molar volume and dipole moment/molar volume of ethylene glycol and ethanol are close, the latter is less absorbed. The Flory interaction parameter χ for ethylene glycol/PA6I is estimated at 2.25 (based on the Hansen interaction parameter δ = 32.9 $MPa^{1/2}$ for ethylene glycol [132] and equation (1.22)), intermediate between water (7.45) and ethanol/PA6I (0.02). Contrary to ethanol which is a very good solvent, the compatibility between ethylene glycol and PA6I is lower.

If we consider that the only difference to ethanol is the additional hydroxyl group, the ethylene glycol molar intake multiplied by two should give the ethanol molar intake. Or, the ratio between the two varies from 1/3, 1/2 or 1/1 ethylene gylcol/ethanol molecule, depending on the polyamide matrix. There is no general tendency to this behavior. This is another indication that the accessibility of the amorphous phase might vary. The molar intakes in Figure 3.22 are reported to the entire amorphous phase. An exact distribution of solvent molecules in the Rigid and Mobile Amorphous Fraction would allow a more precise calculation of the ratio of solvent molecules/amide group. Also, a precise knowledge of sorption modes is necessary. If solvent molecules form clusters for example, the molar intake does not provide an accurate description of the solvent/amide ratio.

3.3 Conclusions

The diffusion of water and alcohols in amorphous and semi-crystalline polyamides was investigated in order to better understand the influence of the crystalline phase. The study was done on a 100% amorphous semi-aromatic PA6I and Selar (PA6I/6T 70/30) and semi-crystalline A1007 (PA6I/6T 30/70). These polymers were chosen because of their almost identical chemical structure, with the exception of the position of substituents on the aromatic ring. It was therefore considered that the study was done at *iso*-chemical structure, which is crucial if we want to distinguish only the effect of the semi-crystalline structure.

It should be highlighted however that, although the polymers have the same molecular structure, the packing of the chains is slightly different. The density of a pure PA6I amorphous is 1.16 g/cm^3 [136], compared to 1.19 g/cm^3 for amorphous PA6I/6T 70/30 (Selar Material Safety Data Sheet) and estimated 1.23 g/cm^3 for amorphous PA6T (see Section 3.1). Since pure PA6I and Selar have the same sorption behavior, this variation does not influence our results.

In the case of water, diffusion follows a Fickian mechanism and there is no influence of crystallinity on the diffusion coefficients, at least in the range 0 to 25% crystalline ratio. In the case of alcohols, diffusion is non-Fickian. For amorphous polyamides, this is probably caused by the formation of cavities and crystallization. For semi-crystalline polymers, it is unclear why alcohols diffusion is non-Fickian. A possible cause would be the increase in the crystalline ratio of A1007, as measured by DSC. Alcohols of different sizes have also been compared and it can be observed that small molecules diffuse faster, as it is well-established in the literature [46, 47, 149].

Contrary to results on diffusion, water sorption at equilibrium is different in amorphous and semi-crystalline polyamide. We estimate that a small percentage of the amorphous phase might not accessible to water. This percentage is in good agreement with the amount of Rigid Amorphous Fraction in the polymer. These results are in line with previous NMR studies on the accessibility of the amorphous phase in polyamide [52, 54, 55, 58].

Since the small molecule of water has a limited accessibility, one could intuitively assume that molecules of different size and polarity cannot access the same number of sorption sites. The comparison of water and alcohols in PA6,6, PA6,10 and A1007 shows that size does not have a reproducible effect from one matrix to another, suggesting again an influence of accessibility. If we want to compare different solvents in the same matrix or different polymer matrixes, a more intensive knowledge of the phase distribution, solvent accessibility and solvent distribution at a molecular level is needed. This information can be obtained from NMR studies and sorption isotherms.

Chapter 4

Sorption modes in polyamide

In Chapter 3, it was highlighted that a more intensive understanding of sorption mechanisms and amorphous phase distribution was needed in order to compare for instance solvents of different size in the same polymer matrix. Information on sorption mechanisms can be obtained from sorption isotherms and the amorphous phase distribution can be investigated by low-resolution NMR. The previous semi-aromatic polyamides were however unsuitable for this study because of their high glass transition temperature (approx. 130°C), too close to the maximum temperature limit of our NMR spectrometer. For this reason, aliphatic polyamides with a lower T_g were chosen. In addition, the T_g of aliphatic polyamides decreases under the experimental temperature upon solvent sorption, which makes sorption and diffusion mechanisms more interesting to study.

The chosen aliphatic polyamides are PA6,6 and PA6,10. The films were prepared by different processing methods and have different crystalline ratios, which has to be taken into account if we want to compare the two. For this reason, in an inital step, each polymer matrix was studied individually. In a second step, the structure of the dry and water-saturated films was investigated by NMR in order to ellucidate their phase distribution. Based on the structural information, the two films could be compared.

4.1 Sorption isotherms

The analysis of sorption isotherms gives important information on the effect of solvents on the polymer matrix. It allows the identification of sorption models (sorption in specific sites for polyamide?) and clustering. This knowledge is essential when making hypotheses on molar intakes for example.

A Dynamic Vapor Sorption experiment was used to access the mass intake at equilibrium as a function of solvent activity. Activity steps of 0.1 were used in the range 0.1 to 0.9. These experimental conditions were also chosen in order to study solvent diffusion in these polymers, as it will be described in detail in Chapter 5. Several temperatures were used in the range 29 to 51°C. The values of water and ethanol uptake at equilibrium for each activity and temperature are reported in Figure 4.1 as sorption isotherms. It should be highlighted that sorption isotherms report values at equilibrium and are therefore independent of the DVS protocol.

The sorption at equilibrium in liquid solvent (a=1) was also recorded for these samples at 40°C and added to Figure 4.1. Before looking more in-depth into sorption mechanisms, the XRD scans of dry and solvent saturated samples were recorded. In the XRD scans in Figure 4.2 it can be observed that the main peaks around 20° are better resolved and the distance $\Delta 2\theta$ between them increases slightly in presence of solvents. This is associated to an evolution towards a more perfect crystalline phase and has been observed in the litterature on several occasions [27, 51, 12]. In order to check if the evolution of the crystalline phase has an influence on sorption at equilibrium, polyamide films were dried and re-immersed in solvent. The solvent intake at equilibrium was the same as the first sorption cycle, meaning that the changes in the crystalline phase did not influence sorption. Lastly, it was confirmed by GPC that the molecular weight and molecular weight distribution did not change in presence of solvents. Note that at very long immersion times, other phenomena were observed. Appendix C presents all these observations and how they were investigated by XRD and GPC.

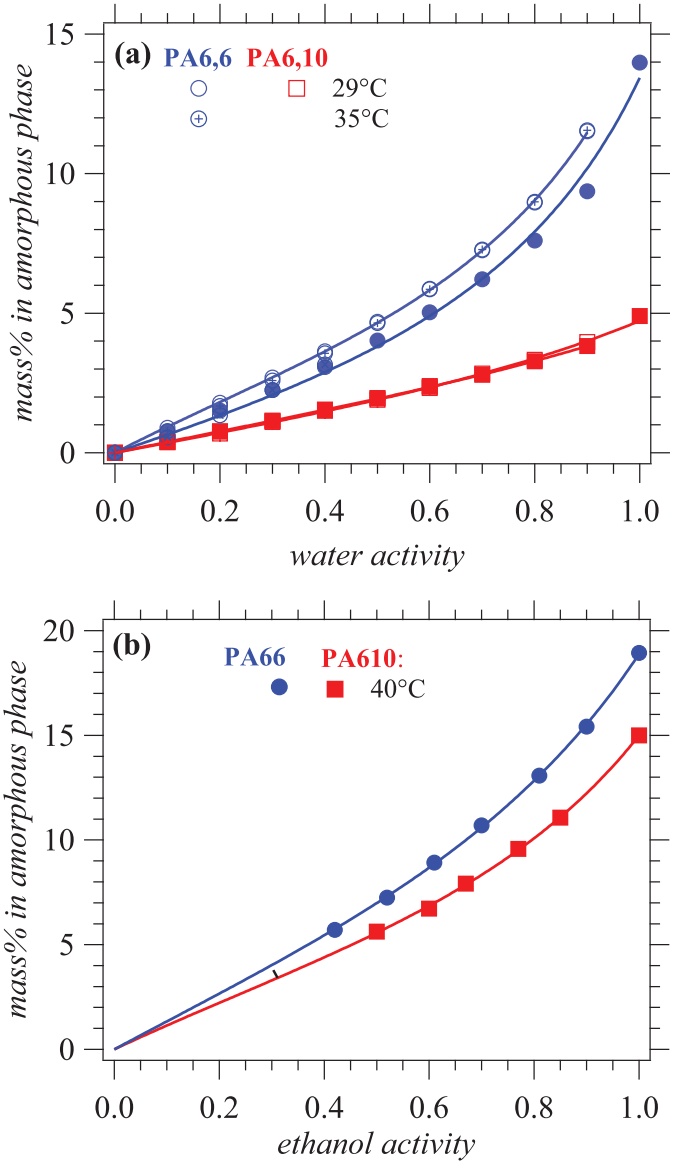

Figure 4.1: (a) Sorption isotherms for water in PA6,6 and PA6,10 at different temperatures (for PA6,10, data at all temperatures roughly superimpose; for PA6,6, data at 29 and 35°C and data at 40 and 51°C roughly superimpose). (b) Sorption isotherms for ethanol in PA6,6 and PA6,10 at 40°C. The full lines were obtained by fitting the data with a GAB model.

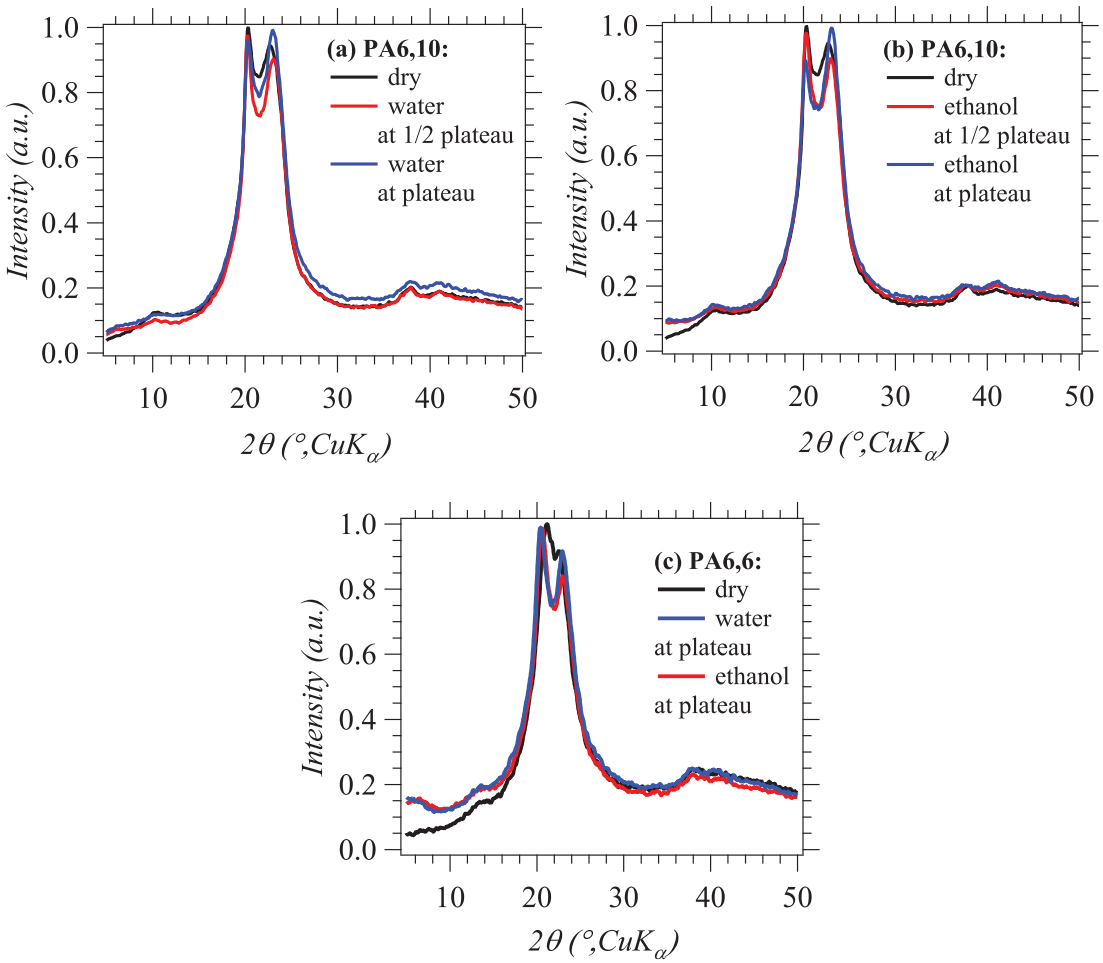

Figure 4.2: XRD scans of (a) PA6,10 + water (b) PA6,10 + ethanol and (c) PA6,6+water and ethanol.

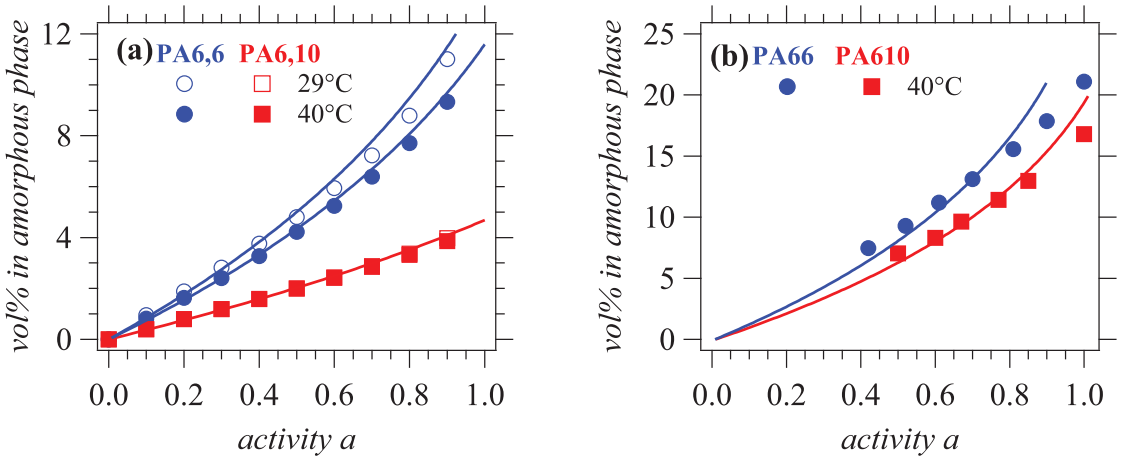

Figure 4.3: (a) Sorption isotherms for water in PA6,6 and PA6,10 at different temperatures. (b) Sorption isotherms for ethanol in PA6,6 and PA6,10 at 40°C. The solid lines were obtained by fitting the data with a Flory-Huggins model.

Since the two polymers were prepared by different processing methods, the comparison between them is not straightforward. Indeed it is well established that morphology and phase composition are influenced by processing and thermal history of semi-crystalline polyamide [54, 55, 56, 58]. In the previous section, it has also been highlighted that water sorption does not follow a simple two phase law in model aromatic polyamides. For sorption isotherms, each matrix will be analyzed individually.

Measured sorption isotherms are in agreement with those reported in the literature for water [2, 71, 150, 151] or ethanol [50, 60]. The upward curvature of sorption isotherms might be associated to the swelling of the matrix or to the existence of solvent clusters [2, 150, 152]. The Flory-Huggins model for binary mixtures takes into account the swelling of the matrix and was used to fit the experimental data with equation (1.23). Equation (1.23) does not fit ethanol sorption isotherms (Figure 4.3) but provides a good quality fit for most of water experimental data (Figure 4.3). The obtained χ values are 1.5 for PA6,6 at 29°C, 1.63 for PA6,6 at 40°C and 2.32 for PA6,10 at 29 and 40°C. A higher Flory-Huggins parameter in PA6,10 suggests that water is a worse solvent for PA6,10 than for PA6,6, which is in accordance with PA6,10 being more hydrophobic.

The value of the interaction parameter χ can alternatively be estimated with equation (1.22) [63]. The reported values for Hildebrand solubility parameters are 27.8 $MPa^{1/2}$ for PA6,6 [145, 146], 26 $MPa^{1/2}$ for PA6,10 (calculated with group contribution [148]) and 48 $MPa^{1/2}$ for water as a pure liquid [63]. Based on equation (1.22) and the reported values of solubility parameters, the values of the Flory interaction parameter χ would be 5.05 for PA6,6/water and 6.75 for PA6,10/water at 40°C. These values are much larger than the χ values obtained from fitting the sorption isotherms. Experimental water intake is thereby much higher than predicted from the calculated χ values. Moreover, in the Flory approach, the water intake should increase with temperature, entropy being the driving force for sorption. However, it is found that the water intake either decreases (PA6,6) or is roughly constant (PA6,10) as a function of temperature. This suggests that the enthalpy of sorption is more likely to be the driving force for sorption, and therefore, that an enthalpy-driven model with specific sorption sites is more appropriate.

The Guggenheim, Anderson and De Boer (GAB) [65, 66, 67] model assumes the existence of preferential sorption sites (in the present case amide groups). The model allows sorption in

Polymer	Solvent	T (°C)	M_m (%)	A	C	Mean Cluster Size
PA6,6	water	29	4.99	0.71	2.74	2
PA6,6	water	35	4.99	0.72	2.58	2
PA6,6	water	40	4.99	0.65	2.4	1.7
PA6,6	ethanol	40	10.22	0.59	2.24	2
PA6,10	water	29	3.61	0.47	2.26	1.3
PA6,10	water	40	3.61	0.46	2.39	1.3
PA6,10	water	51	3.61	0.48	2.11	1.3
PA6,10	ethanol	40	6.94	0.62	2.74	2

Table 4.1: GAB parameters for water and ethanol sorption isotherms and calculated Mean Cluster Size

several layers and differentiates between the water molecules from the first sorbed layer and the ones from the additional layers. The sorption isotherms can be fitted with equation (1.24) (fit shown in Figure 4.1).

The GAB model gives excellent fits for both water and ethanol isotherms. The resulting parameters are listed in Table 4.1. The values of the GAB parameters are in agreement with the literature [2, 50]. The obtained water content in the first layer M_m is 5% in PA6,6 and 3.6% in PA6,10, which in molar intake gives 0.31 and 0.28 respectively. The ethanol content in the monolayer is 10% in PA6,6 and 7% in PA6,10, which in molar intake gives 0.25 and 0.21 respectively. The Guggenheim constants C and constant A have close values in the two polyamides, indicating that there is little difference in the adsorption energy of a water molecule in PA6,6 or in PA6,10.

The GAB parameters can also be used to estimate the size of solvent clusters (Mean Cluster Size, MCS) with equation (1.25) [68]. The MCS values reported in Table 4.1 are in agreement with literature data for PA6,6 [2, 150] (and with results of molecular dynamic simulations for water [153]). A low MCS value of 1.3 for water in PA6,10, as well as the linear shape of the sorption isotherms, suggest that water does not form clusters in PA6,10. On the other hand, ethanol forms clusters of two molecules in the same polymer. Altogether, this indicates that water is distributed in polyamide down to molecular size (or length scale) or nearly (cluster size 1.5-2) and does not form nanodomains (ordered or not) like for example in lyotropic systems (surfactant/water mixtures). This implies that diffusion will be isotropic, not affected by structuration at nanometer scale.

The net isosteric heat of water sorption in PA6,6 was calculated based on equation (1.15), from the slope of $\ln a_C$ as function of 1/T at constant water concentration (Figure 4.4(a)). ΔH is the heat of water sorption at a constant mass intake. The obtained values are shown in Figure 4.4(b). The low values of ΔH at low water intake provide evidence for the existence of specific interactions between water and polyamide. The values of the net isosteric heat of sorption are roughly in agreement with those obtained by Lim *et al.* (-10 to -3 kJ/mol in the range 25-45°C) [2] and Skirrow and Young (-5 to 0 kJ/mol in the range 36-90°C) [60]. For PA6,10, sorption isotherms are independent of temperature, as it can be seen in Figure 4.1. Therefore, the net isosteric heat of sorption is zero over the whole range of water concentrations (Figure 4.4(b)). The enthalpic contribution to water sorption is lower in PA6,10 than in PA6,6.

If we want an accurate assessment of the effect of hydrogen bond density on sorption, the molar intakes of solvents have to be compared in PA6,6 and PA6,10. It is observed that water is more absorbed by PA6,6 than by PA6,10: molar intake at equilibrium Δn = 0.94 and 0.51 respectively for a=1 at 40°C. The number of polar amide groups/g of polymer is 23% higher

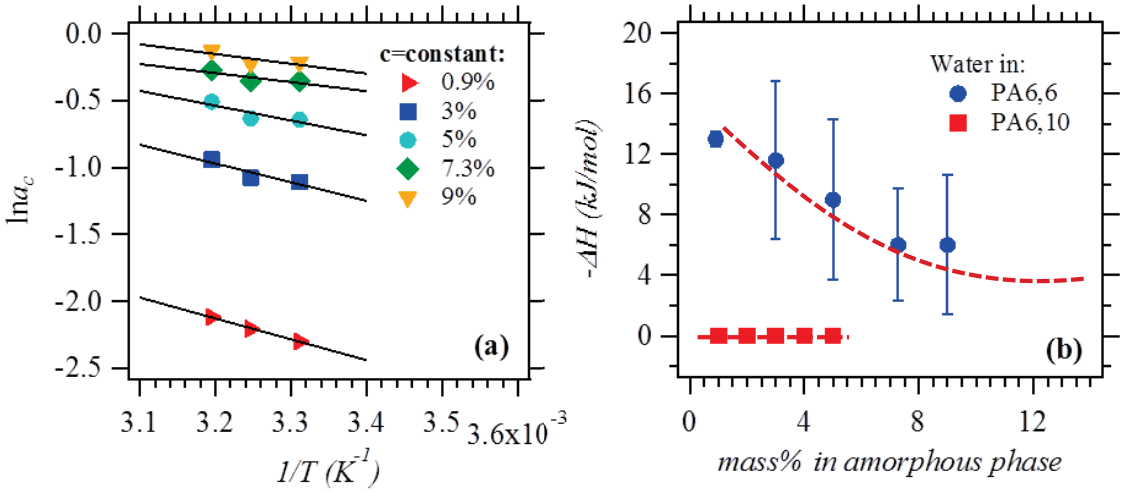

Figure 4.4: (a) $\ln a_c$ as a function of 1/Temperature (29, 35, 40°C) for constant water concentrations in PA6,6. Black lines were obtained with a linear fit. (b) Net isosteric heat of sorption of water in PA6,6 (calculated based on the slopes in (a) and equation (1.15)) and in PA6,10. Dashed lines are a guide for the eye.

in PA6,6 than in PA6,10, making PA6,6 more hydrophilic. However, the difference in water intake is much higher than the difference in amide group density. For ethanol at activity a=1, the molar intake at equilibrium is 0.46 in both polymers. The difference in amide group density doesn't seem to have any influence on the sorption of ethanol. These observations do not follow any trend, indicating that some other factors have to be taken into account. As highlighted in Chapter 3, more information on the amorphous phase heterogeneity is needed.

4.2 Analysis of phase composition by ^{1}H T_2 relaxation

The crystalline fraction, the proportion of RAF and MAF determined by DSC are different in the two polymers (Table 4.2). Also, the observation of the polyamide films by cross-polarization in microscopy shows a different morphology of the films (Figure 4.5). PA6,6 presents a well-defined spherulitic structure, whereas PA6,10 has small spherulites that give a weak polarization. In order to better grasp the heterogeneity of the amorphous phase and the influence of water, the ^{1}H NMR relaxation was measured by low-resolution NMR for dry and D_2O saturated polyamide. D_2O molecules do not contribute to the proton NMR relaxation, so the plasticization effect of water can be assessed by comparing the T_2 relaxation data of the dry and D_2O saturated polyamide [55].

	χ_C (%)	RAF%	MAF%
PA6,6	38	33	29
PA6,10	23	47	30

Table 4.2: Crystalline, RAF and MAF mass fractions obtained by DSC and MDSC for PA6,6 and PA6,10 films

The T_2 relaxation decay obtained by FID and MSE for PA6,6 is illustrated in Figure 4.6. Similar behavior was observed for PA6,10. The use of MSE allows the recovery of the inital part of the signal that is lost because of the receiver dead time in FID.

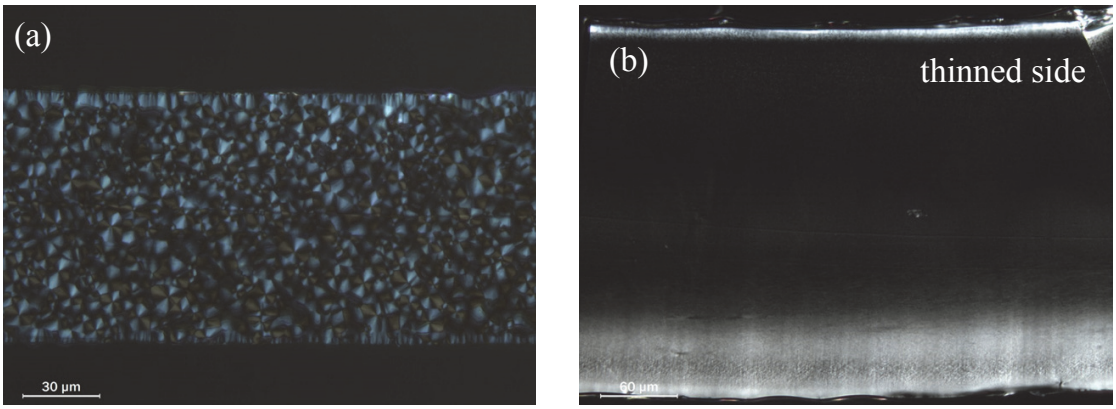

Figure 4.5: Observation of (a) PA6,6 and (b) PA6,10 films by cross-polarization in microscopy. Magnification=40 and 20 × 1.6, respectively

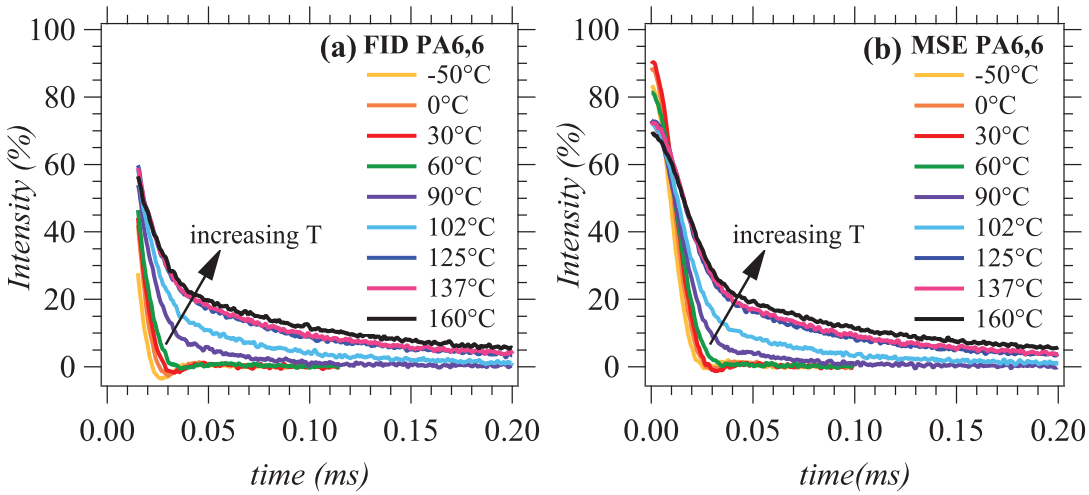

Figure 4.6: PA6,6 100 *µm* film (a) FID and (b) relaxation signal obtained after a MSE sequency (time zero corresponds to the top of the echo), at different temperatures

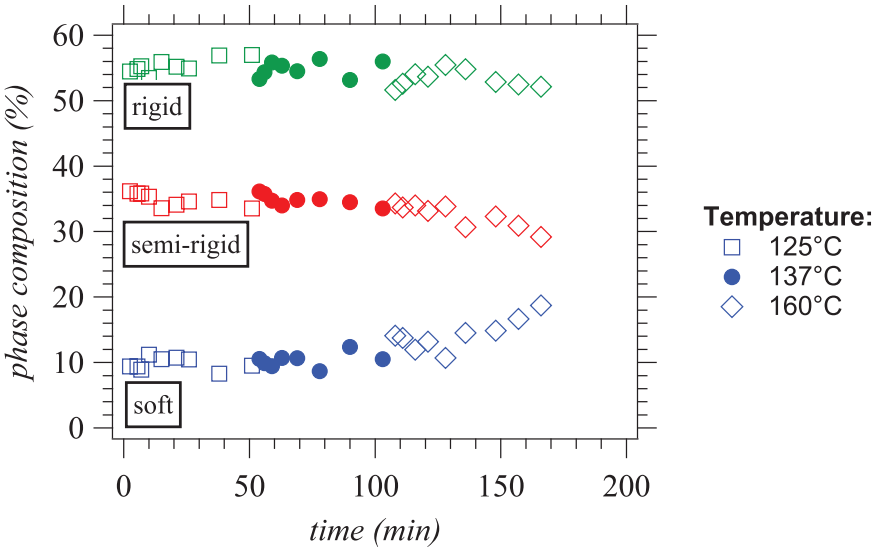

Figure 4.7: PA6,6 100 μm film phase composition as a function of measurement time at successive temperatures

At low temperatures, all the sample is rigid and the signal decays rapidly in less than 20 μs. When the temperature increases, the amorphous phase becomes more mobile and an additional decay with a longer relaxation time appears. The contribution of the amorphous phase becomes larger as the temperature is well above T_g. High temperatures, up to 160°C have to be used in order to fully activate the molecular mobility in the amorphous phase.

Since the experiments are performed at high temperatures well above T_g, sample exposure to elevated temperatures can cause changes in the phase composition and morphology (annealing). Therefore, the samples were checked for annealing under the experimental conditions. A measurement at a temperature T takes approximately 50 minutes: 20 min for temperature equilibration and 30 minutes of measurements. The phase composition was followed in the high temperature range 125-160°C as a function of time. The NMR spectra are fitted with a three phase model (equation (2.12)), which provides the relaxation times and phase composition for the fast (rigid, crystalline?), intermediate (semi-rigid, RAF?) and long (soft, MAF?) components of the relaxation. The phase composition for the PA6,6 film is presented in Figure 4.7 as a function of time and temperature.

For each temperature, the phase composition is stable during the 50 minutes of measurement. At 160°C however, the amorphous phase composition started to change after this period (t>150 min). For this reason, special care was taken not to exceed 50 min of measurement at 160°C. The absence of annealing was also confirmed by DSC measurements: the glass transition temperature and crystalline ratio did not change after temperature treatment.

The absence of annealing being confirmed, the phase composition and T_2 relaxation times of dry and D_2O saturated polyamide are shown in Figure 4.8 and 4.9 respectively. The values are in agreement with the literature on PA6/water systems [55]. Three distinct T_2 relaxation components can be resolved at high temperatures. As the temperature increases, the percentage of rigid phase decreases in favor of a more mobile phase. At high temperature, it can be considered that most of the amorphous phase is mobile and that the rigid contribution to the signal comes from the crystalline phase. Therefore, the last measured percentage of the rigid phase should be close to the crystalline ratio obtained by other techniques. At the highest temperature (160°C for dry and 95°C for D_2O saturated), the phase composition is given in

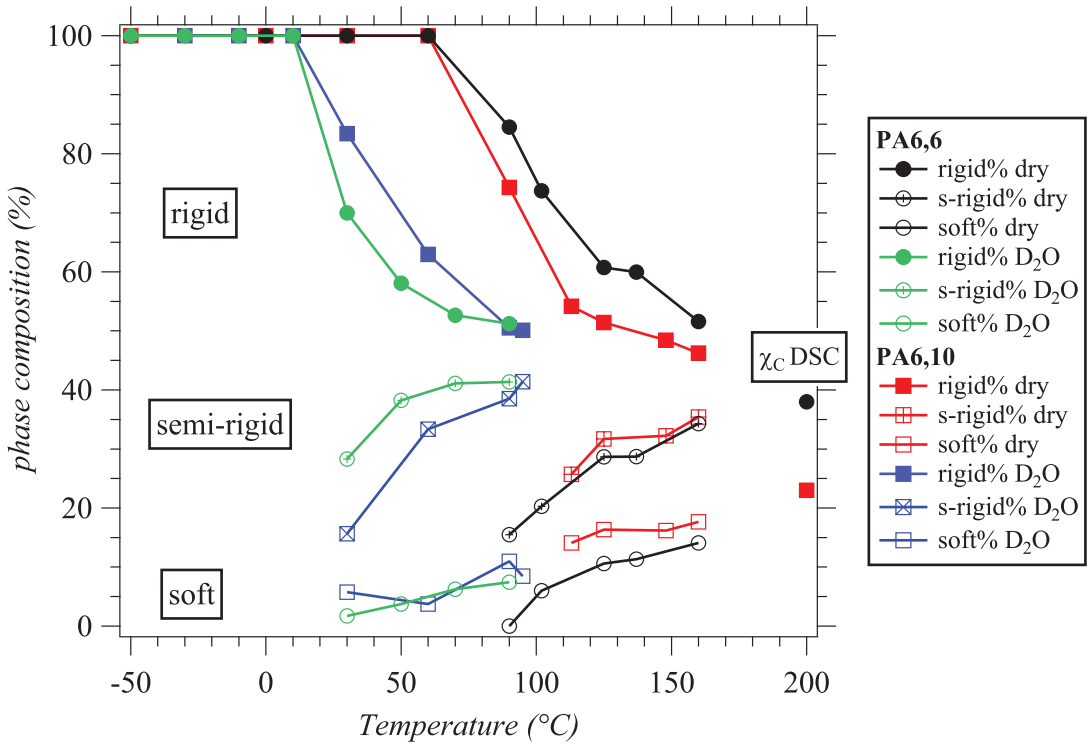

Figure 4.8: Phase composition of PA6,6 100 μm film and PA6,10 300 μm plate, dry and D_2O saturated. Notation in legend: s-rigid= semi-rigid. The crystalline ratio obtained by DSC χ_C is added for comparison.

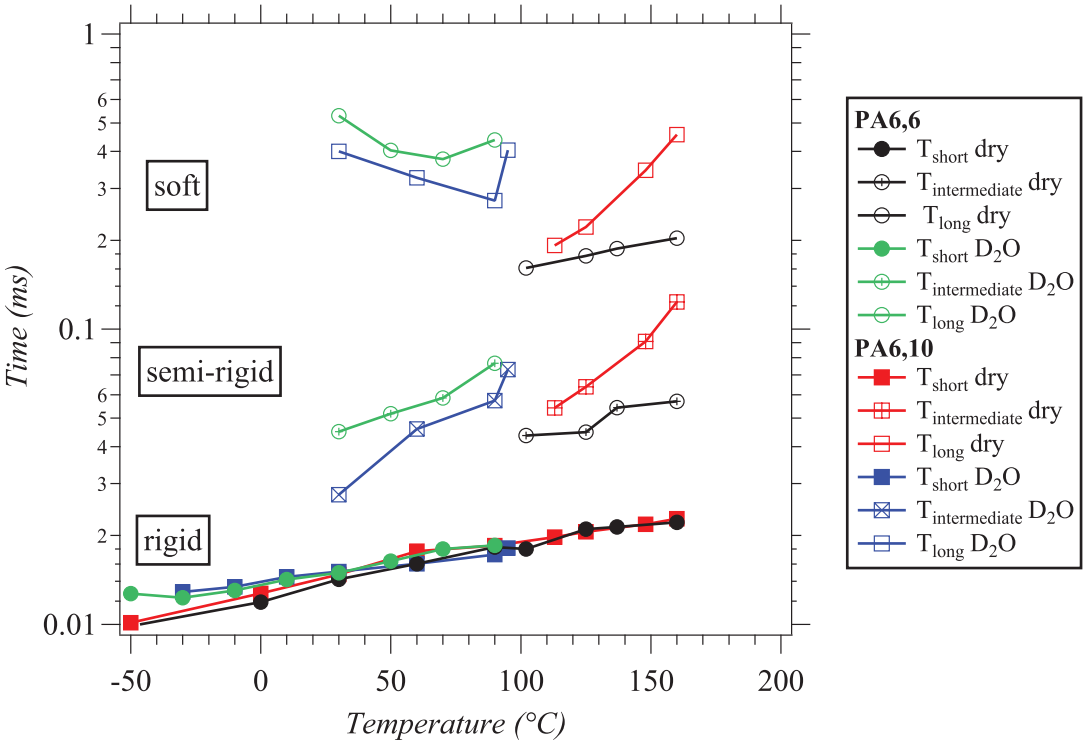

Figure 4.9: T_2 relaxation times of phase components of PA6,6 100 μm film and PA6,10 300 μm plate, dry and D_2O saturated

	rigid %	semi-rigid %	soft %
PA6,6 dry 160°C	52	34	14
PA6,6 D_2O 40°C	64	33	3
PA6,6 D_2O 95°C	51	41	8
PA6,10 dry 160°C	46	35	17
PA6,10 D_2O 40°C	76	22	5
PA6,10 D_2O 95°C	50	41	9

Table 4.3: Phase composition of the two PA at highest temperature (160°C for dry and 95°C for D_2O saturated) and at 40°C. The relative error is estimated at 5% of the values [55].

Table 4.3.

The crystalline ratio of PA6,6 (38%) and PA6,10 (23%), as determined by DSC, is significantly smaller than the crystallinity ratio obtained by NMR (approximately 50%). This difference has already been observed in the literature [55, 56] for NMR, DSC and WAXS and was explained by the intrinsically different nature of the measurements. Discrimination of the amorphous phase from the crystalline phase is made based on the enthalpy of melting (DSC), long-range periodicity (WAXS) and molecular mobility (NMR relaxometry). Compared to WAXS, NMR crystallinity accounts for both large and small nanosize crystals as well as disordered crystals. In DSC, morphological rearrangements can occur during heating and might complicate the analysis.

As seen in Chapter 5, the presence of water in PA6,6 and PA6,10 results in a decrease in the glass transition temperature. T_g can be read at the inflection point in the variation of the percentage of rigid phase. The value is roughly 30°C above the value determined by DSC and corresponds to the T_g value determined by dielectric spectroscopy at 20 kHz as expected. Water acts as a plasticizer and the molecular mobility of the amorphous phase increases. This can be observed as well in NMR, the glass transition of the water/polyamide systems being shifted to lower temperatures by about 50 to 70°C in Figure 4.8 (primary effect). For each polymer matrix, the presence of water results in an increase of the semi-rigid phase percentage, a decrease in the soft phase percentage and longer T_2 relaxation times.

The variation of the T_2 relaxation times does not follow the expected trend in presence of water. T_2 should vary following [154]:

$$T_2^{-1} = \omega_0^2 \tau_C \tag{4.1}$$

where $\omega_0/2\pi$ = 20 kHz (order of magnitude of proton-proton couplings) and τ_C is a correlation time for molecular movements, supposed to decrease when temperature increases. Based on equation (4.1), T_2 should therefore increase with temperature. This is indeed the case for the dry samples. However, T_2 of the soft phase in presence of water decreases with temperature. The polymer films were immersed in an excess of D_2O, under an argon blanket and the tube was closed with a cap and parafilm. In spite of these precautions, water might have evaporated during the measurements, which could explain the decrease in T_2. The phase composition and T_2 relaxation times for polyamide/D_2O at high temperatures is therefore only an estimation. On the other hand, water evaporation is not significant at 30-40°C, as evidenced for other measurements (DSC, BDS) in this PhD work. The determined composition at 40°C is close to reality and can be compared. It should be highlighted that PA6,6 and PA6,10 do not have the same phase distribution in presence of D_2O. The distributions are listed in Table 4.3 at 40°C (one of DVS temperatures) for comparison. The rigid fraction and its T_2 relaxation time at high temperatures do not vary in presence of solvent: some fraction of polyamide (crystalline

phase) is indeed impermeable to water.

Lastly, equation (4.1) provides an estimation of the correlation time for molecular movements τ_C. It is interesting to compare τ_C to the relaxation chart of polyamide obtained by Dielectric Spectroscopy measurements (Figure 5.10). In Figure 5.10, the values of τ_C correspond to a frequency range of $10^8 - 10^9$ Hz in the 1000/T range from 2.3 to 2.75. This range is equivalent to the region in which all polymer relaxations (α, β, γ) would overlap. Indeed, well above T_g, all segmental motions are fast and it becomes difficult to distinguish the various motions corresponding to the different relaxation processes. The estimated value of τ_C indicates that in NMR, all these fast motions contribute to the relaxation.

4.3 Discussion

Up to this point, each polymer matrix was studied individually and provided results on sorption mechanisms and solvent clustering. It is observed experimentally that solvents are less absorbed in the amorphous phase of PA6,10 than in PA6,6. In an attempt to compare the influence of the density of hydrogen bonds, the ratio of the molar intakes in the two polymers can be compared to the theoretical ratio of amide groups ($\Delta n = 1.23$). The experimental ratios are listed in Table 4.4 at equilibrium at activity $a = 1$, T=40°C.

	$\frac{\Delta n_{6,6}}{\Delta n_{6,10}}$ water	$\frac{\Delta n_{6,6}}{\Delta n_{6,10}}$ ethanol
a = 1	2.26	1

Table 4.4: Ratio of solvent molar intake in PA6,6 and PA6,10 at 40°C. The theoretical value, given by the ratio of amide groups, is $\Delta n = 1.23$

It is observed that the values are different from the theoretical ratio of 1.23. The difference depends on the type of solvent, which might be explained either by a different accessibility of the amide groups in the amorphous phase and/or by secondary phenomena like swelling or clustering. As discussed above, the clustering behavior of water is slightly different in the two polyamides (MCS=1 in PA6,10 compared to 2 in PA6,6) but the same for ethanol (MCS=2). On the other hand, our study on amorphous and semi-crystalline aromatic polyamide showed that water does not penetrate in all the amorphous phase. The comparison of water and alcohols of different sizes showed that accessibility might also depend on the type of molecule. All in all, if we want to compare the two polymers, their morphology should be taken into account.

With this aim, the phase distribution of dry and D_2O saturated polyamides was measured by low-resolution ^{1}H NMR up to elevated temperatures. The results of this study are in agreement with the literature [55, 56, 57]. It was shown that the dynamics of the polymer change in presence of water, which can penetrate in the semi-rigid and soft phases. If we want to interpret the sorption data, we are mainly interested in this phase distribution at the DVS experimental temperature, for instance 40°C. Previous NMR studies [33, 58] on PA6/water systems at room temperature have shown that only a small fraction of the amorphous phase was occupied and plasticized by water: 6% of the amorphous phase had a clearly enhanced mobility, 26% of the amorphous phase had a slightly increased mobility and the remaining percentage (approx. 70%) was either non-plasticized amorphous, or the crystalline phase. Our findings are similar: approx. 70% of each polyamide gives a rigid signal and the remaining 30% is affected by water.

Based on these results, we estimate that water changes the dynamics of 27% of PA6,10 and 36% of PA6,6 film. If we consider that water actually penetrates only in this small percentage of the polymers, we obtain a ratio of water molecules/amide groups (Δn) of 1.1 and 1.51 for PA6,10 and PA6,6 respectively. The ratio between the two polymers is then 1.37, closer to the theoretical

ratio of 1.23. However, the proportions of semi-rigid and soft phases are different in PA6,6 and PA6,10, indicating that water does not have the same accessibility of the amorphous phase and that the distribution of the latter depends on the polymer. Therefore, the comparison of the two polyamides is only speculative: the influence of the density of hydrogen bonds cannot be assessed accurately.

4.4 Conclusion

The sorption isotherms of water and ethanol were recorded in two polyamides of different density of hydrogen bonds, PA6,6 and PA6,10. A GAB model provides an excellent description of the sorption isotherms for both polymers, predicting sorption in preferential sites and mean cluster sizes of 1-2 molecules of solvent. It indicates that water is distributed in polyamide down to molecular size, meaning that diffusion will be isotropic.

In order to assess the influence of the density of hydrogen bonds, the number of accessible sorption sites must be determined. As highlighted in several literature studies [54, 55, 56], morphology and phase composition are influenced by the processing and the thermal history of semi-crystalline polyamide. Also, it was shown in Chapter 4 that the amorphous phase of a semi-crystalline polyamide was not entirely accessible to solvents. In the attempt to discriminate the phase composition of PA6,6 and PA6,10 films prepared by different processing methods, low-resolution ^{1}H NMR measurements were performed.

Three phases were identified in the polymer films (denoted rigid, semi-rigid and soft), with characteristic T_2 relaxation times in agreement with the literature [55, 33, 58]. At 40°C, the two polyamides did not have the same phase distribution in presence of water. A comparison between them would therefore be speculative. This chapter highlights once again the importance of taking into account polymer morphology when analyzing solvent sorption.

Chapter 5

Diffusion mechanisms in polyamide: influence of solvent and polymer relaxations

In Chapter 3, it was observed that water diffusion followed a Fickian mechanism, whereas ethanol diffusion followed a non-Fickian mechanism in semi-aromatic polyamides. The semi-aromatic polyamide systems were however not the best suited to understand their respective Fickian and non-Fickian diffusion mechanisms. Although there is no cavitation in A1007, sorption equilibriums were too long to attain with ethanol. Therefore, other semi-crystalline polyamides are more adapted for this study.

The aliphatic PA6,6 and PA6,10 were chosen for this investigation. The analysis of the sorption isotherms of water and ethanol evidenced that the solvents were distributed at a molecular level and that diffusion should be isotropic. In this Chapter, the diffusion mechanisms of water and ethanol will be investigated. A DVS experiment was used in order to measure diffusion coefficients as a function of solvent activity or equivalently solvent concentration. Moreover, dielectric spectroscopy measurements gave access to the characteristic relaxation times of water/polyamide systems. Therefore, the influence of polymer relaxations (dynamics) on diffusion mechanisms will be assessed. As highlighted in Chapter 4, the polyamide films have a different phase distribution and their comparison is not straightforward. For this reason, each matrix will be analyzed individually.

5.1 Influence of solvent: water vs. ethanol

5.1.1 Diffusion of liquid solvents

In the attempt to understand why water diffusion is Fickian and ethanol diffusion is non-Fickian in polyamide, two commercial polyamides have been investigated: PA6,10 (films of 300 μm) and PA6,6 (films of 100 μm). The sorption of liquid water and ethanol in the two polyamides was measured at three temperatures (25, 40 and 55°C). The curves at 40°C are presented in Figure 5.1, the shapes being the same for all temperatures. Since the films did not have the same thickness, the x axis was normalized with respect to each thickness in centimeters.

For water in PA6,10, the normalized water intake $M(t)/M_{eq}$ increases linearly with $t^{1/2}$ and a Fickian model fits the experimental data perfectly for all temperatures. The calculated diffusion coefficients are 3×10^{-9}, 1.1×10^{-8} and 3.5×10^{-8} cm^2/s for the three temperatures respectively. Assuming that the diffusion coefficient dependence on temperature follows an Arrhenius law, an activation energy of 66 kJ/mol is obtained for the diffusion of water in PA6,10. This value is within the range of 60 to 80 kJ/mol activation energies reported for diffusion of water in PA6,6 [2, 14].

The curves obtained for the diffusion of ethanol in PA6,10 and both water and ethanol in PA6,6 at 40°C have a sigmoidal shape with an upward inflexion point. This indicates that the diffusion mechanism is not Fickian; diffusion accelerates in the course of the sorption experiment. Consequently, the experimental data cannot be fitted with equation (1.11) (see Figure 5.1(b) for water).

Before looking more in-depth into diffusion or sorption mechanisms, the XRD scans of dry

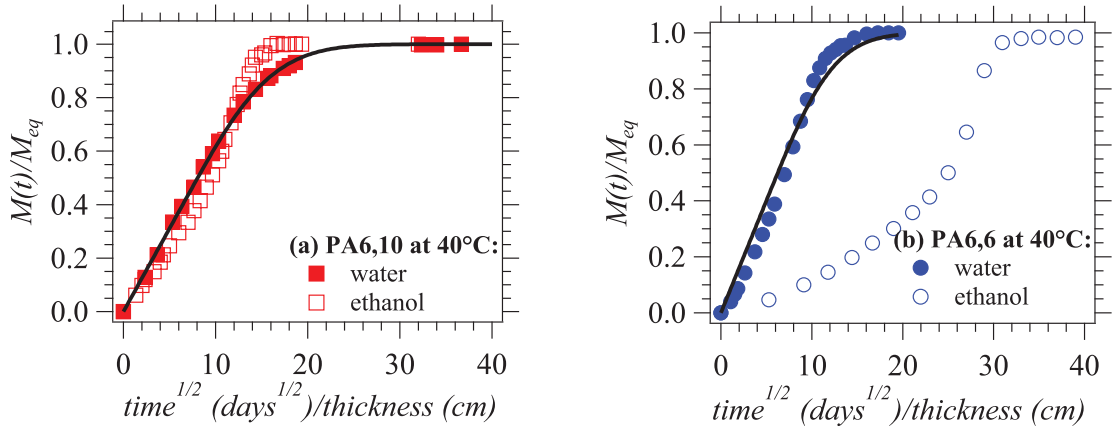

Figure 5.1: Sorption kinetics of liquid water and ethanol at 40°C in (a)PA6,10 and (b)PA6,6. Solid lines are obtained by fitting the data with equation (1.11) for Fickian diffusion.

and solvent saturated samples were recorded (see Figure 4.2 and discussion in Chapter 4). It was evidenced that the crystalline phase was perfected, as it has been observed in the literature on several occasions [12, 27, 51].

The evolution of the crystalline phase might have an influence on diffusion mechanisms. In order to test this concept, solvent saturated polyamide films were dried and then re-immersed in solvent (cycle 2 of sorption). XRD scans confirmed that the "perfected" crystalline structure was maintained after drying. The new sorption kinetics curves superimposed perfectly to the inital curve, meaning that the crystalline phase evolution did not influence diffusion mechanisms. Therefore, other phenomena might occur after a first step of linear Fickian diffusion: concentration dependent diffusion coefficient, swelling and/or polymer relaxation.

5.1.2 Dynamic Vapor Sorption

A Dynamic Vapor Sorption experiment was designed to separate the diffusion process from other phenomena. Swelling kinetics, polymer relaxation and concentration fronts appear when the solvent/polymer system is not at equilibrium. In DVS experiments, a polymer film can be kept through small activity steps from 0.1 to 0.9 so that the polymer reaches equilibrium at each step at water activity a before the next sorption experiment is launched at activity $a + \Delta a$. Therefore, the system should stay close to thermodynamic equilibrium when a new water population diffuses. If the activity steps are sufficiently small, diffusion occurs in a homogeneously relaxing environment, with limited swelling and a relatively constant water concentration. Solvent diffusion should then follow a Fickian mechanism at each activity step. However, for practical reasons related to the precision of the balance and the time span of the experiment, infinitesimal activity steps cannot be set up. In general, a good compromise consists in increasing the activity by 0.1 in the range 0.1 to 0.9. A typical curve obtained following this protocol has been shown in Figure 2.21 in Chapter 2.

Following this protocol, water sorption was recorded at 29, 35, 40 and 51°C for PA6,6 and 29, 40 and 51°C for PA6,10. The highest temperature (51°C) is close to the limit of the DVS device (60°C) so the 0.9 activity could not be reached. The measurements repeatedly stopped at activity 0.4 for PA6,6 and 0.6 for PA6,10. Ethanol sorption was recorder only at 40°C, for the reasons presented in the paragraphs below. The sorption isotherms associated to these DVS measurements were shown and discussed in Chapter 4.

Ethanol sorption was more difficult to set up in DVS. For PA6,10, the same protocol as

water was applied for ethanol sorption at 40°C: start at activity 0.1, wait for equilibrium and then increase activity by a step of 0.1. For water, the equilibrium had been reached in two days/activity step. For ethanol, the equilibrium was still not reached after 7 days at activity 0.1. The activity was then increased manually to 0.3 then to 0.4 and equilibrium was reached after an additional 8 days. At activity 0.5, the equilibrium was reached in 4 days and at the next activity steps, equilibrium was reached in 2 days. This accounted for a total time of 26 days for the measurement of ethanol sorption in PA6,10 at 40°C. During this time, the solvent bottle had to be changed several times, inducing variations in the ethanol activity setpoint. The ethanol sorption curves were therefore less smooth as in the case of water diffusion. Due to the difficulty and the time span of measurements with ethanol, only one temperature (40°C) was recorded for this solvent.

Ethanol sorption was also slow in PA6,6 at 40°C. For water, the equilibrium had been reached in 10 hours/activity step. For ethanol, the first activity step was set at 0.4 and equilibrium was reached after one week. For the next activity steps, time to equilibrium decreased from 2 days to one day. This accounted for a total time of 2 weeks of measurements, during the ethanol activity could not always be kept at the setpoint.

In order to obtain information on diffusion coefficients, the solvent uptake for each activity step is treated individually and plotted as the normalized mass intake as a function of the square root of time. Figures 5.2(a) and (b) illustrate the sorption kinetics of water in PA6,10 at 40°C. Similar curves were obtained at 29°C and 51°C. A linear increase of the normalized mass uptake is observed as a function of $t^{1/2}$. The diffusion mechanism is Fickian from activity 0.1 up to activity 1. A fit with equation (1.11) gives excellent superposition with experimental data and provides the values of the diffusion coefficients for each water activity. In the case of PA6,6, for which non-Fickian diffusion was observed in liquid water, the DVS experiment gave the expected Fickian diffusion mechanisms for low activities, as illustrated in Figure 5.2(c). However, a change occurred around activity 0.7, at which point the slightly sigmoidal shape of the curve suggests that the condition of quasi-equilibrium is no longer fully satisfied (Figure 5.2(d)), or that water diffusion is intrinsically anomalous. An estimate of the diffusion coefficients can still be provided by the fit with equation (1.11). The same type of behavior was obtained at 29, 35 and 51°C.

Figure 5.3 illustrates the sorption kinetics of ethanol in PA6,10 and PA6,6 at different activities. As stated before, some curves are less smooth due to variations in ethanol activity (see Figure 5.3(a) and (c)). A linear increase of the normalized mass uptake is observed as a function of $t^{1/2}$. For PA6,10, the diffusion mechanism is Fickian from activity 0.5 up to activity 0.9. A fit with equation (1.11) gives an excellent description of experimental data and provides the values of the diffusion coefficients for each ethanol activity. By applying small activity steps, ethanol diffusion mechanism passed from non-Fickian to Fickian in PA6,10.

For PA6,6 on the other hand, experimental curves can be fitted with equation (1.11) only from activity 0.5 to 0.7 (Figure 5.3(c)). For higher values of activity, a change is slope is observed around $M(t)/M_{eq} \simeq 0.8$. The data is no longer in agreement with a Fickian diffusion mechanism (Figure 5.3(d)). However, it would seem that a first plateau is reached at $M(t)/M_{eq} \simeq 0.8$, follwed by a slow approach to the final equilibrium. This type of curves, called two-step sorption, has already been observed in other polymers [39, 38, 155] and could be explained, to some extent, by slow polymer relaxation or swelling. In order to analyze two-step sorption, Berens and Hopfenberg [39] suggested an empirical model based on the linear superposition of Fickian diffusion and relaxation processes (equation (5.1)):

$$\frac{M(t)}{M_\infty} = (1-\alpha_R)\left(1 - \sum_{n=0}^{\infty} \frac{8}{(2n+1)^2\pi^2} exp\left(\frac{-D(2n+1)^2\pi^2 t}{l^2}\right)\right) + \alpha_R exp\left(-\frac{t}{\tau_R}\right) \tag{5.1}$$

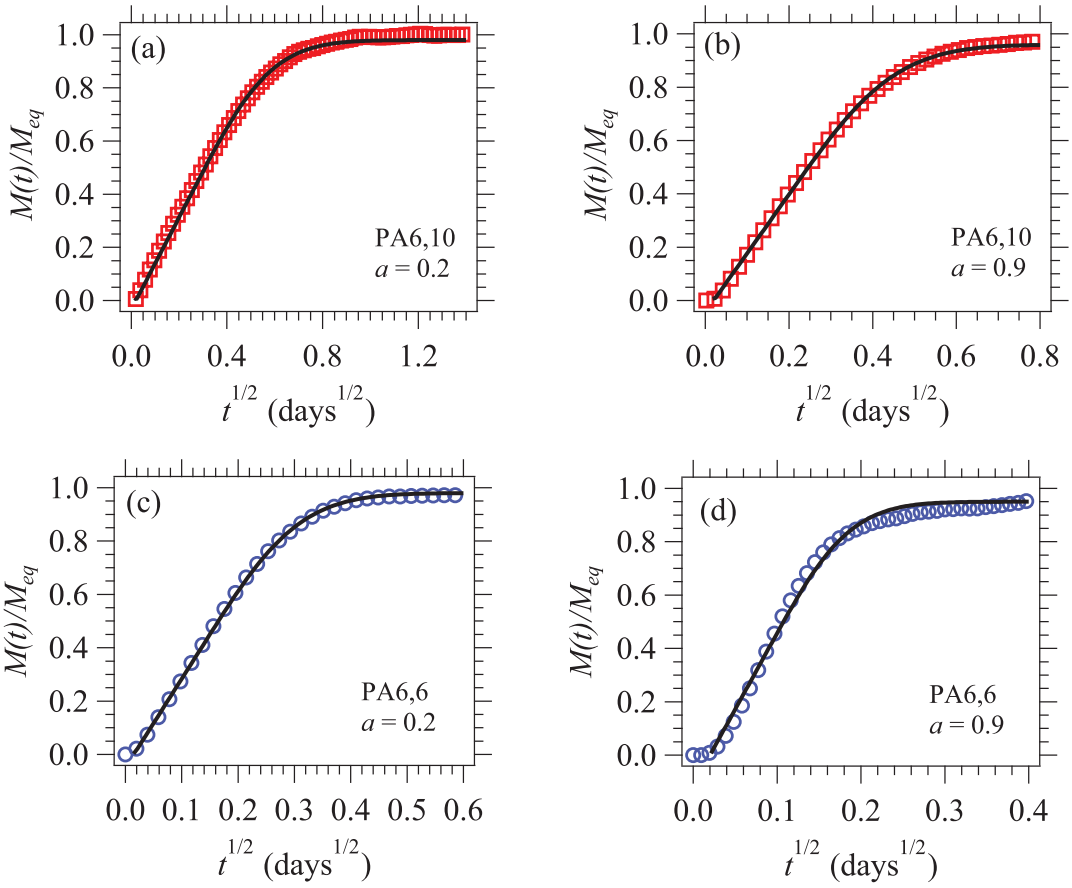

Figure 5.2: Experimental data and Fickian fits for the normalized mass increase as a function of $t^{1/2}$ for water sorption at 40°C: in PA6,10 at activities (a) 0.2 and (b) 0.9 and in PA6,6 at activities (c) 0.2 and (d) 0.9. Symbols are experimental points and lines are Fickian fits.

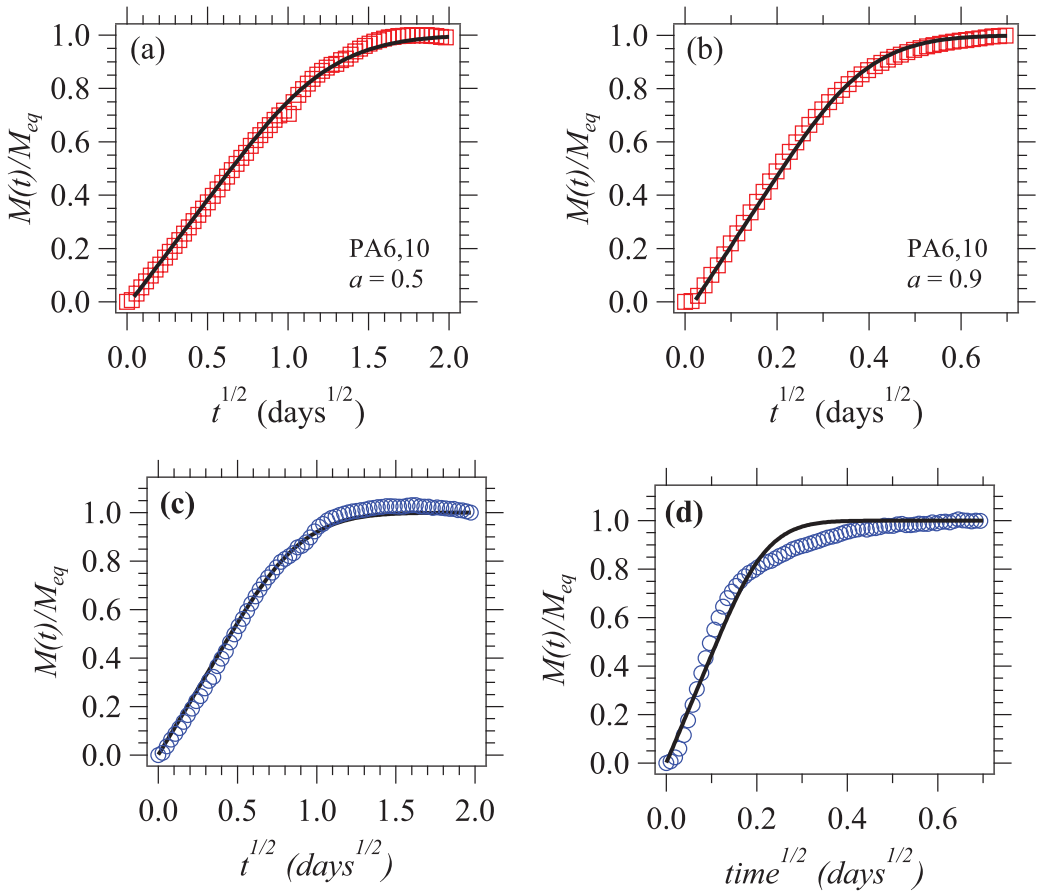

Figure 5.3: Experimental data and Fickian fits for the normalized mass increase as a function of $t^{1/2}$ for ethanol sorption at 40°C: in PA6,10 at activities (a) 0.5 and (b) 0.9 and in PA6,6 at activities (c) 0.5 and (d) 0.9. Symbols are experimental points and lines are Fickian fits.

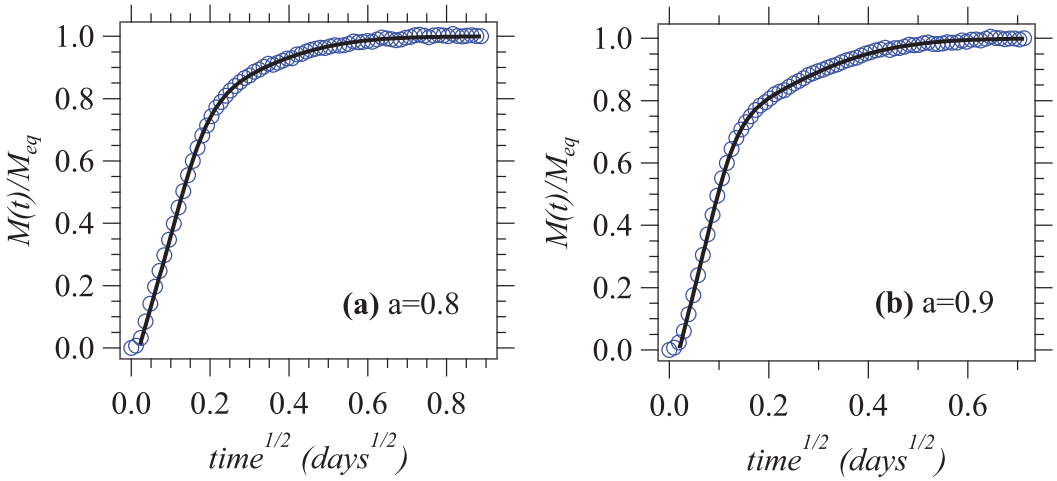

Figure 5.4: Sorption kinetics of ethanol at 40°C in PA6,6 at (a) a=0.8 and (b) a=0.9. Symbols are experimental points and lines are fits with the Berens-Hopfenberg model.

activity	D (cm^2/s) at 40°C	α_R	τ_R (days)
0.8	7.39e-9 ± 1.18e-10	0.257 ± 0.006	0.12 ± 0.002
0.9	1.7e-8 ± 1.55e-10	0.29 ± 0.002	0.09 ± 7e-4

Table 5.1: Values of Berens-Hopfenberg fit parameters for PA6,6/water systems in Figure 5.4

where (1-α_R) and α_R are the fractions of mass uptake in the overall sorption contributed by Fickian diffusion and relaxation processes, respectively and τ_R is the first-order time constant associated with the long time drift in mass uptake. The long time drift in sorption kinetics is usually ascribed to mass uptake controlled by the viscoelastic relaxation of the polymer chains to accommodate the penetrant [39].

In the initial stage the polymer is penetrant-free so the diffusion is dominated by a rapid Fickian process. As the sorption advances, the relative contributions of the polymer relaxations become more important. For a better fit of experimental data, McDowell *et al* [156] introduced the hypothesis that the relaxation process might not start at t=0 but rather at a later time. This idea was expressed by adding a delay time, t_D, to the relaxation process:

$$\frac{M(t)}{M_\infty} = (1-\alpha_R)\left(1 - \sum_{n=0}^{\infty} \frac{8}{(2n+1)^2\pi^2} exp\left(\frac{-D(2n+1)^2\pi^2 t}{l^2}\right)\right) + \alpha_R exp\left(-\frac{t-t_D}{\tau_R}\right) \quad (5.2)$$

It should be noted that this model supposes that the diffusion controlled process is essentially complete before the relaxation process begins. Moreover, the relaxation process is triggered at t_D. For a more accurate description of the transition behavior, a distribution around t_D and τ_R should be taken into account.

As it can be seen in Figure 5.4 the Berens-Hopfenberg model decribes well the experimental data. No delay time t_D was used for the fit. The values of the fit parameters are presented in Table 5.1.

The variation of the water diffusion coefficients as a function of activity and temperature is shown in Figure 5.5 for both polyamides. It is observed that diffusion coefficients are not constant. They vary slightly in PA6,10, increasing by a factor 2 at most. In PA6,6, diffusion coefficients are much more dependent on activity, increasing by a factor about 5.

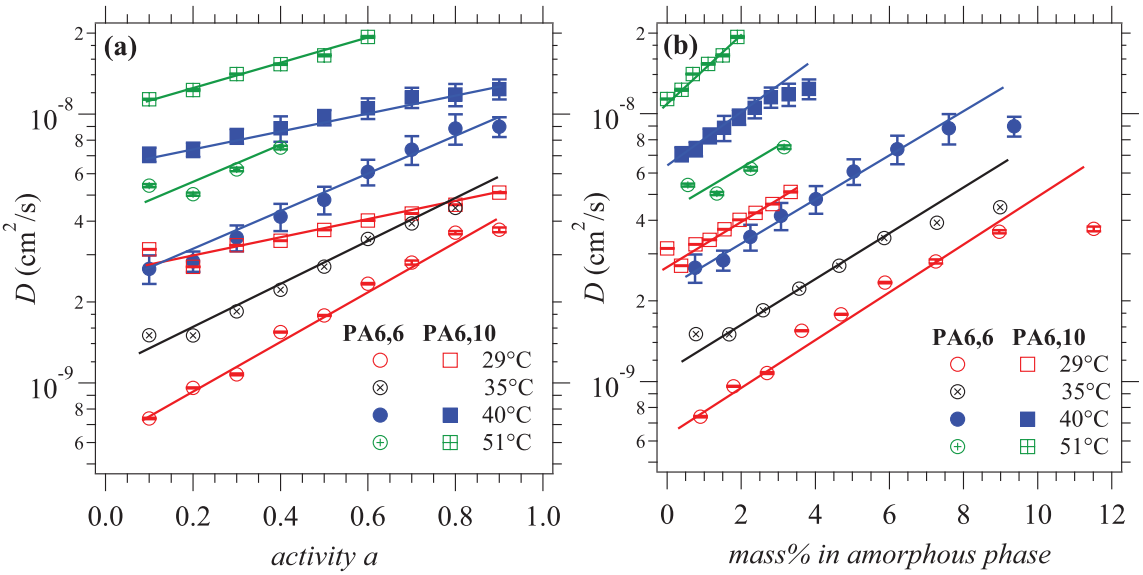

Figure 5.5: Variation of diffusion coefficients of water in PA6,6 and PA6,10 at different temperatures as a function of (a) water activity and (b) water intake (weight %) in the amorphous phase. Lines are guides for the eye.

Moreover, Figure 5.5 illustrates that water diffusion is faster in PA6,10 than in PA6,6 at the same experimental temperature, especially at low activities. As the activity increases, the values of the diffusion coefficients in PA6,6 approach those in PA6,10. The experimental temperatures were also chosen so as to have equivalent $T - T_g = 24°C$, as is the case for PA6,6 at 40°C and PA6,10 at 29°C or $T - T_g = 13°C$, as is the case for PA6,6 at 51°C and PA6,10 at 40°C. As it will be highlighted in the next section, the glass transition temperature of the water-polyamide systems varies rapidly as water is absorbed so this initial condition of equivalent mobility of the polymer chains is no longer valid. Additionally, it can be noticed that diffusion coefficients are slightly higher in PA6,10 than in PA6,6 for the two equivalent values of $T - T_g$.

Ethanol diffusion coefficients are presented in Figure 5.6 for both polyamides as a function of water activity and ethanol intake in the amorphous phase. In this case as well, diffusion coefficients are not constant. They vary by one decade for PA6,10 and by two decades for PA6,6 from activity 0.5 to activity 0.9. It should be highlighted that the values of the diffusion coefficients obtained for PA6,6 at activities 0.8 and 0.9 with the Berens-Hopfenberg model are in the continuity of the diffusion coefficients obtained with a Fickian model. The Berens-Hopfenberg model gives therefore a good description of the diffusion of ethanol at high activities in PA6,6.

5.1.3 Discussion

The sorption kinetics of water and ethanol were recorded in PA6,10 and PA6,6 at several temperatures. It was observed that the diffusion mechanism is Fickian for water in PA6,10 but non-Fickian for water in PA6,6. Also, it was observed that ethanol diffusion followed a non-Fickian mechanism in both polymers. In order to better understand the reasons behind these mechanisms, a Dynamic Vapor Sorption experiment was designed. In DVS, small activity steps can be applied to a polymer film, allowing it to reach equilibrium at an activity a before a new solvent population is added at activity $a+0.1$. Therefore, the polymer film is in a quasi-equilibrium state and diffusion can be decoupled from other phenomena like swelling or

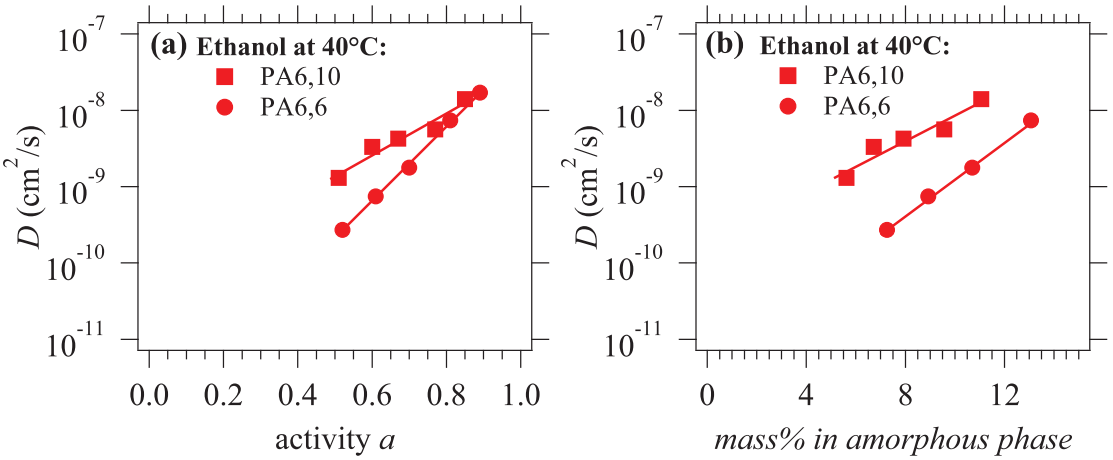

Figure 5.6: Variation of diffusion coefficients of ethanol in PA6,6 and PA6,10 at 40°C as a function of (a) ethanol activity and (b) ethanol intake in the amorphous phase. Lines are guides for the eye.

polymer relaxation. This experiment design produces Fickian diffusion for each activity step, provided that the steps are small enough.

Indeed, Fickian diffusion was obtained for water or ethanol at intermediate activities (except for a slight drift for water and ethanol at high activities in PA6,6). Diffusion coefficients were obtained as a function of solvent activity/mass intake in the amorphous phase. It is observed that water diffusion coefficients are almost constant in PA6,10 as a function of activity. Since Fickian diffusion is characterized by a constant diffusion coefficient, this explains why liquid water diffusion is Fickian in PA6,10. On the other hand, water diffusion coefficients vary by a factor 5 in PA6,6. A concentration dependent diffusion coefficient is one of the origins of non-Fickian diffusion mechanisms [35], which might explain the sigmoidal sorption profile of water in PA6,6. The same explanation applies for ethanol diffusion in PA6,6 or PA6,10. Ethanol diffusion coefficients vary by more than a decade, which explains the strong non-Fickian profiles of liquid ethanol diffusion in the two polymers.

The comparison of water and ethanol diffusion coefficients is illustrated in Figure 5.7 as a function of solvent activity. Ethanol diffusion coefficients vary much more with the solvent activity, which might account for the stronger non-Fickian profile of ethanol diffusion. This difference is exacerbated in PA6,6, with diffusion coefficients varying over several decades for ethanol, compared to a factor 5 for water.

On the whole, it would seem that ethanol diffuses much slower than water. Several explanations could exist for this slow diffusion: ethanol molecule is bigger than water so it is inherently slower, ethanol might not have the same accessibility of sorption sites or that the PA matrix is plasticized. The hypothesis of ethanol accessibility could have been tested on model amorphous and semi-crystalline polyamides in Section 3.1 but unfortunately other phenomena (cavitation, crystallization) prevented any conclusions. For plasticization, the glass transition temperature of water and ethanol/polyamide systems was measured at different solvent intakes. The shift in the glass transition temperature is shown in Figure 5.8 as a function of the number of solvent molecules/amide group (Δn defined in Chapter 2). As it can be seen in Figure 5.8, ethanol plasticizes polyamide more than water. It would be interesting thus to evaluate the influence of polymer dynamics on diffusion mechanisms.

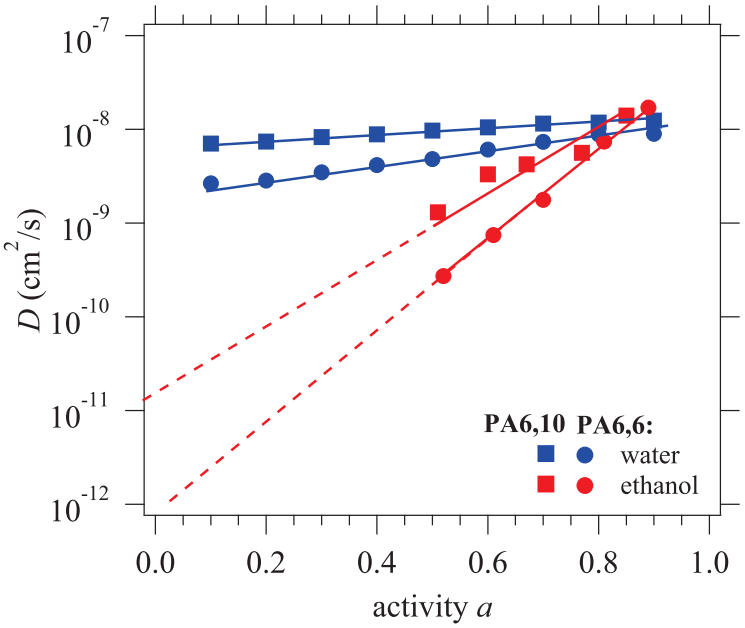

Figure 5.7: Comparison of diffusion coefficients (logarithmic scale) of water and ethanol in PA6,6 and PA6,10 at 40°C as a function of solvent activity. Lines are guides for the eye. Dotted lines are an extrapolation for low activities of ethanol, based on the slopes at high activities.

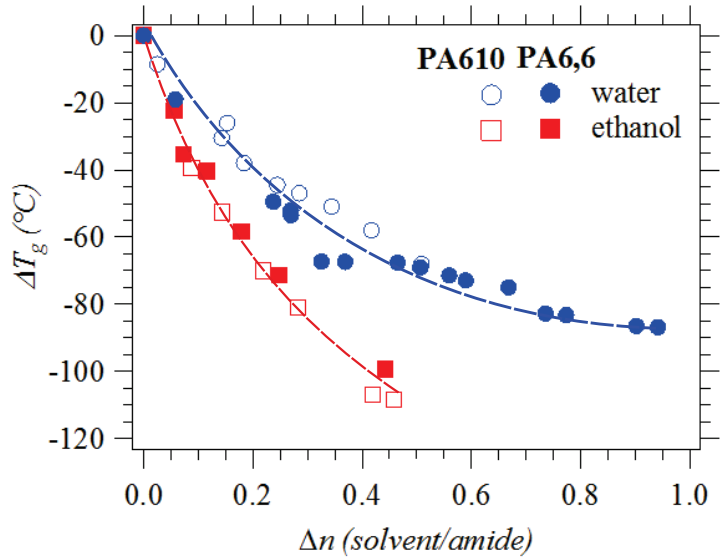

Figure 5.8: Shift in the glass transition temperature PA6,6 and PA6,10 in presence of water and ethanol. Lines are guides for the eye.

5.2 Diffusion mechanisms and polymer relaxation

As seen in the previous section, non-Fickian diffusion mechanisms can be caused by the variation of diffusion coefficients with solvent concentration. It is unclear however if polymer relaxations have an influence on diffusion mechanisms. In order to decouple polymer relaxations and water diffusion, a step-by-step experiment has been adopted by using Dynamic Vapor Sorption (DVS). This protocol has allowed the measurement of diffusion coefficients in a wide range of temperatures and water activities. The same systems can be investigated in Dielectric Spectroscopy in order to better understand their dynamics and attempt a correlation to diffusion mechanisms. Since ethanol diffusion was difficult and extremely long to measure in DVS, this study was only done for water.

Spatially resolved water uptake was studied quantitatively by NMR imaging [33, 58, 59]. The most recent study has shown that a plasticization lag exists, meaning that a few percentages of water were absorbed in the material before plasticization was visible [59].

Thus, it would be interesting to study if there is a correlation between penetrant diffusion and the mobility of the polymer chains due to amorphous phase heterogeneity or plasticization. To the best of our knowledge, no previous study has investigated directly the correlation between the diffusion coefficient and the polymer relaxations (main α relaxation and more local, secondary relaxations) in polyamides.

The objective of this study is to investigate the relationship between water diffusion and the various relaxation processes in polyamides. For this, we have measured water diffusion coefficients and the polymer relaxation times as a function of water activity. Two different polyamides with slightly different ratios of amide/methylene groups (PA6,6 and PA6,10), obtained with different processing conditions, have been studied. The main purpose is to understand diffusion mechanisms, in particular whether or not diffusion is coupled to polymer relaxation. The influence of the ratio of amide/methylene groups, *i.e.* the density of hydrogen bonds, is tentatively discussed.

5.2.1 α relaxations of water-polyamide systems

Anomalous or non-Fickian effects might be related to the influence of the evolving polymer mobility on diffusion or to the internal stresses (swelling) exerted as diffusion proceeds [35, 45]. Since water decreases the glass transition temperature of polyamide [2, 3], it is interesting to study if there is a correlation between diffusion and the mobility of polymer chains.

To begin with, the glass transition temperatures T_g of the two polyamide-water systems were measured by Differential Scanning Calorimetry (DSC) at intermediate water mass uptakes corresponding to different activity values (Figure 5.9). PA6,10 absorbs less water than PA6,6 in the activity range 0.1 to 0.9 (for details, see Chapter 4). The overall decrease in the glass transition temperature is thus smaller in PA6,10/water system at equilibrium than in PA6,6/water (-50°C compared to -80°C, respectively).

More detailed information on the polymer mobility can be obtained by dielectric spectroscopy. This technique gives access to the characteristic times of the polymer relaxations as a function of temperature. The α relaxation in dielectric spectroscopy is associated to the glass transition so the α relaxation times give an indication about the polymer mobility. The glass transition temperature measured by DSC can be added to these data by considering that the equivalent relaxation time in DSC measurements is approximately 100 seconds [25]. The relaxation times were initially measured for the dry and water equilibrated PA6,6 and PA6,10 films (Figure 5.10). It was observed that all relaxations shifted to lower temperatures in presence of water. In order to check if this shift was gradual, the relaxation times of water/polyamide

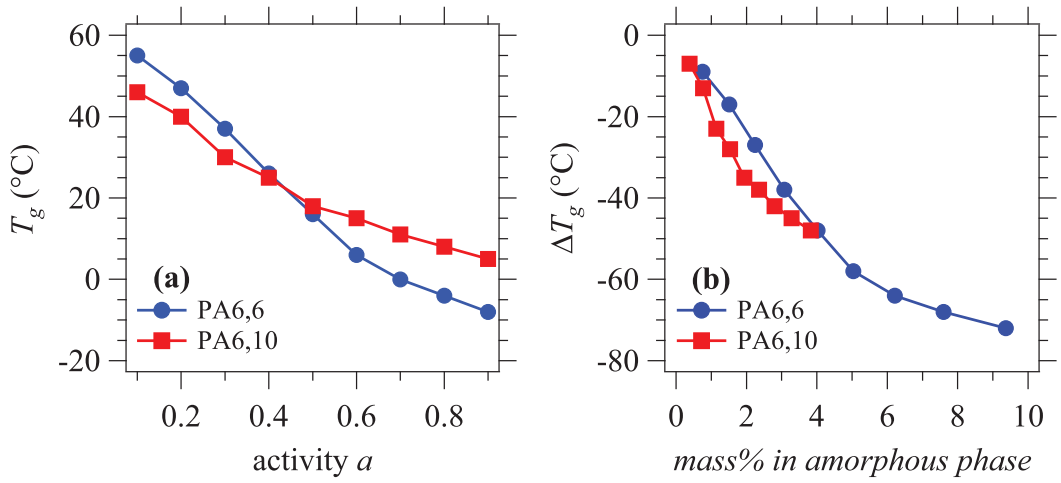

Figure 5.9: Shift in the glass transition temperature T_g measured by DSC in PA6,6 and PA6,10 as a function of (a) water activity and (b) water mass intake. Lines are guide for the eye.

systems prepared with saturated salt solutions (activity 0.5, 0.75 and 0.84) were measured. The α relaxation times are shown in Figure 5.11(a).

The α relaxation times as a function of temperature for both the dry (activity $a = 0$) and liquid-water equilibrated ($a = 1$) polyamide can be fitted by a Vogel-Fulcher-Tammann (VFT) equation (equation (1.4)), which can be rewritten as:

$$\frac{1}{T} = \frac{1}{T_0 + \frac{A_{VFT}}{\ln(\tau/\tau_0)}} \tag{5.3}$$

where the VFT parameters T_0, A_{VFT} and τ_0 depend on the activity.

It was observed that the relaxation times for intermediate activities could be obtained by an interpolation method based on the position of the data points for DSC glass transition temperature ($\ln \tau \simeq 4.6$) and their distances to the dry and liquid-water equilibrated polyamide VFT curves $\ln \tau$ as a function of $1/T$. Based on the notations in Figure 5.11a, this semi-empirical interpolation method is given by Equation (5.4):

$$\frac{1}{T(a)} = \frac{x}{x+y}\frac{1}{T(a=1)} + \frac{y}{x+y}\frac{1}{T(a=0)} \tag{5.4}$$

where all temperatures correspond to the same value of $\ln \tau$ and x and y are the differences between the inverse $1/T_g$ of the polymer with water at activity a and $1/T_g$ of the dry and water equilibrated polymer respectively. Equation (5.4) is analogous to the Fox-Flory mixing rule for the T_g of miscible blends [157]. It is an experimental finding here that the α relaxation times for the systems equilibrated at intermediate water activities are well described by equation (5.4). Indeed, in Figure 5.11(a) it is observed that the dashed lines obtained from equation (5.4) superimpose over the experimental relaxation times represented by the markers, for the three intermediate activities. Equation (5.4) expresses the fact that the T_g of polyamide/water systems vs. activity curve (as shown in Figure 5.9) is independent of the frequency of the measurement.

The DSC glass transition temperature was available for all intermediate activities between 0.1 and 0.9. Therefore, the VFT curves for the α relaxation times vs temperature at intermediate activities from 0.1 to 0.9 were estimated based on this interpolation method using equation (5.4). Finally, from the set of interpolated curves (as shown in Figure 5.11(b)), the relaxation time as a function of activity at a given experimental temperature was obtained by taking the

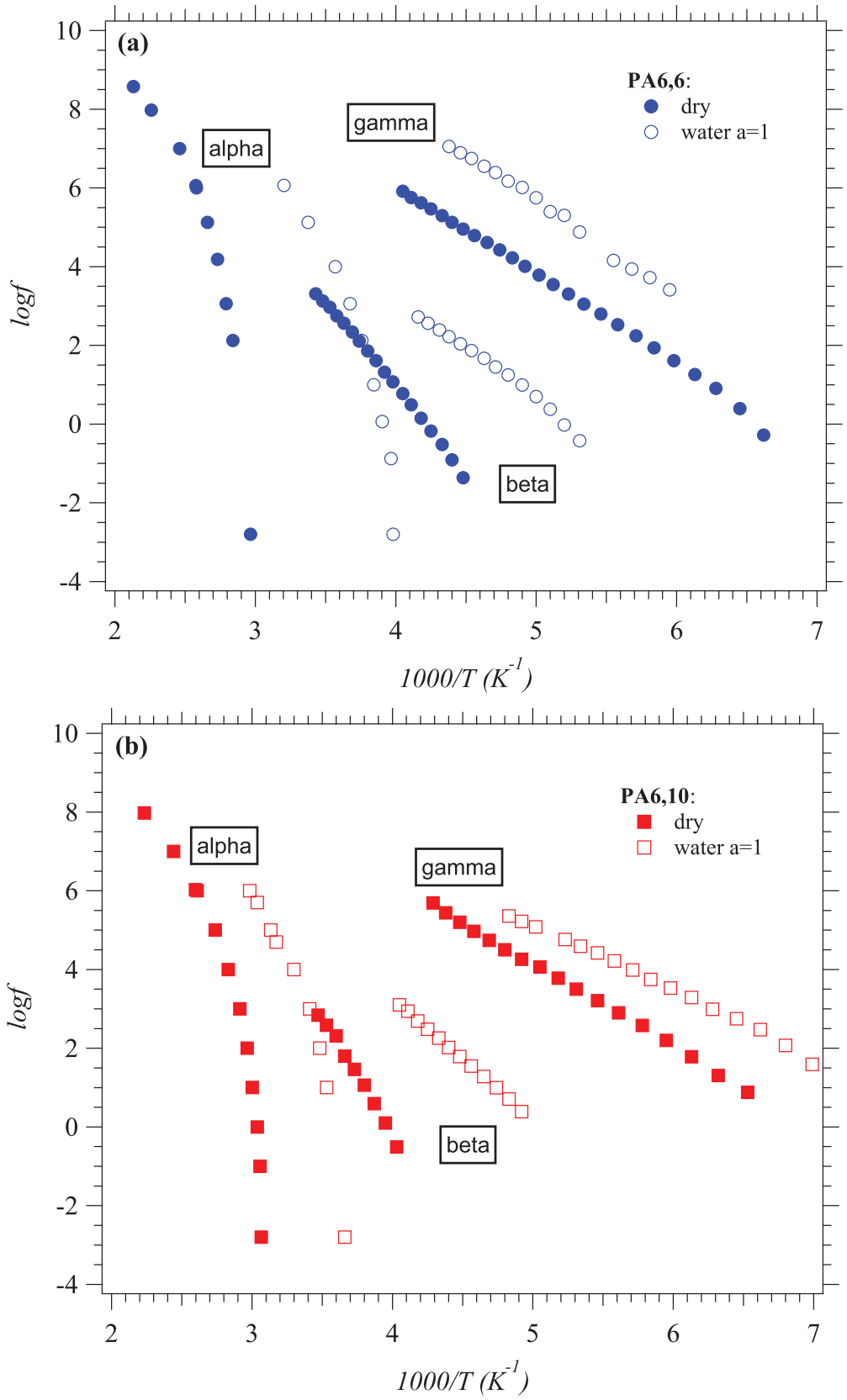

Figure 5.10: Relaxation charts obtained from Dielectric Spectroscopy measurements for dry and water-saturated (a) PA6,6 and (b) PA6,10

intersections of the experimental temperature (vertical straight line Figure 5.11(b)) and of the interpolated relaxation time curves (Figure 5.11(b)).

The characteristic relaxation times τ_α of PA/water systems at different temperatures are illustrated in Figure 5.12(a) and (b) as a function of water mass intake in the polyamide amorphous phase. First of all, it can be noticed that α relaxation times decrease when the water concentration increases, which is in agreement with polyamide being plasticized by water. Also, as expected, the α relaxation times of the polymer systems decrease when temperature increases. At equivalent water intake, τ_α of the PA6,10/water systems are shorter than τ_α of the PA6,6/water systems for all temperatures.

5.2.2 β relaxations of water-polyamide systems

The β relaxation is strongly affected by the presence of water [34]. In a dry polyamide, the β relaxation is symmetrical and corresponds to the relaxation denoted β_{dry} in Figure 5.13. When water is introduced, the initial position of the beta relaxation does not change significantly but a second, more intense beta relaxation β_w appears in the high frequency side. As the water concentration increases, this relaxation shifts to higher and higher frequencies. It should be highlighted that in PA6,10, two relatively well distinct processes can be observed in the presence of water (Figure 5.13(a-b)). In PA6,6 however, it is very difficult to clearly distinguish between the two processes, especially at high water activities (Figure 5.13(d)). For this reason, the position of the β relaxation determined for the dry polymer was introduced manually in the fits, with varying dielectric strength. The relaxation denoted β_w is considered to be representative of the local chain dynamics of hydrogen bonded amide groups in the presence of water. It is thus the one discussed in this work in relation to water diffusion.

It should be highlighted that polymer processing and the resulting distribution of rigid and mobile amorphous fractions can have an influence on polymer relaxations. A comparison has been done between the PA6,6 100 μm film and a PA6,6 0.8 mm injected plate. The effect of processing is mainly noticeable on the α relaxation associated to the glass transition, since the crystalline fractions and the glass transition temperatures of the two samples are slightly different. However, no effect was noticed on the secondary, more local β or γ relaxations, for which the obtained characteristic relaxation times superimposed. As a consequence, the characteristic relaxation times presented in this study can be extended to polyamides prepared with different processing methods.

The corresponding relaxation maps for the β_w relaxation in the presence of water in both polymers are shown in Figure 5.14. For both polymers, the characteristic β_w relaxation times at a constant temperature become shorter in presence of water. The variation of the relaxation times can be fitted with an Arrhenius equation (1.5) and gives the parameters listed in Table 5.2.

The activation energy for a β secondary relaxation should be around 30-40 kJ/mol [25]. In this case, the activation energies are more than doubled and the values of τ_0 have no physical relevance ($\tau_0 < 10^{-16}$ s). This is an indication that the β relaxation in polyamide is not a simple process involving the rotation of a single amide group or the dissociation of a single hydrogen bond. The complexity could be due to cooperative movements of the amide groups.

The Arrhenius equation and the parameters in Table 5.2 were used in order to extrapolate the characteristic β_w relaxation times at the experimental DVS temperatures (see extrapolation in Figure 5.14(a)). The variation of the characteristic β_w relaxation time as a function of water content in both polymers at DVS experimental temperatures are shown in Figure 5.15. The obtained values are considered to be representative of the local chain dynamics of hydrogen bonded amide groups. Although β relaxation times approach α relaxation times in presence of water, the two processes are still sufficiently separated to be studied individually. As in the case of the α relaxation, β relaxation times decrease when the water content or temperature

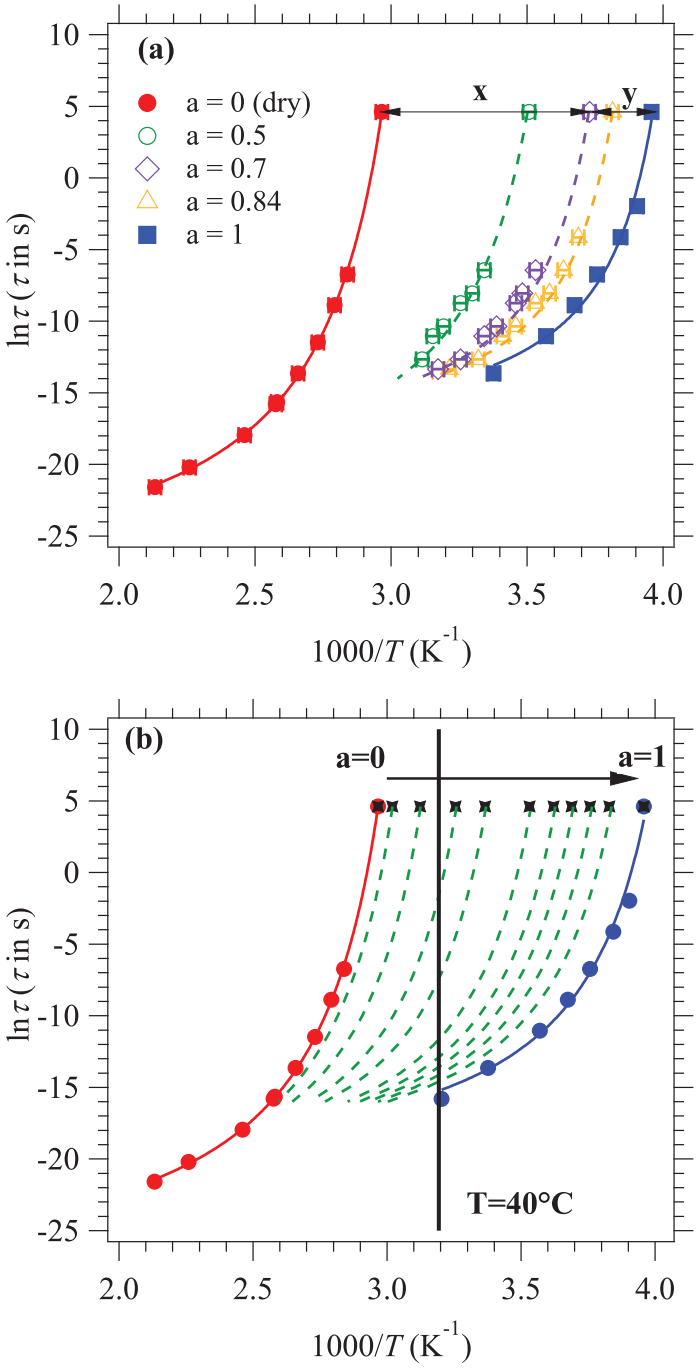

Figure 5.11: (a) Experimental α relaxation times obtained from ϵ''_{dielec} isochrones (markers), VFT fits (solid lines) and interpolation results (dashed line) for dry and water equilibrated (a = 0.5, 0.75, 0.84 and 1) PA6,6; (b) Set of interpolated curves for all DVS intermediate activities and intersection with experimental temperature 40°C. Black markers correspond to the T_g measured by DSC for polyamide/water systems at intermediate activities.

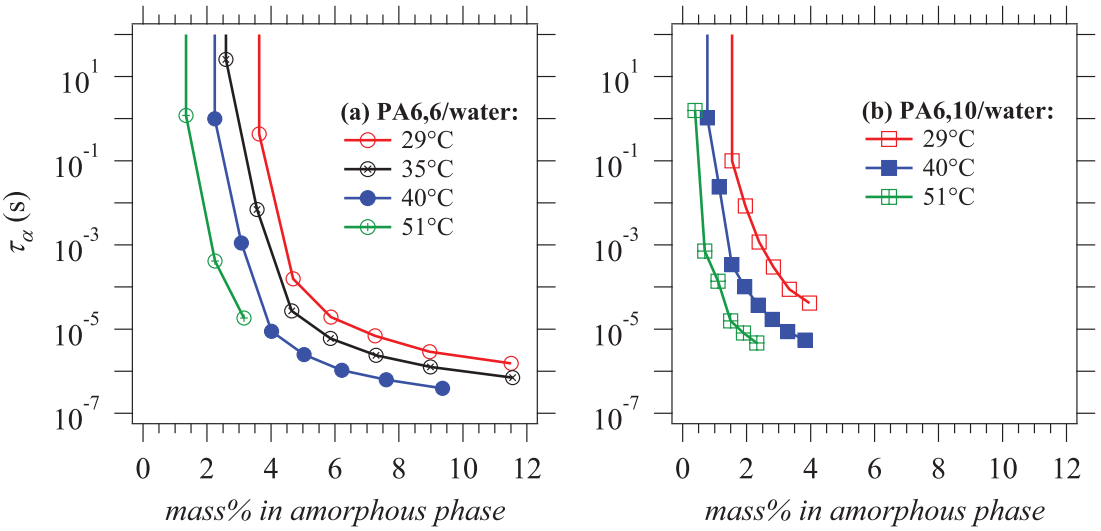

Figure 5.12: α relaxation times in logarithmic scale for (a) PA6,6/water and (b) PA6,10/water systems as a function of water intake in the amorphous phase at different temperatures. Lines are guides for the eye.

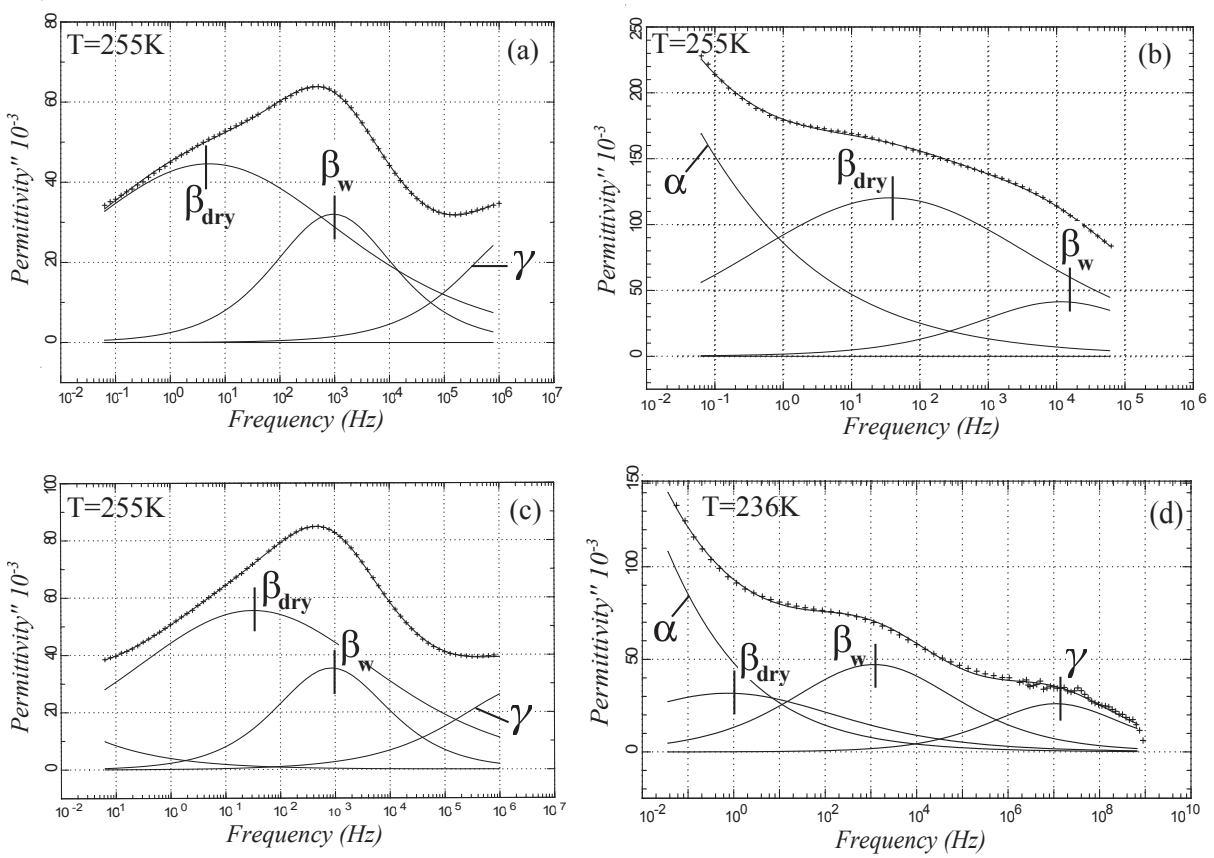

Figure 5.13: Isotherms of loss permittivity ϵ'' in the region of the β relaxation in PA6,10 at water activity 0.11 (a) and 1 (b) and in PA6,6 at water activity 0.11 (c) and 1 (d), together with corresponding Havriliak-Negami fits.

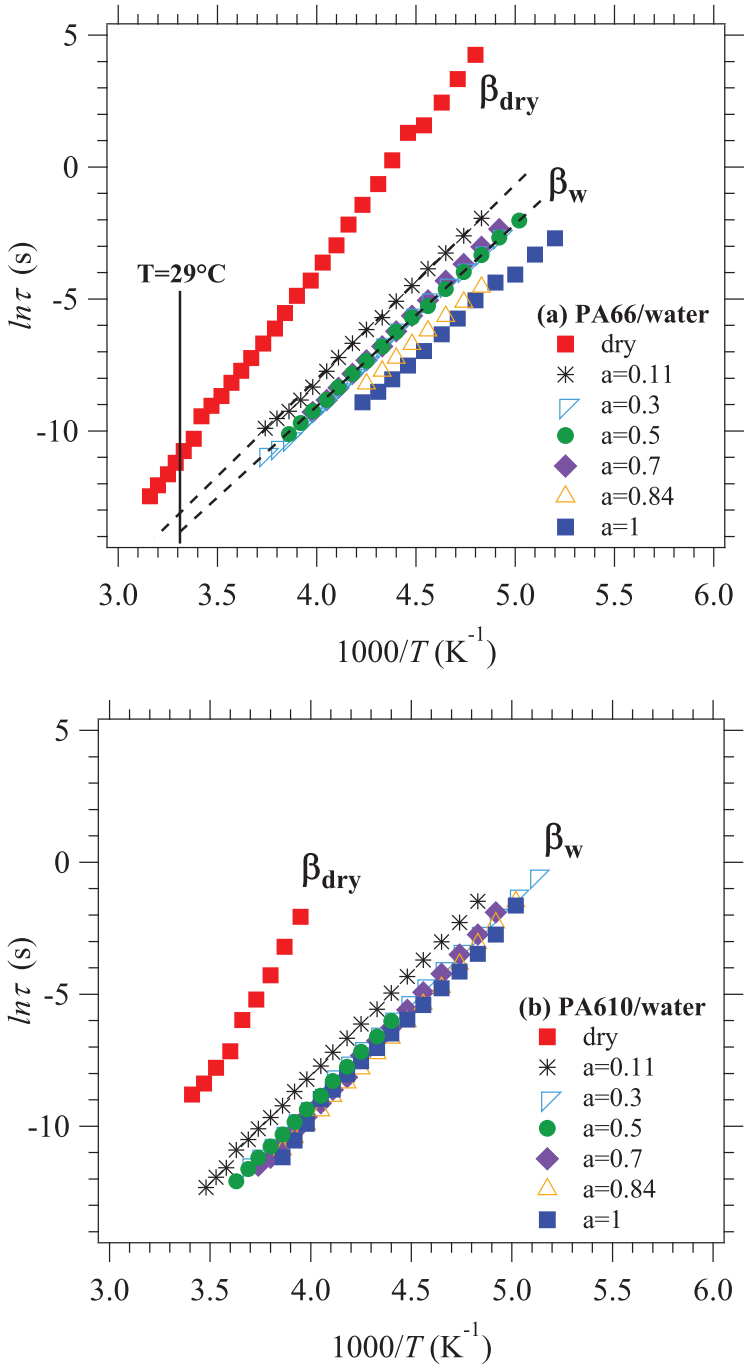

Figure 5.14: Relaxation maps for the β relaxations for (a) PA6,6 and (b) PA6,10 for various water activities. The dotted lines in figure (a) are the Arrhenius fits of the relaxation times, which can be extrapolated to obtain the characteristic β relaxation times at DVS experimental temperatures (*e.g.* 29°C)

	PA6,6		PA6,10	
activity	**E_a (kJ/mol)**	**τ_0 (s)**	**E_a (kJ/mol)**	**τ_0 (s)**
0 (dry)	85	3.6e-20	103	4.3e-23
0.11	62	2.2e-17	66	5.2e-18
0.3	60	3.0e-17	65	2.7e-18
0.5	58	7.9e-17	65	2.3e-18
0.7	62	1.2e-17	68	4.5e-19
0.84	54	2.9e-16	67	6.3e-19
1	54	1.2e-16	64	2.7e-18

Table 5.2: Arrhenius parameters from the β relaxation maps of PA6,10 and PA6,6 at various water activities shown in Figure 5.14.

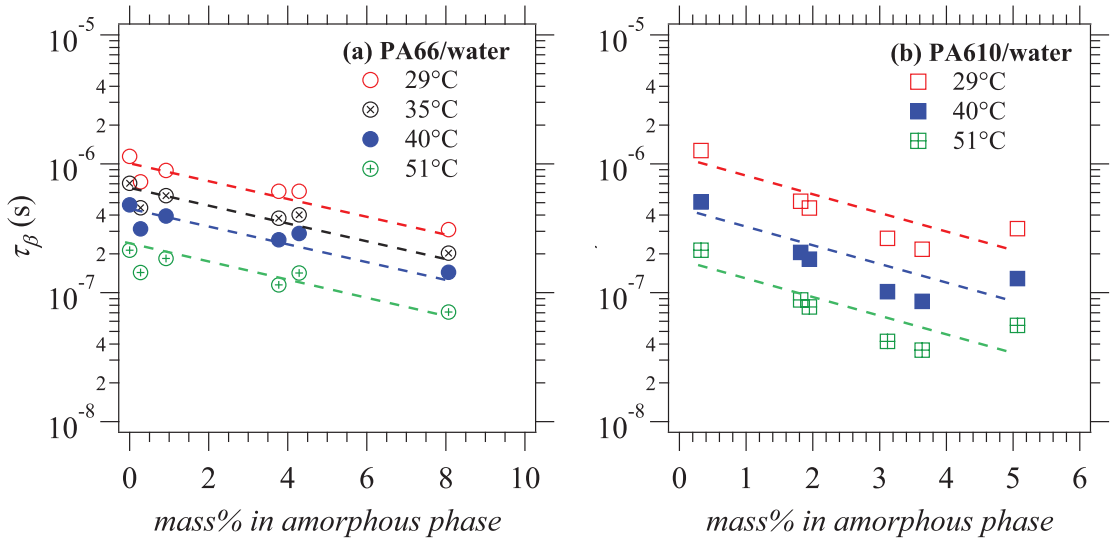

Figure 5.15: Characteristic β relaxation times as a function of water uptake in the amorphous phase of (a) PA6,6 and (b) PA6,10 corresponding to DVS experimental temperatures. Lines are guides for the eye.

increases. The same order of magnitude, 0.1 to 1 μs, is observed in both polymers.

5.2.3 Discussion

The correlation between water diffusion and polyamide relaxations is now discussed. The diffusion coefficients and relaxation times of polyamide/water systems were measured for different water activities/intakes. For a given temperature, the diffusion coefficient can therefore be plotted as a function of the relaxation times as the water concentration or activity varies. This is first done for the α relaxation in Figure 5.16.

At each temperature, diffusion coefficients vary by a factor 2 to 5, whereas τ_α relaxation times vary over 7 orders of magnitude. Thus, there is a huge difference between the magnitude of the variation of diffusion coefficients and τ_α as a function of water content: the two processes seem to follow distinct timescales. These results are in agreement with NMR studies that showed a few percentages of water already penetrate in polyamide before the plasticization sets in [59]. The authors concluded on the existence of a plasticization lag, which also suggests that plasticization and diffusion are not directly correlated.

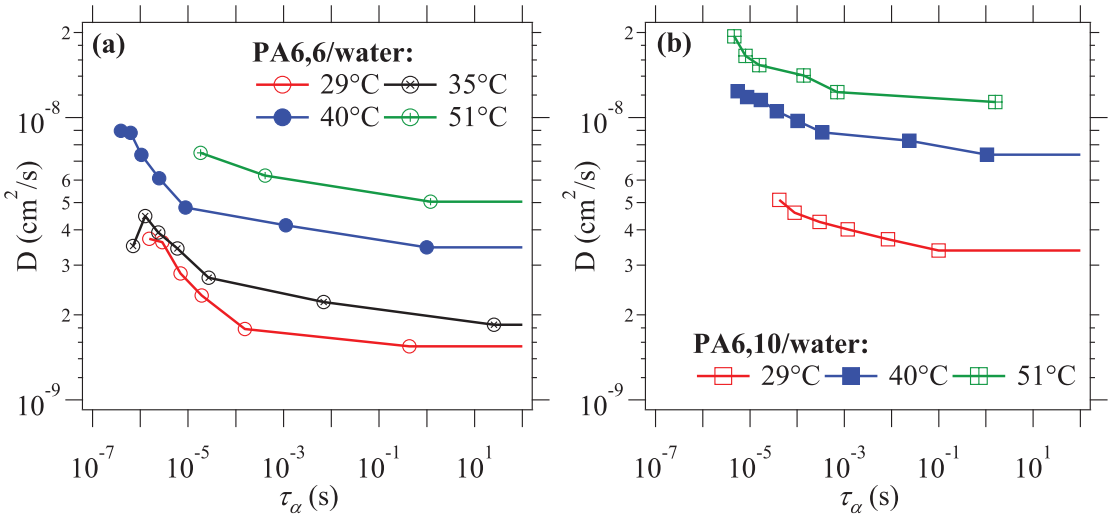

Figure 5.16: Water diffusion coefficient D as a function of the α relaxation times τ_α at different temperatures for (a) PA6,6/water and (b) PA6,10/water systems.

In addition, this set of data gives access to the variation of the diffusion coefficients as a function of temperature, for a constant characteristic rate of segmental motions of the matrix. The variation of D with temperature can be represented at constant τ_α of the matrix (Figure 5.17).

Figure 5.17 shows that the variation of the diffusion coefficients may reasonably be considered to be Arrhenian with temperature, for each different relaxation times of the polyamide/water system. The curves can be fitted with an Arrhenius-like law to give access to an activation energy for diffusion. The fits are presented in Figure 5.17 as dashed lines. The associated activation energies are 46 ± 10 kJ/mol for PA6,6 and 43 ± 10 kJ/mol for PA6,10. The activation energy for diffusion seems to be independent of the relaxation state of the polymer. Along with the distinct timescales of the diffusion and relaxation processes, this would suggest that there is no direct correlation between the two phenomena.

The activation energies for diffusion are only slightly different in PA6,6 and PA6,10, suggesting that water diffusion mechanisms at molecular scale are similar. Note, however, that activation energies for diffusion of various gas and water molecules are found to be of the order 30-60 kJ/mol in a wide variety of amorphous or semi-crystalline polymers [14]. Thus, such values for the activation energy do not allow discriminating a particular mechanism *per se*.

At a molecular level, it is then interesting to investigate the correlation of diffusion to local movements, more specifically the β relaxation. This secondary relaxation combines conformational changes around amide groups and hydrogen bond relaxation. There are several concordant indications that diffusion may be controlled by the lifetime of hydrogen bonds, that is, by the local environment around a water molecule being hydrogen-bound to an amide group. First, in polyamides, strong interactions exist between water molecules and the amide preferential sorption sites, as already mentionned before. Another argument is the fact that diffusion coefficients are only little affected by the huge variation of the polymer matrix α relaxation time, as described above.

Following the same procedure as for the α relaxation, the water diffusion coefficients are plotted as a function of the high frequency β relaxation times for various water activities and various temperatures in both PA6,6 and PA6,10 in Figure 5.18.

In this case, the variations of the diffusion coefficients and β relaxation times are of the same

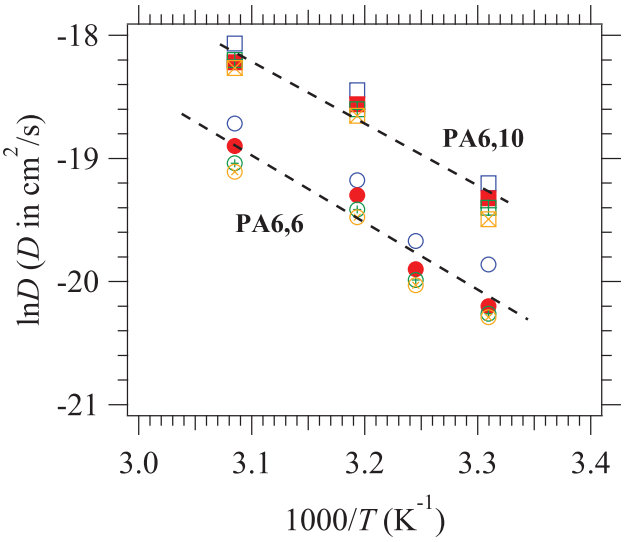

Figure 5.17: Variation of diffusion coefficients as at different temperatures for constant τ_α relaxation times. PA6,10 (squares): $\tau_\alpha = 10^{-4}$ s (blue), 10^{-3} s (red), 10^{-2} s (green), 10^{-1} s (orange); PA6,6 (circles): $\tau_\alpha = 2 \times 10^{-5}$ s (blue), 10^{-3} s (red), 10^{-1} s (green), 1 s (orange).

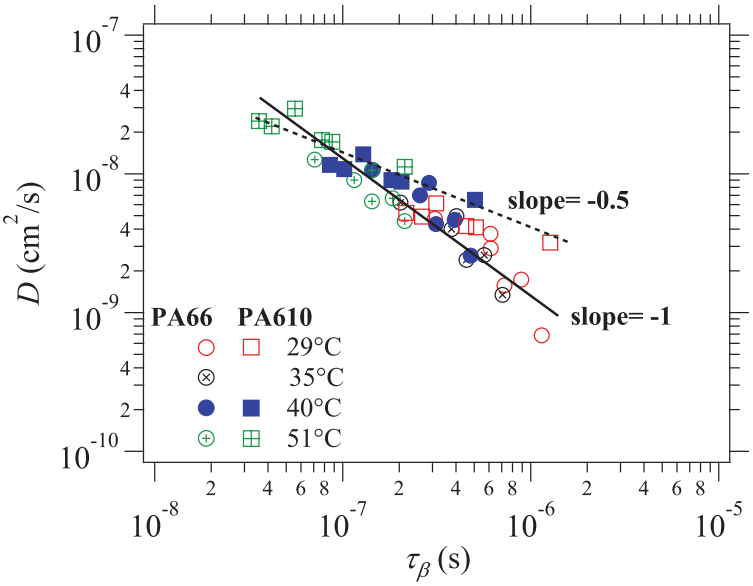

Figure 5.18: Water diffusion coefficients D as a function of the characteristic β relaxation times at different temperatures for PA6,6/water and PA6,10/water systems. Each series of points corresponds to a given T, each point in a series corresponds to a given water activity. The line with a slope of -1 (PA6,6) and -0.5 (PA6,10) is a guide for the eyes.

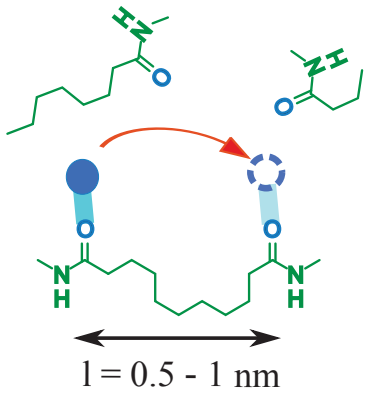

Figure 5.19: Schematic representation of water diffusion between preferential sorption sites (amide groups) in polyamide

order of magnitude. A small difference of slope is observed however in this variation for PA6,10 (slope close to -0.5) compared to PA6,6 (slope close to -1). This might be an effect of different polarity or different amide groups configuration in PA6,10 compared to PA6,6. For now, this interpretation in only speculative, more data on other polyamide/solvent systems would be needed to confirm this trend.

To assess the contribution of the β relaxation and hydrogen bonding to the diffusion process, the diffusion characteristic time can be compared to the β relaxation time and the lifetime of a hydrogen bond. Assuming that water molecules diffuse between neighboring amide groups (Figure 5.19), the characteristic time for diffusion is proportional to the square length of distance over the diffusion coefficient. Based on elementary density arguments, the average distance d between amide groups can be evaluated to approximately 0.7 nm in PA6,6 (in agreement with simulation results [158]) and 0.8 nm in PA6,10, due to the additional methylene groups. For both polymers, the calculated characteristic diffusion times $t_D \approx d^2/2D$ range from 10^{-7} to 10^{-6} s. Estimations for water-amide group interaction energy can be found in the literature [9, 142], based on ab-initio calculations for peptide-water systems in vacuum. The interaction energy thus obtained is approximately 30-35 kJ/mol. In a polymer environment, this interaction energy might be different because of hydrophobic contributions. Taking the relaxation time of a hydrogen bond as Arrhenian with a characteristic τ_0 of 10^{-12} to 10^{-10} s^{-1} and an activation energy E of 30-35 kJ/mol [48], the lifetime of a hydrogen bond is estimated between 10^{-7} and 10^{-5} s in the experimental temperature range.

Note that β relaxation has an apparent activation energy of the order of 60 kJ/mol (as mentioned before), which indicates that it involves more complex, perhaps more cooperative processes than just the rotation of an amide group or breaking of one hydrogen bond. In any case, the characteristic β relaxation times are found experimentally in the range 10^{-7} and 10^{-6} s, as illustrated in Figure 5.18. Therefore, the characteristic diffusion time, the β relaxation time and the lifetime of the hydrogen bond are of the same order of magnitude, which suggests that diffusion of water in polyamide may indeed be limited by the departure of the water molecule from the amide sorption site. Consequently, the hoping in between sites should be very fast.

Thus, the values of the diffusion coefficients themselves seem to be compatible with a very simple picture in which diffusion would be controlled by hoping from one amide group to the neighboring one (Figure 5.19).

Since the two polyamides studied here have not been processed with the same method, a direct comparison would somehow be hazardous. The type of mechanism suggested above would predict a faster diffusion through a polymer that has sorption sites separated by longer

distances (if t_D is similar, then $D \sim \frac{d^2}{2t_d}$ is higher when d is higher), which is in accordance with the experimental observation that water diffusion is faster in PA6,10 than in PA6,6, either we compare at the same temperature or at equivalent $T - T_g$. Measured diffusion coefficients in PA6,10 are 2 to 4 times larger than in PA6,6. However, this ratio is significantly larger than predicted from the ratio of average distances between amide groups in both polymers. This difference might arise from the samples microstructures. The study of the influence of crystallinity on diffusion coefficients (Section 3.1) on model PA showed that there was no influence in the range 0-26% crystalline ratio . However, the crystalline ratio of PA6,6 (38%) is larger than 26%. Also, the crystalline fraction is much higher in PA6,6 (38%) compared to PA6,10 (23%). Therefore, crystallites, as well as the rigid amorphous phase, may affect diffusion coefficients in these systems. The measured diffusion coefficient D can be expressed by equation (1.12), as a function of the diffusion coefficient in the bulk amorphous polymer D^*, a chain immobilization factor that relates to the fraction of rigid amorphous phase (β_{imm}) and a tortuosity factor that accounts for the increased diffusion path in order to bypass crystallites (ξ) [41, 42]. One expression for the tortuosity factor proposed in the context of polymers nanocomposites with layered clay fillers of aspect ratio f is of the form $\xi \simeq 1 + \frac{f}{6} X_c$, where X_c is the volume fraction of layered objects (taken to be here crystalline lamellae or lamellar stacks) and integration has been done over all possible lamella orientations [44, 43]. With X_c varying from 23% to 38%, it is easy to explain the ratio between diffusion coefficients with reasonable values of the aspect ratio. Also, the chain immobilization factor should not be the same in the two polymers. Note again, that a direct comparison of diffusion coefficients between polyamides with different amide group densities would require a detailed control of the processing conditions and an extensive characterisation of the microstructure.

5.3 Conclusions

The diffusion mechanisms in two aliphatic semi-crystalline polyamides (PA6,6 and PA6,10) were studied independently and similar conclusions were reached for each of them. The influence of the density of hydrogen bonds was tentatively discussed.

First, it was found that the diffusion of liquid water is apparently Fickian in PA6,10 and non-Fickian or anomalous in PA6,6. Ethanol diffusion is non-Fickian in both polymers. In order to get a more detailed insight on diffusion mechanisms, a quasi-equilibrium experiment was set up to measure selectively the variation of the diffusion coefficient as a function of solvent activity/concentration at equilibrium.

It was thus shown that the diffusion coefficient of water in PA6,6 increases significantly as the water concentration increases, which accounts for the non-Fickian diffusion in this polymer. In PA6,10, this variation is much less pronounced, which supports an apparent Fickian diffusion. Ethanol diffusion could no longer be fit with a simple Fickian model at high activities in PA6,6. The Berens-Hopfenberg model adds a relaxation process (generally identified as swelling) to the Fickian model and describes the data accurately. Ethanol diffusion coefficients vary to a much larger extent than water in each polymer matrix, which accounts for the strongly non-Fickian profile of sorption kinetics curves. Since ethanol plasticizes polyamide more than water, the next question was if the polymer dynamics could give this difference in diffusion mechanisms. Ethanol sorption being too long in DVS, only water was investigated.

Thus, the polymer relaxation times associated to the glass transition (α relaxation) and to the β secondary relaxation of the amorphous phase of the polyamides were measured or estimated as a function of temperature and water concentration by Broadband Dielectric Spectroscopy. The α relaxation times decrease by several orders of magnitude, illustrating the polymer plasticization by water molecules. This variation (typically 6 orders of magnitude) is much more

extensive than the variation of diffusion coefficients (a factor 2 to 5 at most) over the activity range from 0 to one, indicating that diffusion is not controled primarily by the α relaxation in polyamide. Conversely, the variation of the diffusion coefficient with water concentration is coherent with that of the β relaxation time.

On the whole, the existence of strong interactions between the solvents and the amide groups in polyamide affects diffusion at a molecular level. The results on polymer dynamics related to diffusion are compatible with a diffusion process controled by the hoping of water molecules between preferential adsorption sites (amide groups), with which they form hydrogen bonds. For water, there is no correlation between α relaxation and solvent diffusion. However, this observation might not be true for ethanol, whose diffusion coefficients vary by several orders of magnitude (estimated at 4 decades), compared to a factor 2-5 for water. Ethanol diffusion might therefore be coupled to some extent to the polymer α relaxation (to be investigated).

Another possible explanation would be that the dependence of diffusion coefficients on β relaxation is different for ethanol. This hypothesis could not be tested because ethanol plasticizes polyamide more than water: the α relaxation domain superimposes on the β relaxation domain and the latter is not visible anymore in dielectric spectroscopy measurements.

To finish with, since PA6,6 and PA6,10 were prepared by different processing methods, it is hasardous to compare the two polymers for the role of hydrogen bonds density. A direct comparison of diffusion coefficients between polyamides would require a detailed control of the processing conditions and an extensive characterisation of the microstructure.

Chapter 6

Effects of interchain interactions on the dynamics of polyamide

Although polyamide is an industrially important polymer, systematic studies of its rheological behavior are scarce (see Chapter 1). The main reasons are the difficulties related to chemical stability and to the presence of a crystalline phase that limits the measurement range to temperatures above the melting point. The use of blocked, amorphous polyamides was identified as a solution to both problems (see Chapter 1). Several polyamides of varying molecular weight and with systematic variations in the interacting groups were synthesized (Chapter 2). The main purpose of this study is to investigate the possible influence of interactions (hydrogen bonds, ionic) on the viscoelasticity of polyamide. The effects of the different interacting groups on the dynamics in both the molten and solid states are presented, taking into account the analysis of their molecular structure.

6.1 Molecular structure

In order to interpret dynamical data, a complete analysis of the molecular structure is needed. As evidenced in the literature review, polydispersity and branching have an important effect especially on the viscoelasticity (*i.e.* the dynamics in the molten state) so they have to be accurately assessed.

The molecular weight and molecular weight distributions (MWD) for the polymers were measured by GPC, following the method described in Section 2.2.1.1. The number average molecular weight was also obtained by NMR for the short polymers and by end-group titration, as described in Section 2.2.1.1. The summary of the analyses results is shown in Table 6.1. The molecular weight distributions from GPC are shown in Figure 6.1. The sample coding was chosen as follows: type of polyamide (PA6I, PA6HIA or PA6I/PA6LiSIPA), followed by the number average molecular weight as determined by GPC in kg/mol (*e.g.* 2k...) and, for the copolymers, the molar proportion of each type (PA6I/PA6LiSIPA 95/5). Since only one composition was synthesized, the 95/5 indication is omitted in the following sections.

The number average molecular weights obtained by GPC, NMR or end-group titration are identical within ±10%. PA6HIA was insoluble in the solvent for the end-group titration so this value is missing from Table 6.1. The weight average molecular weight obtained by GPC yields polydispersity indices (PDI) between 2.2 and 2.9, except for the PA6HIA which has a PDI of 3.3. These values are much higher than the expected PDI value of 2 for linear polycondensation [6].

In order to understand this difference, the experimental GPC data (transformed following $w = \frac{dw}{dlogM}\frac{M_0}{2.303M}$, where M_0 is the mass of the repeating unit) were fitted with a Flory distribution. The original data and their fits with equation (1.2) for linear polycondensation are shown in Figure 6.2. It can be observed that, except for PA6I 2k, the Flory distribution does not describe the MWD of these aromatic polyamides well. In some cases, clear shoulders are visible in the distributions, indicating that the synthesis did not result in a statistical pool of linear chains.

A possible explanation for this deviation is the occurrence of branching. The source of branching was explained in Chapter 1, via the synthesis of bis(n-alkyl)triamine. The amount of bis(hexa-methylene)triamine (BHT) can be measured after complete hydrolysis of the polyamide chains and consequently the amount of branched amide groups can be assessed. The concentration of BHT measured in each sample is reported in Table 6.1.

Sample code	M_n(kg/mol) - target	M_n(kg/mol) - NMR	M_n(kg/mol) - GT	M_n(kg/mol) - GPC	M_w(kg/mol) - GPC	PDI	[BHT]±10% (ppm)	mol% BHT/amide groups	T_g ±1 (°C)
PA6I 2k	2	2.0	2.0	2.0	4.9	2.5	4400	0.25	106
PA6I 5k	10	-	4.8	5.6	16.4	2.9	4400*	0.25	121
PA6I 12k**	12	-	12.3	12.8	37.1	2.9	2000	0.12	126
PA6HIA 3k	2	3.0	-	3.3	11.0	3.3	4000	0.24	147
PA6I/6LiSIPA 95/5 2k**	2	-	2.0	2.8	6.2	2.2	2600	0.15	117
PA6I/6LiSIPA 95/5 6k**	10	-	5.0	6.5	14.6	2.3	2600	0.15	133

Table 6.1: Average molecular weight (targeted in the synthesis, NMR, terminal groups - GT, GPC-absolute), polydispersity index, concentration of bis(hexa-methylene) triamine (BHT) and glass transition temperatures (DSC) of semi-aromatic polyamides. *Since the same reaction conditions were used for PA6I 2k and 5k, we expect the same [BHT] in PA6I 5k as the one measured for PA6I 2k. **Small amounts of catalyst were used for these syntheses. The uncertainty on M_n is 10% and on M_w is 5% (provided by Solvay Analytical Lab).

The molar percentage of branched amide groups was calculated as follows:

$$\text{mol\% BHT/amide group} = \frac{\text{moles BHT}}{\text{moles amide groups}} = \frac{\text{[BHT](in g/g PA)}\, M_{PA}}{M_{BHT}} \tag{6.1}$$

where M_{PA} is the molar mass/amide group (123 g/mol for PA6I, 131 g/mol for PA6HIA and 125 g/mol for PA6I/6LiSIPA 95/5) and M_{BHT} = 220 g/mol is the molar mass of BHT. A molar percentage of 0.25 means that 1 in 400 amide groups are branched.

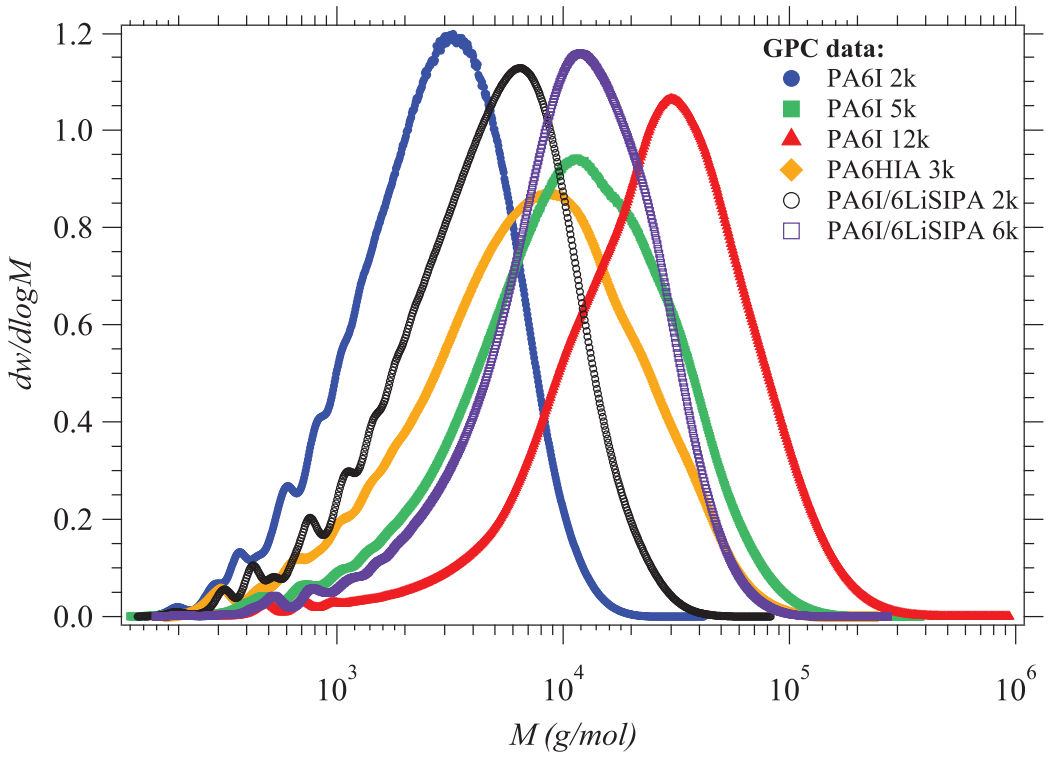

Figure 6.1: Molecular weight distribution as obtained by GPC for the semi-aromatic polyamides

The concentration of BHT varies between 2000 and 4500 ppm, which gives between 0.1 and 0.25 molar percent of BHT over amide groups. Therefore, 1 in 400 or 1 in 1000 amide groups are branched. The majority of the chains is thus linear, since on average there are between 20 and 100 monomers/chain. Although PA6HIA has a similar concentration of BHT as PA6I, this sample has a higher PDI and a much higher molecular weight than the target. This suggests that other side reactions might occur in the synthesis of this sample. The hydroxy isophthalic acid monomer in PA6HIA has an additional phenol group that might react with the acid groups (either from a blocker or another HIA monomer). This reaction results in an ester, which can account for a lateral group (Figure 6.3(a)) or an additional branching point (Figure 6.3(b)). Traces of ester groups were identified in NMR and might explain the unusual behavior of this polymer.

Last, the glass transition temperatures of the polyamides were measured by Modulated DSC, following the method presented in Chapter 2 (±2°C every 60s, heating rate of 3°C/min). The values are reported in Table 6.1. The glass transition temperatures of the PA6I series increase from 106 to 126°C as the molecular weight increases. The same observation is made for the PA6I/6LiSIPA series, which is in accordance with the general behavior of the T_g of polymers with molecular weight, *i.e.* following the Fox-Flory equation [77]. The addition of 5% PA6LiSIPA results in an increase of approximately 10°C in the glass transition temperature. As explained in Chapter 2, lithium cations can coordinate up to 4 amide groups and high energy complexes (up to 50 kJ/mol [122]). This shift in T_g is similar to the one reported by Weiss *et al.* for sulfonated PS [104], in which the energy of ionic association was estimated to be 65 kJ/mol at 135°C [103]. The glass transition temperature of PA6HIA is higher than those of the PA6I or PA6I/6LiSIPA of corresponding molecular weight. This effect might be due to the fact that each acid monomer in PA6HIA has an additional phenol group capable of forming hydrogen bonds of higher energy than an amide-amide hydrogen group (40 kJ/mol compared to 25 kJ/mol [117]).

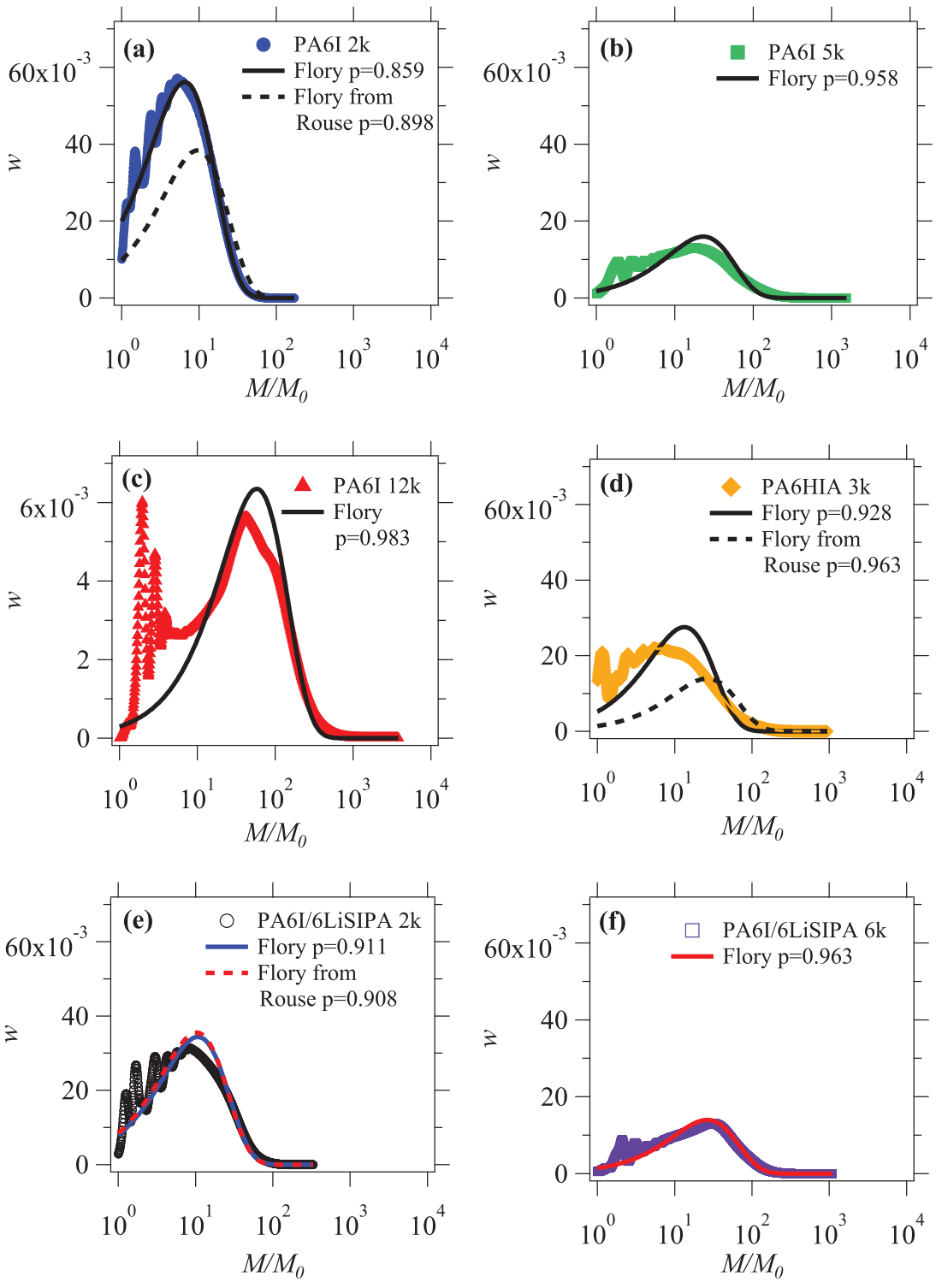

Figure 6.2: Molecular weight distributions and corresponding fits (solid lines) with the Flory equation (1.2) for linear polycondensation (a) PA6I 2k, (b) PA6I 5k, (c) PA6I 12k, (d) PA6HIA, (e) PA6I/6LiSIPA 2k and (f) PA6I/6LiSIPA 6k. For the short chains, the dashed lines were extracted from the viscoelastic data using a Rouse model for linear chains (see Section 6.2.2). The scale in Figure (c) is different than the other for a better observation.

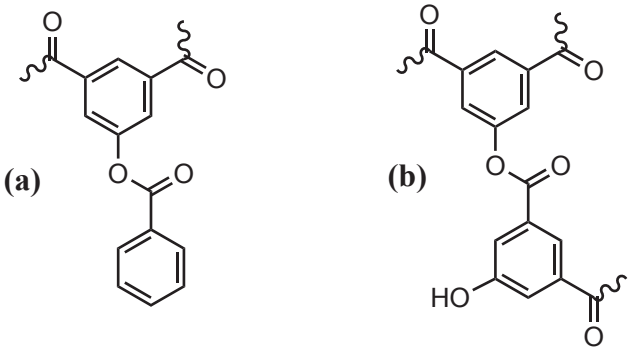

Figure 6.3: Chemical structure of an ester formed between the HIA monomer and (a) a blocker or (b) another HIA monomer

6.2 Dynamics in the molten state

In this section, the dynamics of polyamide in the molten state will be presented. The master curves of relaxation moduli were obtained by time-temperature superposition. For the long chains, the master curves provided information on the plateau modulus and molecular weight between entanglements. The different short polymers were tentatively described with a Rouse model in order to identify inconsistencies with the classical behavior that could hint to an influence of interactions.

6.2.1 Time-temperature superposition and viscoelastic master curves

The experimental procedure for rheological measurements was presented in Chapter 2. The efficiency of the end-capping was tested by measuring the stability of the polymer with time at each experimental temperature. All polyamides in this study were stable for at least 30 min. The highest experimental temperature of 210°C was much lower than the temperature of synthesis in the reactor (>270°C). After determination of the linear viscoelastic region, small amplitude dynamic oscillatory measurements for varying frequencies were performed at temperatures between the glassy and terminal regime. The master curves were obtained by time-temperature superposition (horizontal and vertical shift, as explained in Chapter 2) and then shifted to the glass transition temperature T_g. The master curves at T_g are shown in Figures 6.4 and 6.5. The corresponding horizontal shift factors a_T are presented in Figure 6.6 as function of temperature. The vertical shift factors b_T were calculated based on the temperature variation assuming a constant, temperature independent density. This assumption is supported by molecular modelling of PA6I thermal properties, in which the density was found to vary from 1.160 to 1.155 over this range of temperatures [136].

Time-temperature superposition (tTS) did not work for the complete temperature range for the low molecular weight samples. Namely, tTS failed close to the glass transition; the rheological complexity is clear in the $\tan\delta$ representation, as the curves obtained at different temperatures do not overlap. This effect disappears for the higher molecular weights: tTS works reasonably well for PA6I 12k. Thermo-rheological complexity has previously been observed for example for low molecular weight polyisoprene [159]. This effect is common in short polymers and not specific to polyamide. To the best of our knowledge, this behavior has not been formalized yet by a theoretical model.

The dynamic moduli of the PA6I (Figure 6.4) and the PA6I/6LiSIPA (Figure 6.5(a)) series show the classical polymer behavior with increasing molecular weight: gradual appearance of a plateau and shift of the G'/G" crossover towards lower frequencies. The PA6I 2k, PA6HIA

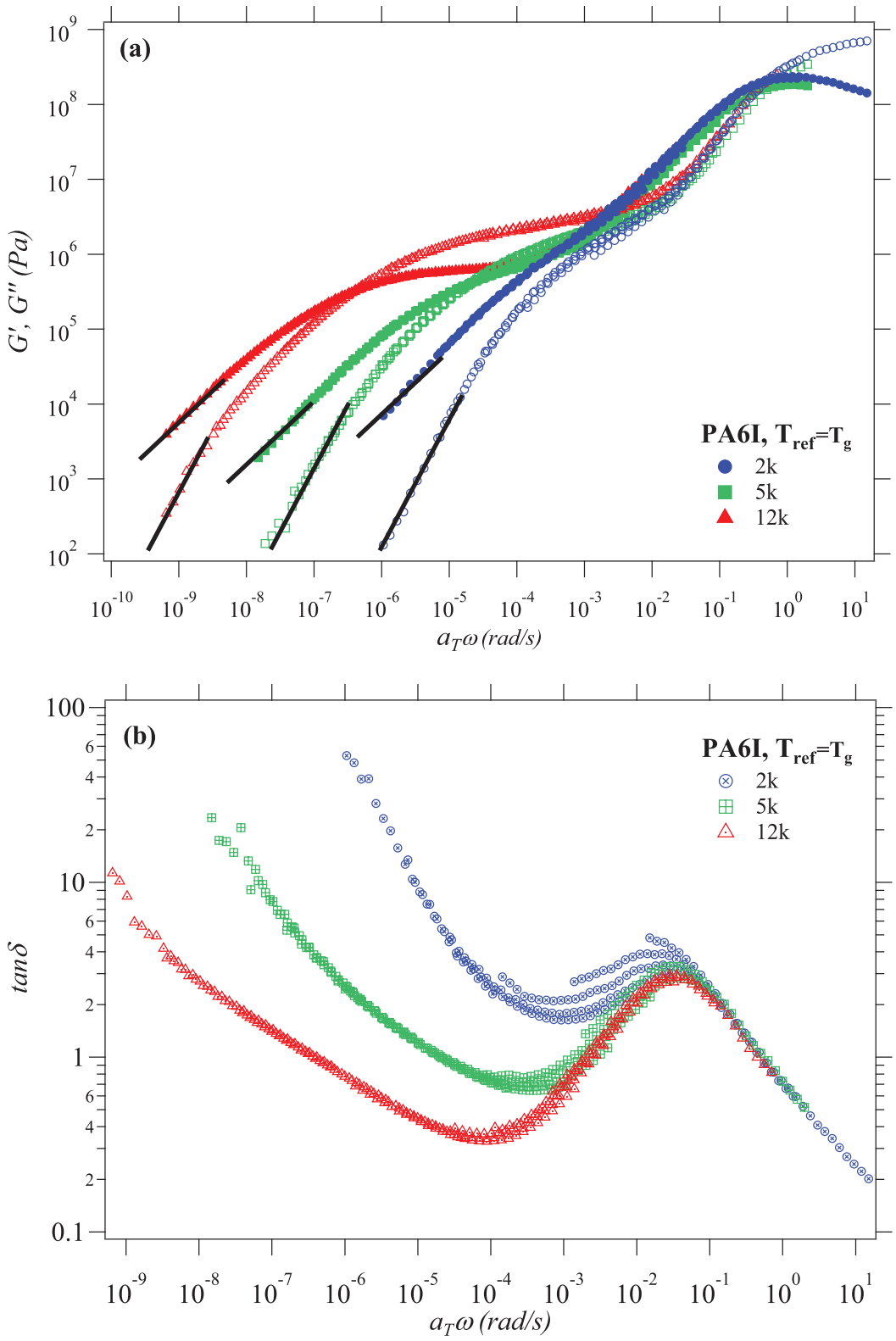

Figure 6.4: (a) Master curves of the dynamic moduli at T_g for the PA6Is of increasing molecular weights (filled markers G″, empty markers G′). Solid lines represent the expected slopes of 1 and 2 in the terminal regime for G″ and G′ respectively. (b) Corresponding damping factor for this series.

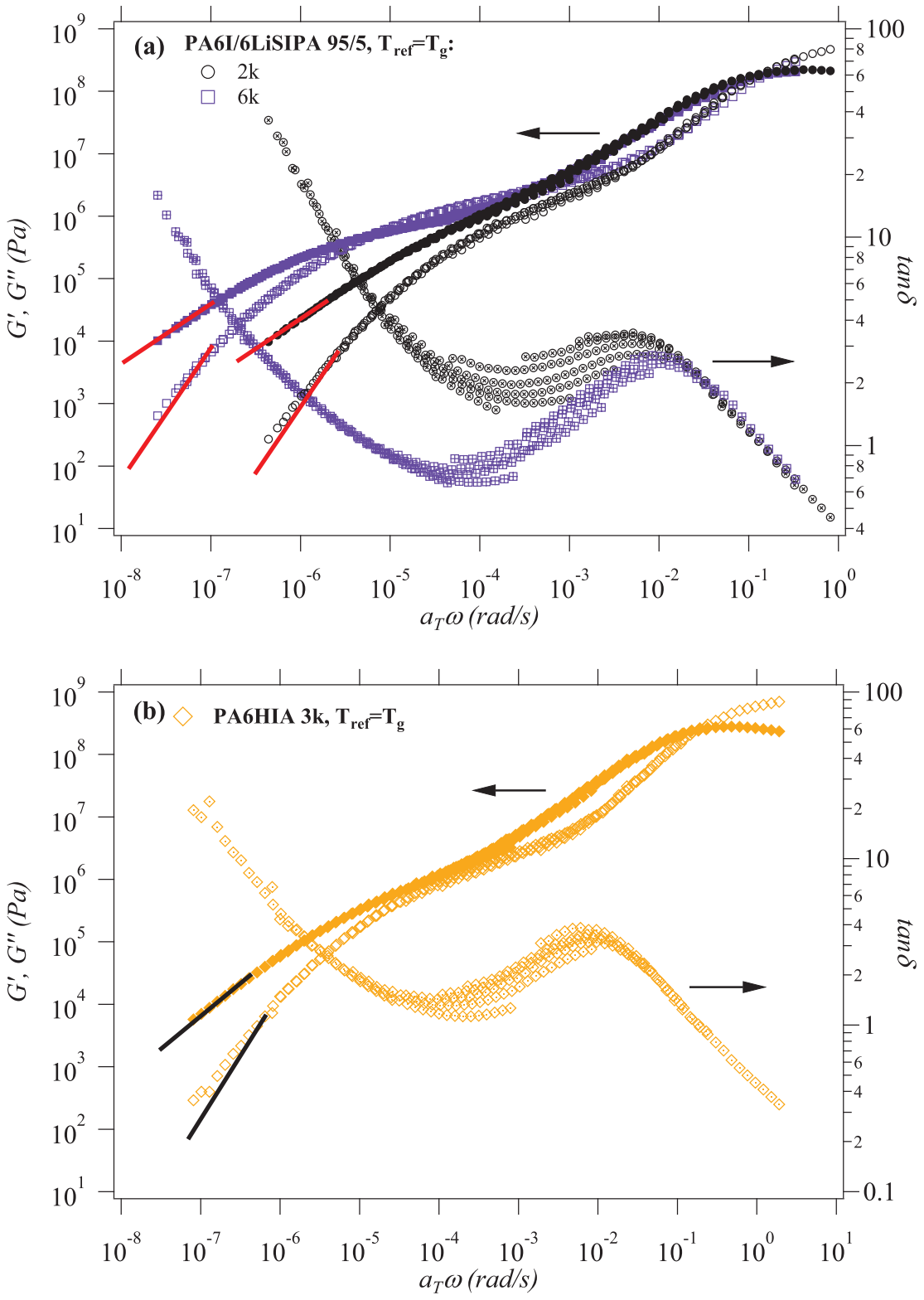

Figure 6.5: Master curves of the dynamic moduli (filled markers G″, empty markers G′) and the damping factor at T_g (a) PA6I/6LiSIPA of increasing molecular weights and (b) PA6HIA 3k. Solid lines represent the expected slopes of 1 and 2 in the terminal regime for G″ and G′ respectively.

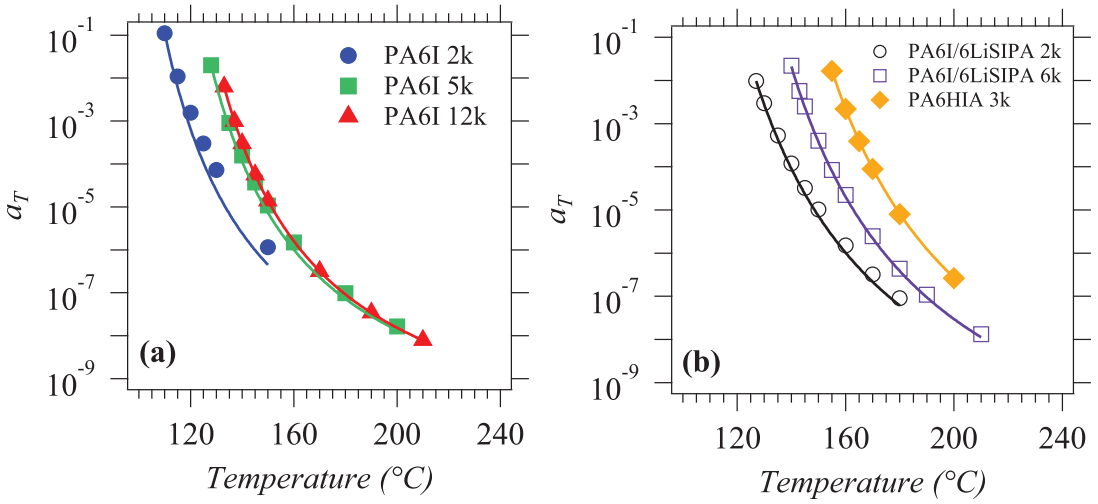

Figure 6.6: Horizontal shift factors used to obtain the master curves at $T_{ref} = T_g$ in Figures 6.4 and 6.5. Solid lines correspond to fits with the WLF equation.

and PA6I/6LiSIPA 2k display the typical behavior of unentangled polymers. PA6I 5k and PA6I/6LiSIPA 6k are mildly entangled, with a short elastic plateau and a slope close to 1/2 for G′ and G″ at frequencies above the terminal region crossover. A clear rubbery plateau can be observed for the PA6I 12k. The value of the plateau modulus $G_N^0 = 2.2$ MPa was taken as the value of G' at the minimum of $\tan\delta$ and provides an estimation of the molecular weight between entanglements [76]:

$$G_N^0 \simeq \frac{\rho RT}{M_e} \tag{6.2}$$

The density value at T_g was taken as 1160 kg/m^3, as estimated by molecular modelling [136]. The obtained M_e is 1.8 kg/mol for $T = T_g = 399.15$ K, which is in agreement with the value of 2.0 kg/mol tabulated for PA6 [88, 160]. Based on the value of the plateau modulus, the packing length of PA6I can be calculated with [160]:

$$G_N^0 = \frac{kT}{a^2 p} = \frac{kT}{\left(14\exp\left(\frac{T}{1270}\right)\right)^2 p^3} \tag{6.3}$$

We obtain a value of 1.9Å for the packing length, which is slightly lower than the 2.0Å value for PA6 [160]. The packing length is defined as [160]:

$$p = \frac{M_k}{\rho N_A b^2} \tag{6.4}$$

where b and M_K are the length and the molecular weight of a Kuhn segment respectively. Their values, obtained by molecular modelling for PA6I, are the following: $b = 9.8$ Å and $M_k = 0.128$ kg/mol (communicated by authors of reference [161]). With these parameters, a value of 2.2Å is obtained for the packing length, which is 20% higher than the value obtained based on the plateau modulus.

The horizontal shift factors are fitted with a WLF equation (equation (2.17), fits in Figure 6.6). The resulting C_1 and C_2 parameters are listed in Table 6.2, referred to $T_{ref} = T_g$, superscript g. C_1 and C_2 values are close for all polyamides; the product of C_1 and C_2 is between 370 and

Sample	T_{ref}=T_g (°C)	C_1^g	C_2^g (K)	$C_1^g C_2^g$	f_g	E_a^{Ferry} (kJ/mol)
PA6I 2k	106	12.4	47.9	594.6	0.035	119
PA6I 5k	121	11.5	37.5	431.2	0.038	107
PA6I 12k	126	11.2	32.9	369.2	0.039	98
PA6HIA 3k	147	12.6	48.7	614.0	0.035	144
PA6I/6LiSIPA 2k	117	12.7	50.6	644.3	0.034	132
PA6I/6LiSIPA 6k	133	12.6	46.1	579.8	0.035	133

Table 6.2: WLF fit parameters at T_g, fractional free volume at T_g and flow activation energies calculated with equation (6.6) at T_g + 100 for semi-aromatic polyamides.

643, in the low limit of the 449-2305 range mentioned in the literature [77]. Based on the value of C_1^g, the fractional free volume at T_g can be calculated based on [77]:

$$f_g = \frac{1}{\ln(10) C_1^g} \tag{6.5}$$

The values of f_g listed in Table 6.2 are slightly higher than the 0.025 universal value reported in the literature [77]. The fractional free volume at T_g was measured independently by Positron Annihilation Lifetime Spectroscopy for several polymers and it was shown that polymers containing double bonds or aromatic rings have a higher fractional free volume at T_g, of the order 0.030-0.035 [162]. Therefore, the difference can possibly be attributed to the semi-aromatic nature of the PA6I backbone.

In the PA6I series in Figure 6.6, the horizontal shift factors of the 2k polymer has a different behavior than those of the 5k and 12k polymers, whose curves of the horizontal shift factors nearly superimpose. This can be explained by the fact that the glass transition temperature is lower in low molecular weight samples, leading to slightly different WLF parameters [159]. Other forms of the WLF equation have been proposed, taking into account the T_g variation with molecular weight [77, 159]. However, a full series of molecular weights is needed for an accurate interpretation. Since only three molecular weights were available for the PA6I series, this approach has not been used in the present study.

Finally, the variation of the horizontal shift factors can be plotted as a function of T_g/T in an Angell plot (Figure 6.7) [163]. In this approach, materials that have an Arrhenius-like dependency (*i.e.* linear) are defined as "strong" glass formers and those with a WLF dependency as "fragile" glass formers. The strenght of the temperature dependency at the glass temperature is often considered in the terms of the "fragility" parameter and is given by the slope of the curves in Figure 6.7 at $T = T_g$. Compared to other polymers in Figure 6.7, the semi-aromatic polyamides are relatively "strong". This might be explained by the polar nature of the polymer and the existence of interchain interactions.

6.2.2 Influence of interactions

The main purpose of this study is to investigate the possible influence of interactions (hydrogen bonds, ionic) on the viscoelasticity of polyamide. The strenght of interactions has been fine-tuned by adding functional groups on a PA6I backbone. Two different series of constant molecular weight were targeted: 2 and 5 kg/mol. Experimentally, the number average molecular weight varied between 2-3 kg/mol for the first series and 5-6 kg/mol for the second. In this section, the different polymers will be compared in each series to identify the possible influence of interactions on viscoelasticity.

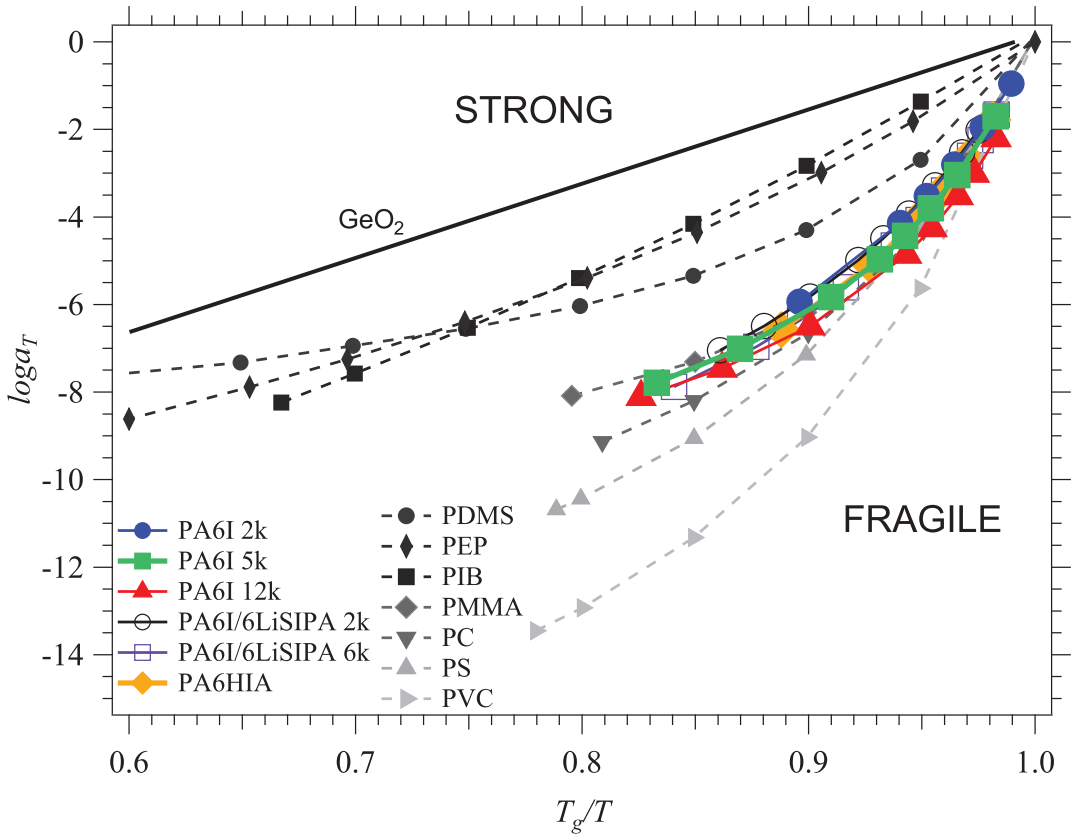

Figure 6.7: Angell plot for the segmental relaxation shift factors for our semi-aromatic polyamides and several polymers (data from [164])

6.2.2.1 Direct comparisons of the 2k and 5k series

The master curves of the 2k (PA6I, PA6HIA and PA6I/6LiSIPA) and 5k series (PA6I and PA6I/6LiSIPA) are shown in Figure 6.8(a) and (b) at $T_{ref} = T_g$. In this representation, the master curves of PA6HIA and PA6I/6LiSIPA are slightly shifted towards lower frequencies, which is mainly due to the difference in the glass transition temperature. It was observed that the data can be shifted artificially to superimpose (Figure 6.8(c) and (d)) by changing the reference temperature by a few degrees. This shift is compatible with the standard deviation of T_g values from DSC measurements and the relative broadness of the glass transition peaks obtained by taking the derivative of the MDSC ReversibleC_p signal with respect to time (Figure 6.9). The master curves of PA6I and PA6I/6LiSIPA overlay perfectly, indicating that the introduction of ionic groups does not influence the viscoelasticity of PA6I. In addition, it should be highlighted that at 2 kg/mol these polyamides are unentangled and no plateau is visible. These two observations are in strong contrast with the observations on unentangled polystyrene, for which 5% of sulfonate groups changed the master curves substantially, with a clear plateau appearing at $T_{ref} = T_g + 45 \simeq 130°C$ due to the interactions [104]. Note that for PA6I/6LiSIPA 2k, there is one sulfonate group per two chains compared to two sulfonate groups per chain for polystyrene.

PA6HIA seems to have a different behavior, with a higher modulus and the terminal region shifted to lower frequencies. The molecular weight of this polymer is slightly higher (3 kg/mol) compared to the other samples and additional branching probably occured via the hydroxy group (Figure 6.3). Although it is tempting to subscribe the difference to the presence of stronger H-bonds, as the structure of this polymer has not been fully elucidated, we can only speculate on the discrepancy.

Up to this point, the samples only display clear differences in T_g. Another quantity that can be compared is the activation energy for flow, which can be calculated from the slope of the Arrhenius plot of $\ln a_T$ as a function of $1/T$ [77]:

$$E_a^{Ferry} = \frac{ln(10)RC_1C_2T^2}{(C_2 + T - T_{ref})^2} \tag{6.6}$$

with T in Kelvin. Since the curve is not linear in the range (T_g, T_g + 100), this "apparent" activation energy increases accordingly when approaching T_g. Therefore, different materials have to be compared at the same distance to T_g. Usually, T is taken as T_g + 100, which is representative for processing [77]. The values of the activation energies obtained at $T_g + 100$ for $T_{ref} = T_g$ are listed in Table 6.2.

It is observed that the activation energy for flow increases by 10 to 50 kJ/mol when functional groups are added. This increase has already been observed for sulfonated polystyrene, but to a much larger extent. For instance, E_a^{Ferry} at T_g+100 increases from 126 kJ/mol for pure polystyrene to 220 kJ/mol for 6% sulfonated polystyrene [165].

6.2.2.2 Molecular modelling of the viscoelasticity of the short chains

Surprisingly, the master curves of polymers of similar molecular weight and molecular weight distribution could be forced to overlap close to T_g, indicating that the strength of the interactions does not significantly affect their dynamics. To confirm this point, a regular polydisperse Rouse model will be tested in order to fit the mastercurves of the unentangled polyamides.

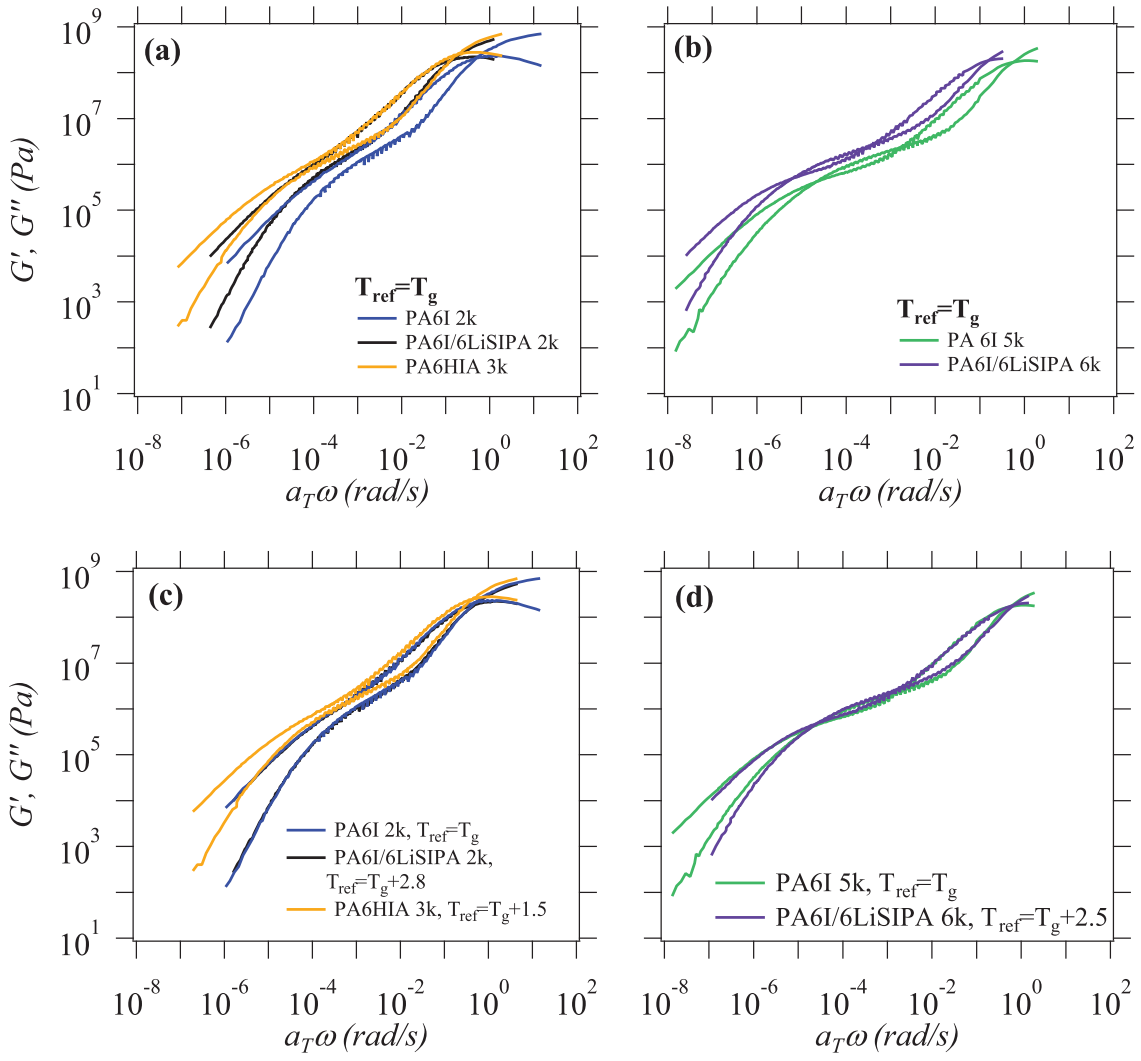

Figure 6.8: Comparison of master curves for the 2k and 5k series at (a) and (b) $T_{ref} = T_g$ and (c) and (d) shifted to superimpose

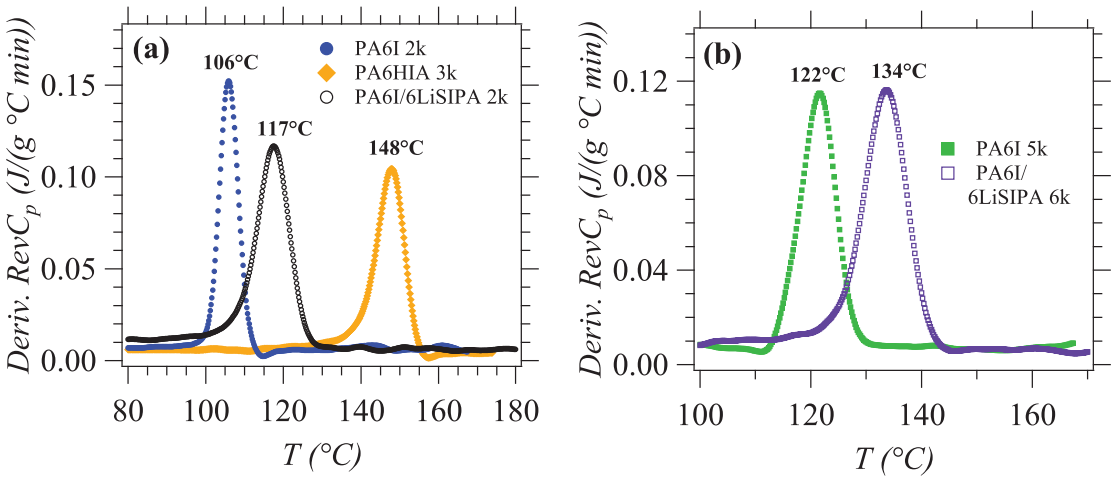

Figure 6.9: Comparison of the broadness of the glass transition process in the (a) 2k and (b) 5k series

6.2.2.2.1 Polydisperse Rouse model using the experimental molecular weight distribution

To begin with, the experimental molecular weight distribution (MWD) obtained from GPC was inserted in the Rouse equations (1.39) and (1.40) for a polydisperse, linear polymer. The characteristic time of the Rouse mode p is taken from equation (1.38), which leaves only one fitting parameter $f = \frac{\zeta b^2}{M_K}$ (where ζ is the monomeric friction coefficient). As stated previously, b and M_K were obtained by molecular modelling for PA6I and are supposed to be b = 9.8 Å and M_k = 0.128 kg/mol [161]. For PA6HIA and PA6I/6LiSIPA with a PA6I backbone, we make the hypothesis that b does not change significantly upon the introduction of lateral groups. Since the molecular weight of a PA6HIA monomer (0.262 kg/mol) or average molecular weight of a PA6I/6LiSIPA monomer (0.250 kg/mol) do not change much compared to the PA6I monomer (0.246 kg/mol), the same value was used for M_k as well. The fit was done with a Matlab program, using a least square minimization algorithm on a logarithmic scale. Only the data in the low frequency range was fitted, since the Rouse model does not describe the glass transition region. The data was cut off at different frequencies (10^{-2}, 10^{-3} and 10^{-4} s); this procedure provided slight variations in the values of the fit parameters and allows us to define an error, but the quality of the fit was similar. The experimental data and the corresponding fits with a Rouse model are reported in Figure 6.10.

As can be seen in Figure 6.10, the Rouse model for polydisperse, linear polymers provides an excellent description of the experimental data for the 2k series. The parameter f and the estimated ζ are reported in Table 6.3. The estimated monomeric friction coefficients are in the $10^{-2} - 10^{7}$ kg/s range of reported values of ζ at T_g for various polymers [77]. The excellent fit with the Rouse model suggests that interactions do not play a role in the viscoelasticity of these polymers. Last but not least, this also indicates that the small amount of branching by BHT (approx. 0.25 mol% of the amide groups are branched) or esters in the case of PA6HIA does not exert a significant influence on the rheological behavior, at least for the low molecular weights.

The monomeric friction coefficient obtained for PA6I 2k was applied to PA6I 5k, along with the experimental MWD. The resulting curve of the Rouse model does not describe the experimental points accurately, as can be seen in Figure 6.10(d). Indeed, the PA6I 5k is mildly entangled and a small rubbery plateau is observed. Hence, the Rouse model is no longer applicable.

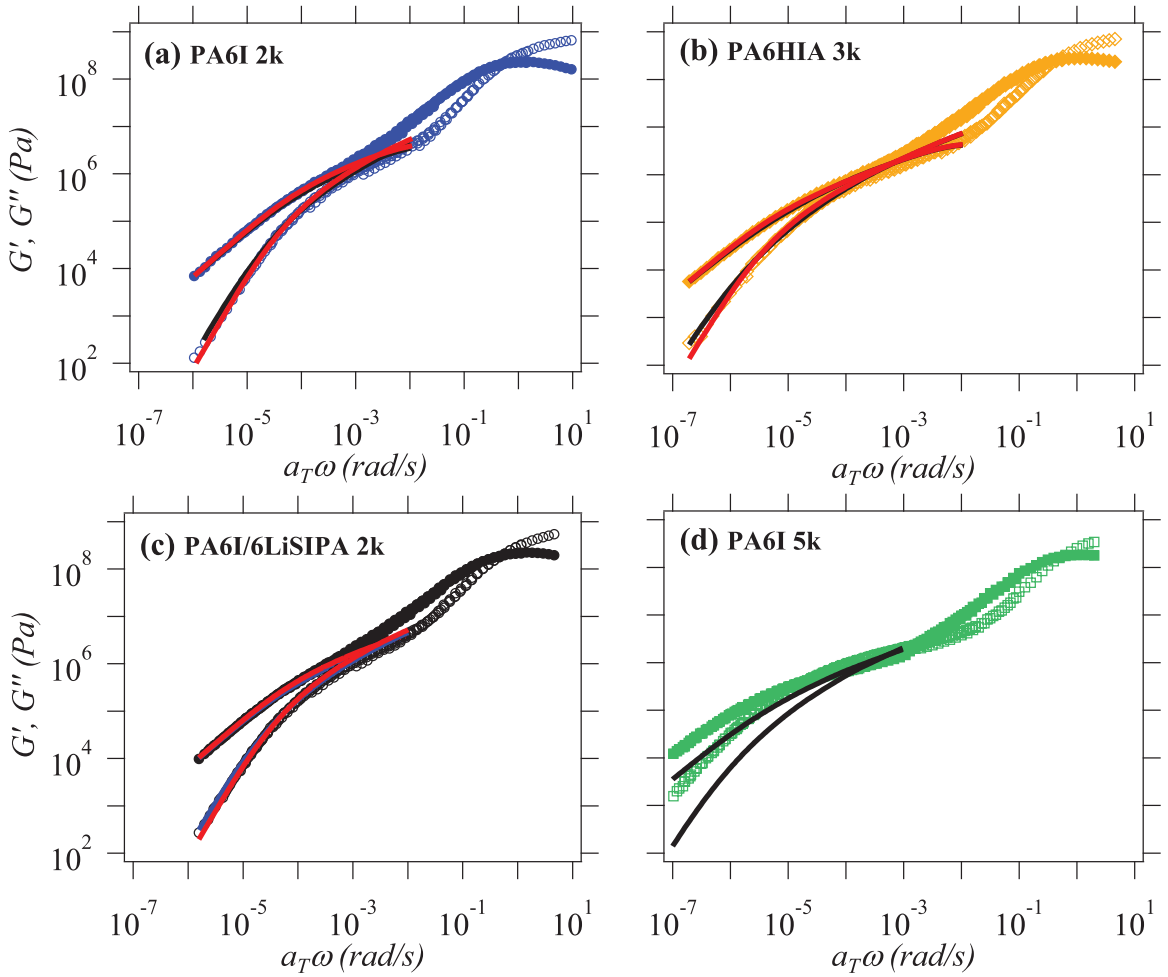

Figure 6.10: Experimental data in the terminal region ($T_{ref} = T_g$) and their corresponding fits with a Rouse model using the experimental GPC molecular weight distribution (black or blue lines) and with the molecular weight distribution as a free parameter (red lines). For PA6I/6LiSIPA 2k blue and red lines superimpose.

	Rouse with measured MWD		Rouse assuming a Flory MWD		
Sample	parameter f ($= \frac{\zeta b^2}{M_K}$)	ζ (kg/s)	p	parameter f ($= \frac{\zeta b^2}{M_K}$)	ζ (kg/s)
PA6I 2k	(3.1 ± 0.1) 10^{-17}	4.1 ± 0.1	0.8983 ± 0.008	(2.2 ± 0.2) 10^{-17}	2.9 ± 0.3
PA6HIA 3k	(3.6 ± 0.1) 10^{-17}	4.8 ± 0.1	0.9628 ± 0.003	(3.5 ± 0.3) 10^{-17}	4.6 ± 0.3
PA6I/6LiSIPA 2k	(1.5 ± 0.1) 10^{-17}	2.1 ± 0.1	0.9083 ± 0.009	(2 ± 0.3) 10^{-17}	2.6 ± 0.3

Table 6.3: Fit parameter obtained by describing the master curves of dynamic moduli at T_g with a Rouse model. M_k = 0.128 kg/mol and b = 9.8 Å [161]. The standard deviation was obtained from fitting the data with different high frequency cut-offs from 10^{-2} to 10^{-4} s.

6.2.2.2.2 Polydisperse Rouse model assuming an ideal Flory distribution

The Rouse model can also be used in a reverse approach in order to obtain the molecular weight distribution of the polymer. Supposing that the polyamides have a Flory molecular weight distribution (equation (1.2)), the rheological data can provide an estimation of monomer conversion p, which is then an additional free parameter in the fit. The fit procedure has therefore two parameters instead of one: p and f. Figure 6.10 illustrates the Rouse fits obtained with this approach. The corresponding fit parameters are listed in Table 6.3.

The quality of the fits is roughly equivalent to those obtained with the experimental MWD. The values of the monomeric friction coefficients are in agreement with the previous values. ζ is however much closer for PA6I and PA6I/6LiSIPA than in the previous fit. In order to better apprehend the monomer conversion p, the resulting Flory distributions are represented together with the experimental MWD from the GPC in Figure 6.2 (dotted lines). Small variations in the value of p have important consequences on the shape of the distribution. For PA6I/6LiSIPA 2k, the predicted and experimental MWDs are in excellent agreement. For PA6I 2k and PA6HIA 3k, the predicted Flory distributions are shifted to higher molecular weights compared to the GPC data. In any case, the master curves are well described by a simple polydisperse Rouse model and hence there are no obvious effects of the bonds on the viscoelasticity (apart perhaps an effect on ζ for PA6HIA).

6.3 Dynamics in the solid state (below T_g)

So far, it was found that the interchain interactions in semi-aromatic polyamides had an effect on T_g but did not have any pronounced influence on the viscoelastic properties. To extend our study to the dynamics in the solid state and possibly assess the effect of the bonds, dielectric spectroscopy measurements were performed on the semi-aromatic polyamides.

Three relaxations have been identified in polyamides [26]: γ, supposedly corresponding to the rotation of the aliphatic sequences, β, a combination of the configuration changes around the amide groups and the dissociation of the hydrogen bonds and α, associated to the glass transition (Chapters 1 and 5). Three relaxation processes are also visible in the polyamides of this study (Figure 6.11). Their characteristic relaxation times are illustrated in Figure 6.12 as function of temperature for PA6I 2k and 12k, PA6HIA 3k and PA6I/6LiSIPA 2k.

The γ relaxation is observed in the typical temperature range from -130 to -30°C [26]. However, the β relaxation is found at much higher temperatures than usual (60 to 100°C compared to -70 to 10°C for aliphatic polyamides [26, 127, 34, 166]). The α relaxation is also observed in at higher temperatures compared to aliphatic polyamides, which is in agreement with the higher T_g values measured by DSC. Being shifted towards higher temperatures where the conductivity of the samples increases and closer to T_g, the β relaxation could not be discriminated for PA6I 2k and PA6I/6LiSIPA 2k. In the latter, the presence of ions could also have resulted in a relaxation process, as it was the case for the ionomers of Chen *et al.* [105, 103]. However, no additional relaxation process could identified in this sample at high temperature. The ion concentration is probably too low (5%, 1 ionic group/2 chains) for ionic groups to form aggregates and therefore contribute to an additional, distinct relaxation.

The variation of the characteristic relaxation times for the secondary relaxations can be fitted with Arrhenius-like equations. The resulting activation energies E_a and characteristic relaxation times at infinite temperature (τ_0) are reported in Table 6.4. For the γ relaxation, the activation energy is in the usual range of 40 kJ/mol as for aliphatic polyamides [26, 25]. On the other hand, the activation energy for β is higher than the typical value of 60-70 kJ/mol for aliphatic polyamides [26, 34]. Along with the non physical value of τ_0^β (the range $\tau_0^\beta \sim 10^{-15} - 10^{-18}$ s is

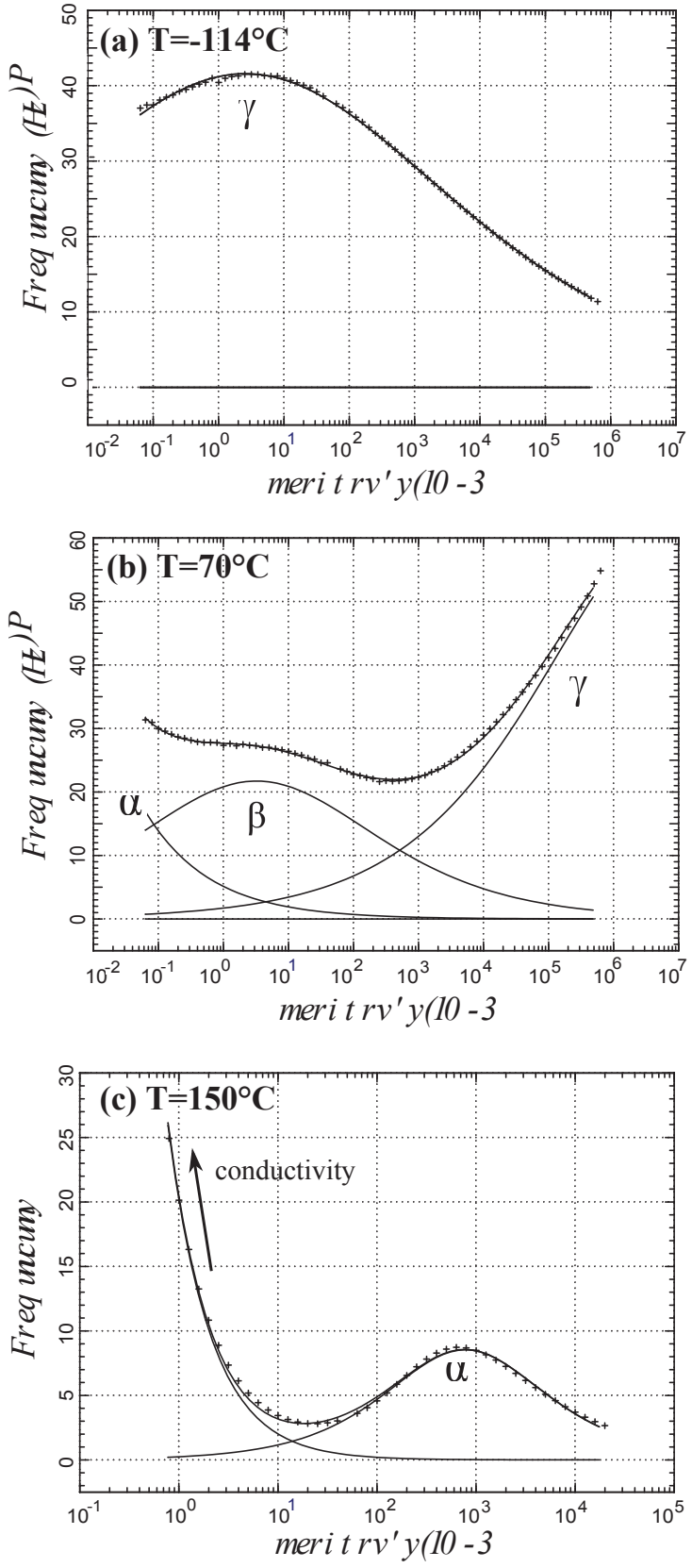

Figure 6.11: Isotherms of the loss permittivity ϵ'' in the region of the (a) γ, (b) β and (c) α relaxations in PA6I 12k, together with the corresponding fits with a Havriliak-Negami empirical equation (2.11).

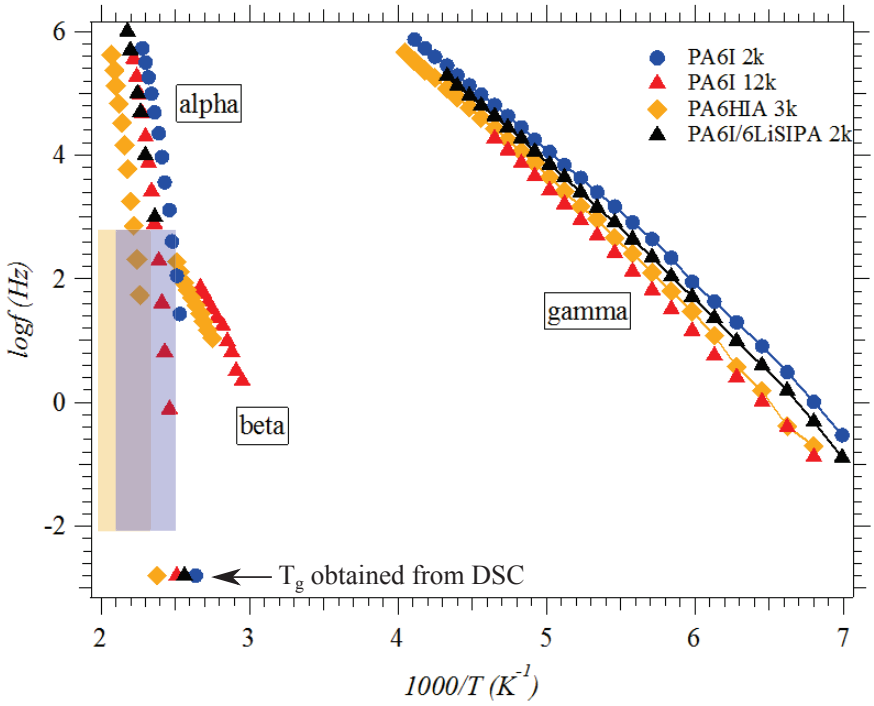

Figure 6.12: Relaxation chart evidencing the characteristic α, β and γ relaxation times as a function of increasing temperature for the PA6I 2k and 12k, PA6HIA 3k and PA6I/6ALiSIPA 2k. The β relaxation is not visible in PA6I 2k and PA6I/6LiSIPA 2k. Colored areas correspond to the temperature and frequency ranges available in rheometry for PA6I 2k and PA6HIA 3k with the same color code as the symbols. Lines are guides for the eye.

Sample	E_β (kJ/mol)	τ_0^β (s)	E_γ (kJ/mol)	τ_0^γ (s)
PA6I 2k	-	-	41	$2.9\ 10^{-16}$
PA6I 12k	109	$1.0\ 10^{-18}$	42	$1.9\ 10^{-16}$
PA6HIA 3k	92	$7.9\ 10^{-16}$	44	$1.3\ 10^{-16}$
PA6I/6LiSIPA 2k	-	-	43	$1.0\ 10^{-16}$

Table 6.4: Activation energies and characteristic τ_0 times for β and γ relaxations in aromatic polyamides

even beyond the value of 10^{-16} s where atomic or electronic entities respond; dipole orientation occurs in dielectric spectroscopy only down to 10^{-12} – 10^{-13} s [25]), this suggests that the process is more complicated than a simple configuration change around an amide group or the dissociation of a single hydrogen bond. Cooperative movements of the amide groups or an entropic contribution might explain this complexity.

The comparison of the relaxation charts of the samples is not straightforward. The characteristic relaxation times of all relaxations (α, β and γ) are shifted, but they do not display a clear trend. For instance, the γ relaxation in PA6HIA 3k is shifted to lower temperatures compared to PA6I 12k, whereas the β and α relaxations are shifted to higher temperatures. It is also unclear why the γ relaxation times vary to such a large extent, considering that the γ relaxation is supposedly associated to the rotation of the $-CH_2-$ sequences, which are the same in all samples. Lastly, the variation of the α relaxation is consistent with the T_g variation determined by DSC. Although we cannot comment more on the observed relaxations, the most important conclusion is that no other relaxation was observed above the α relaxation, as it was the case in other systems [93, 103, 105]. The interchain interactions would then break during the α or β relaxations.

6.4 Discussion

The viscoelastic master curves of amorphous polyamides were reported for varying molecular weights and varying types of interacting groups. The samples show a classical behavior with increasing molecular weight and no apparent strong influence of the interacting groups on the viscoelasticity. Indeed, the master curves of the short polymers are well described by "common" polydisperse Rouse models. In order to better understand these systems, their dynamics in the solid state was investigated by Dielectric Spectroscopy, which has proven to be a valuable technique for providing characteristic relaxation times of interacting groups in other rheological studies [93, 103, 105].

In comparison to the studies in the literature, we do not observe an α^* relaxation associated to the bond dynamics. The relaxation of hydrogen bonds in which amide groups participate is supposedly encompassed in the β and α relaxations [26]. Their influence on rheological properties can be eventually observed only if they are active in the temperature and frequency range available in rheometry. However, rheological measurements are only done above the α relaxation. For comparison, the temperature and frequency ranges in rheometry were added to Figure 6.12.

This was not the case for instance in the studies of Stadler *et al.* [89, 93] or Chen *et al.* [103, 105], where the relaxation of the interactions (H-bonds and ionic interactions, respectively) occured at temperatures above the α relaxation. All the polymers with H-bonds studied in the literature had a glass transition temperature well below 0°C. Hence, at room temperature, the energy RT is about 2.5 kJ/mol, much lower than the association energy of the stickers (25 to 70 kJ/mol, see

Table 1.3). However, a plateau due to the association of the stickers appeared only for stickers with a high energy of interaction (70 kJ/mol) [97].

In the case of polyamide, no effect is observed for PA6I, PA6HIA or PA6I/6LiSIPA. *RT* is between 3.2 and 4 kJ/mol in the tTS range (110-210°C), lower than the energy of a hydrogen bond in polyamide, estimated around 25-27 kJ/mol [9, 117]. The introduction of phenol or ionic groups should lead to phenol/amide H-bonds or complexes of Li^+ and carbonyl groups, with estimated energies of 40 kJ/mol [9] and between 12 and 50 kJ/mol [122], respectively, as explained in Chapter 2. A clear effect can be observed on the glass transition temperature, which increases for instance by 10°C with 5% of ionic groups LiSIPA. For comparison, 5% ions produced the same effect on the glass transition of polystyrene and led to the appearance of a clear plateau in the modulus of the unentangled polymer [104]. However, the energy of ionic association/dissociation of these systems was estimated to be 65 kJ/mol [103].

Generally speaking, it seems that a plateau is observed only if the interaction energies are high enough (>60 kJ/mol?). It was also the case for Chen *et al.* [103], who had a plateau in unentangled ionomers based on copolymers of poly(tetramethylene oxide) and sulfonated phthalates (energy of interaction of 58 kJ/mol), but not in copolymers of poly(ethylene oxide) and sulfonated phthalates (energy of interaction of 10 kJ/mol). Based on these energies, we can estimate a relative relaxation time of the interactions with an Arrhenius-like equation $\tau = \tau_0 \exp(E/RT)$. At 25°C, $\tau/\tau_0 \sim 10^4$ for an energy of 25 kJ/mol and 10^{12} for an energy of 70 kJ/mol. At 135°C, $\tau \sim 10^3$ s for an energy of 25 kJ/mol, 10^6 s for 50 kJ/mol and 10^8 s for 65 kJ/mol. It is observed that τ/τ_0 shifts strongly with small differences in energy. This might explain why we do not see an effect of the interchain interactions in our systems.

Furthermore, in the case of ionomers, the addition of 5% LiSIPA monomers leads to a ratio of 1 sulfonate group/2 polymer chains. This ratio is not significant to see an effect on rheology, since at best small amounts of star polymers would be formed.

The sole effect of the interacting groups on the viscoelasticty seems to be on the monomeric friction coefficient. Similar values were obtained for PA6I and PA6I/6LiSIPA (Table 6.3) by the two fit methods of the viscoelastic data, since the LiSIPA percentage was too low to see any difference. However, PA6HIA contains a phenol group on each monomer. We systematically obtain a higher value of the monomeric friction coefficient for this polymer, which might be associated to the higher density of interacting groups. In order to test this hypothesis, copolymers with different ratios of PA6I/PA6HIA or higher percentages of 6LiSIPA should be investigated.

6.5 Conclusions

The aim of our investigation was to gain understanding of the effects of the strength and density of interchain interactions on the dynamics of polyamides. In order to achieve this goal, a class of amorphous, blocked polyamides was designed to remove the limitations inherent to polyamide. The strength of the interactions was varied by the introduction of lateral groups (hydroxy, lithium sulfonate) on a PA6I backbone.

First of all, the chemical structure of the polyamides was thoroughly investigated by GPC and the branching was quantified. It was highlighted that, with the exception of the PA6I 2k, these polymers did not have a Flory distribution characteristic of linear polycondensation. Small amounts of branching were identified via the dosage of bis(hexa-methylene)triamine (BHT). Approximately 0.1-0.25% of the amide groups are branched, which accounts for 1 amide group in 400-1000. However, more investigations would be required in order to determine the exact nature of the branches. Especially for PA6HIA, additional branching might occur via the phenol group.

The complete master curves of the dynamic moduli for polyamide were obtained for the first time. For PA6I we observe the occurrence of a plateau in G' around molecular weights of 5 kg/mol. As the molecular weight increases, a clear rubbery plateau appears and the longest relaxation time is shifted to lower frequencies. The introduction of lithium sulfonate or phenol groups results in an increase of the glass transition temperature by 10 to 40°C, respectively, presumably due to their ability to form strong interactions with the amide groups. Surprisingly, when polymers of similar molecular weight and molecular weight distribution are compared at their respective T_g, their master curves roughly overlap, indicating that the strength and density of interactions does not affect the dynamics above T_g significantly. To confirm this point, we described the master curves of the unentangled polyamides with a polydisperse Rouse model taking into account the experimental MWD obtained by GPC.

An investigation by Broadband Dielectric Spectroscopy did not identify an α^* relaxation specific to the interactions, as it was the case in some previous literature studies. The dynamics of hydrogen bonds is encompassed in the the β and α relaxations of the samples, which are not in the temperature and frequency range of rheological measurements. This might explain why the hydrogen bonds do not have a signature on the rheological properties, contrary to previous studies on systems with low T_g polymers and H-bonded stickers. The ionomers PA6I/6LiSIPA did not show any difference in viscoelasticity compared to PA6I (apart from the shift in T_g), probably because the quantity of sulfonate groups was too low (1 per 2 polymer chains). The lack of influence of interchain interactions was tentatively explained by taking into consideration the energy of interaction, which might be too low. The interacting groups do seem to have a mild but systematic influence on the monomeric friction coefficient. Also, semi-aromatic PAs are less "fragile" glass formers (in terms of Angell's plot) compared to non polar polymers.

General conclusions

The main purpose of this PhD thesis was to investigate the dynamics of polyamide, a commercial polymer in which a network of hydrogen bonds exists. Two different aspects have been studied: the dynamics in the solid state in presence of solvents and the dynamics in the molten state.

Since most polyamides are semi-crystalline, this study begins with an assessment of the influence of the crystalline phase on diffusion and sorption (Chapter 3). 100% amorphous semi-aromatic polyamides (PA6I and Selar) were compared to a semi-crystalline polyamide (A1007, up to 26% crystalline ratio), at *iso*-chemical structure. Several solvents were investigated: water and alcohols of different sizes. As it turned out, the amorphous polyamides crystallize and form cavities in presence of alcohols and thus prevented the comparison. The crystallization was thoroughly accounted for through DSC, XRD and SEM imaging. In presence of water on the other hand, the amorphous polyamides do not crystallize. The comparison of the amorphous and semi-crystalline polyamides showed that the diffusion coefficients are similar in the range of 0 to 26% crystalline ratio. However, sorption at equilibrium is influenced by the presence of the crystalline phase. Indeed, polyamide structure is more accurately depicted as a three phase model: crystalline, rigid amorphous fraction (RAF) and mobile amorphous fraction (MAF). The present study suggested that 15% of the amorphous phase was not accessible to water, which roughly corresponds to the percentage of RAF estimated independently by DSC. The comparison of the alcohols sorption in different semi-crystalline polyamides (PA6,6, PA6,10 and A1007) shows a large variability on the equilibrium values, as a function of size or polarity of the solvent. It also suggests that the amorphous phase of a semi-crystalline polyamide is not 100% accessible to solvents. This findings are in agreement with previous literature studies [33, 54, 55, 58, 167].

In Chapters 4 and 5, the sorption and diffusion mechanisms of water and ethanol were investigated in more detail. A Dynamic Vapor Sorption experiment design was used in order to apply small steps of solvent activity to a PA6,6 and PA6,10 matrix. Two different informations were obtained: diffusion coefficients and solvent intake at equilibrium as a function of solvent activity (sorption isotherms). The main purpose of this study was to investigate sorption and diffusion mechanisms individually in each matrix. A second purpose was to assess the influence of the density of hydrogen bonds on these two processes, since the density of hydrogen bonds is lower in PA6,10 than in PA6,6.

In order to provide information on solvent distribution at the molecular level, sorption isotherms were first investigated. Both water and ethanol sorption isotherms can be accurately described by a Guggenheim, Anderson and de Boer (GAB) model, which predicts sorption in specific sites and accounts for the formation of solvent clusters. It was thus shown that water forms clusters of about 1 molecule in PA6,10 and about two molecules in PA6,6. In the case of ethanol, clusters of two molecules were identified in both materials. It is suggested therefore that water and ethanol are distributed in polyamide down to molecular size and do not form nanodomains. This implies that diffusion will be isotropic, *i.e.* not affected by polymer structuration at a nanometer scale in the amorphous phase.

It was suggested by the comparison of amorphous and semi-crystalline polyamide in Chapter 3 that the amorphous phase might not be entirely accessible to solvents. Therefore, more information on structure is needed before comparing the sorption at equilibrium in PA6,6 and PA6,10. Moreover, the two polymers had been processed with different methods (film casting and injection), which might have a high impact on the phase distribution. Following the example of Litvinov *et al.* [55], a quantification of the different polyamide phases (regid, semi-rigid, mobile) was attempted. The results of this study were inconclusive when compared to DSC estimations of the rigid and mobile amorphous fraction. As a consequence, the direct comparison

of PA6,6 and PA6,10 is only speculative.

One of the main interests of this work was the study of diffusion mechanisms in relation to polyamide relaxation. The variation of the diffusion coefficients with solvent concentration could be successfully related to Fickian and non-Fickian diffusion mechanisms. In addition, the characteristic relaxation times of water/polyamide systems were measured by Broadband Dielectric Spectroscopy. It was observed that diffusion is not directly correlated to the polymer α relaxation, associated to the glass transition. This finding is in agreement with previous studies, in which polyamide plasticization was measured long after water penetrated in the material (plasticization lag) [59]. On the other hand, diffusion seems correlated to the β relaxation, which is supposedly a combination of configuration change of the amide groups and hydrogen bond dynamics. Based on this observation, a model of water hopping between sorption sites is proposed, in which the limiting factor is the dissociation of hydrogen bonds.

For future studies, it would be particularly interesting to look into the β relaxation of other polyamide/solvent systems. Since this relaxation encompasses the dynamics of the hydrogen bonds in polyamide, it would be expected to depend on the type of interaction with the solvent (for instance, water, ethanol or phenols). Also, the secondary β relaxation seems to be the key in understanding the mechanical properties of polymers [168], so it is important to characterize it.

The second interest of this work was to study the influence of strong interactions (hydrogen bonds, ionic) on the viscoelasticity of polyamide. Polyamide viscoelasticity has hardly been investigated in the literature, the main reasons being the semi-crystalline nature of most polyamides and the evolution of their molecular weight upon heating (because of post-condensation). The use of end-capped, amorphous polyamides was identified as a solution. The chosen backbone is a semi-aromatic PA6I, that can be functionalized by the addition of small lateral groups on the aromatic ring of the isophthalic acid monomer: *-OH* (PA6HIA, hydrogen bonds) and *-SO_3Li* (PA6I/6LiSIPA, ionic interactions). Different molecular weights were synthesized, from unentangled to entangled. Several difficulties were identified for the synthesis and characterization of the molecular structure. On the one hand, polyamide synthesis presents secondary reactions that lead to branching. On the other hand, the experimental GPC curves do not follow a Flory distribution. The amount of branching could be estimated through the dosage of bis(hexa-methyl)triamine but other branching mechanisms might exist, especially for PA6HIA.

PA6I displays the classical melt behavior with the increase of molecular weight: appearance of a plateau and increase of the longest relaxation time. The molecular weight between entanglements M_e is estimated to be 1.8 kg/mol, which is comparable to the literature value for PA6 [88, 160]. The introduction of lateral groups has important effects on the glass transition temperature. The T_g increases by 10 to 40°C as the amount of lateral interacting groups increases. On the other hand, no significant effect was observed on the viscoelasticity. Master curves of polyamides of similar molecular weight rescaled at T_g superimpose, suggesting that the bonds do not have a pronounced influence on the viscoelasticity. Moreover, the master curves of unentangled polyamides could be well described by a classical Rouse model for polydisperse polymers.

Some elements for understanding this lack of influence of the strong interactions are given by Broadband Dielectric Spectroscopy. No relaxation specific to the interactions (α^*) was identified at temperatures above the α relaxation. The α and β relaxations, directly correlated to the association/dissociation of the hydrogen bonds, are outside the available temperature and frequency range in rheometry. It was not the case in systems previously reported in the literature, for which the relaxation of interacting groups occurred at temperatures above the main α relaxation of the chain, close to room temperature. Moreover, two other hypotheses

were proposed: 1. the energy of interaction is not high enough to influence the dynamics at elevated temperatures and 2. the effect of interchain interactions is encompassed in the friction coefficient. For ionomers, the percentage of LiSIPA was in any case too low (1 sulfonate group/2 chains) to give an effect, *i.e.* even if active, with a long enough lifetime in the molten state, the effects on the viscoelasticity would be minor. The two clear manifestations of the interactions were the increase in glass transition temperature and the lower fragility (in terms of Angell's plot) compared to non-polar polymers.

The study of polyamide viscoelasticity opened the path for future investigations. It identified the blocking strategy for having stable materials, an amorphous structure to have access to the variation of dynamic moduli on a large frequency range, raised several questions on how to accurately describe the molecular structure (Flory distribution? branching?) and reported the first master curves for polyamides. And most importantly, the density and strength of interactions could be modified without changing the polymer backbone. Although some considerations were made on viscoelasticity and the lack of influence of hydrogen bonds, the number of samples and their characterization were not satisfactory in order to be conclusive. More systems, with a higher variation in strength and density of interactions will have to be investigated.

Bibliography

[1] M.I. Kohan. *Nylon Plastics Handbook*. Wilmington:Hanser, 1995.

[2] L.T. Lim, I.J. Britt, and M.A. Tung. Sorption and transport of water vapor in nylon 6,6 film. *Journal of Applied Polymer Science*, 71:197, 1999.

[3] A. Rios de Anda, L. A. Fillot, S. Rossi, D. Long, and P. Sotta. Influence of the sorption of polar and non-polar solvents on the glass transition temperature of polyamide 6,6 amorphous phase. *Polymer Engineering & Science*, 51(11):2129–2135, 2011.

[4] K. Tai and T. Tagawa. Simulation of hydrolytic polymerization of epsilon-caprolactam in various reactors. a review on recent advances in reaction engineering of polymerization. *Industrial & Engineering Chemistry Product Research and Development*, 22(2):192–206, 1983.

[5] B.L. Deopura, R. Alagirusamy, M. Joshi, and B. Gupta. *Polyesters and polyamides*. Woodhead Publishing, 2008.

[6] P.J. Flory. *Principles of polymer chemistry*. Cornell University Press, Ithaca, 1953.

[7] M. Rubinstein and Ralph H. Colby. *Polymer Physics*. Oxford University Press, 2003.

[8] C.H. Bamford and C.F.H. Tipper. *Comprehensive Chemical Kinetics. Vol 15 Non-Radical Polymerization*. Elsevier Scientific Publishing Company, 1976.

[9] W.L. Jorgensen and C.J. Swenson. Optimized intermolecular potential functions for amides and peptides. Hydration of amides. *Journal of the American Chemical Society*, 107(6):1489, 1985.

[10] D. Garcia and H.W. Starkweather. Hydrogen bonding in nylon 66 and model compounds. *Journal of Polymer science: Polymer Physics Edition*, 23(3):537–555, 1985.

[11] G. Serpe and N. Chaupart. Relaxation-structure relationship in bulk and plasticized polyamide 11. *Journal of Polymer Science Part B*, 34:2351–2365, 1996.

[12] M. Laurati, A. Arbe, A. Rios de Anda, L. A. Fillot, and P. Sotta. Effect of polar solvents on the crystalline phase of polyamides. *Polymer*, 55:2867–2881, 2014.

[13] F. Auriemma, V. Petraccone, L. Parravicini, and P. Paolo Corradini. Mesomorphic form (beta) of nylon 6. *Macromolecules*, 30:7554–7559, 1997.

[14] J. Brandrup, E. H. Immergut, and E. A. Grulke. *Polymer Handbook, 4th edition*. 2003.

[15] H.W. Starkweather, J.F. Whitney, and D.R. Johnson. Crystalline order in nylon 66. *Journal of Polymer Science Part A*, 1:715–723, 1963.

[16] H. Haberkorn, K. H. Illers, and P. Simak. Molekülordnung und kristallinität in polyhexamethylenadipamid. *Colloid and Polymer Science Kolloid-Zeitschrift & Zeitschrift Für Polymere*, 257(8):820–840, 1979.

[17] J. Varlet. Cristallinité du polyamide 6 et du polyamide 66: étude comparative des différentes techniques de caractérisation. Technical report, Rhodia Internal Report, 1989.

[18] C. Vergelati, A. Imberty, and S. Pérez. Water induced crystalline transition of PA6,6: A combined X-Ray and molecular modeling approach. *Macromolecules*, 26:4420–4425, 1993.

[19] C. W. Bunn and E. V. Garner. The crystal structures of two polyamides ('nylons'). *Proceedings of the Royal Society A: Mathematical, Physical and Engineering Sciences*, 189(1016):39–68, 1947.

[20] L. Penel-Pierron, C. Depecker, R. Seguela, and J.M. Lefebvre. Structural and mechanical behavior of nylon 6 films. Part I. Identification and stability of the crystalline phases. *Journal of Polymer Science Part B*, 39:484–495, 2001.

[21] R. Brill. *Journal für praktische Chemie*, 161:49, 1942.

[22] R. Brill. *Die Makromolekulare Chemie*, 18/19:294, 1956.

[23] H.-J. Radusch, M. Stolp, and R. Androsch. Structure and temperature-induced structural changes of various polyamides. *Polymer*, 35(16):3568–3571, 1994.

[24] P.J. Flory. On the morphology of the crystalline state in polymers. *Journal of the American Chemical Society*, 84(15):2857–2868, 1962.

[25] F. Kremer and A. Schönhals. *Broadband Dielectric Spectroscopy*. Springer, 2003.

[26] N.G. McCrum, B.E. Read, and G. Williams. *Anelastic and Dielectric Effects in Polymeric Solids*. Wiley, 1967.

[27] A. Rios de Anda. *Influence of the solvent sorption, additivation, and chemical modification on the molecular mobility dynamics of Polyamide 6,6 amorphous phase and its consequences on the tensile and impact strength properties of this polymer*. Thesis, 2012.

[28] H Vogel. *Physikalische Zeitschrift*, 22:645, 1921.

[29] G.S. Fulcher. Analysis of recent measurements of the viscosity of glasses. *Journal of the American Ceramic Society*, 8:339, 1923.

[30] G. Tammann and W. Hesse. Die abhängigkeit der viscosität von der temperatur bie unterkühlten flüssigkeiten. *Zeitschrift für anorganische und allgemeine Chemie*, 156:245, 1926.

[31] H.W. Starkweather. The sorption of water by nylons. *Journal of Applied Polymer Science*, 2(5):129, 1959.

[32] N. S. Murthy. Hydrogen bonding, mobility, and structural transitions in aliphatic polyamides. *Journal of Polymer Science Part B*, 44:1763–1782, 2006.

[33] N.J.W. Reuvers, H.P. Huinink, H.R. Fischer, and O.C.G. Adan. Quantitative water uptake study in thin nylon-6 films with NMR imaging. *Macromolecules*, 45:1937–1945, 2012.

[34] M. Laurati, P. Sotta, D. R. Long, L. A. Fillot, A. Arbe, A. Alegrìa, J. P. Embs, T. Unruh, G. J. Schneider, and J. Colmenero. Dynamics of water absorbed in polyamides. *Macromolecules*, 45(3):1676–1687, 2012.

[35] J. Crank. *The Mathematics of Diffusion, 2nd edition*. Clarendon Press - Oxford, 1975.

[36] T. Alfrey and E.F. Gurnee. Diffusion in glassy polymers. *Journal of Polymer Science Part C*, 12:249–261, 1966.

[37] U. Yamamoto and K.S. Schweizer. Microscopic theory of the long-time diffusivity and intermediate-time anomalous transport of a nanoparticle in polymer melts. *Macromolecules*, 48:152–163, 2015.

[38] David A. Bond and Paul A. Smith. Modeling the transport of low-molecular-weight penetrants within polymer matrix composites. *Applied Mechanics Reviews*, 59(5):249, 2006.

[39] A.R. Berens and H.B. Hopfenberg. Diffusion and relaxation in glassy polymer powders: 2. separation of diffusion and relaxation parameters. *Polymer*, 19:489–496, 1978.

[40] M.S. Hedenqvist and U.W. Gedde. Parameters affecting the determination of transport kinetics data in highly swelling polymers above Tg. *Polymer*, 40:2381–2393, 1999.

[41] A.S. Michaels and R.B. Parker. Sorption and flow of gases in polyethylene. *Journal of Polymer Science*, 41:53–71, 1959.

[42] A.S. Michaels and H.J. Bixler. Flow of gases through polyethylene. *Journal of Polymer Science*, 50:413–439, 1961.

[43] R. K. Bharadwaj. Modeling the barrier properties of polymer-layered silicate nanocomposites. *Macromolecules*, 34:9189–9192, 2001.

[44] L. E. Nielsen. Models for the permeability of filled polymer systems. *Journal of Macromolecular Science*, A1:929–942, 1967.

[45] M.H. Klopffer and B. Flaconnèche. Transport properties of gases in polymers: Bibliographic review. *Oil & Gas Science and Technology – Rev. IFP*, 56(3):223–244, 2001.

[46] K. S. Kwan, C. N. P. Subramaniam, and T. C. Ward. Effect of penetrant size and shape on its transport through a thermoset adhesive: I. n-alkanes. *Polymer*, 44(10):3061–3069, 2003.

[47] K. S. Kwan, C. N. P. Subramaniam, and T. C. Ward. Effect of penetrant size, shape, and chemical nature on its transport through a thermoset adhesive. II. esters. *Polymer*, 44(10):3071–3083, 2003.

[48] W. Camacho, M. S. Hedenqvist, and S. Karlsson. Near infrared (NIR) spectroscopy compared with thermogravimetric analysis as a tool for on-line prediction of water diffusion in polyamide 6,6. *Polymer International*, 51(12):1366–1370, 2002.

[49] M. Broudin, P. Y. Le Gac, V. Le Saux, C. Champy, G. Robert, P. Charrier, and Y. Marco. Water diffusivity in PA66: Experimental characterization and modeling based on free volume theory. *European Polymer Journal*, 67:326–334, 2015. Broudin, M. Le Gac, P. Y. Le Saux, V. Champy, C. Robert, G. Charrier, P. Marco, Y.

[50] M. Sabard. *Etude de films PA6 et nanocomposites. Effet des conditions de procédé et des nanocharges sur la morphologie et les propriétés de sorption à l'eau et à l'éthanol*. Thesis, 2006.

[51] N.S. Murthy, M. Stamm, J.P. Sibilia, and S. Krimm. Structural changes accompanying hydration in nylon 6. *Macromolecules*, 22:1261–1267, 1989.

[52] J. L. Hutchison, N. S. Murthy, and E. T. Samulski. Deuterium NMR studies of water in oriented nylon 6 fibers. *Macromolecules*, 29(17):5551–5557, 1996.

[53] N.S. Murthy and M.K. Akkapeddi. Analysis of lamellar structure in semicrystalline polymers by studying the absorption of water and ethylene glycol in nylons using small-angle neutron scattering. *Macromolecules*, 31(1):142–152, 1998.

[54] P. Adriaensens, A. Pollaris, R. Carleer, D. Vanderzande, J. Gelan, V. M. Litvinov, and J. Tijssen. Quantitative magnetic resonance imaging study of water uptake by polyamide 4,6. *Polymer*, 42(19):7943–7952, 2001.

[55] M. Litvinov and J. P. Penning. Phase composition and molecular mobility in Nylon 6 fibers as studied by proton NMR transverse magnetization relaxation. *Macromolecular Chemistry and Physics*, 205:1721–1734, 2004.

[56] V. M. Litvinov, O. Persyn, V. Miri, and J. M. Lefebvre. Morphology, phase composition, and molecular mobility in polyamide films in relation to oxygen permeability. *Macromolecules*, 43(18):7668–7679, 2010.

[57] V. M. Litvinov, C. E. Koning, and J. Tijssen. The effect of annealing of linear and branched polyamide 46 on the phase composition, molecular mobility and water absorption as studied by DSC, 1H and 2H solid-state NMR. *Polymer*, 56(0):406–415, 2015.

[58] N.J.W. Reuvers, H.P. Huinink, and O.C.G. Adan. Water plasticizes only a small part of the amorphous phase in nylon-6. *Macromolecular Rapid Communications*, 34(11):949–953, 2013.

[59] N.J.W. Reuvers, H.P. Huinink, and O.C.G. Adan. Plasticization lags behind water migration in nylon-6: An NMR imaging and relaxation study. *Polymer*, 63:127–133, 2015.

[60] G. Skirrow and K.R. Young. Sorption, diffusion and conduction in polyamide-penetrant systems: 1. sorption phenomena. *Polymer*, 15(12):771–776, 1974.

[61] L.D. Landau and E.M. Lifshitz. *Physique Statistique*.

[62] I. Langmuir. The constitution and fundamental properties of solids and liquids. Part I. Solids. *Journal of the American Chemical Society*, 38(11):2221, 1916.

[63] A. F. M. Barton. *A. F. M. Barton, Handbook of Solubility Parameters and Other Cohesion Parameters, 1983*. CRC Press, Boca Raton, FL., 1983.

[64] Emmett P.H. Teller E. Brunauer, S. Adsorption of gases in multimolecular layers. *Journal of the American Chemical Society*, 60(2):309–319, 1938.

[65] R.B. Anderson. Modification of the Brunauer, Emmett and Teller equation. *Journal of the American Chemical Society*, 69:686–691, 1946.

[66] J.H. de Boer. *The dynamic character of adsorption*. Oxford Clarendon Press, 1953.

[67] E.A. Guggenheim. Application of statistical mechanics. *Oxford Clarendon Press*, pages 186–206, 1966.

[68] Z. Zhang, I. J. Britt, and M. A. Tung. Water absorption in EVOH films and its influence on glass transition temperature. *Journal of Polymer Science Part B*, 37:691–699, 1999.

[69] S. W. Lasoski and W. H. Cobbs. Moisture permeability of polymers. I. Role of crystallinity and orientation. *Journal of Polymer Science*, 36(130):21–33, 1959.

[70] D. H. Weinkauf and D. R. Paul. *Effects of Structural Order on Barrier Properties*, volume 423 of *ACS Symposium Series*, book section 3, pages 60–91. American Chemical Society, 1990.

[71] R. Puffr and J. Sebenda. On the structure and properties of polyamides.XXVII. the mechanisms of water sorption in polyamides. *Journal of Polymer Science Part C*, 16:79–93, 1967.

[72] W. Liu, B. Breault, and J. Brisson. Solvent-induced crystallization of Nylon-6I. *Journal of Polymer Science Part B*, 33:619–627, 1995.

[73] Y. S. Hu, S. Mehta, D. A. Schiraldi, A. Hiltner, and E. Baer. Effect of water sorption on oxygen-barrier properties of aromatic polyamides. *Journal of Polymer Science Part B*, 43(11):1365–1381, 2005.

[74] R.I. Tanner and K. Walters. *Rheology: An historical perspective*. Elsevier Science B.V., 1998.

[75] H.A. Barnes, J.F. Hutton, and K. Walters. *An introduction to rheology*. 1989.

[76] W.W. Graessley. *Polymeric Liquids and Networks: Dynamics and Rheology*. Garland Science, 2008.

[77] J.D. Ferry. *Viscoelastic properties of polymers, 3rd edition*. John Wiley & Sons, Inc, 1980.

[78] R. M. L. Evans, M. Tassieri, D. Auhl, and T. A. Waigh. Direct conversion of rheological compliance measurements into storage and loss moduli. *Physical Review E*, 80(1):012501, 2009.

[79] J. Zhao, S. F. Hahn, D. A. Hucul, and D. M. Meunier. Thermal and viscoelastic behavior of hydrogenated polystyrene. *Macromolecules*, 34(6):1737–1741, 2001.

[80] G. C. Berry and T. G. Fox. The viscosity of polymers and their concentrated solutions. *Advances in Polymer Science*, 5:261–357, 1968.

[81] H. J. Unidad, M. A. Goad, A. R. Bras, M. Zamponi, R. Faust, J. Allgaier, W. Pyckhout-Hintzen, A. Wischnewski, D. Richter, and L. J. Fetters. Consequences of increasing packing length on the dynamics of polymer melts. *Macromolecules*, 2015.

[82] S. F. Edwards. The statistical mechanics of polymerized material. *Proceedings of the Physical Society*, 92(1):9, 1967.

[83] P. G. de Gennes. Reptation of a polymer chain in the presence of fixed obstacles. *The Journal of Chemical Physics*, 55(2):572–579, 1971.

[84] M. Doi and S. F. Edwards. Dynamics of concentrated polymer systems. Part 1 to 3. *Journal of the Chemical Society, Faraday Transactions 2: Molecular and Chemical Physics*, 74(0):1789–1832, 1978.

[85] A. E. Likhtman and T. C. B. McLeish. Quantitative theory for linear dynamics of linear entangled polymers. *Macromolecules*, 35(16):6332–6343, 2002.

[86] E. van Ruymbeke, S. Coppola, L. Balacca, S. Righi, and D. Vlassopoulos. Decoding the viscoelastic response of polydisperse star/linear polymer blends. *Journal of Rheology*, 54(3):507–538, 2010.

[87] J.M. Dealy and R.G. Larson. *Structure and Rheology of Molten Polymers: From Structure to Flow Behavior and Back Again*. Hanser Publishers, 2006.

[88] E. Van Ruymbeke, J.J.M. Slot, M. Kapnistos, and P.A.M. Steeman. Structure and rheology of branched polyamide 6 polymers from their reaction recipe. *Soft Matter*, 9:6921, 2013.

[89] R. Stadler and L.L. de Lucca Freitas. Thermoplastic elastomers by hydrogen bonding 1. Rheological properties of modified polybutadiene. *Colloid and Polymer Science*, 264:773–778, 1986.

[90] L.L. de Lucca Freitas and R. Stadler. Thermoplastic elastomers by hydrogen bonding. 3. Interrelations between molecular parameters and rheological properties. *Macromolecules*, 20:2478–2485, 1987.

[91] L.L. de Lucca Freitas and R. Stadler. Thermoplastic elastomers by hydrogen bonding 4. Influence of hydrogen bonding on the temperature dependence of the viscoelastic properties. *Colloid and Polymer Science*, 266:1095–1101, 1988.

[92] M. Müller, U. Seidel, and R. Stadler. Influence of hydrogen bonding on the viscoelastic properties of thermoreversible networks: analysis of the local complex dynamics. *Polymer*, 36(16):3143–3150, 1995.

[93] M. Müller, F. Kremer, F.J. Stadler, E.W. Fischer, and U. Seidel. The molecular dynamics of thermoreversible networks as studied by broadband dielectric spectroscopy. *Colloid and Polymer Science*, 273:38–46, 1995.

[94] L. Leibler, J.M. Rubinstein, and R.H. Colby. Dynamics of reversible networks. *Macromolecules*, 24:4701–4707, 1991.

[95] M. Rubinstein and A. N. Semenov. Thermoreversible gelation in solutions of associating polymers. 2. Linear dynamics. *Macromolecules*, 31(4):1386–1397, 1998.

[96] M. Rubinstein and A. Semenov. Dynamics of entangled solutions of associating polymers. *Macromolecules*, 34:1058–1068, 2001.

[97] C. L. Lewis, K. Stewart, and M. Anthamatten. The influence of hydrogen bonding side-groups on viscoelastic behavior of linear and network polymers. *Macromolecules*, 47(2):729–740, 2014.

[98] A. Shabbir, H. Goldansaz, O. Hassager, E. van Ruymbeke, and N. J. Alvarez. Effect of hydrogen bonding on linear and nonlinear rheology of entangled polymer melts. *Macromolecules*, 48(16):5988–5996, 2015.

[99] K.E. Feldman, M.J. Kade, E.W. Meijer, C.J. Hawker, and E.J. Kramer. Model transient networks from strongly hydrogen-bonded polymers. *Macromolecules*, 42:9072–9081, 2009.

[100] C. Osterwinter, C. Schubert, C. Tonhauser, D. Wilms, H. Frey, and C. Friedrich. Rheological consequences of hydrogen bonding: Linear viscoelastic response of linear polyglycerol and its permethylated analogues as a general model for hydroxyl-functional polymers. *Macromolecules*, 48(1):119–130, 2015.

[101] X. Callies, C. Fonteneau, C. Vechambre, S. Pensec, J. M. Chenal, L. Chazeau, L. Bouteiller, G. Ducouret, and C. Creton. Linear rheology of bis-urea functionalized supramolecular poly(butylacrylate)s: Part I- weak stickers. *Polymer*, 69:233–240, 2015.

[102] R. A. Weiss and Wei-Ching Yu. Viscoelastic behavior of very lightly sulfonated polystyrene ionomers. *Macromolecules*, 40(10):3640–3643, 2007.

[103] Q. Chen, G. J. Tudryn, and R. H. Colby. Ionomer dynamics and the sticky Rouse model. *Journal of Rheology*, 57(5):1441–1462, 2013. Chen, Quan Tudryn, Gregory J. Colby, Ralph H. Chen, Quan/J-8052-2013 Chen, Quan/0000-0002-7771-5050.

[104] R. A. Weiss and Hongying Zhao. Rheological behavior of oligomeric ionomers. *Journal of Rheology*, 53(1):191–213, 2009.

[105] Q. Chen, S. Liang, H. Shiau, and R. H. Colby. Linear viscoelastic and dielectric properties of phosphonium siloxane ionomers. *ACS Macro Letters*, 2(11):970–974, 2013.

[106] G. Pezzin and G.B. Gechele. *Journal of Applied Polymer Science*, 8:2195, 1964.

[107] P. Parrini, D. Romanini, and G.P. Righi. Melt rheology of some aliphatic polyamides. *Polymer*, 17:377–381, 1976.

[108] H.M. Laun. Das viskoelastische verhalten von polyamid-6-schmelzen. *Rheologica Acta*, 18:478–491, 1979.

[109] Khanna Y.P., P.K. Han, and E.D. Day. New developments in the melt rheology of nylons. i: Effect of moisture and molecular weight. *Polymer Engineering & Science*, 36(13):1745–1754, 1996.

[110] D.J. Dijkstra. Guidelines for rheological characterization of polyamide melts (IUPAC technical report). *Pure and Applied Chemistry*, 81(2), 2009.

[111] S. Acierno and P. Van Puyvelde. Rheological behavior of polyamide 11 with varying initial moisture content. *Journal of Applied Polymer Science*, 97(2):666–670, 2005.

[112] F. Wolff and H. Münstedt. Artefacts of the storage modulus due to bubbles in polymeric fluids. *Rheologica Acta*, 52(4):287–289, 2013.

[113] D. Graebling, R. Muller, and J. F. Palierne. Linear viscoelastic behavior of some incompatible polymer blends in the melt. Interpretation of data with a model of emulsion of viscoelastic liquids. *Macromolecules*, 26(2):320–329, 1993.

[114] U. Jacobs, M. Fahrländer, J. Winterhalter, and C. Friedrich. Analysis of Palierne's emulsion model in the case of viscoelastic interfacial properties. *Journal of Rheology*, 43(6):1495–1509, 1999.

[115] R.J. Gaymans, J. Amirtharaj, and H. Kamp. Nylon 6 polymerization in the solid state. *Journal of Applied Polymer Science*, 27:2513–2526, 1982.

[116] J.G. Dolden. Structure-property relationships in amorphous polyamides. *Polymer*, 17:875–891, 1976.

[117] J. Hartikainen, O. Lehtonen, T. Harmia, M. Lindner, S. Valkama, J. Ruokolainen, and K. Friedrich. Structure and morphology of polyamide 66 and oligomeric phenolic resin blends: Molecular modeling and experimental investigations. *Chemistry of Materials*, 16:3032–3039, 2004.

[118] P. Rajagopalan, J-S. Kim, H.P. Brack, X. Lu, A. Eisenberg, R.A. Weiss, and W. Risen. Molecular interpretation of miscibility in polyamide-6 blends with alkali ionomers of sulfonated polystyrene. *Journal of Polymer Science Part B*, 33:495–503, 1995.

[119] Y. Feng, A. Schmidt, and R.A. Weiss. Compatibilization of polymer blends by complexation. 1. Spectroscopic characterization of ion-amide interactions in ionomer/polyamide blends. *Macromolecules*, 29:3909–3917, 1996.

[120] X. Lu and R. A. Weiss. Specific interactions and miscibility of blends of poly(epsilon-caprolactam) and sulfonated peek ionomer. *Journal of Polymer Science Part B*, 34:1795–1807, 1996.

[121] Y. Ghebremeskel and R. A. Weiss. Near infrared analysis of blends of sulfonated polystyrene ionomers and poly(epsilon-caprolactam). *Journal of Polymer Science Part B*, 46(15):1602–1610, 2008.

[122] A. Eilmes. A quantum-chemical study of Li+ C=O interactions in polyester-based polymer electrolytes. *Solid State Ionics*, 179(13-14):458–464, 2008.

[123] W. Souheng. Chain structure and entanglement. *Journal of Polymer Science Part B*, 27:723–741, 1989.

[124] T. Q. Nguyen. Molecular weight distribution of polyamides by GPC-viscometry. a comparison between high temperature and low temperature eluants. *Journal of Liquid Chromatography & Related Technologies*, 24(18):2727–2747, 2001.

[125] A. Xenopoulos and B. Wunderlich. Thermodynamic properties of liquid and semicrystalline linear aliphatic polyamides. *Journal of Polymer Science Part B*, 28:2271–2290, 1990.

[126] H.M. Le Huy and J. Rault. Remarks on the α and β transitions in swollen polyamides. *Polymer*, 35:136, 1994.

[127] E. Laredo and M.C. Hernández. Moisture effect on the low- and high-temperature dielectric relaxations in nylon-6. *Journal of Polymer Science Part B*, 35:2879, 1997.

[128] E. Laredo, F. Grimau, F. Sánchez, and A. A. Bello. Water absorption effect on the dynamic porroperties of nylon-6 by dielectric spectroscopy. *Macromolecules*, 36:9840, 2003.

[129] S. Havriliak and S. Negami. A complex plane representation of dielectric and mechanical relaxation processes in some polymers. *Polymer*, 8:161–210, 1967.

[130] A. Maus, C. Hertlein, and K. Saalwachter. A robust proton NMR method to investigate hard/soft ratios, crystallinity, and component mobility in polymers. *Macromolecular Chemistry and Physics*, 207:1150–1158, 2006.

[131] C.D. Hodgman. *CRC Handbook of Chemistry and Physics 44th edition*. CRC Press, Cleveland, 1962.

[132] C. M. Hansen. *Hansen solubility parameters: A user's handbook*. CRC Press, Boca Raton, FL, 2007.

[133] Anthony J. Fontana. *Appendix A: Water Activity of Saturated Salt Solutions*, pages 391–393. Blackwell Publishing Ltd, 2008.

[134] M. Williams, R. Landel, and J. Ferry. The temperature dependence of relaxation mechanisms in amorphous polymers and other glass-forming liquids. *Journal of the Americal Chemical Society*, 77:3701–3706, 1955.

[135] J. Dealy and D. Plazek. Time-temperature superposition - a users guide. *Rheology Bulletin*, 78(2):16–31, 2009.

[136] T. Cousin, J. Galy, and J. Dupuy. Molecular modelling of polyphthalamides thermal properties: Comparison between modelling and experimental results. *Polymer*, 53(15):3203–3210, 2012.

[137] J. Honerkamp and J. Weese. A nonlinear regularization method for the calculation of relaxation spectra. *Rheologica Acta*, 32(1):65–73, 1993.

[138] P. W. Morgan and S. L. Kwolek. Polymides from phenylenediamines and aliphatic diacids. *Macromolecules*, 8(2):104–111, 1975.

[139] J. L. McPeak. *Solvent-induced crystallization of poly(ether ether ketone)*. Thesis, 1999.

[140] C. J. Durning and W. B. Russel. A mathematical model for diffusion with induced crystallization: 1. *Polymer*, 26(1):119–130, 1985.

[141] C. J. Durning and W. B. Russel. A mathematical model for diffusion with induced crystallization: 2. *Polymer*, 26(1):131–140, 1985.

[142] C.-L. Sun, X.-N. Jiang, and C.-S. Wang. An analytic potential energy function evaluation for the amide–amide and amide–water intermolecular hydrogen bonds in peptides. *Journal of Computational Chemistry*, 30(15):2567–2575, 2009.

[143] M. Nagaraju and G. Narahari Sastry. Effect of alkyl substitution on h-bond strength of substituted amide-alcohol complexes. *Journal of Molecular Modeling*, 17(7):1801–16, 2011.

[144] S. Goudeau, M. Charlot, C. Vergelati, and F. Müller-Plathe. Atomistic simulation of the water influence on the local structure of PA66. *Macromolecules*, 37:8072–8081, 2004.

[145] R.L. Patrick. *Treatise on Adhesion and Adhesives Vol. 1*. Marcel Dekker, New York, 1967.

[146] H.J. Vandenburg, A.A Clifford, K.D. Bartle, R.E. Carlson, J. Carroll, and I.D. Newton. A simple solvent selection method for accelerated solvent extraction of additives from polymers. *Analyst*, 124:1707–1710, 1999.

[147] L. J. Hughes and G. E. Britt. Compatibility studies on polyacrylate and polymethacrylate systems. *Journal of Applied Polymer Science*, 5(15):337–348, 1961.

[148] E. Stefanis and C. Panayiotou. Prediction of Hansen solubility parameters with a new group-contribution method. *International Journal of Thermophysics*, 29:568–585, 2008.

[149] N. B. Hatzigrigoriou, C. D. Papaspyrides, C. Joly, and P. Dole. Effect of migrant size on diffusion in dry and hydrated polyamide 6. *Journal of Agricultural and Food Chemistry*, 58(15):8667–8673, 2010.

[150] H.W. Starkweather. Some aspects of water clusters in polymers. *Macromolecules*, 8(4):476, 1975.

[151] I. Auerbach and M.L. Carnicom. Sorption of water by nylon 6,6 and Kevlar 29. *Journal of Applied Polymer Science*, 42:2417, 1991.

[152] B. H. Zimm and J. L. Lundberg. *Journal of Physical Chemistry*, 60:425, 1956.

[153] H. Eslami and F. Müller-Plathe. Molecular dynamics simulation of water influence on local structure of nanoconfined polyamide-6,6. *The Journal of Physical Chemistry B*, 115:9720–9731, 2011.

[154] C. Kittel. *Introduction to solid state physics, 7th edition*. John Wiley & Sons, 2011.

[155] E. M. Davis, M. Minelli, Marco Giacinti B., and Y. A. Elabd. Non-fickian diffusion of water in polylactide. *Industrial & Engineering Chemistry Research*, 52(26):8664–8673, 2013.

[156] C.C. McDowell, B.D. Freeman, and G.W. McNeely. Acetone sorption and uptake kinetic in poly(ethylene terephthalate). *Polymer*, 40:3487–3499, 1999.

[157] T.G. Fox. Influence of diluent and of copolymer composition on the glass temperature of a polymer system. *Bulletin of the American Physical Society*, 1:123, 1956.

[158] H. Eslami and F. Müller-Plathe. How thick is the interphase in an ultrathin polymer film? Coarse-grained molecular dynamics simulations of polyamide-6,6 on graphene. *The Journal of Physical Chemistry C*, 117(10):5249–5257, 2013.

[159] D. Auhl, J. Ramirez, A. E. Likhtman, P. Chambon, and C. Fernyhough. Linear and nonlinear shear flow behavior of monodisperse polyisoprene melts with a large range of molecular weights. *Journal of Rheology*, 52(3):801–835, 2008.

[160] L. J. Fetters, D. J. Lohse, and R. H. Colby. *Chain Dimensions and Entanglement Spacings*, book section 25, pages 447–454. Springer New York, 2007.

[161] A. Bocahut, J.-Y. Delannoy, D.R. Long, and P. Sotta. Modeling molecular relaxation mechanisms in amorphous polymers: application to polyamides. *to be published*, 2015.

[162] J. Bartos. Free volume microstructure of amorphous polymers at glass transition temperatures from positron annihilation spectroscopy data. *Colloid and Polymer Science*, 274:14–19, 1996.

[163] C. A. Angell. Formation of glasses from liquids and biopolymers. *Science*, 267(5206):1924–1935, 1995.

[164] G. B. McKenna. Deformation and flow of matter: Interrogating the physics of materials using rheological methods. *Journal of Rheology*, 56(1):113–158, 2012.

[165] R.A. Register. *Melt Rheology*, pages 208–260. 1997.

[166] F.-M. Preda, A. Alegría, An. Bocahut, L.-A. Fillot, D. R. Long, and P. Sotta. Investigation of water diffusion mechanisms in relation to polymer relaxations in polyamides. *Macromolecules*, 48(16):5730–5741, 2015.

[167] P. Adriaensens, A. Pollaris, R. Rulkens, V. M. Litvinov, and J. Gelan. Study of the water uptake of polyamide 46 based copolymers by magnetic resonance imaging relaxometry. *Polymer*, 45:2465–2473, 2004.

[168] L. Monnerie, J.L. Halary, and H.-H. Kausch. *Deformation, Yield and Fracture of Amorphous Polymers: Relation to the Secondary Transitions*, volume 187 of *Advances in Polymer Science*, book section 136957, pages 215–372. Springer Berlin Heidelberg, 2005.

[169] J.A. Dean and N.A. Lange. *Lange's handbook of chemistry*. McGraw-Hill, 1992.

[170] L.W. Cornell and R.E. Montonna. Studies in distillation. II. Liquid-vapor equilibria in the systems ethanol-water, methanol-water and acetic acid-water. *Industrial and Engineering Chemistry*, 25(12):1331–1335, 1933.

[171] J. Beguinel. Rapport de stage Solvay, 2012.

[172] C. El-Mazry, O. Correc, and X. Colin. A new kinetic model for predicting polyamide 6-6 hydrolysis and its mechanical embrittlement. *Polymer Degradation and Stability*, 97:1049–1059, 2012.

APPENDIX

A Water infiltration in sorption experiments

In a classical sorption experiment, a polymer film is immersed in a solvent at controlled temperature, under atmospheric pressure. We consider here the case in which the sorption cell is an open system, meaning that the solvent is in contact with air humidity. Water may thus infiltrate the solvent and the polymer until a thermodynamic equilibrium is reached and small amounts of water can be measured in solvent/polyamide systems (Table A). This appendix presents some general considerations on the thermodynamics of water/solvent mixtures, experimental results on water infiltration and its impact on the glass transition temperature of polyamide/solvent systems.

A.1 Thermodynamics of water/solvent mixtures

Consider a mixture of solvents A and B with molar composition in the liquid x_A and $x_B = 1 - x_A$. The saturated vapor pressure of each component as a function of temperature is described by the curves $p_A^{sat}(T)$ and $p_B^{sat}(T)$. For water and ethanol for example, the variation of the saturated vapor pressure with temperature is illustrated in Figure A.

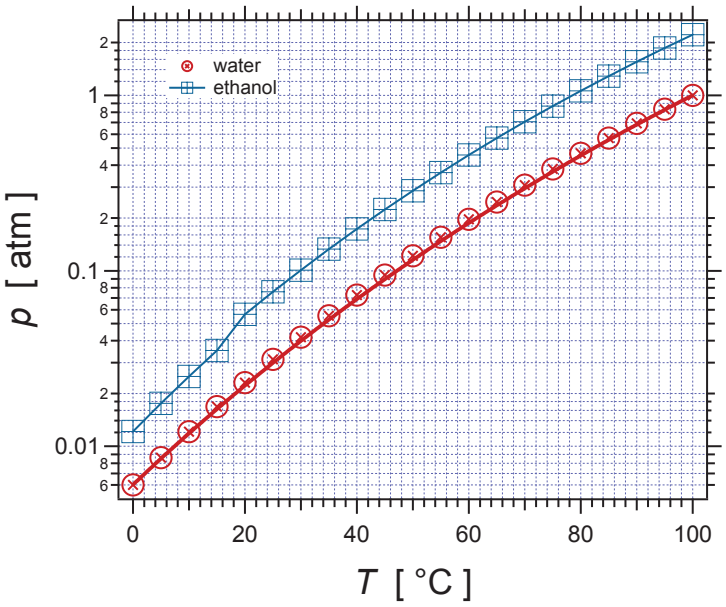

Figure A: Saturated vapor pressure of water and ethanol as a function temperature. Data points are from reference [169]. For water, line is obtained with $P_s(T) = {P_s}^0 \exp\left[-\frac{Q}{T}\right]$, where ${P_s}^0 = 1.14181 \times 10^6$ atm (1 atm = 1.012 bar), T in K and $Q = 5202.65$ K [61].

For an ideal mixture, the activity of A is equal to the molar fraction x_A (same for B). The composition of the vapor phase on top of the mixture at a temperature T can be calculated based on the partial vapor pressures of A ($x_A p_A^{sat}(T)$) and B ($x_B p_B^{sat}(T) = (1 - x_A) p_B^{sat}(T)$):

$$y_A(T) = \frac{x_A p_A^{sat}(T)}{x_A p_A^{sat}(T) + (1 - x_A) p_B^{sat}(T)} = \frac{x_A p_A^{sat}(T)}{p_B^{sat}(T) + x_A (p_A^{sat}(T) - p_B^{sat}(T))} \tag{A-1}$$

Thus, even for an ideal mixture, because of the difference between the saturated vapor

pressures $p_A^{sat}(T)$ and $p_B^{sat}(T)$, the molar composition in the vapor $y_A(T)$ is not exactly equal to the molar composition in the liquid $x_A(T)$.

In this study, we are particularly interested in water/solvents mixtures, more specifically in water/ethanol or water/toluene mixtures, which are *not ideal*.

A.1.1 Water/ethanol mixtures

For non-ideal mixtures, the activities are not equal to the molar fractions in the liquid phase and must be calculated in the vapor phase (assumed to be an ideal gas). To begin with, Figure B illustrates the phase diagram of water/ethanol mixtures at 40°C. The total vapor pressure P_{tot} on top of mixture (the sum of water and ethanol vapor pressures) is given as a function of the water molar content. For a given pressure, the molar fractions of water in the liquid (X_{water}) and vapor phase (Y_{water}) are given by the blue and red curve respectively. The inital point of the curves at molar fraction zero (P = 17.92 kPa) is the saturated vapor pressure for pure ethanol at 40°C and the final point at molar fraction one (P = 7.49 kPa) is the saturated vapor pressure for pure water at 40°C (see Figure A).

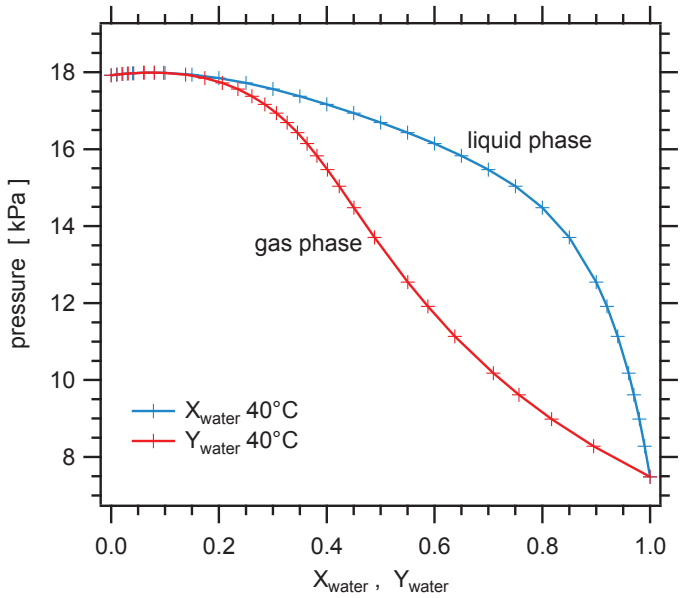

Figure B: Phase diagram of water-ethanol mixture at 40°C (X = molar fraction in the liquid, Y = molar fraction in the vapor). Data from [170]

The partial vapor pressure of water is then $P_W = Y_W P_{tot}$ and for ethanol it is $P_E = Y_E P_{tot} = (1 - Y_W)P_{tot}$. The solvent activities are then $a_W = P_W/p_W^{sat}(T)$ for water and $a_E = P_E/p_E^{sat}(T)$ for ethanol. Both activities are plotted as a function of the molar content of water in the liquid mixture in Figure C, together with the total activity $a_{tot} = a_W + a_E$. The sum of the activities is larger than one, suggesting that there might be a synergistic effect of purely thermodynamic origin, *i.e.* the global uptake in polyamide/solvent mixture may then increase compared to the pure solvents.

Suppose that initially dry ethanol is kept under humid atmosphere, for instance at RH50, *i.e.* $a_W = 0.5$, at 40°C. Then the liquid mixture will uptake water up to equilibrium at the same water activity in the liquid phase, as illustrated in Figure D. In this particular case for RH50, molar fraction of water will be $X_W \approx 0.27$ in the liquid mixture, which corresponds to a weight fraction of 0.13 and a volume fraction of 0.1. The ethanol activity in the mixture is 0.78 (Figure D).

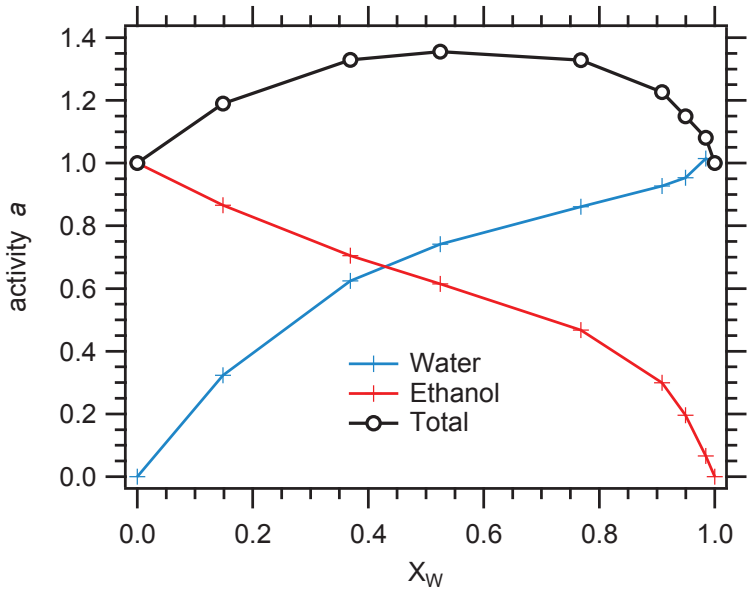

Figure C: Activities of water (blue) and ethanol (red) as a function of the molar fraction of water in the liquid mixture, at 40°C, together with their sum (black line and markers).

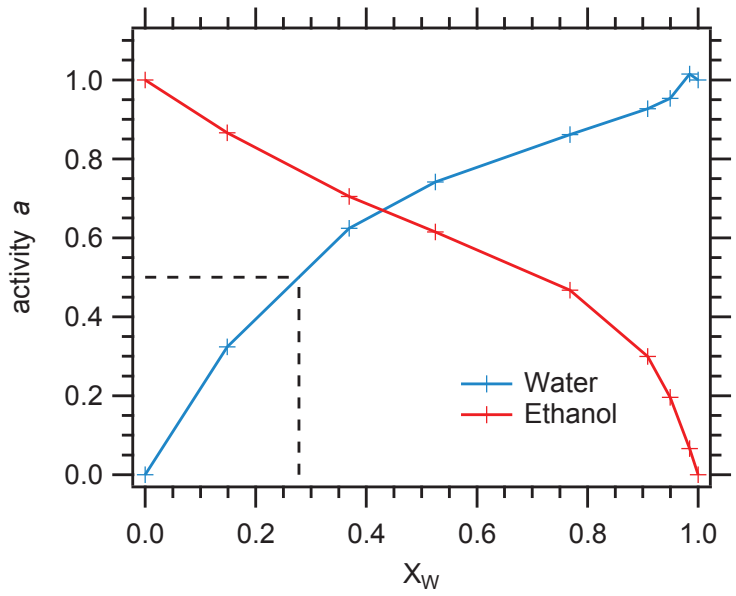

Figure D: The activities of water and ethanol as a function of the molar fraction of water in the liquid mixture, at 40°C. At RH50 (water activity $a_W = 0.5$) the liquid molar fraction is $X_W \approx 0.27$, as indicated by dashed lines.

In order to estimate the global intake (assuming that sorption of one solvent does not impact the other one), we need to know the sorption isotherms for each pure solvent. The sorption isotherms for water and ethanol at 40°C in PA6,6 were measured during this PhD (Chapter 4) and are shown in Figure E.

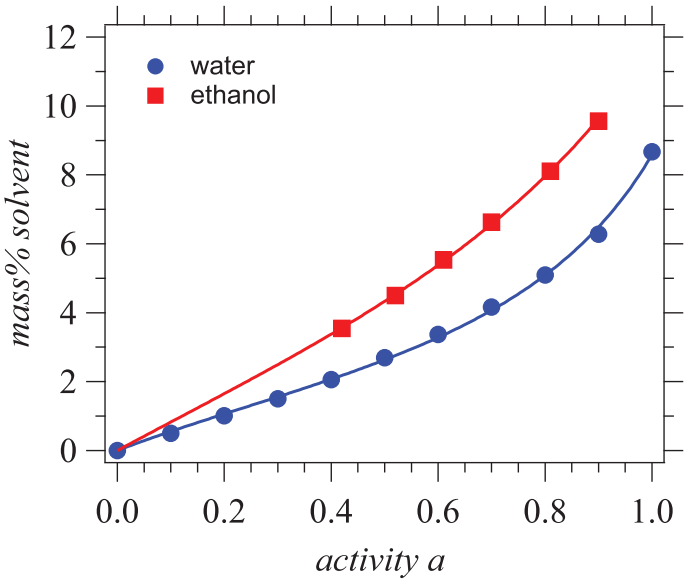

Figure E: Sorption isotherms for water and ethanol at 40°C in PA6,6.

From Figure E, the mass intake of water is 2.6% at activity 0.5 and the mass intake of ethanol is 7.8% at activity 0.78, which would account for a total mass intake of 10.4% in ethanol/water mixture at equilibrium at 40°C. The experimental mass intake is 11-12%, slightly higher than the calculated one. A synergistic effect was observed in the shift of the glass transition temperature of polyamide in presence of ethanol/water mixtures [171] (Figure F(a)).

A semi-quatitative value of the water intake in polyamide/solvent films can be obtained by Karl Fischer titration. This method was validated in an internship [171] on the sorption of ethanol/water mixtures in polyamide. It was shown that the water concentrations determined by Karl Fischer titration were in good agreement with the concentrations obtained by gas chromatography after solvent desorption (internal Solvay setup). The obtained quantities of water are reported in Table A. It can be seen that in the case of ethanol in PA6,6, between 1 and 2% water was found in the films, out of the total 11-12% ethanol/water absorbed. Although this measurement was done on films at 25°C, this value is close to the estimated 2.6% intake at 40°C.

A.1.2 Water/toluene mixtures

The case of water/toluene mixtures is particular, since toluene is a non-polar solvent that does not mix with water. However, a weight fraction of 0.05 water is found at equilibrium in this solvent under RH = 100 [169] (Figure G). At RH50, the weight fraction of water in toluene can be estimated to be 0.025 (see Figure G). Although the amount of water is extremely small, its activity is equal to the external activity (0.5) at equilibrium, which will drive its sorption in the polymer. Since the sorption isotherms of toluene are not available, the total amount of solvent cannot be estimated. Based on the sorption isotherms of water however, 2.6% and 1.5% water are absorbed at a=0.5 in PA6,6 and PA6,10 respectively.

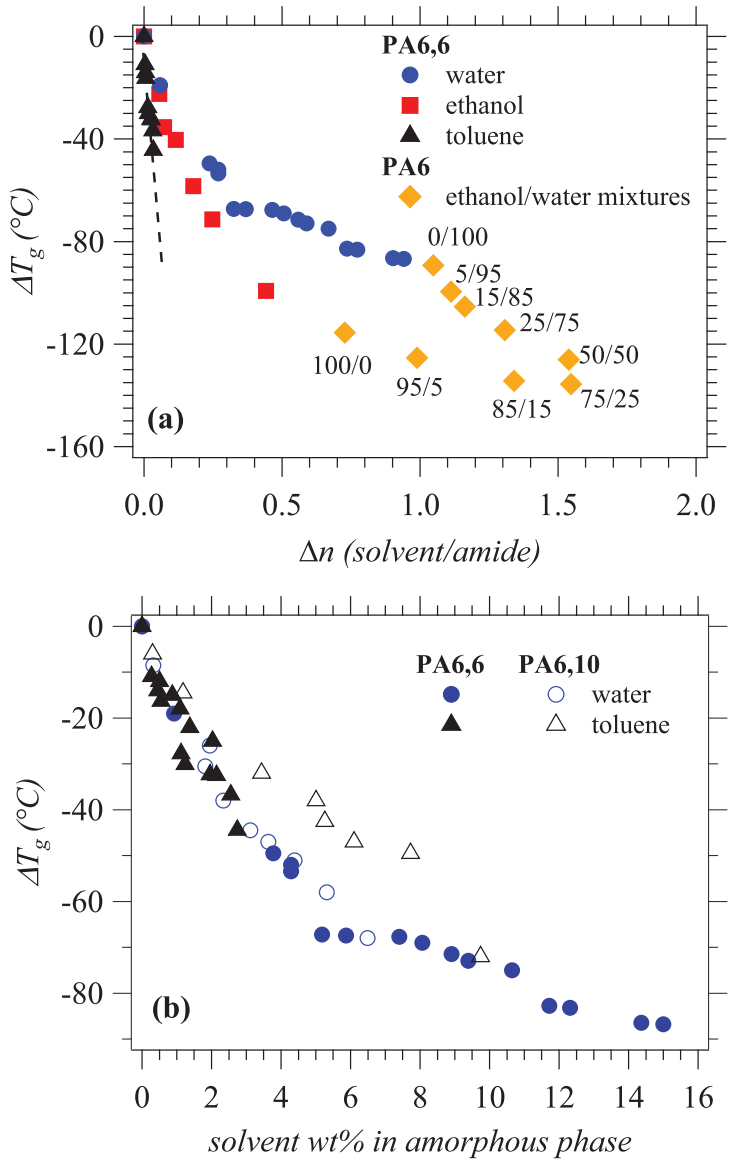

Figure F: (a) Shift in the glass transition temperature of PA6,6 in presence of water, ethanol, toluene and ethanol/water mixtures (volume fractions in the liquid are indicated on the figure next to the symbols), as a function of the molar intake Δn (solvent molecule/amide group). (b) Shift in the glass transition temperature of PA6,6 and PA6,10 in presence of water, ethanol and toluene as a function of the solvent mass intake in the amorphous phase. For water, ethanol and toluene in PA6,6, data from reference [27]. For water and ethanol at low Δn in PA6,6 and all solvents in PA6,10, data measured during this PhD. For ethanol/water mixtures in PA6, data from [171]. Since PA6,6 and PA6 have the same repeating unit, the effect of solvents on T_g should be close.

Polymer	Solvent	T (°C)	Total mass intake (%)	water % (Karl Fischer)	Solvent %
A1007	Ethanol*	25	12	1.1	10.9
	Ethanol*	25	10	1.0	9.0
	Ethanol*	40	12.7	1.0	11.7
	Ethanol*	40	11.4	1.1	10.3
	Ethanol*	40	11.4	1.2	10.2
PA6I	Ethanol*	25	20	1.5	18.5
	Ethanol*	25	19.5	1.1	18.4
	Ethanol*	40	19.3	1.0	18.3
	Ethanol*	40	18.5	0.9	17.6
	Methanol*	23-24	17	1.6	15.4
Selar	Ethanol*	25	21	2.1	18.9
	Ethanol*	40	21	1.3	19.7
PA6,10	Toluene	25	1.6	0.3	1.3
	Toluene*	25	2.7	0.4	2.4
	Toluene*	25	6.2	1.7	4.6
	Toluene*	40	3.4	0.2	3.3
	Ethanol*	25	11.7	0.3	11.4
	Ethanol*	25	10.7	0.3	10.4
	Ethanol	25	7.1	0.4	6.7
PA6,6	Toluene	25	1.7	2.1	0
	Toluene	25	0.3	0.5	0
	Toluene	25	0.4	0.5	0
	Toluene	25	0.4	0.5	0
	Toluene	40	0.5	0.3	0
	Ethanol	25	12.1	2.0	10.1
	Ethanol	25	11.3	1.0	10.3
	Ethanol	25	11.1	0.7	10.4

* Solvent with desiccant (3Å molecular sieves)

Table A: Total solvent mass intake at equilibrium for different polyamides and the estimated amount of water by Karl Fischer dosage

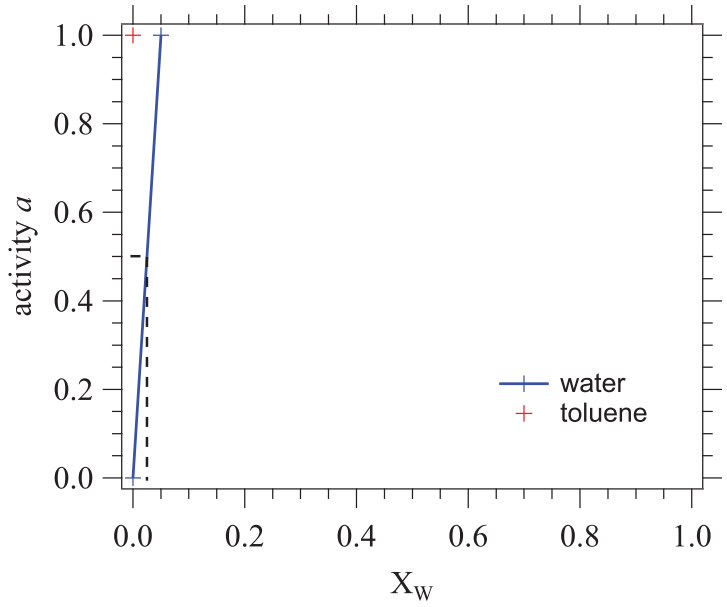

Figure G: Activities of water (blue) and toluene (red) as a function of the molar fraction of water in the liquid mixture, at 25°C

The sorption of toluene in PA6,6 was studied during the PhD of A. Rios [27]. It was observed that toluene penetrated in small quantities in PA6,6 but apparently had a very important effect on the glass transition temperature of the polyamide films (Figure F(a)). This behavior could not be accurately accounted for at the time, so more measurements were done during the current work. The sorption curves of toluene in PA6,6 or PA6,10 films (same materials as for the sorption isotherms in Chapter 4) were recorded at different temperatures (25, 40, 55°C) by immersion in a non-hermetic sorption cell containing initially anhydrous toluene. The obtained curves are shown in Figure H.

At the first equilibrium plateau, small quantities of 1-3% solvent are absorbed in the amorphous phase. However, a second step of sorption equilibrium appears in all cases at long immersion times (several months). The solvent mass intake reaches high values up to 8%. Moreover, it was observed that the sorption kinetics curves varied significantly from one polymer film to another in a series of repeated experiments or if the measurements were done in winter or summer (variability in air humidity). In addition, the first part of the curves up to the first equilibrium corresponds roughly with the sorption curves of water at activity 0.5 measured for these systems.

Karl Fischer (KF) measurements provided estimations of the water content for these systems, as it can be seen in Table A. An accurate estimation of the toluene concentration might be obtained however by desorption and gas chromatography [27] (to be eventually done in future work).

In PA6,6 with toluene, the KF dosage of water corresponds roughly to the total amount of solvent in the polymer up to 2%. Therefore, it would seem that only water enters the polymer. This hypothesis is confirmed by the curve in Figure F(b), in which the T_g shift corresponding to a supposed mass intake of toluene superimposes perfectly on the T_g shift for the mass intake of water at 25°C. Therefore, the important effect seen on T_g in Figure F(a) would be only an artefact from the calculation, which takes into account the molar mass of toluene (92 g/mol » 18 g/mol for water).

In PA6,10 with toluene, increasing amounts of water are found in the polymer as the total

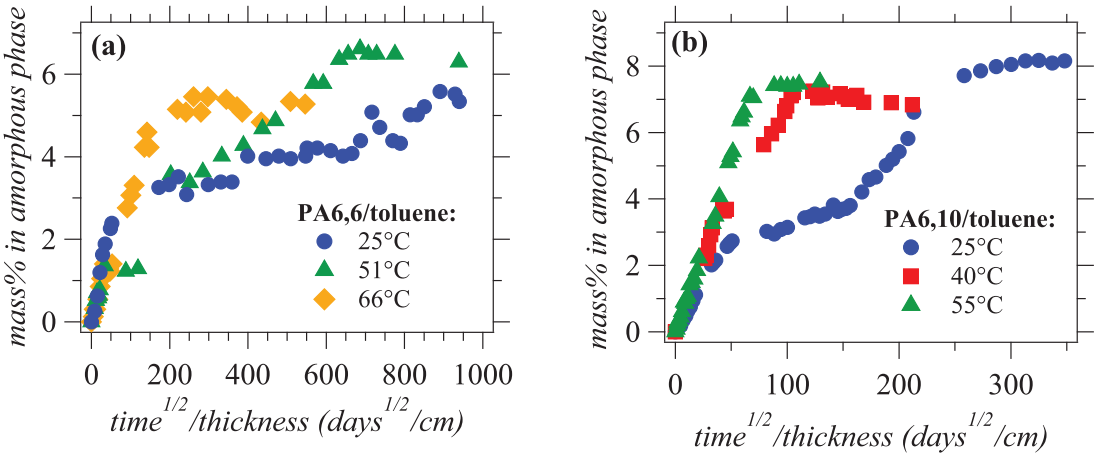

Figure H: Sorption kinetics curves of toluene in (a) PA6,6 and (b) PA6,10

solvent intake increases (Table A, toluene 25°C in PA6,10). It would seem that water and toluene penetrate simultaneously in PA6,10. The T_g shift in Figure F(b) confirms this hypothesis: the curve of toluene does not superimpose to that of water. Once again, there might be a synergistic effect of the mixture. It should be highlighted that the sorption mechanism is different in PA6,6 and PA6,10. Indeed, in PA6,6, water penetrated first, followed by toluene, whereas in PA6,10 both solvent penetrate simultanously. The different polarity of the polymers could be at the origin of this behavior.

A.2 Conclusion

In this appendix, we have presented thermodynamic calculations to prove water infiltration in polyamide/solvent systems. Ethanol and water can be mixed in all proportions and their phase diagram allows us to calculate the amount of water at equilibrium with ethanol at 40°C in a sorption cell in contact with ambient atmosphere. The sorption isotherms of water provide then the mass% of water in the polyamide film. This quantity is in agreement with Karl Fischer measurements. A synergistic effect is evidenced in these systems from simple thermodynamics, *i.e.* the amount of absorbed solvents from the mixture is higher than the absorbed amount of individual solvents. The same synergistic effect was evidenced on the glass transition shift in presence of water/ethanol mixtures.

Toluene and water are not miscible in all proportions because of their difference in polarity. Under atmospheric conditions, toluene will absorb 0.05% water [169]. The sorption kinetics curves for toluene (+water) show a peculiar behavior and the effect on T_g is very important for small amounts of (hypothetically) absorbed toluene. This effect could be mainly attributed to the water infiltration. A different sorption behavior was highlighted in PA6,6 and PA6,10.

In addition, there might exist "dynamic" synergistic effects related to the influence of one solvent on the dynamics of the polymer (or H-bonds network...), which would in turn influence the sorption of the other solvent (or conversely). However, the quantification of this effect requires first to take into account the non-ideal nature of solvent mixtures.

In conclusion, it is very important to: 1. study solvent sorption (other than water) in closed systems like the Dynamic Vapor Sorption device and 2. take into account the phase diagram in non-ideal mixtures.

B DSC scans of PA6I and Selar after immersion in solvents and drying

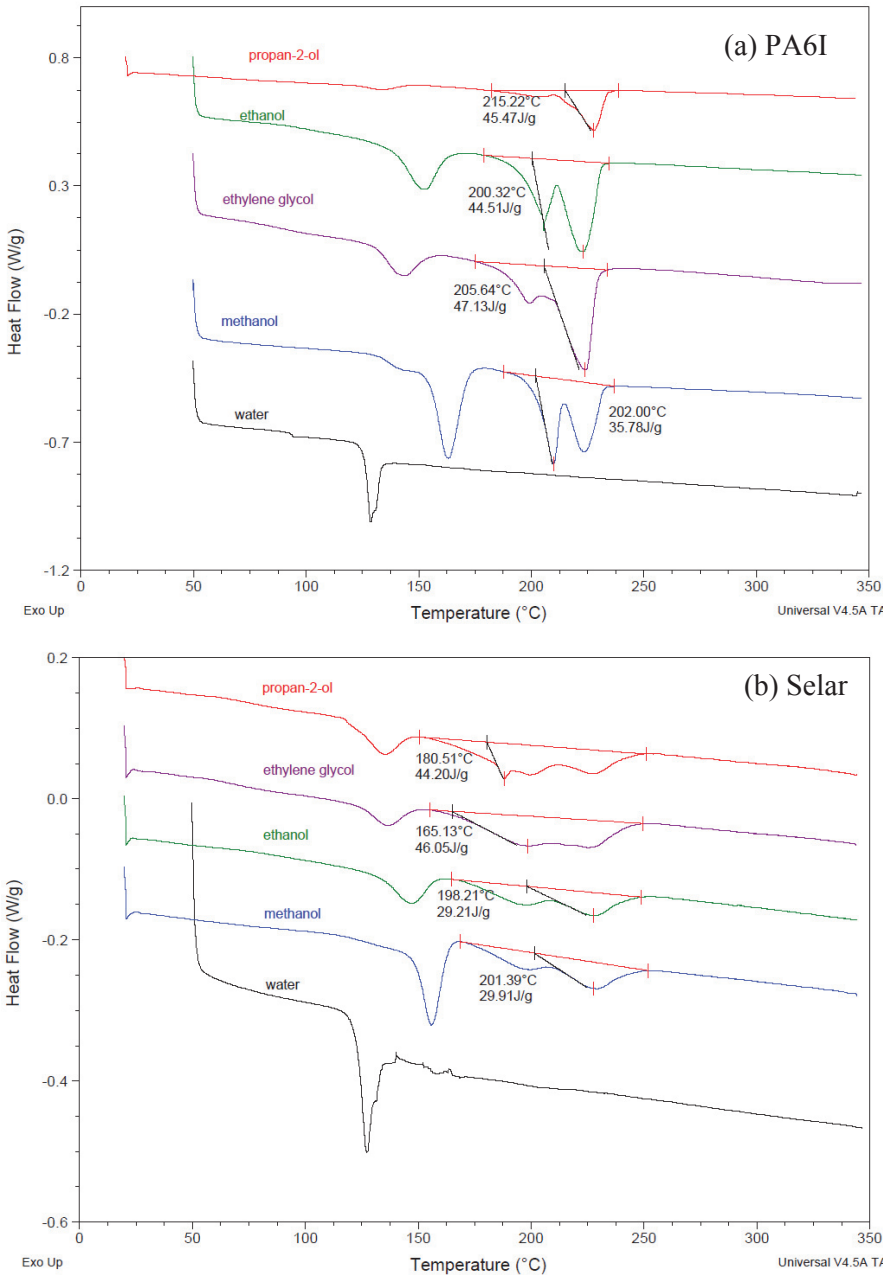

Figure I: DSC scans of (a) PA6I and (b) Selar after immersion in solvents and drying. The melting peaks were integrated and the values are reported on the figure.

C Changes at long timescales

Once the sorption equilibrium was attained, polyamide films were left immersed in the solvents for long periods in order to check for additional changes in structure. For some polyamides, a second sorption plateau or a gradual decrease in the solvent mass intake was observed and investigated for possible crystalline evolutions. It is important to note that for solvents other than water, small quantities of water were measured by Karl-Fischer dosage at long timescales (see Appendix A). Even though special precautions were taken to avoid water infiltration during the sorption experiment (use of absolute or anhydrous solvents, isolation with parafilm, use of dessicant), some samples contained between 0.3 and 2% of water. Therefore, the observed changes correspond to the action of the solvent plus infiltrated water.

C.1 PA6,6

PA6,6 films immersed in water and ethanol at 25°C did not show any evolution in the mass uptake up to one year of immersion. The WAXS scans were recorded for dry samples, immediately after equilibrium was attained and after one year immersion. The scans are shown in Figure J.

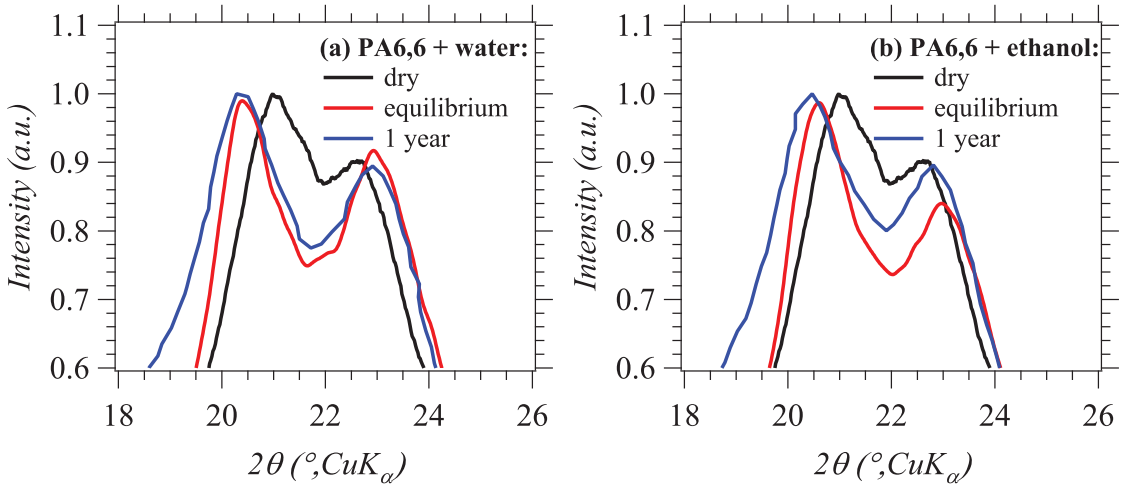

Figure J: Zoom on main WAXS peaks of PA6,6 dry, with solvents at equilibrium and after a one year immersion: (a) water and (b) ethanol

There is no significant evolution in the spectra between the moment the plateau is reached and up to one year. Therefore,it can be implied that the structural changes occur fast, as soon as the solvent penetrates the material. Once at equilibrium, no further changes are observed. As stated in Chapter 4, sorption kinetics curves for PA6,6 immersed in water, then dried and re-immersed superimposed. This suggests that crystalline changes do not affect sorption. Indeed, computer simulations of PA6,6 in presence of water suggested that crystalline changes are local, caused by the slight rotation of the polymer chains in the crystalline phase [18].

The integrity of PA6,6 after immersion in water was also checked by GPC. At equilibrium, no changes were observed in the molecular weight or molecular weight distribution (MWD) of PA6,6. However, after a long immersion time of one year, the GPC spectra are significantly different (Figure K). It can be observed in Figure K(a) that the molecular weight distribution is shifted towards small M_w. If we integrate the area under the MWD at different M_w, the plots in Figure K(b) and (c) are obtained. They confirm the shift towards smaller M_w, which

would indicate that the chains were hydrolysed in water at 25°C. Also, the zoom in Figure K(c) shows that the small masses are no longer present, meaning that monomers and oligomers were desorbed from the film. Therefore, two phenomena seem to occur: small M_w desorption and hydrolysis. In particular, hydrolysis at this low temperature (25°C) is very surprising.

An interesting phenomenon was also observed on PA6,6 films immersed in water at 66°C. The initial sorption equilibrium was attained fast, in only ten minutes. But as the film was left in water for a longer time, a few changes were observed in the initially transparent polymer film. White regions became apparent until the whole films turned opaque (L). At this final completely white step, the film disintegrated upon drying with a flow of compressed air.

When the film broke, the absorbed amount of water was already divided by two. This decrease in water uptake can be seen in Figure L. A DSC scan of the water immersed samples showed that the fusion and cold crystallization peaks had moved to lower temperatures (Figure M(a)). The crystalline fraction increased from 38 to 45%. WAXS spectra showed better resolved crystalline peaks, with a higher $\Delta 2\theta$ distance of 3.47, which is close to the value of 3.55 tabulated for the stable crystalline lattice α_I (Figure M(b)). Therefore, the crystalline fraction increased and the crystalline phases are more stable. In addition, SAXS spectra (Figure N(a)) show a shift towards smaller values of lamellar spacing (5.86 instead of 7.85 nm for the reference), which is an indication of a closer packing.

An increase in the crystalline fraction explains the subsequent opacity of the film and the decrease in the water uptake. If the crystalline ratio increases by 7%, this percentage of the amorphous phase would become unavailable for the solvent, leading to a decrease of 10% in the solvent mass intake. However, in Figure L it can be seen that there is a 40% mass loss between the end of the first plateau and the equilibrium. The experimental amount of expulsed solvent is therefore superior to the expected amount due to the increase in crystallinity. Other phenomena might take place.

The only hypothesis for this increase of crystallinity is that polyamide is hydrolyzed at 66°C. This hypothesis is supported by previous work done by El-Mazry *et al.* [172], who showed that PA6,6 hydrolysis and mechanical embrittlement started at 60°C. GPC measurements (Figure N(b)) confirm the hydrolysis of PA6,6; the average molecular weight decreased from 25000 g/mol to 5000 g/mol.

In conclusion, at long times scales and low temperatures (25-55°C) no additional structural changes occur compared to the initial equilibrium in water and ethanol. However, water immersion for 1 year at 25°C results in a change in the molecular structure. More specifically, the molecular weight distribution shifts to smaller molecular weights and monomers/oligomers are desorbed. Also, water sorption at high temperatures (above 60°C) for long periods results in the hydrolysis of PA6,6 chains.

C.2 PA6,10

PA6,10 films were also immersed for long periods of time in water and ethanol. In the case of ethanol, the mass intake at equilibrium remained constant up to 18 months of measurement. WAXS spectra were recorded regularly during all this period (Figure O). Immediately after equilibrium, it was discussed in Chapter 4 that the peaks are better resolved and the distance $\Delta 2\theta$ between the main crystalline peaks increases. There is a much more pronounced difference between $\Delta 2\theta$ at equilibrium (2.7°) and at 12 or 18 months of immersion (3.36 and 3.19° respectively), indicating a continuous evolution of the crystalline phase. The SAXS spectra (Figure O) give a small variation between the long period of the reference (7.8 nm) and the one year immersed sample (7.5 nm).

In the case of water at 25°C, the first sorption plateau is followed by a gradual increase of the mass uptake until 4 months (Figure P). After this second stage is attained, the mass of the

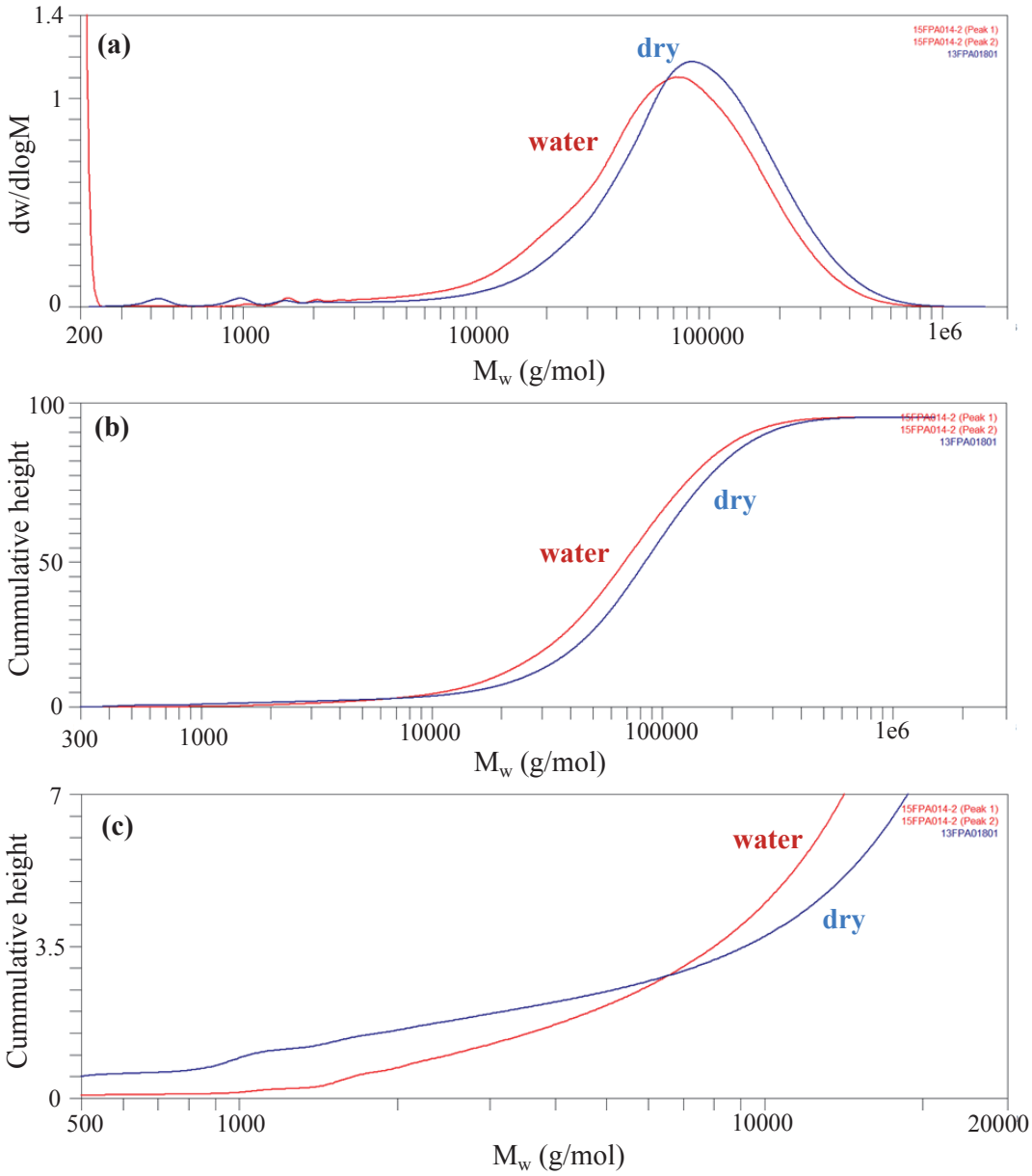

Figure K: PA6,6 films dry (blue) and after 1 year immersion in water (red): (a) GPC molecular weight distribution, (b) Cummulative height of the GPC molecular weight distribution as a function of molecular weight and (c) Zoom on cummulative height as a function of molecular weight for small M_w molecules

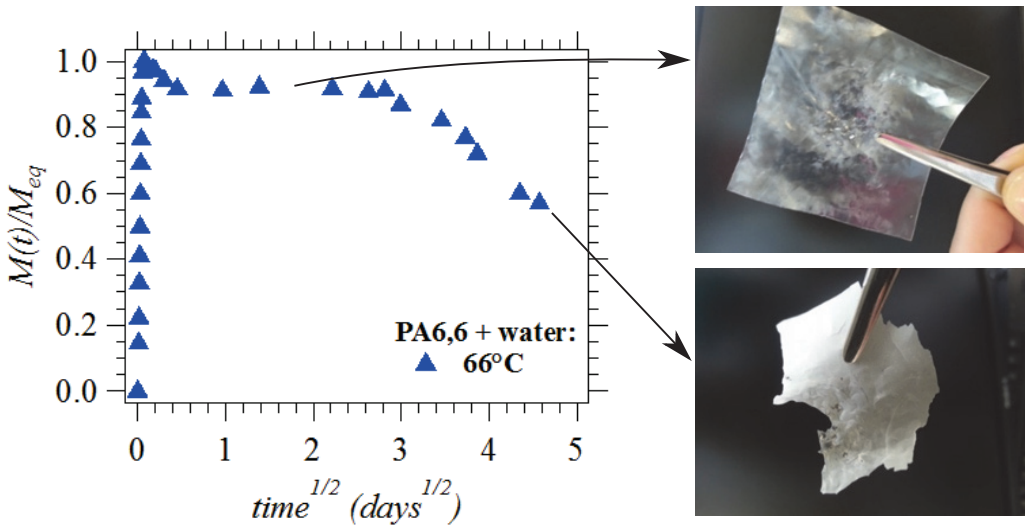

Figure L: Sorption kinetics curve of water in PA6,6 at 66°C and images of changes in the film appearence

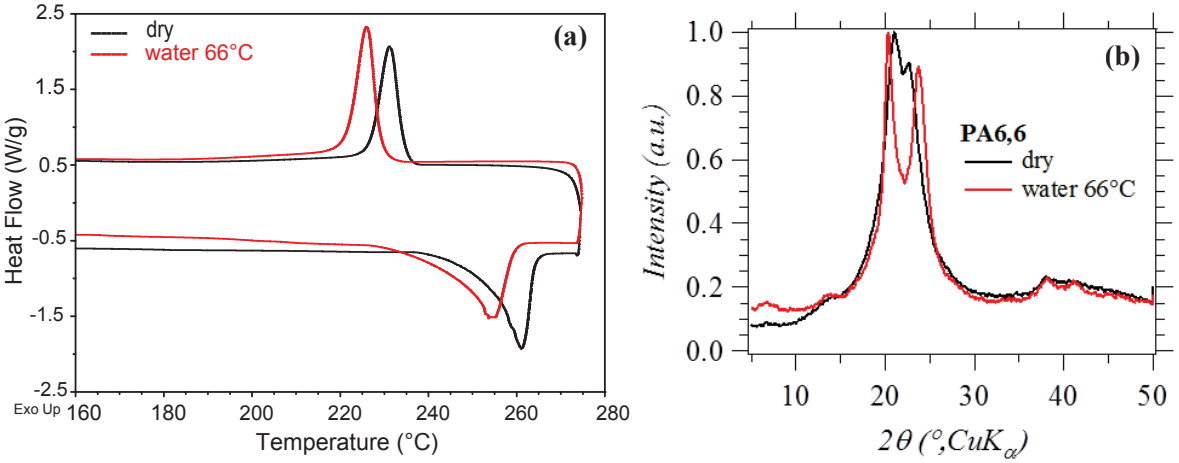

Figure M: (a) DSC and (b) WAXS scans of PA6,6 dry and after water sorption at 66°C

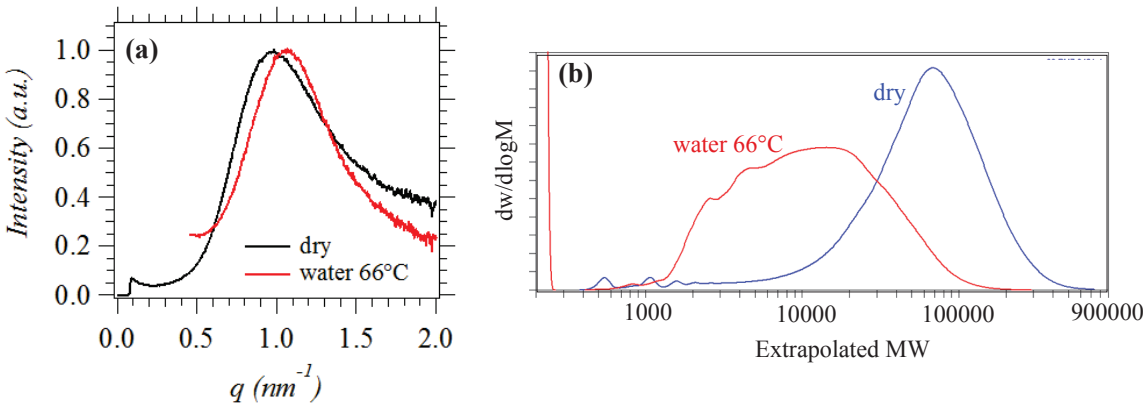

Figure N: (a) SAXS scans and (b) GPC curves of PA6,6 dry and after water sorption at 66°C

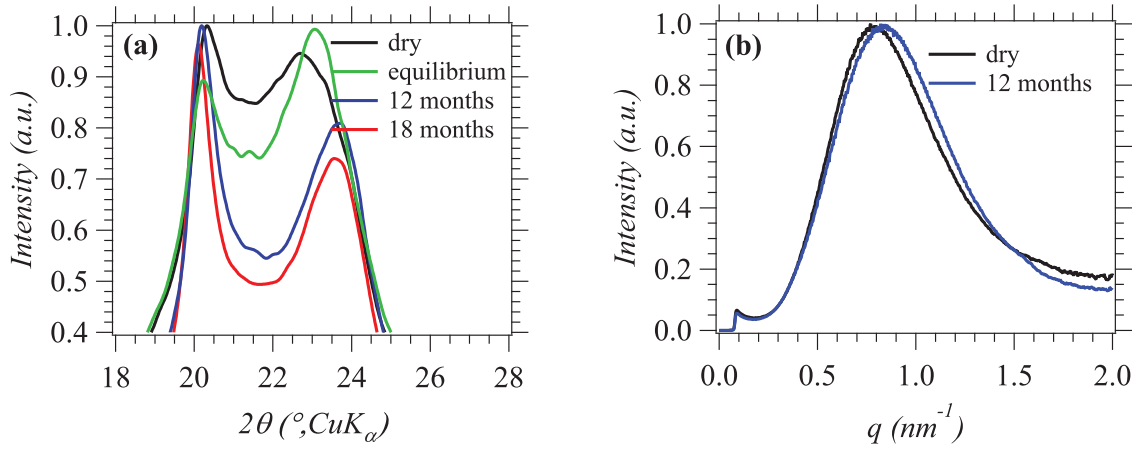

Figure O: (a) WAXS and (b) SAXS scans of PA6,10 dry and after immersion in ethanol at 25°C for long periods

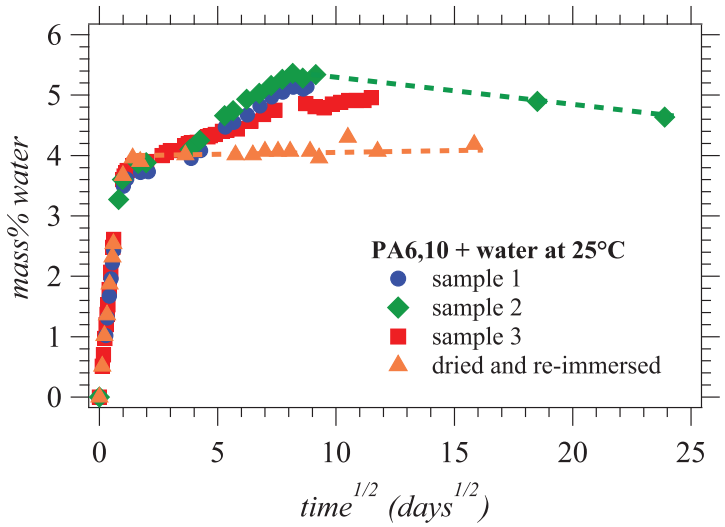

Figure P: Water sorption in several PA6,10 films at 25°C after a long immersion time

sample slowly decreases up to 18 months of immersion. It should be noticed in Figure P that the evolution of the water intake is sample-dependent in the second stage sorption.

PA6,10 films that were immersed in water were dried after reaching the first plateau (1 day), the second plateau (4 months) and after a long period immersion (18 months). 6 days under vacuum at 50°C were needed to remove all water. The sorption kinetics of the dried films were recorded and added at Figure P. All three dried films have similar kinetics, superimposing with the initial measurements up to the first plateau. On the other hand, the second plateau is not present in any of these samples. The mass intake remained constant up to 9 months of measurement. Therefore, it would seem that the second plateau can be removed by drying the sample.

As mentioned before, this type of two-stage sorption has been observed in other polymers in the literature [39, 38, 155] and for PA6,6/ethanol systems in this study. The Berens-Hopfenberg model [39] (equation (5.2)), combining Fickian diffusion and a relaxation process, was used once again to fit the experimental data. The second plateau appears in PA6,10 after a first stable

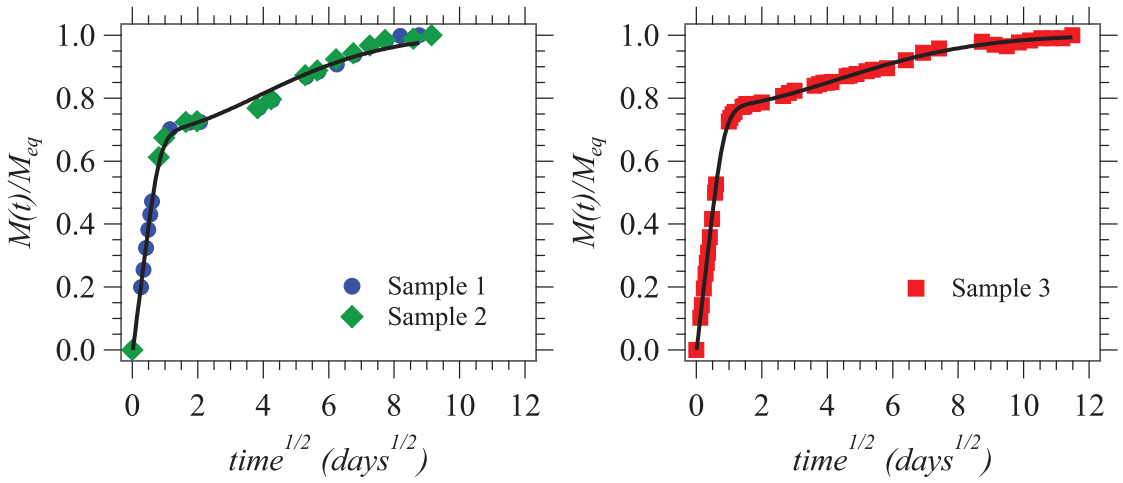

Figure Q: Water sorption in several PA6,10 films at 25°C after a long immersion time and their corresponding fits (solid lines) with the Berens-Hopfenberg model in equation (5.2)

	D (cm^2/s)	α_R	τ_R (days)	τ_D (days)
Sample 1 and 2	$3.4\ 10^{-9}$	0.3	30	1.3
Sample 3	$3.3\ 10^{-9}$	0.22	37	1.1

Table B: Parameters obtained from fitting experimental data with a Berens-Hopfenberg model in Figure Q

period of a few days. Therefore, equation (5.2) with a delay time was found more adapted to fit the experimental data. The resulting fits are illustrated in Figure Q and the corresponding fit parameters are listed in Table B.

Some variability is observed on the values of D, α_R, τ_R and t_D in Table B but the same range is obtained for all parameters in the three samples. The value of the delay time t_D (1.1-1.3 days) suggests that the relaxation process starts after the inital equilibrium is attained at 1 day. The characteristic time for relaxation τ_R is of the order of 30 days, indicating a long process. During this time, 20 to 30% mass increase is observed in the material. The fact that the parameters are sample dependent might come from the residual stresses in the sample. 5×5 cm films were cut from 10×10 cm plates, meaning that each film was positioned differently from the injection point on the side of the plate.

WAXS and SAXS scans were recorded at different immersion times in the attempt to understand the origins of the relaxation process. WAXS scans (Figure R(a)) of the water-equilibrated PA6,10 samples are similar from the end of the first plateau until the end of the second plateau ($\Delta 2\theta \simeq 2.5°$). In addition, the SAXS scans of the dry sample (lamellar spacing 7.5 nm) and at the second plateau (lamellar spacing 7.8 nm) are similar as well (Figure R(b)). Therefore, there is no change in the crystalline structure, nor lamellar spacing during the second plateau. This would suggest that there is little or no swelling during this period.

After the end of the second plateau, the weight of the PA6,10 film decreases in Figure P (sample 3). WAXS scans at 12 and 18 months are not significantly different from the ones at the first or second plateau. $\Delta 2\theta$ increases slightly from 2.5° at the second plateau to 2.8° at 18 months. The main crystalline peaks are somewhat better resolved at 18 months. On the other hand, SAXS measurements (Figure R(b)) are much different at 12 months of immersion. The lamellar spacing increases from 7.5 nm in the dry polymer to 9.2 nm at 12 months. During all

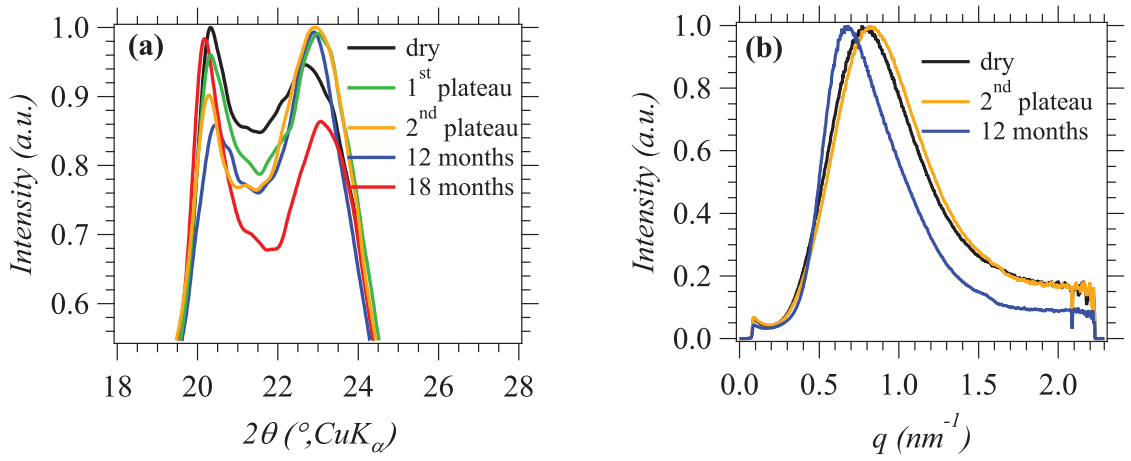

Figure R: (a) WAXS and (b) SAXS scans of PA6,10/water at different immersion times

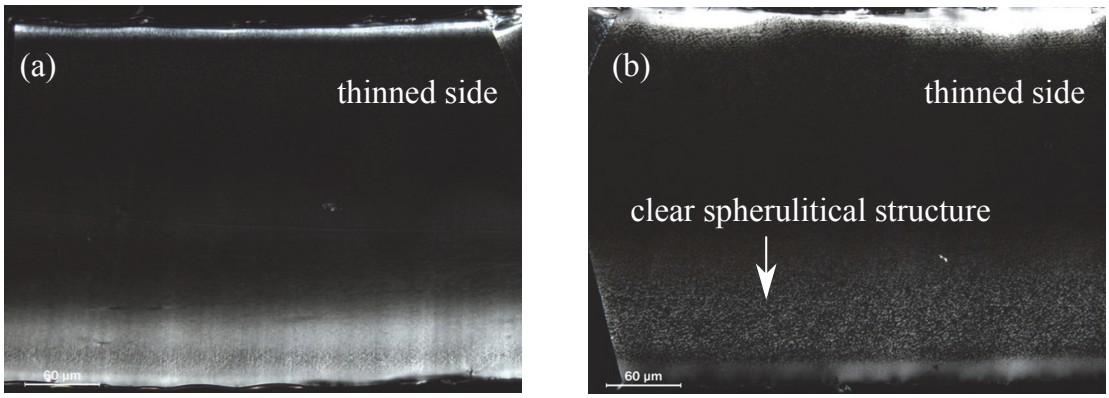

Figure S: Optical microscopy observation of PA6,10 films under polarized light (a) reference and (b) after 2 years of immersion in water. Magnification = 20 × 1.6

the immersion time, DSC measurements did not show any change in the crystalline ratio, in the limits of the uncertainty. However, the films show a more clear spherulitical structure in PA6,10 with time (Figure S).

In order to investigate if the loss of mass resulted from the desorption of oligomers, the GPC spectra of the dry and water immersed (2 years) PA6,10 films were recorded (Figure T). Although small differences are observed, there is no significant desorption of the lower mass components. Therefore, we do not have an explanation up to date for the mass decrease at long times.

The Berens-Hopfenberg model was previously applied for the diffusion of gas or solvents in glassy polymers. The slow mass uptake that follows diffusion is caused by the viscoelastic relaxation of the polymer chains to accommodate the penetrant. Or, PA6,10 has a glass transition temperature of -5°C at the first plateau and -15°C at the second plateau, which is much lower than the experimental temperature (25°C). At 30-40 degrees above T_g, polymer chains should relax sufficiently fast to accomodate the solvent. The viscoelastic relaxation time of this polymer could be obtained by studying its linear viscoelasticity. However, no rheological measurements can be done on these semi-crystalline polymers for several reasons (see Chapter 6), especially in presence of water.

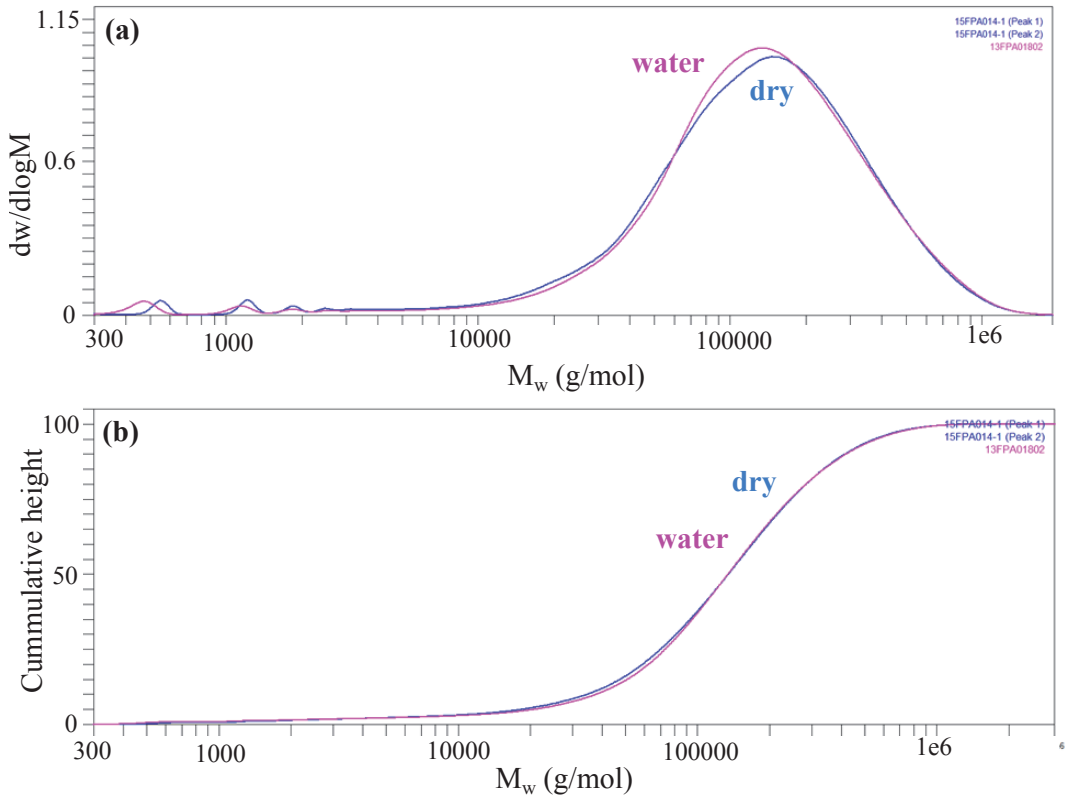

Figure T: PA6,10 films dry (blue) and after 2 years of immersion in water (pink): (a) GPC molecular weight distribution, (b) Cummulative height of the GPC molecular weight distribution as a function of molecular weight

C.3 Conclusion

In this appendix, changes at long timescales in presence of solvents were discussed. After the initial sorption equilibrium is attained, the weight of the polymer films was either kept constant, increased or decreased, indicating that the system was not yet at thermodynamic equilibrium.

The structural changes observed up to the first equilibrium generally remain constant over time: it was the case of PA6,6 with water or ethanol and PA6,10 with water. However, a continuous evolution towards a more stable crystalline phase is observed for PA6,10 immersed in ethanol up to 18 months.

At high temperatures (66°C), PA6,6 was found to hydrolyse. This phenomenon has already been observed in the past at temperatures between 60 and 90°C and led to the mechanical embrittlement of the samples [172]. More surprisingly, the molecular weight distribution of PA6,6 changed significantly after one year of immersion in water at 25°C, indicating hydrolysis and desorption of small mass components.

A two step sorption was observed for PA6,10 at long immersion times. WAXS and SAXS scans of the polymer are similar between the first and the second plateau and the crystalline ratio does not change, making it difficult to explain this phenomenon. A Berens-Hopfenberg model was used to fit the curves and a slow relaxation process with a characteristic time of 30 days was evidenced. After this second plateau, another interesting phenomenon occurs: the mass of the polymer film decreases, the lamellar spacing increases and the spherulitical structure becomes more pronounced. However, there is no change in the crystalline ratio in the limit of DSC uncertainty, nor desorption of small M_w components. No explanation was found up to date for the behavior of PA6,10/water system at long immersion times.

Observations at long timescales are particularly important for predicting the ageing of a material. Since hydrolysis or an increased amount of water might lead to changes in mechanical properties [1, 172], special attention must be paid to the end-user conditions of these materials, to avoid loss of performance over time for a certain application.

D Creep measurements for semi-aromatic polyamides

The conversion of the creep compliance data did not always provide satisfactory results. Since the data do not bring significant additional elements for the discussion in Chapter 6, it was included as an appendix. The obtained superposition between dynamic and creep converted data is remarkable in most cases. Oscillations on G′ are likely to be artefacts from the conversion method.

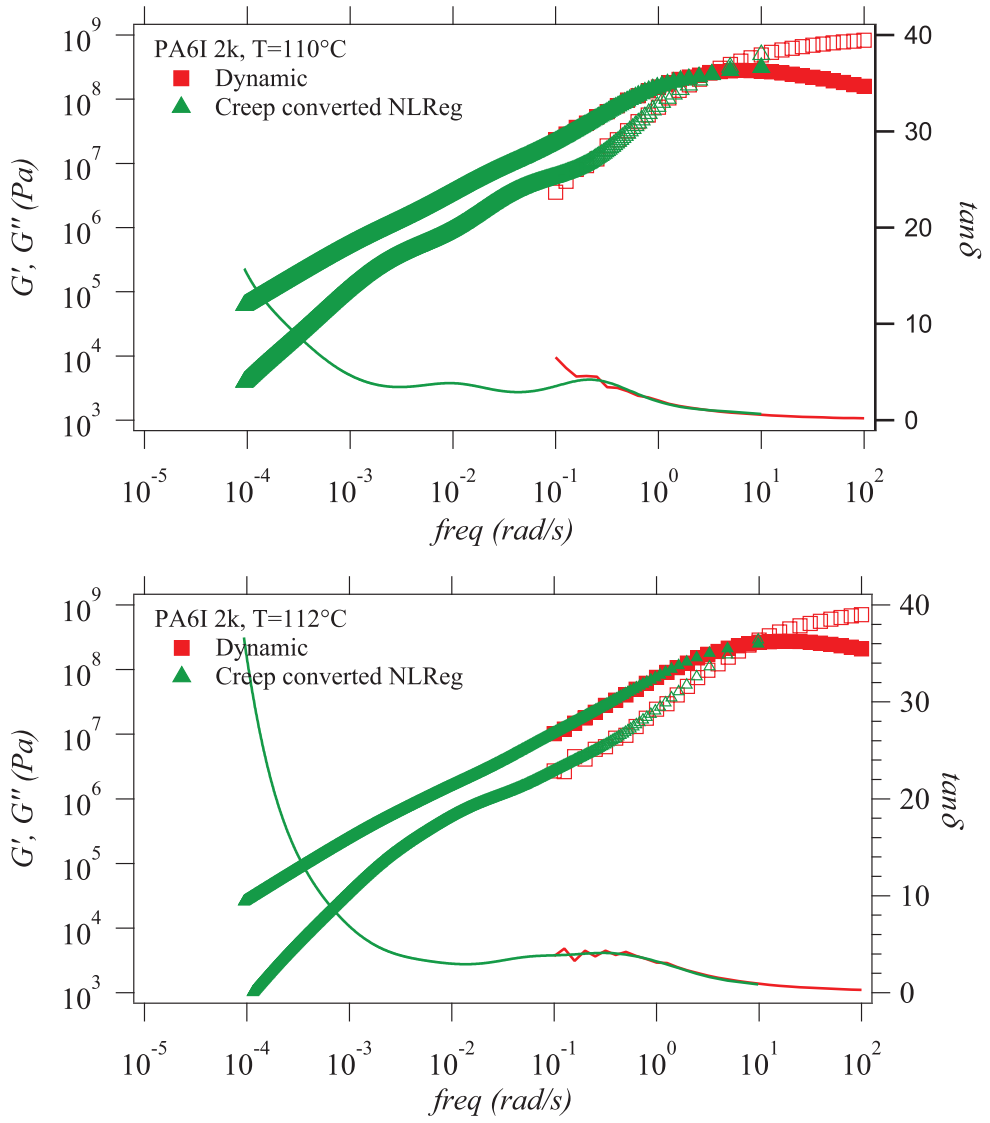

Figure U: Creep compliance conversion to dynamic moduli and dynamic measurements for different temperatures in PA6I 2k. G′=empty markers, G″=filled markers, tan δ=line

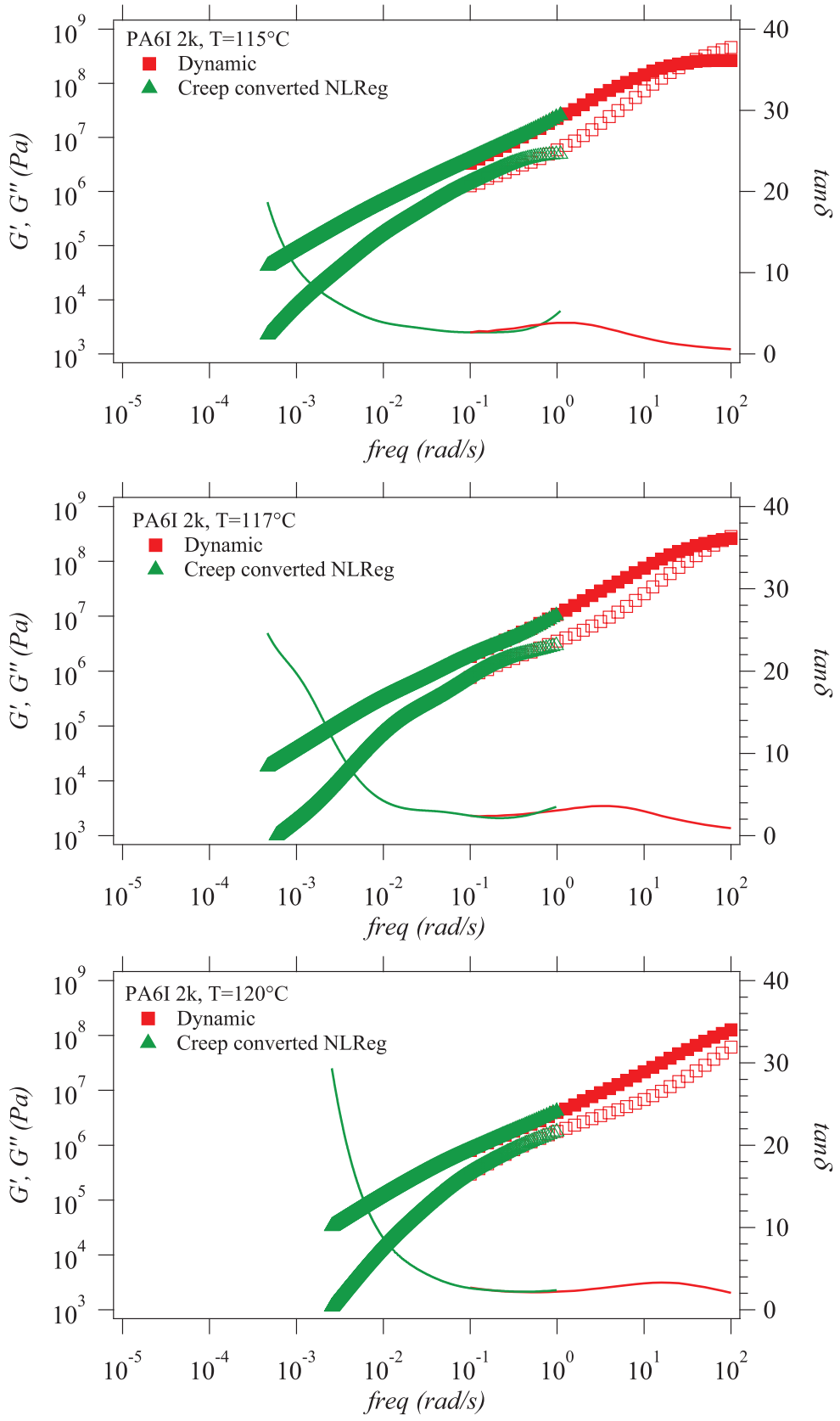

Figure V: Creep compliance conversion to dynamic moduli and dynamic measurements for different temperatures in PA6I 2k. G′=empty markers, G″=filled markers, tan δ=line

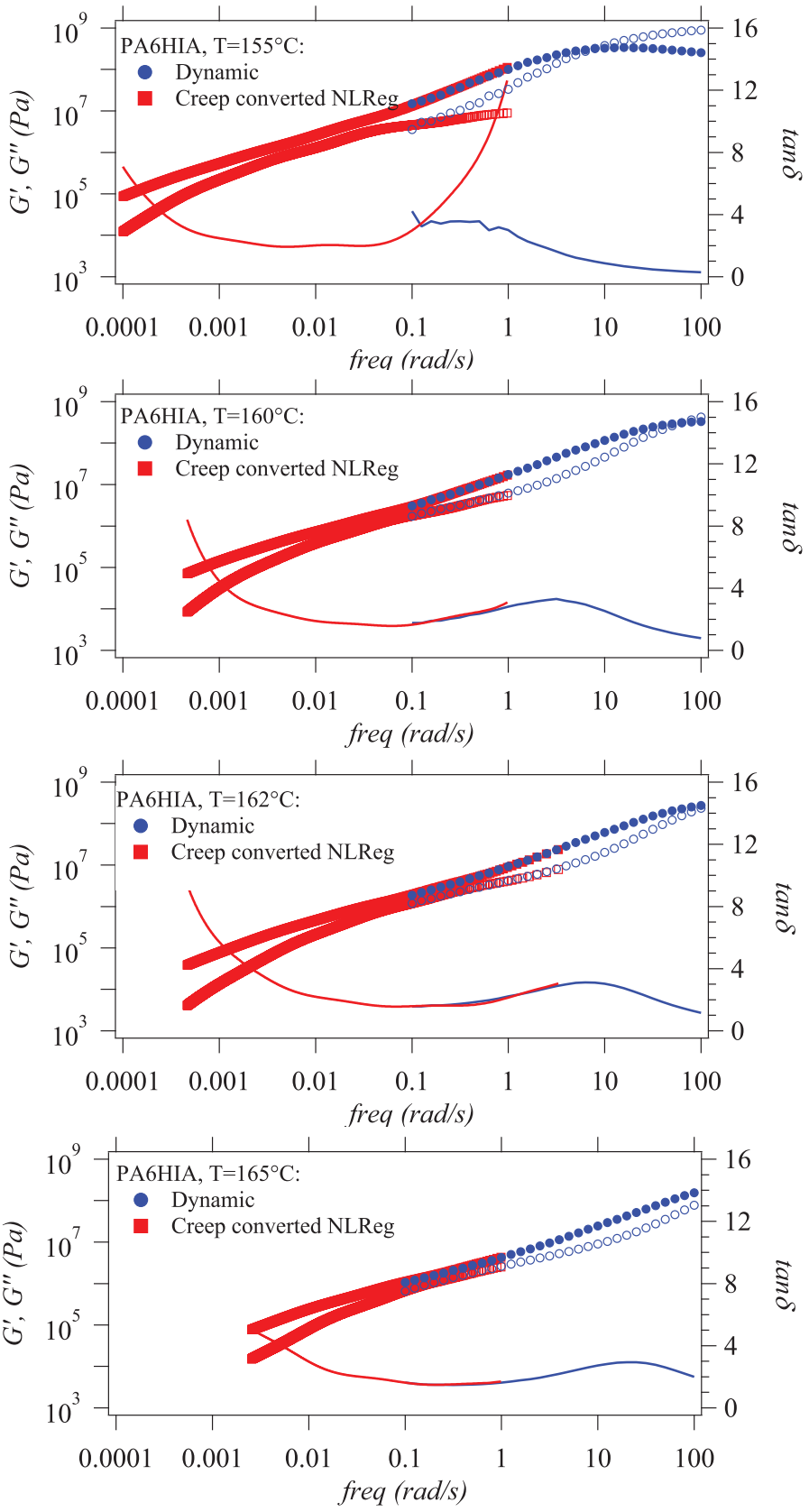

Figure W: Creep compliance conversion to dynamic moduli and dynamic measurements for different temperatures in PA6HIA 3k. G'=empty markers, G"=filled markers, tan δ=line

Résumé étendu en français

Ce travail de thèse a été consacré à l'étude de l'effet possible des liaisons intermoléculaires fortes (liaison hydrogène, complexation ionique) sur la dynamique du polyamide dans l'état solide en présence de solvants et à l'état fondu. Le contexte, l'approche et les conclusions de l'étude sont résumés ci-dessous.

1. Dynamique du polyamide dans l'état solide en présence de solvants

Les polyamides sont une famille de polymères thermoplastiques semi-cristallins largement utilisés dans l'industrie automobile grâce à leur excellente stabilité thermique et propriétés mécaniques. Cependant, ces propriétés peuvent être affectées par la sorption de l'eau présente dans l'atmosphère ou de l'éthanol présent dans les biocombustibles. Les cinétiques de sorption et la sorption à l'équilibre dépendent des mécanismes d'interaction entre le solvant et le polyamide et des mécanismes de sorption et de diffusion.

La diffusion et la sorption de solvants dans les polymères sont des phénomènes complexes à cause de l'existence possible d'interactions spécifiques (polaire ou apolaires), d'hétérogénéités dynamiques dans la phase amorphe, de changements dans la dynamique du polymère en présence de solvants et de l'existence d'une phase cristalline. Tous ces éléments doivent être pris en compte dans les systèmes polyamide/solvants. Tout d'abord, les solvants peuvent interagir avec les groupements amides présents dans le polyamide et induire une diminution de la température de transition vitreuse, c'est à dire une augmentation de la mobilité des chaînes polymère (Rios De Anda, A.; Fillot, L. A.; Preda, F. M.; Rossi, S.; Long, D. R.; Sotta, P., *Sorption and plasticization effects of ethanol–toluene–isooctane ternary mixtures in polyamide 6,6 and induced plasticization effects*. European Polymer Journal 2014, 55, 199-209). Ensuite, même si la phase cristalline est considérée comme imperméable aux solvants, sa présence induit un gradient de mobilité dans la phase amorphe, qui par conséquent est souvent représentée comme un milieu formé de deux régions distinctes, une phase amorphe mobile et contrainte.

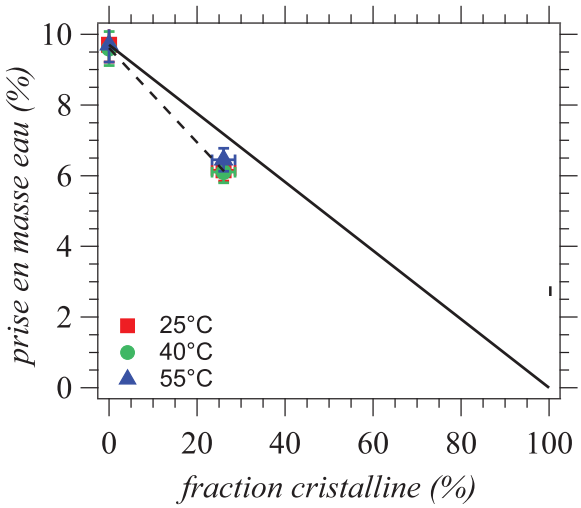

Figure A: Prise en masse d'eau dans un polyamide amorphe et son homologue semi-cristallin. La prise en masse en est dessous de la courbe prédite pour un modèle à deux phases (cristalline et amorphe), ce qui semble indiquer qu'une fraction de la phase amorphe ne serait pas accessible pour l'eau.

Puisque l'accessibilité de la phase amorphe peut avoir une influence sur les mécanismes

de diffusion et de sorption, la première partie de cette étude a été consacrée aux polyamides modèles. La diffusion et la sorption de différents solvants (eau, alcools de tailles différentes) ont été comparés dans un polyamide 100% amorphe (PA6I, PA6I/6T 70/30 molaire) et son homologue semi-cristallin (PA6I/6T 30/70 molaire). Nous avons confirmé que la phase amorphe d'un polymère semi-cristallin n'est pas entièrement accessible à l'eau (Figure A), ce qui est en accord avec la littérature [33, 55, 58, 59]. Dans le cas des alcools, la comparaison des polyamides amorphes et semi-cristallins n'a pas été possible à cause de phénomènes secondaires (cristallisation, cavitation) dans le polyamide amorphe. Les processus de cristallisation et cavitation ont été soigneusement documentés.

Une deuxième partie de cette étude a été consacrée à la relation entre la diffusion de solvants et la dynamique de la phase amorphe dans deux polyamides avec une densité de liaisons hydrogène différente (PA6,6 et PA6,10). Le but principal est d'étudier chaque matrice individuellement (sorption de l'eau, coefficients de diffusion, temps caractéristiques de relaxation) et de comprendre les mécanismes de diffusion, en particulier si la diffusion est couplée à la relaxation du polymère. Un autre objectif est d'évaluer l'influence de la densité de liaisons hydrogène sur la sorption et la diffusion.

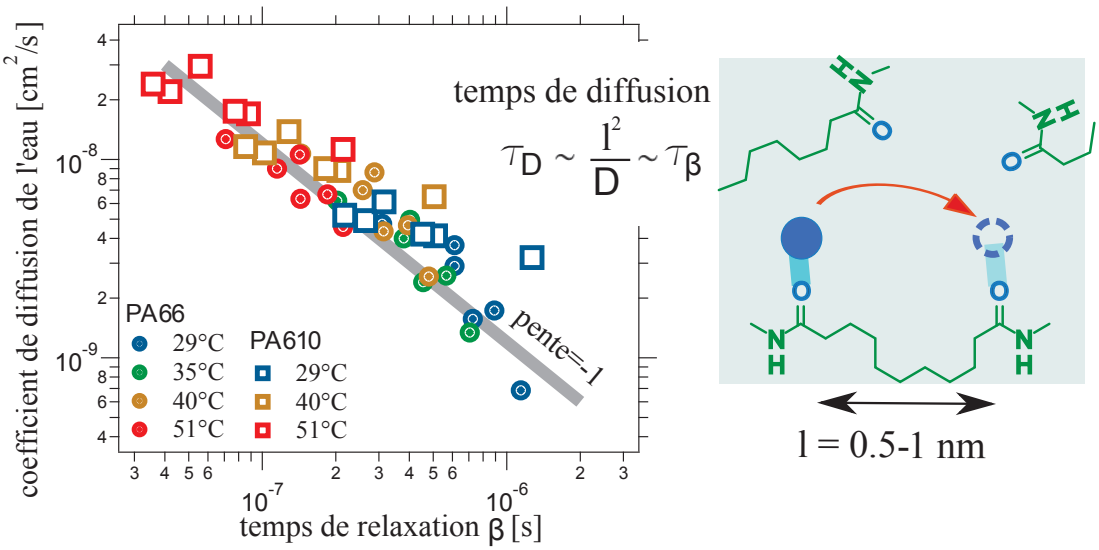

Figure B: Coefficients de diffusion de l'eau dans le PA6,6 et PA6,10 à différentes températures en fonction tu temps de relaxation β et représentation schématique du saut d'une molécule d'eau entre deux groupements amide

Premièrement, nous avons mis en évidence que la diffusion de l'eau liquide est Fickienne dans le PA6,10 et non-Fickienne dans le PA6,6. Pour avoir un aperçu plus clair des mécanismes de diffusion, nous avons effectué des mesures à quasi-équilibre avec un outil de Sorption Dynamique de Vapeur (Dynamic Vapor Sorption, DVS), pour mesurer sélectivement la variation des coefficients de diffusion en fonction de l'activité de l'eau ou, de façon équivalente, la concentration d'eau à l'équilibre. Deuxièmement, l'influence de la relaxation du polymère a été évaluée par Spectroscopie Diélectrique. Nous avons mesuré les temps caractéristiques de la relaxation α, qui est associée à la transition vitreuse et de la relaxation β, qui est liée à la dynamique locale du polymère (changements de conformation des groupements amide et relaxation de liaisons hydrogène) [26]. Une simple comparaison des échelles de temps de la diffusion et de la relaxation α indique que les deux phénomènes ne sont pas directement corrélés. Cependant, la diffusion semble corrélée à la relaxation secondaire β (Figure B), qui décrit la dynamique locale des groupements amide en présence d'eau. Nous proposons un mécanisme

de diffusion basé sur le piégeage des molécules d'eau dans les sites de sorption (groupements amide) et le saut des molécules d'eau d'un site à l'autre. La diffusion semble limitée par le temps de relaxation des liaisons hydrogène entre l'eau et les groupements amide et les changements de conformation de ces dernières (Preda, F.-M.; Alegría, A.; Bocahut, A.; Fillot, L.-A.; Long, D. R.; Sotta, P., *Investigation of Water Diffusion Mechanisms in Relation to Polymer Relaxations in Polyamides*, Macromolecules 2015, 48 (16), 5730-5741).

2. Dynamique du polyamide à l'état fondu

Bien que le polyamide soit un polymère industriel de grande importance, les études systématiques de son comportement rhéologique sont rares dans la littérature. Les raisons principales sont les difficultés liées à la stabilité chimique de ce polymère et à l'existence d'une phase cristalline qui limite les mesures à des températures au-dessus de son point de fusion.

Le but de notre étude est de comprendre les effets de la force et de la densité de liaisons intermoléculaires (liaisons hydrogène, interactions ioniques) sur la dynamique du polyamide à l'état fondu. Pour atteindre ce but, des polyamides amorphes ayant des bloqueurs de chaînes ont été synthétisés (Figure C). La force d'interaction a été variée en introduisant des groupements latéraux sur des chaines polymères par ailleurs identiques (PA6I). En effet, l'énergie d'interaction entre un groupement phénol (40 kJ/mol [9]) ou sulfonate de lithium (50 kJ/mol [122]) et un groupement amide est plus importante que l'énergie d'interaction entre deux groupements amides (25 kJ/mol [9]).

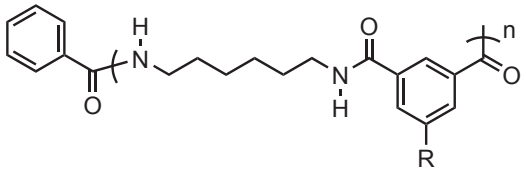

R= H PA6I
OH PA6HIA
SO_3Li PA6LiSIPA

Figure C: Structure chimique des polyamides semi-aromatiques avec des groupements latéraux

Les courbes maîtresses complètes pour les modules dynamiques ont été obtenues pour la première fois pour le polyamide en appliquant le principe de superposition temps-température. Dans la série de polyamides 6I, nous observons l'apparition d'un plateau sur le G' pour des masses moléculaires d'environ 5000 g/mol. Quand la masse moléculaire augmente, un plateau caoutchoutique distinct apparaît et le temps de relaxation le plus long est déplacé vers les fréquences plus basses. L'introduction de sulfonate de lithium ou du groupement phénol provoque une augmentation de la température de transition vitreuse de 10 à 40°C respectivement, ce qui est probablement dû à leur capacité à former des interactions plus fortes avec les groupements amide. De manière surprenante, les courbes maitresses des polymères de masse moléculaire comparable se superposent à même distance à la T_g, ce qui indique que la force d'interaction n'influence pas leur dynamique en fondu. Pour confirmer cette hypothèse, nous avons décrit la variation des modules dynamiques des polymères non-enchevêtrés avec un modèle classique de Rouse. Une étude de ces matériaux par Spectroscopie Diélectrique a mis en évidence que la relaxation des interactions se fait dans une gamme de température et de fréquence qui n'est pas accessible pour les mesures rhéologiques. Par comparaison avec les polymères apolaires, on observe cependant que les PA étudiés ont une fragilité (définie au sens d'Angell) réduite.